5-2004

Analytical and Numerical Investigation of a Mechanically Stabilized Earth Wall on I-15

Aaron S. Budge
Utah State University

ANALYTICAL AND NUMERICAL INVESTIGATION OF A MECHANICALLY STABILIZED EARTH WALL ON I-15

by

Aaron S. Budge

A dissertation submitted in partial fulfillment
of the requirements for the degree

of

DOCTOR OF PHILOSOPHY

in

Civil and Environmental Engineering

Approved:

James A. Bay
Major Professor

Joseph A. Caliendo
Committee Member

Loren R. Anderson
Committee Member

Robert T. Pack
Committee Member

Steven L. Folkman
Committee Member

Laurens H. Smith Jr.
Interim Dean of Graduate Studies

UTAH STATE UNIVERSITY
Logan, Utah

2004

ABSTRACT

Analytical and Numerical Investigation of a Mechanically Stabilized Earth Wall on I-15

by

Aaron S. Budge, Doctor of Philosophy

Utah State University, 2004

Major Professor: Dr. James A. Bay
Department: Civil and Environmental Engineering

This dissertation is the culmination of extensive research into the behavior of a mechanically stabilized earth (MSE) wall at I-15 and 3600 South in Salt Lake City, Utah. The wall is about 30 ft tall and is constructed on a compressible, soft clay foundation. Research on this project has included extensive instrumentation and monitoring of stresses and deformations in the wall and its foundation, a study of the effects of drilling and sampling method on disturbance of samples, and extensive laboratory testing to determine strength and deformation properties of soils at the site. The results of these portions of the project are summarized. All of this work has been used to develop and calibrate an analytical model of the MSE wall. This dissertation presents this analytical model.

The analytical model of this wall is a valuable and powerful tool to understand the behavior of tall MSE walls on compressible foundations. By using such a model, the effects of pore pressure dissipation during construction can be evaluated. This allows for

accurate evaluation of the stability of the embankment during construction and long term for any construction sequence. The model can be used to evaluate soil reinforcement interaction and to evaluate different reinforcement configurations.

This research contains discussions of the soil model that was developed for Bonneville clay, a comparison between measured and calculated deformations in the wall foundation, the time-settlement behavior of the wall, soil-reinforcement interactions, and stability evaluations, as well as a comparison of traditional slope stability analysis results to the finite element results obtained from this model.

(221 pages)

ACKNOWLEDGMENTS

A number of people have been essential in making this research project possible. First of all, I would like to thank the Utah Department of Transportation, specifically Blaine Leonard and Clifton Farnsworth, for their guidance and interest from the initial stages of this project. Jon Bischoff and Darren Sjoblom were also very helpful with their insights relating to the work performed. Each of them took time to review preliminary reports to give feedback on progress and help the project move along in the right direction.

Next, I wish to thank the other graduate students that have been involved in various phases of this project since its conception. Mark Goodsell instigated the project, setting up the initial instrumentation plan and obtaining the initial measurements. Jon Hagen and Todd Colocino spent hours in the field and in the laboratory working on sample disturbance analyses and obtaining very detailed soil properties, making my job that much easier. Additional students were also involved throughout the process, helping take measurements, set up instrumentation, retrieve buried instrumentation, etc. In order to not leave anyone out, I won't attempt to name each of these students. However, they need to know they are very much appreciated.

Without the help of our department "McGyver," I would never have been able to collect the data needed for the final analysis. Thanks to Ken Jewkes, who can literally do anything required for any project, and can remember details that everyone else had long since forgotten. Thanks Ken!

Thanks to my committee members for their guidance and advice, not only relating to this project, but also to my professional career goals. Many thanks to Dr. Caliendo, Dr. Anderson, Dr. Pack, and Dr. Folkman for helping me these past years.

I give a special thanks to my major professor, Dr. Jim Bay, for his patience and guidance throughout the project. Several times it seems my wheels were just spinning, and little progress seemed to be made. Jim helped to get things back into gear so we could make headway, and in the end we came up with a pretty good model.

I give a huge thanks to my family for their support all along the way. My brothers and sisters have shown interest and support throughout my research. In fact, Mike helped out on a nasty chore for many hours on a cold fall day at 3600 South. My mother made our life easy, playing the role of daycare for Brady for the years it took to complete this research. Thanks, Mom! Thanks also to my father, who has since passed on, for his example, and for having instilled in me the ability to work hard. Thanks, Dad!

Finally, thanks to my beautiful wife, Anita, for her great patience and gentle persuasion these past years. She made it possible for me to earn two graduate degrees and somehow make it through graduate school without any monetary distress. Her love and support have been priceless, literally! Thank you, Sweetheart!

Aaron S. Budge

CONTENTS

LIST OF TABLES

LIST OF FIGURES

CHAPTER 1

INTRODUCTION

This dissertation is the culmination of extensive research into the behavior of a Mechanically Stabilized Earth (MSE) wall at I-15 and 3600 South in Salt Lake City, Utah. The wall was designated R-346-1C by the Utah Department of Transportation. The final wall is about 30 ft (9.1 m) tall and is constructed on a compressible, soft clay foundation. A schematic showing the typical wall system used on I-15 is given in Fig. 1.1. The location of the wall is shown in Fig. 1.2. Several photographs showing the wall during and after construction are given in Fig. 1.3.

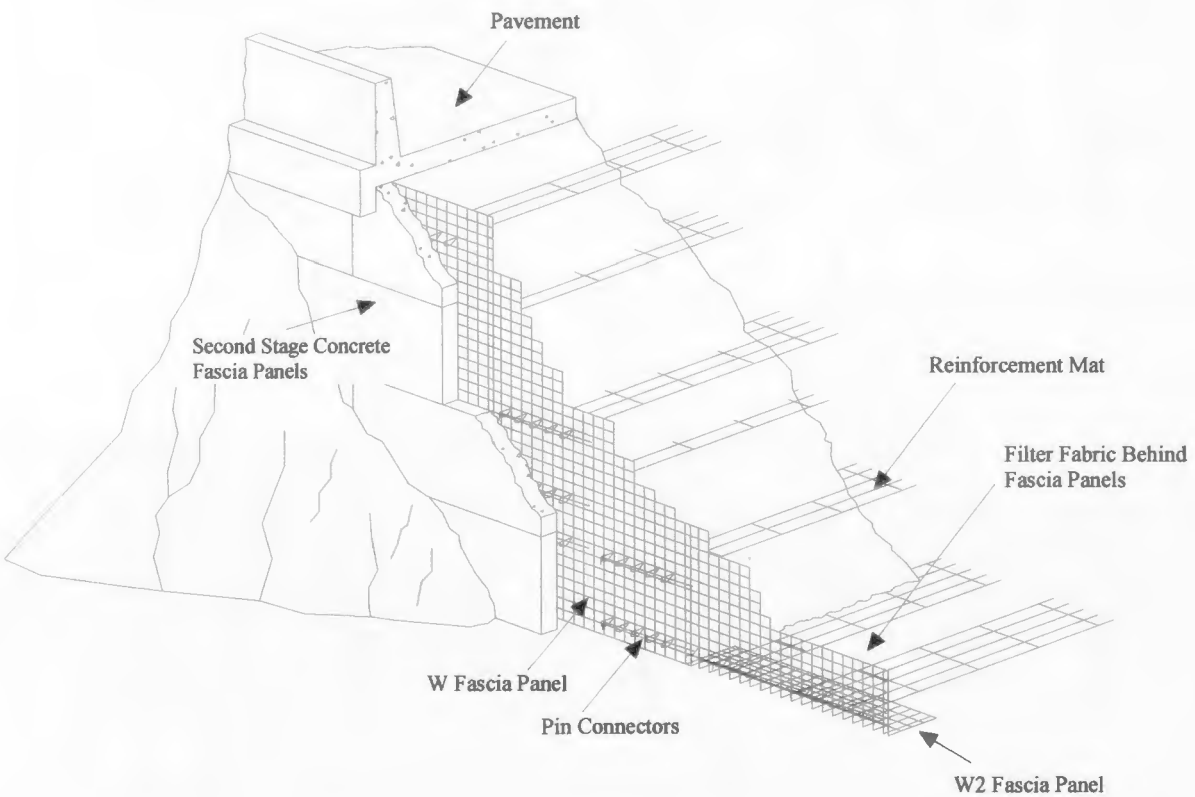

Fig. 1.1 Schematic of a typical MSE wall system used on the I-15 reconstruction project

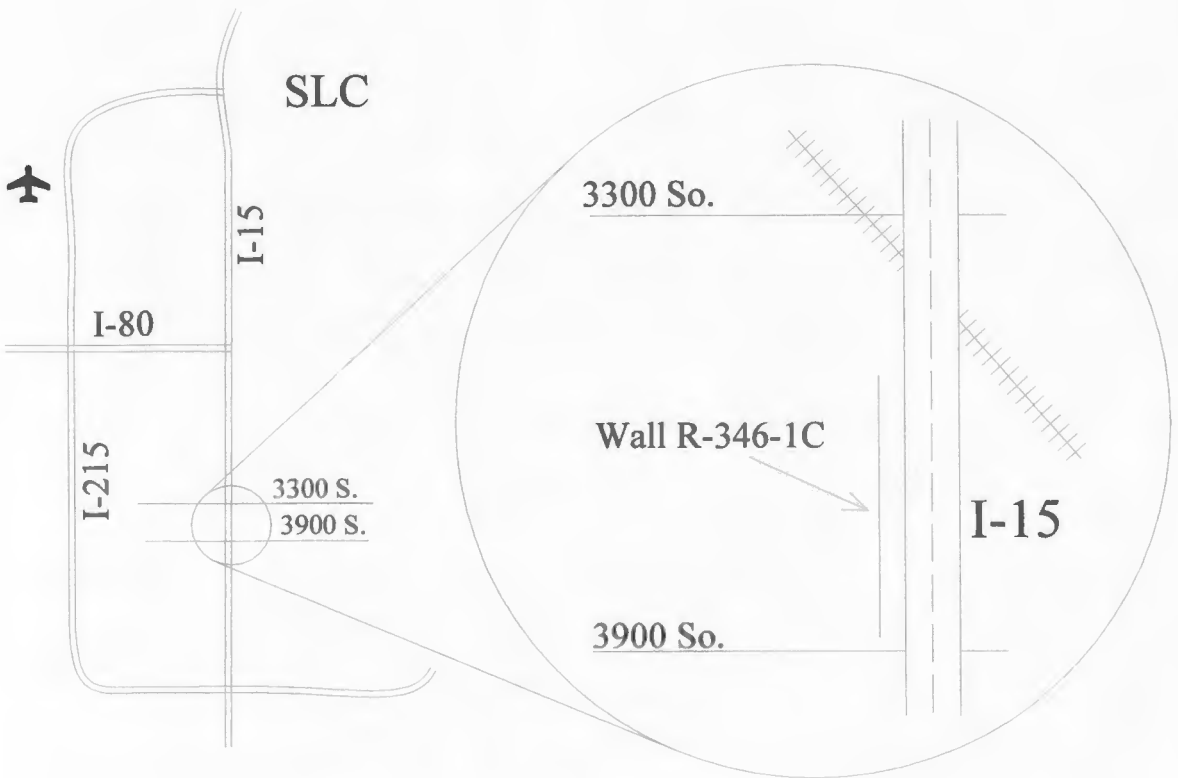

Fig. 1.2 Location of MSE Wall R-346-1C

This project has included four significant components, each of which will be addressed in this dissertation. The first component involved the placement of extensive instrumentation in the wall and foundation material. This allowed for the monitoring of stresses and deformations in the wall and foundation during the course of construction and through the end of primary consolidation. The second component of this research involved long-term monitoring of the wall to investigate the effects of secondary consolidation and ensure minimal long-term movement. The third component of this research involved a careful study of the effects of drilling and sampler type on the extent of sample disturbance for soil samples obtained. Extensive laboratory testing not only

Fig. 1.3 Photographs showing Wall R-346-1C during and after construction

provided a means of quantifying the extent of sample disturbance, but also provided valuable strength and consolidation properties for the foundation soil. The end result of this project, the fourth component of the study, used the data collected from each of the previous stages to develop and calibrate an analytical finite element model of the MSE wall. Each of these portions of the project will be addressed in this dissertation, with a special emphasis given to the finite element model of the wall and the conclusions reached from that model. An overview of each of the components associated with this project will now be given.

1.1 LITERATURE REVIEW

Chapter 2 presents a literature review of several references considered pertinent to this project. This literature review was performed by the author. Four topics were considered to be appropriate for the purposes of this research.

First, a general background on Mechanically Stabilized Earth (MSE) walls is given. Many research projects, professional papers, and professional conferences have focused on MSE wall design and behavior. This literature review discusses the basics of MSE walls as developed through the years, but is by no means an all-encompassing review of the hundreds of available references. Additional references may be found in Goodsell (2000).

Second, an investigation into finite element analysis studies of geotechnical structures was performed. Finite element analysis has been used to investigate the response of such structures as traditional embankments, earth- and rock-fill dams, MSE

walls, and other geotechnical structures. Several studies that were found to be applicable for the purposes of this research are summarized.

Third, a discussion of the Hardening Soil Model is given. This model is the most robust model currently available in publicly available software packages such as Plaxis. Traditional strength parameters are used for a given soil, but stress-dependent modulus values allow the moduli of a given soil layer to vary with depth. Thus, fewer layers of soil are required to appropriately model a quite complex foundation system. A few of the details regarding this soil model are given.

As the final section of Chapter 2, a review of literature relating to soil-reinforcement interaction is given. The finite element model used for this research does only a fair job of modeling this complicated interaction. Some of the simplifications required and a comparison to the actual complexities of the interaction are given.

1.2 WALL INSTRUMENTATION AND PERFORMANCE

Chapter 3 presents the instrumentation installation plans and the measurements obtained for mechanically stabilized earth (MSE) wall R-346-1C located along the I-15 reconstruction project in Salt Lake City, Utah. This chapter contains the initial instrumentation plan and the monitoring of wall behavior during the construction process and in the first three years following construction.

Much of the work involved with this chapter was performed by Mark W. Goodsell. A complete version of this work can be found in the thesis prepared by Goodsell (2000) and in a report to the Utah Department of Transportation as given by Bay et al. (2003a, Report No. UT-03.11). Several students assisted Goodsell in collecting

the data during the construction process. The author performed some of the data analysis in cases where mistakes had been found. However, the majority of the initial analysis was performed by Goodsell. The author and several additional students obtained the post-construction measurements, and the author performed all of the data analysis for these measurements.

Important findings have been observed during and following the construction of this MSE wall. These include conclusions relating to the internal stability of the wall and also the internal and external wall displacements. These conclusions are based on data collected from extensive instrumentation located within the wall and in the foundation material beneath the wall. This instrumentation includes over 500 strain gages in the reinforcement bar mats and fascia panels, three vertical and two horizontal inclinometers, three Sondex settlement systems, five pressure cells, and 60 horizontal extensometers.

1.2.1 Conclusions Regarding Internal Stability

A number of conclusions are made concerning the internal stability of the wall.

- The maximum tension in the bar mats was much less than the allowable tension to which the bar mats could be subjected. The minimum ratio of the allowable yield stress to the tensile stress existing in the longitudinal bars of the reinforcement is 2.5 for one strain gage position, with only four gage positions having ratios less than 5.0 (out of more than 90 functional positions). Thus, the vast majority of the bar mats are subjected to tensile forces less than 20 percent of the yield strength of the material. The allowable stresses used in calculating these ratios considered the entire cross section of the

longitudinal bar, not taking into account corrosion of the steel over time, which decreases the cross-sectional area.

Similar calculations were performed to account for the decrease in the cross-sectional area of the bars due to corrosion throughout the design life of the wall. For a 75 year design life, and allowing for 16 years for loss of the galvanization of the steel, the minimum ratio of the allowable yield stress to the tensile stress existing in the longitudinal bars of the reinforcement is 2.0, again for one strain gage position. Only four gages have ratios less than 4.2 after the same 75-year design life.

- From the measured lateral earth pressure coefficient K-values (as back calculated from tension measurements in the bar mats) it appears that the design K-value currently required by AASHTO (1998) is conservative. Fig. 1.4 shows some of the K-values measured in the wall. A number of the back calculated K-values shown in Fig. 1.4 appear to exceed the current AASHTO design envelope, but closer inspection shows that these values occur in the mats near the bottom of the wall early in the construction process. These mats show values well within the design envelope once the construction has progressed. It is concluded that these higher values of K can be attributed to residual compaction stresses, and are not of concern.

- The vertical stress distribution followed a pattern similar to other instrumented MSE walls, with low vertical stresses near the face of the wall, stresses increasing to a maximum value approximately 6 ft (1.83 m) from the wall face, then decreasing to the stress expected from overburden ($\sigma_v = \gamma h$) at some distance from the wall face. The measured vertical stresses obtained during the application of the surcharge load during wall construction are presented in Fig. 1.5.

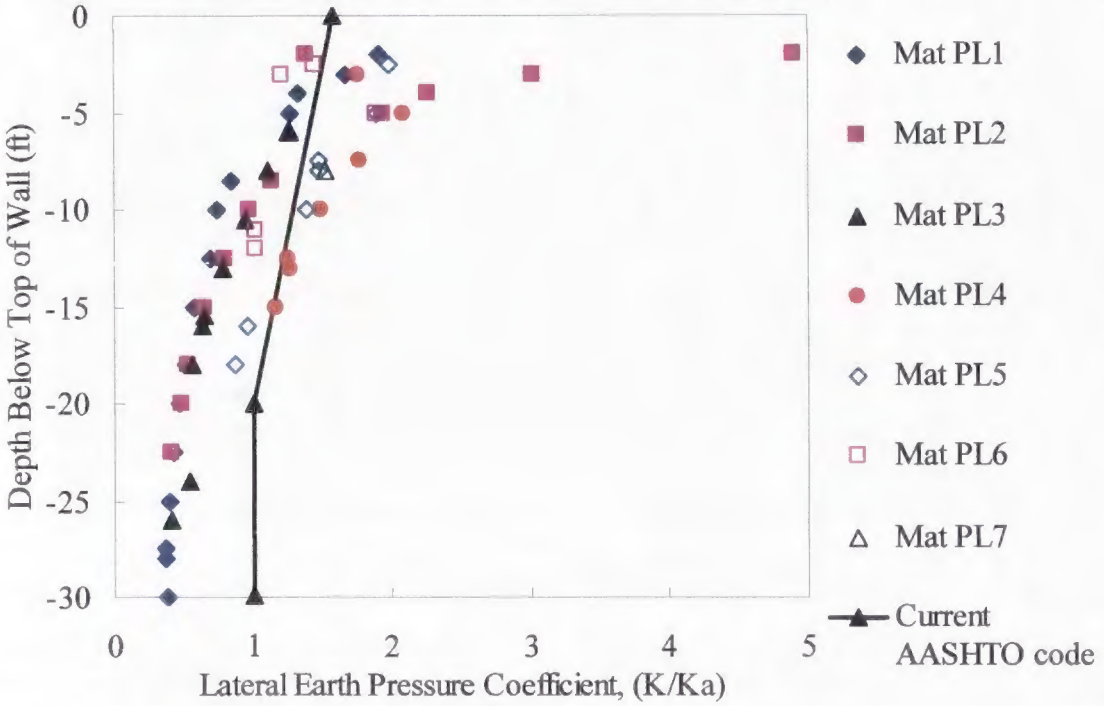

Fig. 1.4 Normalized values of K for the section of Wall R-346-1C with primary reinforcement only

Also shown in this figure is the vertical stress calculated due to overburden (γh) at the time the surcharge was applied, as well as the stress calculated using the Meyerhof equation as per AASHTO (1998). Due to the fairly significant wall height of 36 ft (11 m) with maximum surcharge, the eccentricity associated with the Meyerhof equation becomes large, producing calculated vertical stresses near the wall face that far exceed the vertical stresses measured in the wall. Thus, the measured vertical stress distribution in the wall recorded in this study is not reflective of the stresses required for use in design by AASHTO (1998).

Minimal internal deformations were measured. Data collected from the horizontal extensometers showed that the wall essentially moved as a rigid body, with little differential movement. Practically no differential movement occurred between

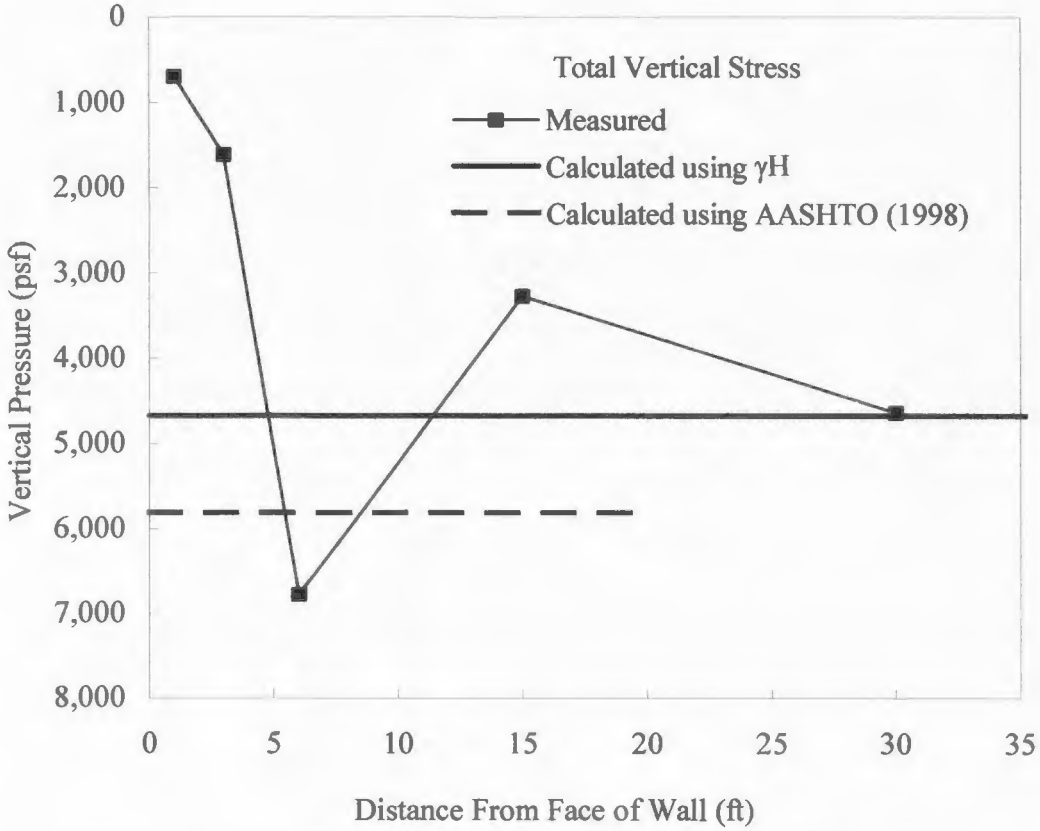

Fig. 1.5 Plot of vertical pressure versus distance from wall face during time in which surcharge was applied to the wall

extensometers located 4 ft (1.22 m) from the wall face and extensometers located 16 ft (4.88 m) from the wall face. There was some movement within the soil mass from the wall face to a distance of 4 ft (1.22 m) from the face, possibly due to the fact that less compaction energy was used close to the wall face.

The overall movement of the extensometers was on the same order as the movement of the entire wall measured by the vertical inclinometer measurements, again confirming the rigid movement of the wall. On average, the vertical inclinometers measured a horizontal displacement of 3.5 inches (89 mm) at the base of the wall.

Extensometers in the same general area also near the base of the wall showed 3 inches (76 mm) of movement 16 ft (4.88 m) from the wall face, with increasing movement toward the face of the wall.

Extensometer measurements showed a decrease in lateral movement moving from the base of the wall to the top of the wall, with incremental movements decreasing near the base of the wall throughout the construction process. Some deformations were monitored in the wall face near the toe of the wall, but these deformations were determined to be localized and not indicative of global instability in the wall.

- Vertically, during construction, the wall settled approximately 1.5 ft (0.46 m). Most of this settlement occurred in the two soft clay layers located in the upper 22 ft (6.7 m) of the soil profile beneath the rubble backfill on which the wall was constructed. Survey monuments showed that no measurable settlement occurred outside the wick drain zone, while monuments within the wick drain zone verified the settlements measured using the horizontal inclinometers.

- Total wall deformations are shown in Fig. 1.6, in which the movements are exaggerated for clarity. Wall settlement was approximately 20 inches (0.51 m) at the time the most recent measurements were taken. Horizontal movement at the base of the wall was 3.5 inches (89 mm). Rotation of the wall was on the order of 0.2 degrees. Each of these deformations will continue to be monitored over time to observe secondary consolidation effects. Horizontal movement outside the wick drain zone (I-15 right-of-way) was 0.3 inches (7.6 mm) at the ground surface and decreased with depth.

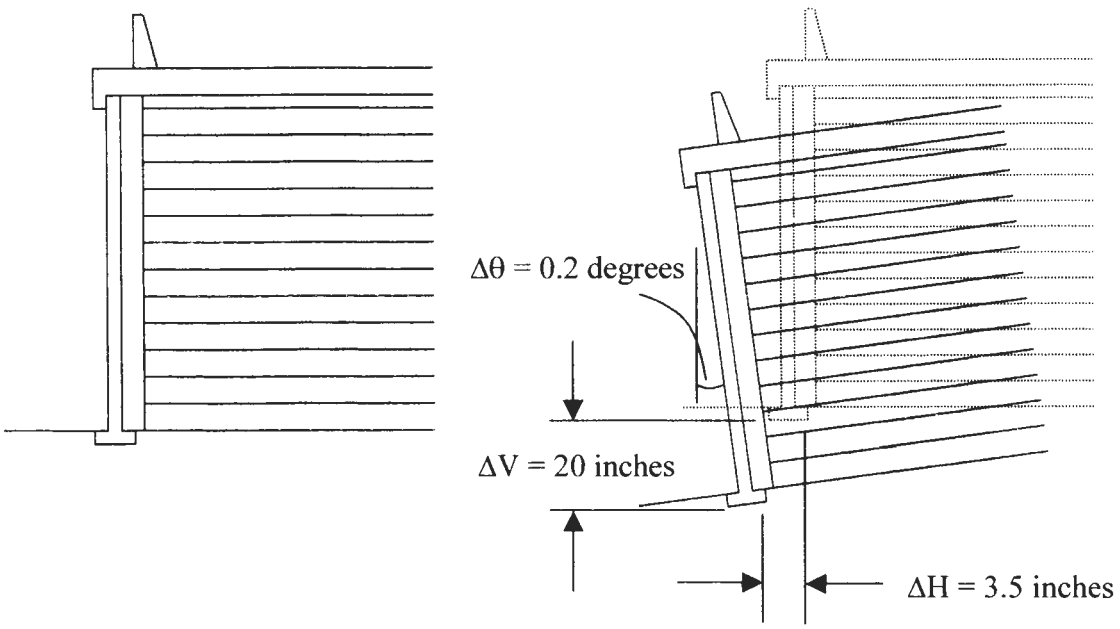

a) Undeformed Wall b) Exaggerated Deformed Wall

Fig. 1.6 Comparison of the undeformed wall to an exaggeration of the deformed wall

1.2.2 Conclusions from Comparison of Reinforcement Systems

The portion of wall that was instrumented contained two reinforcements systems. One section, referred to as the primary reinforced only section, contained the initial design used by VSL, with 24 ft (7.32 m) long bar mats with a 30 inch (0.76 m) vertical spacing between reinforcement layers. This system had experienced some problems with constructibility due to some significant face deformations near the base of the wall at some other walls along the I-15 corridor. These constructibility issues as well as concerns regarding the stability of this system caused a design change. This resulted in the addition of intermediate layers of reinforcement in the bottom half of the wall. These bar mat layers were 10 ft (3.05 m) long, and were placed halfway between the layers of primary reinforcement. Instrumentation was placed in sections of the wall containing

both systems to compare the behavior of the two sections as well as determine the stability of both sections. Conclusions relating to these two systems are given here.

- As the primary purpose of the intermediate reinforcement was to reduce the excessive bulging that had been noted near the base of several other walls, steps were taken to monitor this bulging during construction for both sections of the wall. In the section containing only primary reinforcement, a bulge on the order of 4 inches (102 mm) developed during wall construction and extended over a fairly large distance (approximately 17 ft (5.18 m)). The maximum bulge found in the section containing both primary and intermediate reinforcement was only 2.7 inches (69 mm) and was only prominent for a distance of approximately 4 ft (1.22 m). Thus, it appears that the addition of intermediate reinforcement did reduce the bulging near the toe of the wall significantly. It should be noted, however, that neither of the bulges monitored at the two sections of wall was found to be indicative of a stability problem.

- The section containing both primary and intermediate reinforcement was subjected to higher tensile stresses than the section with only primary reinforcement. One possible reason for this is that the section with additional reinforcement is behaving more rigidly, such that less internal deformation takes place. This causes the soil to stay closer to the at-rest condition, such that stresses in the soil are higher than for soil allowed to deform and move toward the active state. These increased stresses in the soil are transferred to the reinforcement, causing the increased stresses to be observed in the section with additional reinforcement.

- Both systems are stable. When considering both internal and external stability, both the section containing only primary reinforcement and the section containing primary and intermediate reinforcement are stable and in good condition.
- The intermediate reinforcement could have been omitted if other methods of controlling the deformation had been found. Possible alternatives that may be considered are the following:

    1. Using a uniform gravel as fill near the wall face,
    2. Temporary support of the wall face during compaction.

1.2.3 Overall Conclusions Regarding Instrumentation

Overall, throughout construction and in the years following construction the wall is performing well. Results of this study show that there is adequate reinforcement within the wall, with stresses in the reinforcement being well below the allowable. The wall has been determined to be internally stable. The deformations near the wall face were determined to be localized and not due to internal instability. The wall has also been found to be stable externally. The expected large primary settlement of the wall did occur, but little secondary settlement has taken place. Finally, a comparison of the section of wall containing only primary reinforcement to that containing primary and intermediate reinforcement led to the following conclusions:

- Intermediate reinforcement was not necessary for stability of the wall, since the section of wall not containing additional reinforcement was found to be both internally and externally stable,

- Intermediate reinforcement did decrease the deformations of the wall face in the lower portion of the wall, resolving the constructibility issues that had been a problem with previous walls not containing the intermediate reinforcement, and
- Intermediate reinforcement could be omitted without consequence if another method to control deformations of the wall face is utilized.

1.2.4 Long-term Monitoring

Chapter 3 also presents the long-term monitoring of MSE Wall R-346-1C during the first three years following wall construction. The steps taken to protect the instrumentation for long-term monitoring are given, and a number of challenges that were overcome are explained. Each of the instruments for which data was collected during construction is addressed to illustrate the post-construction changes in the wall and any changes in the ability to take such measurements.

The author performed the work contained in this chapter. Several students were involved with some of the physical work required to access several of the instruments and in taking the necessary readings. The author performed all of the data analysis contained in this section.

In general, minimal movement has occurred within the wall and foundation material since the end of construction of the wall. Data collected from the vertical inclinometers show that some additional horizontal movement has taken place, but this movement appears to be due to secondary consolidation effects which have caused slight tipping of the wall over time.

Horizontal inclinometer and Sondex consolidation system measurements show that minimal vertical movement has occurred since the end of construction. From the end of primary consolidation until the most recent measurements were taken (around 2.5 years after the end of construction), only 0.3 inches (7.6 mm) of wall settlement has occurred. This deformation is due to secondary consolidation of the foundation soils, and will continue to be monitored for a number of years. Assuming the wall continues to follow secondary consolidation behavior, it appears the design criterion of a maximum of 3.0 inches (76.2 mm) of post-construction movement in the first 10 years after construction will easily be met.

Extensive work was required in order to clean the strain gage connectors to allow additional tension readings in the reinforcement to be taken. Readings were taken, but the data obtained was found to be questionable. The reason for these misleading readings has not yet been determined, but at this point additional strain gage readings would be considered unreliable.

Four of the five pressure plates appear to be fully functional at the most recent readings. The four functional plates showed a decrease in vertical effective stress from the final reading taken during construction. This makes sense because the final construction readings were taken while the 6 ft (1.8 m) surcharge was still in place. When the surcharge was removed, the pressure decreased, as was noted in the most recent set of pressure plate readings.

Due to construction of the second-phase concrete fascia panels, the horizontal extensometers were no longer accessible. Thus, it was not possible to obtain any additional information as to relative movement within the wall since the end of

construction. Similarly, the toe bulges that were monitored during the course of construction were no longer accessible, which again prevented any additional measurements of face deformations to be taken.

In general, the post-construction behavior of the wall is in accordance with all expectations. Some secondary consolidation has taken place, which has yielded additional horizontal and vertical movement since the end of construction. This movement will continue to be monitored over coming years. It appears that the long-term deformation requirements established by the Utah Department of Transportation will be met, and that the wall will continue to behave in a predictable manner.

1.4 SOIL SAMPLING AND LABORATORY TESTING

Chapter 4 presents the effects of sampling method on sample disturbance in soft Bonneville clays. To obtain samples for this work, two drilling methods, rotary wash and hollow stem auger, were used. Samples were obtained using a shelby tube sampler and two different piston samplers. Sample disturbance was evaluated using radiograph images of the specimens, and laboratory consolidation and triaxial tests.

The research performed to obtain the results given in this chapter was completed primarily by Jon C. Hagen and Todd M. Colocino. Hagen has submitted a thesis containing the full results of his study, given in Hagen (2001). A report has also been submitted to the Utah Department of Transportation (Bay et al., 2003b, Report No. UT-03.14). Colocino has not yet submitted his final thesis, but his results have been submitted to the Utah Department of Transportation as Report No. UT-03.13 (Bay et al., 2003c). A summary of their efforts and results is given in Chapter 4.

Comparisons of piston and shelby tube samples indicate that piston samples are less disturbed than shelby tube samples. X-rays show significantly fewer fractures in piston samples than shelby tube samples. The average radius of the consolidation curves at the points of maximum past pressure was less (indicating a sharper break between reconsolidation and virgin consolidation) for the piston samples than the shelby tube samples, resulting in less uncertainty in maximum past pressure predictions.

Interestingly, there was no significant difference in maximum past pressure or $C_{c\varepsilon}$ between the piston and the shelby tube samples. This may be because the radiograph images were used to select portions of the sample to use in consolidation tests. Thus, the most disturbed portions of the samples were not tested. The piston samples also exhibited higher initial moduli (E_{50}) values than the shelby tube samples in the unconfined compression test. This is also indicative of less sample disturbance. The shape of the consolidation curves for piston samples are generally better than those of shelby tube samples with the same drilling method.

The differences in sample disturbance were not as recognizable or significant between the two drilling methods. The quantities of fractures and cracks identified in radiograph images were practically identical for the two drilling methods. The CRS tests show slightly less disturbance in the rotary wash samples than the hollow stem auger samples. The average radius of the consolidation curves at the points of maximum past pressure was somewhat lower for the rotary wash samples than the hollow stem auger samples, resulting in less uncertainty in maximum past pressure for the rotary wash samples. Again, there was no significant difference in the average maximum past pressure or $C_{c\varepsilon}$ between rotary wash and hollow stem auger samples.

Based upon this research, several recommendations can be made as to methods that should be employed in drilling and sampling to minimize the effects of sample disturbance in soft Bonneville clays. These are:

- Piston samplers along with thin-walled sampling tubes should be used rather than shelby tube samplers for obtaining specimens for consolidation, triaxial, and other critical geotechnical tests.
- Both fixed piston and free piston samplers obtain samples of similar high quality.
- Radiograph (x-ray) images of the soil specimens provide a powerful tool for assessing sample disturbance, selecting the least disturbed portions of the sample for critical tests, and identifying locations of sand lenses in Bonneville clay samples.
- Rotary wash drilling methods result in slightly less sample disturbance than hollow stem auger drilling.
- When hollow stem auger drilling is used, the auger should be advanced slowly using slow rotation (as was done in this work) to minimize disturbance to the surrounding soil.
- Sample recovery can be increased by waiting a period of several minutes after pushing a sample tube before attempting to extract the sample from the ground.

1.5 MSE WALL FINITE ELEMENT MODEL

Chapter 5 presents the results of a finite element model of the mechanically stabilized earth (MSE) wall located on I-15 at 3600 South in Salt Lake City, Utah. The model was created and calibrated using data collected at the construction site during and

after construction of the wall (as given in Chapter 3), as well as using the results of extensive laboratory testing on samples collected at the site (given in Chapter 4). Such a model is a powerful tool in understanding the behavior of a tall MSE wall on a compressible foundation. The author is responsible for the development of this model and the results of the modeling as given in this chapter.

This analytical model includes a number of soil models to represent the range of soils in the foundation of the wall, as well as additional soil models to represent the fill material used for the original I-15 embankment and the new material used to construct the MSE wall. Trench drains, with adjusted soil permeabilities, were used to represent the prefabricated vertical drains (PVDs) used at the site. The bar mat reinforcement used to construct the wall was also modeled, with special consideration as to the effects of soil-reinforcement interaction.

The analytical model was calibrated to match the measured long-term horizontal and vertical deflections at the wall site. Once this was accomplished, the effective permeability of the foundation soil was adjusted and the construction sequence approximated in order to match the time settlement behavior of the wall. When the model was considered to accurately represent the MSE wall for both the long- and short-term behavior, a stability analysis was performed at various stages of construction to observe the global stability of the wall throughout the construction process and in the years following construction.

For the model following the staged construction of the wall, the factor or safety for the original embankment was 1.96. This value increased slightly as the wall was built, since initially the wall acted as a berm, forcing the failure surface up the

embankment. However, once the wall was approximately halfway constructed, the failure surface was forced into the foundation material, and the factor of safety decreased to a minimum value of 1.57 at the application of the surcharge load, then increased with consolidation to a value of 1.81 for the long-term factor of safety for the MSE wall at final grade. A minimum factor of safety of 1.25 was calculated for instantaneous construction of the wall, which increased with consolidation to a value nearly identical to the long-term value obtained from the staged construction.

As determined during the external stability analysis, the failure surface has a V-shape, with total movement being downward and away from the original embankment in the backfill material and the foundation material beneath the wall backfill, and with total movement being upward and away from the wall in the foundation material outside the wall footprint. It is noteworthy that such a failure surface would NOT be predicted using traditional slope stability analyses, where a circular or spiral failure surface would be used to compute a factor of safety. Thus, for this case, it appears that a traditional slope stability approach would not be conservative. This is a key reason for using a finite element program to perform slope stability (or other stability) evaluations instead of the more traditional software packages that may be limited to circular or spiral failure surfaces.

A comparison is given to show the difference between a stability analysis using traditional, commercially available software and the Plaxis analysis performed for this research. The differences were found to be significant.

The effects of pore pressure dissipation during construction can be evaluated, and were taken into account during the stability analyses and in calibrating the time-

settlement behavior. The effects of excess pore pressure were significant. Substantial excess pore pressures developed during the construction process, and dissipated with time. However, the pore pressures that developed were much less than those that would occur if an immediate, undrained construction had occurred. Thus, an undrained strength approach would be quite conservative, while a drained strength approach would be unconservative. Using a soil model that accounts for the generation and dissipation of pore pressures and accounts for those excess pore pressures in performing stability analyses is of the utmost importance.

The ability to model the interaction between the soil and the reinforcement is somewhat limited, due to the limitations in the Plaxis software. However, a model was developed that overestimates the tension in the reinforcement in the lower portion of the wall while underestimating the tension in the upper portion of the wall. With this limited and simplified model of the soil-reinforcement interaction, an analysis of some additional external failure modes was performed. The modes of overturning and sliding were investigated, while internal modes relating to pull-out failure and tensile failure of the reinforcement were not considered. These additional analyses resulted in a factor of safety for sliding of approximately 1.9 and a factor of safety for overturning of approximately 2.1.

CHAPTER 2

LITERATURE REVIEW

2.1 INTRODUCTION

This chapter briefly discusses a number of concepts related both to Mechanically Stabilized Earth (MSE) Walls and Finite Element modeling. Four topics were considered to be appropriate for the purposes of this research. The first topic to be discussed is a background discussion on MSE walls. Since chapters of books, entire books, and numerous professional papers have been devoted to such structures, a full review of such literature has not been attempted. However, a general discussion relating to the most important issues concerning MSE walls will be given.

The second topic gives a review of a number of finite element analyses relating to various geotechnical structures. A number of studies have been performed on MSE walls, but several studies relating to earth-fill dams were also found to be helpful and appropriate to include in this review.

The third topic relates to the Hardening Soil Constitutive Model, which is to be used in the Plaxis model of the MSE wall located at 3600 South and I-15. This soil model is the best constitutive model for soil currently offered in existing publicly-available software packages, and was considered the most appropriate model for the wall addressed in this research project. Although the range of constitutive models used in the above-mentioned Finite Element studies varied from quite simple to exceptionally complex, the Plaxis model was determined to adequately replicate the soil behavior at the site while using a relatively small number of input parameters.

The final topic to be addressed is a discussion of soil-reinforcement interaction. It is difficult to model a three-dimensional problem such as this with a two-dimensional finite element model. Previous work explains some of the simplifications that must be made and discusses some of the appropriate modeling methods to replicate, as accurately as possible, the complex soil-reinforcement interaction.

2.2 MECHANICALLY STABILIZED EARTH WALLS

Many books, chapters of books, and professional journal papers have addressed the theory, design, and response of Mechanically Stabilized Earth (MSE) Walls. A number of symposia have been devoted to relating information obtained from MSE wall studies since such methods of earth reinforcement were first developed. Studies began in Europe in the middle of the 1960s when Henry Vidal developed and patented a technique referred to as "Reinforced Earth" (Vidal, 1969), while at the same time in Japan laboratory tests were being performed to study reinforcement techniques to allow more efficient construction on the widespread soft foundations common in the area (Yamanouchi et al., 1988).

Literally decades later, the progression of technique, application, and studies relating to such walls and such reinforcement has been enormous. Soil reinforcement has been applied to such projects as traditional embankments, foundations on soft soils, pavement support, and earth dams (Koga et al., 1988). The reinforcement used for such projects includes, but is not limited to, geotextiles, geogrids, steel meshes, and steel strips (Mylleville and Rowe, 1988).

The initial idea of steel strip reinforcement, as proposed by Vidal, required backfill material of very high quality in order to obtain the high friction required for the reinforcement to be effective and have sufficient pullout resistance. The development of steel grids (also referred to as bar mats) with longitudinal and transverse bars allowed a lower-quality backfill to be used while maintaining the necessary pullout resistance (Chang et al., 1977).

Additional progress was made when synthetic materials such as polymer grids were introduced as reinforcement. Such materials were not subject to corrosion, as the steel reinforcement had been, and could be produced to have sufficient tensile strength to be applied in constructing substantial walls (Bergado et al., 1992). Later, polymer geotextiles were introduced as adequate alternatives to steel reinforcement for a number of applications (Bergado et al., 1992).

Design specifications have been developed by agencies such as the Federal Highway Administration (FHWA) of the U.S. Department of Transportation (FHWA, 2001) in order to ensure adequate design of MSE wall projects. Fig. 2.1 shows a figure given by FHWA (2001) that shows the terminology given relating to MSE wall structures.

Design of a wall starts by first considering the geometry of an original ground surface or an existing embankment. Some excavation may be necessary before construction of the MSE wall can begin. At this point, lifts of reinforcement and soil are placed to construct the wall to the desired height. A single-stage or two-stage facing may be used. In some cases, the foundation soil may be weak enough that staged construction must be used in order to prevent stability problems from occurring.

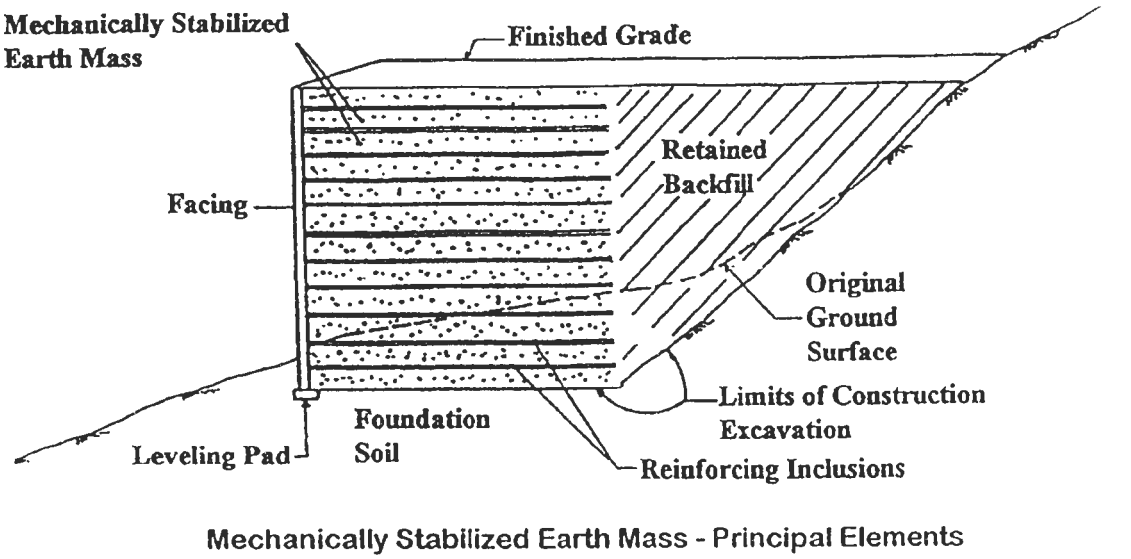

Fig. 2.1 Cross section of MSE wall structure (after FHWA, 2001)

A schematic of the type of MSE wall evaluated for this research project was given in Chapter 1. It has been repeated as Fig. 2.2 for further discussion.

This schematic shows the critical elements involved with MSE walls. Some type of reinforcement must be used to provide the necessary tensile strength to allow a vertical (or near-vertical) face to be constructed. Again, the number of types of reinforcement that have been used on various projects is growing significantly. For the purposes of this research, the focus will be on steel bar mat reinforcement, since welded-wire steel bar mats were used throughout the I-15 reconstruction project.

The longitudinal reinforcement is connected to the fascia material (in this case, the primary fascia mats), which would later be connected to the second stage concrete fascia panels. Specifications relating to the amount of reinforcement, the spacing of the reinforcement, the parameters of the soil backfill, etc. are determined in the design stage of a given project. Design specifications are addressed in FHWA (2001). Work on this

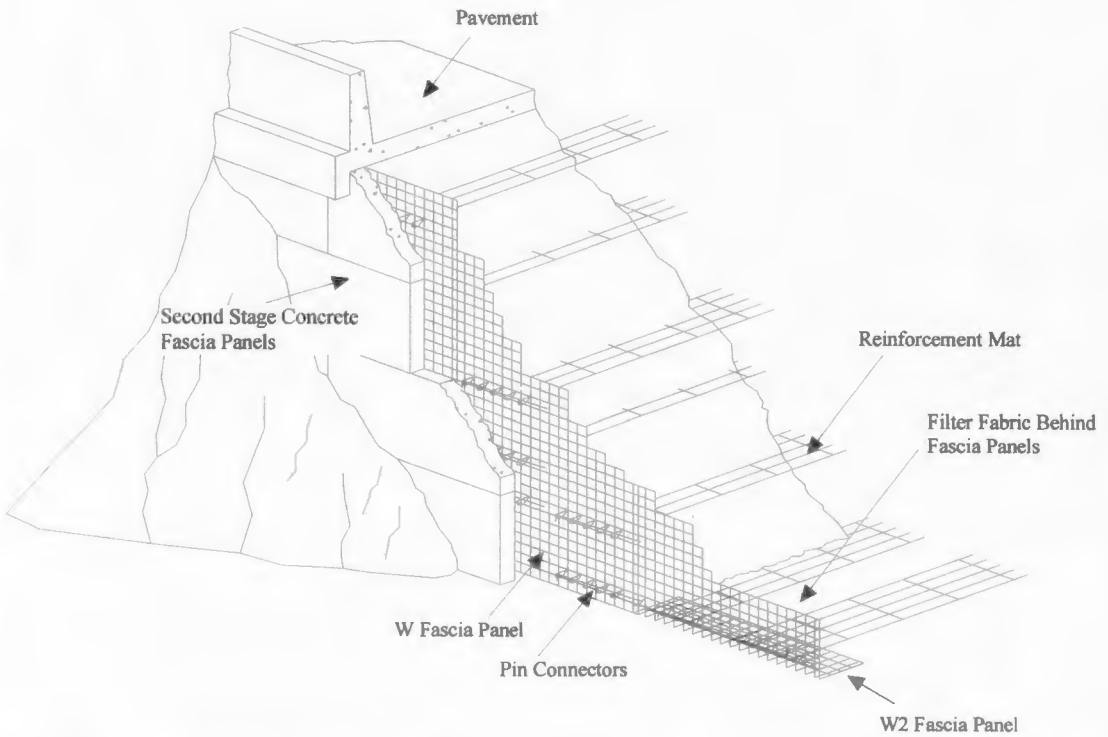

Fig. 2.2 Schematic of a typical MSE wall system used on the I-15 reconstruction project

project and previous studies at Utah State University have noted several limitations in the FHWA design guidelines, and some positive changes have been made in past years. However, especially when considering bar mat reinforced walls, the design guidelines to date are still quite conservative in some aspects. It is not the intent of this literature review to encompass the entire design process, but a more in-depth review of this process can be found in Goodsell (2000).

A number of studies have been performed during the history of such projects to evaluate the response of the walls during and after construction. Two such studies will be mentioned here, which were considered to be the most relevant with respect to this project.

The first study was a more experimental and theoretical evaluation of MSE walls, with the intent of coming up with a suitable design method for such structures (Laba and Kennedy, 1986). This study evaluated the maximum tensile forces mobilized in a reinforced earth retaining wall. The design method proposed determines the magnitude of the maximum tensile force for the reinforcement as a function of the height of the backfill. The method accounts for stress transfer internally, such that overstressed regions of reinforcement are able to transfer stresses to adjacent regions that have not achieved full frictional or strength capacity. No full-scale wall was compared, but the results of the study compared well with the results obtained from model tests performed.

The second study compares very well to this study. Cadden and Harris (1998) presented the instrumentation plan of a 28 ft high MSE wall in Richmond, Virginia. Test borings, piezometers, and inclinometers provided for the collection of field data for the wall, while triaxial tests were performed on soil samples obtained at the site to determine soil parameters. The piezometers evaluated pore pressures during and after construction of the MSE wall. Similar instrumentation was used on the I-15 wall to provide wall response measurements throughout the construction process and following construction of the wall.

2.3 FINITE ELEMENT ANALYSIS OF GEOTECHNICAL STRUCTURES

With the increased popularity of both MSE walls and Finite Element Analysis methods, it should be no surprise that a number of studies have been performed that evaluate MSE structures using the finite element method. This analysis tool is not

limited to MSE walls, however. The applicability of other studies relating to other geotechnical structures with respect to MSE walls will also be presented.

The finite element method was first applied to geotechnical engineering in the 1960s (Bergado et al., 1992). This method was very useful since it can accommodate such difficulties as nonhomogeneous materials, nonlinear stress-strain behavior, complicated boundary conditions, and other complex considerations. Reinforced soil walls have been considered in such research as Hermann (1978), Schaefer and Duncan (1988), Hird and Kwok (1989), and Adib et al. (1990).

In these projects, the constitutive model used to model the soil varied from a simple elastic material, to elastic perfectly-plastic, to nonlinear hyperbolic, to modified Cam clay models (Bergado et al., 1992). It must be remembered that the accuracy of the results obtained from a finite element analysis depends on the use of appropriate material properties (Koga et al., 1988).

Studies such as Mylleville and Rowe (1988) seem to do a reasonable job in predicting the expected failure mechanism for a mechanically stablized earth structure that uses steel strips for reinforcement and is constructed on a soft foundation. Fig. 2.3 shows an example of the results obtained in this study.

Finite element analysis is not only appropriate for modeling an entire MSE wall, but may also be used in examining individual elements in such structures. Bergado et al. (1996) uses a finite element approach to examine pullout resistance of the reinforcement. Such a procedure can be used to evaluate and replicate the soil-reinforcement interaction, as much as possible, and is less time-consuming that attempting to model the entire structure at once.

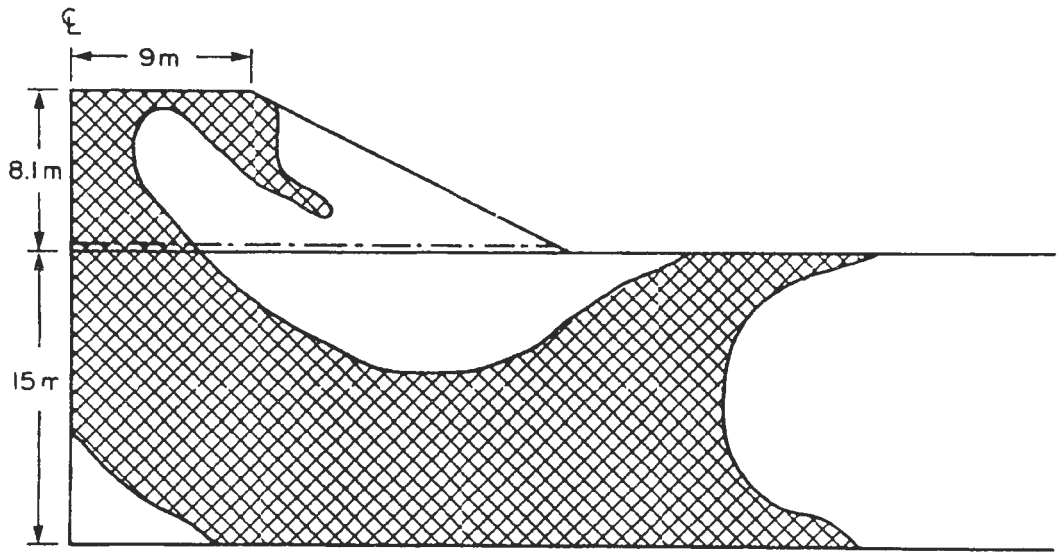

Fig. 2.3 Plastic region developing in Mylleville and Rowe (1988) study

A number of additional sources were reviewed that dealt with finite element studies of mechanically stabilized earth wall. This list includes Abdi et al. (1994), which presents source code (or the results thereof) that calculates the critical height of a soil wall for given foundation conditions. Also included are two references by Siddharthan et al. (2004a and 2004b), which evaluate the seismic deformation of mechanically stabilized earth walls that have been reinforced with bar mats. These sources presents the findings of six MSE walls that were subjected to a range of base excitations using a centrifuge at the University of California at Davis. The walls behaved very well, with no catastrophic failure observed in any of the walls for the range of accelerations to which the walls were subjected. A third investigation (Leshchinsky and Vulova, 2001) used a numerical approach to investigate the effects of geosynthetic spacing on failure mechanisms in MSE walls. The effects of reinforcement spacing, backfill strength, foundation strength,

reinforcement stiffness, interface strength, and intermediate reinforcement layers were analyzed , and the results of the study were presented.

Several additional investigations were researched that relate to other geotechnical structures. These included both dry embankments and earth dams, where the slope stability was investigated. These sources include Zhang (1999), Kiousis et al. (1986), Lechman and Griffiths (2000), and Ishii and Suzuki (1987).

2.4 HARDENING SOIL CONSTITUTIVE MODEL

Much effort was spent in examining the details of the hardening soil model, as applied in Plaxis (1998). This model provides an accurate approximation of real soil behavior with a reasonable number of parameters. The parameters allow for stress dependent stiffness, which most soil models do not. Having this capability allows fewer soil layers to closely approximate soil stiffness with depth, where other models would require a given soil layer to have a fixed stiffness that is independent of stress conditions. This capability is one of the real strengths of this soil model.

The hardening soil model accounts for both the plastic straining due to deviatoric loading (using parameter E_{50}^{ref}) and the plastic straining due to primary compression (using parameter E_{oed}^{ref}), separating the two by using two values of moduli. A third modulus (parameter E_{ur}^{ref}) value allows for elastic unloading and reloading of the soil. Failure of the soil occurs according to the Mohr-Coulomb model, which uses the traditional parameters (Plaxis, 1998). Additional explanation of the details regarding the hardening soil model can be found in Chapter 6.

2.5 SOIL-REINFORCEMENT INTERACTION

The effects of soil-reinforcement interaction were found to be a key factor during the course of this research. The Plaxis model is somewhat limited with respect to modeling the behavior of the soil-reinforcement interface. A number of studies have been performed to evaluate the interface strength associated with MSE walls.

Bergado et al. (1996) has a good discussion of the mechanisms governing soil-reinforcement interaction. Three mechanisms are mentioned that dictate the interaction between the soil and the reinforcement. The mobilization of frictional resistance along the longitudinal members, the passive bearing resistance of the soil on transverse members, and the bending moment in the reinforcement all contribute to some extent to the interaction. The bending moment influence was deemed to be minimal, and can be ignored for the most part (Bergado et al., 1996).

Pullout tests can be performed to evaluate the soil-reinforcement interaction. A number studies related to such tests have been performed over the years, adjusting one or two parameters in order to determine the effects of various factors on the interaction. An in-depth look at such pullout tests was not done as a part of this section, the focus of which is to deal more with the interface elements to be used in the Plaxis model.

Koga et al. (1988) use what are referred to as joint elements to represent the interface behavior between the reinforcement and the wall backfill. No additional details are given as to the features associated with these elements.

Long et al. (1997) gives a more detailed study of interface elements. In this study, an evaluation of the interface factor with respect to wall height is performed. As with Plaxis (1998), the interface factor for Long et al. (1997) was defined to be the strength

reduction factor for a given interface. The strength of the interface will be dictated by the soil cohesion (c) multiplied by this factor and the tangent of the soil friction angle [tan(ϕ)] also multiplied by this factor. The range of values back-calculated by Long et al. (1997) varied from about 0.72 to 0.92, depending on the type of backfill used and the effective stress (a function of position within the wall) at the interface.

The Plaxis manual (1998) recommends a strength reduction factor (R_{inter}) of 0.67 for a sand-steel contact and a factor of 0.50 for a clay-steel contact. Since for real soil-structure interaction the interface is weaker and more flexible than the associated soil layer, a value greater than 1.0 is not recommended (Plaxis, 1998).

CHAPTER 3

MECHANICALLY STABILIZED EARTH WALL INSTRUMENTATION BACKGROUND AND MONITORING

3.1 INTRODUCTION

This chapter presents the instrumentation for and the measurements obtained from a mechanically stabilized earth (MSE) wall located along the I-15 reconstruction project in Salt Lake City, Utah. The wall is on the west side of I-15 at approximately 3600 South. The final wall height is approximately 30 ft (9.1 m). However, surcharge placed during construction made the maximum height of the wall approximately 36 ft (11.0 m). Prefabricated vertical drains (PVDs) were used in the foundation soil within the right of way to speed primary consolidation of the soft clay soil foundation. Surcharging was used to minimize secondary consolidation following the completion of the wall. The extent of the PVDs, the stratigraphy of the foundation material, and the configuration of foundation instrumentation are shown in Fig. 3.1.

Due to the significant consolidation anticipated as a result of the soft clay foundation material, a two-stage MSE wall system was designed for this project. A one-stage MSE wall with an integral face was not expected to perform well, since the significant movement expected during and after the construction process would create problems in appearance and could possibly affect the structural integrity of the wall. The two-stage system utilizes bar mat fascia panels as the first-stage face. After primary consolidation of the foundation material has taken place, the second-stage precast concrete fascia panels were connected to the bar mat fascia panels using a system of rods

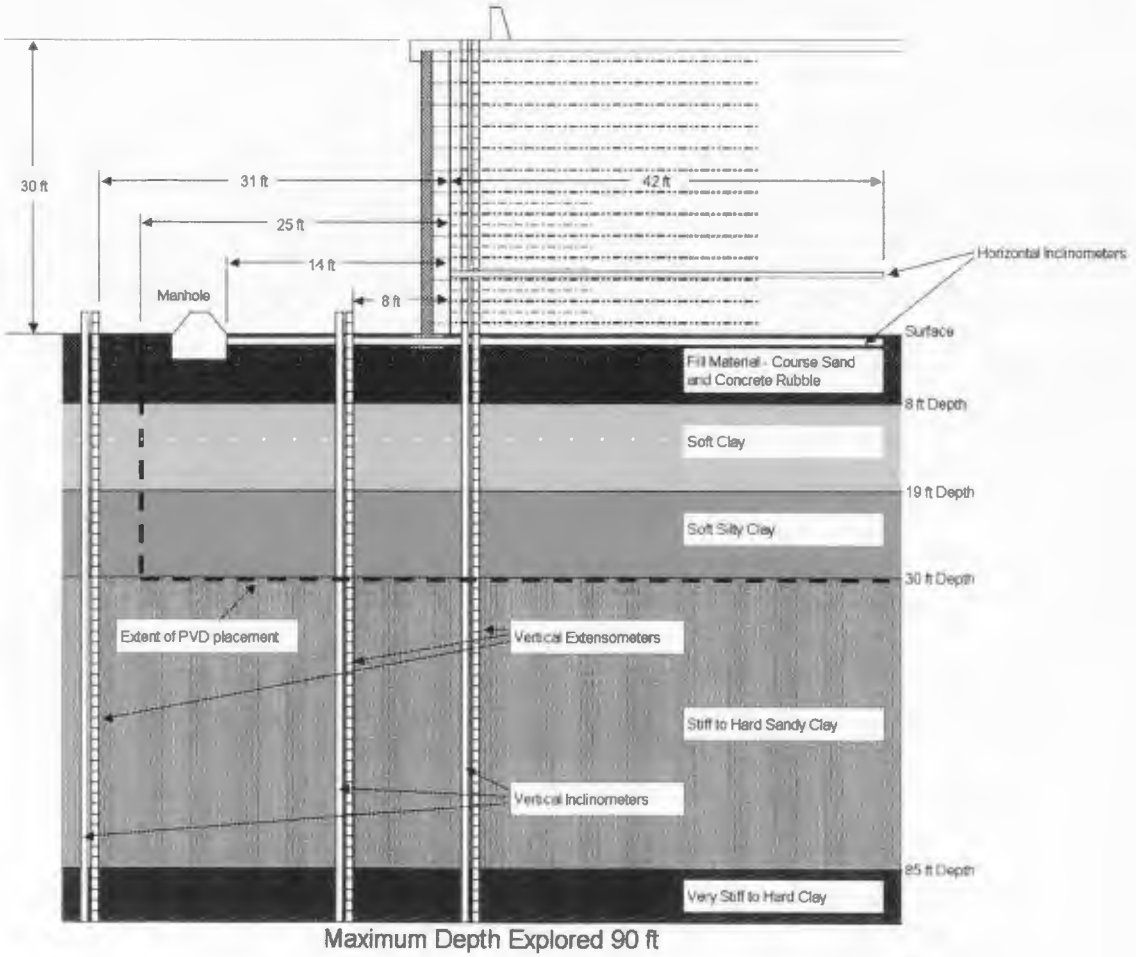

Fig. 3.1 Elevation of wall and foundation showing foundation instrumentation

and turnbuckles, allowing both the structural integrity and the aesthetic appearance of the wall to remain intact. The two-stage system used on this project is shown in Fig. 3.2.

The two-stage MSE wall system developed for this project was designed by the VSL Corporation (Bay et al., 2003a, Report UT-03.11). The design utilized welded-wire reinforcing bar mats. These bar mats varied in width from 1.5 ft (0.46 m) to 2.5 ft (0.76 m). The center-to-center spacing of the mats was 5.5 ft (1.7 m), leaving gaps between consecutive bar mats from 3 ft (0.9 m) to 4 ft (1.2 m). The primary bar mats consisted of

24 ft (7.3 m) long longitudinal wires spaced at 6 in. (152 mm) welded to transverse bars spaced at 12 in. (305 mm) or 24 in. (610 mm), depending on the position of the reinforcement within the wall. The number of longitudinal wires varied from 4 to 6, again depending on the position of the reinforcement within the wall. The bar mat vertical spacing was 30 in. (762 mm). The first-stage bar mat fascia panels consisted of longitudinal and transverse wires spaced at 6 in. (152 mm), with a geofabric beneath the fascia panels.

MSE walls on soft clay foundations are typically subjected to significant deformations. Similar walls built earlier at other locations on this same project had experienced more than 3 ft (0.9 m) of settlement (Bay et al., 2003a, Report UT-03.11). One significant benefit of two-stage walls is their ability to withstand such significant settlement without problems. However, some of the walls on this project had exhibited large deformations such as bulging, sagging, and negative batter of the wall face, which led to some concern. It was not apparent whether these deformations were associated with overstressing of the wall or whether they were merely localized deformations near the face of the wall. Excessive bulging of the wall face, especially at the toe of the wall, was an additional concern since it was causing problems with the constructibility of the second stage of the wall. Also, some toe bulges were large enough that the welds in the fascia panels were breaking, causing concern about the structural stability. Photographs showing toe bulging are shown in Fig. 3.3.

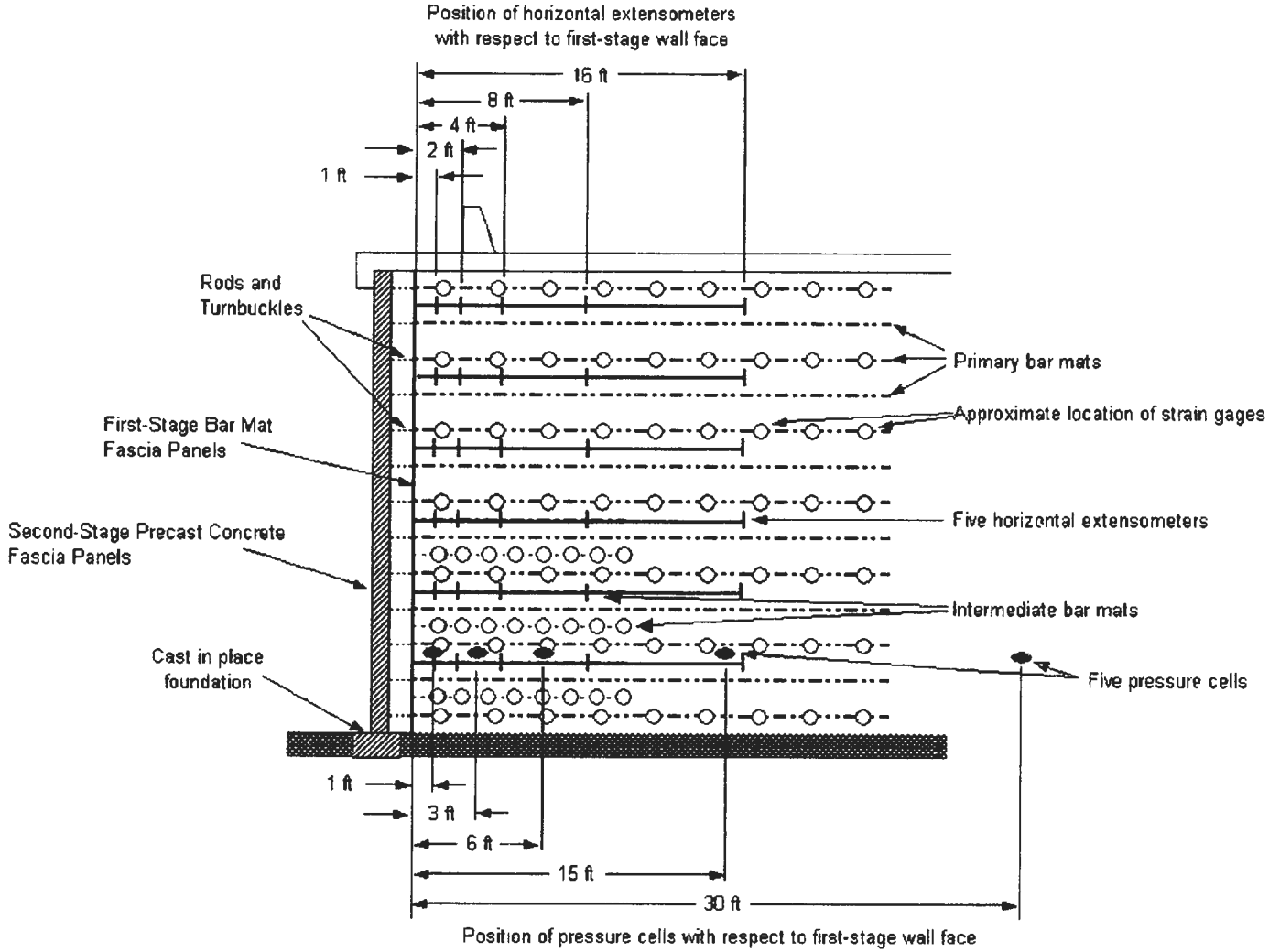

Fig. 3.2 Elevation of MSE wall showing reinforcement, first-stage and second-stage faces, and instrumentation

Fig. 3.3 Photographs showing deformations and toe bulges of first-stage wall face during construction

Because of the concerns described above, a revised design was implemented. This design change added an additional layer of reinforcement between the primary layers of reinforcement in the lower portion of the walls, where the bulging had been most significant. These additional reinforcement mats, referred to as intermediate bar mats, were composed of four 10 ft (3.0 m) long longitudinal wires spaced at 6 in. (152 mm), with transverse wires spaced at 12 in. (305 mm). The center-to-center spacing between consecutive intermediate mats was again 5.5 ft (1.7 m), the same as the spacing between consecutive primary bar mats. These intermediate bar mats were placed between the primary bar mats, so the vertical spacing between successive bar mats was decreased to 15 in. (381 mm) in the bottom portion of the walls

For the wall observed during the course of this project, the majority of the wall was constructed according to the revised design. However, a small section was constructed according to the original wall design in order to make a comparison of the behavior of the two designs. Throughout this dissertation the initial design is referred to as the primary reinforced only section, and the revised design is referred to as the primary and intermediate reinforced section.

Instrumentation was designed to measure the internal stresses, internal deformations, and external deformations to which the wall was subjected. As mentioned in Chapter 1, Mark W. Goodsell was primarily responsible for developing the instrumentation plan and obtaining the initial measurements during construction of the wall. Several undergraduate students assisted Mark with this work. A complete version of this instrumentation plan and the measured wall response during construction may be found in Goodsell (2000) and Bay et al. (2003a, Report UT-03.11).

Instrumentation was placed in a portion of the wall containing each of the reinforcement designs in order to measure the internal stresses and deformations associated with each design, so as to provide a comparison of the behavior of the two designs. Instrumentation was also placed in the foundation soils both inside and outside the wall footprint in order to monitor the external deformations of the wall. The measurements obtained from the instrumentation provided information as to the internal and external stability of the wall.

This chapter presents those measurements made during the construction of the wall and during the first three years following wall construction. The steps taken to protect the instrumentation for long-term monitoring are given, and a number of challenges that were overcome are explained. Conclusions relating to the internal stability of the wall, the internal stresses within the wall, internal deformations within the wall, and external wall displacements are given. Also presented are conclusions relating to the comparison of sections of the wall containing the initial reinforcement design and the revised reinforcement design.

3.2 MECHANICALLY STABILIZED EARTH WALL INSTRUMENTATION

3.2.1 Instrumentation to Measure Stresses

3.2.1.1 Strain Gages on Longitudinal Reinforcement Bars. Reinforcement for this MSE wall consists of 13 layers of primary bar mats, as shown in Fig. 3.2. Seven of the 13 layers were instrumented with strain gages, such that every other mat was instrumented. For each instrumented layer, 13 or 14 strain gage points were chosen for

the primary reinforcement bar mats. Over 400 strain gages were placed on the longitudinal bars of the bar mats to measure the increase in strain throughout construction of the wall. The layers of reinforcement that were instrumented and the approximate location of the strain gages for these layers are shown in Fig. 3.2. Fig. 3.4 shows the reinforcement bar mats located at the base of the wall (level 1) with the strain gage configuration.

Each bar mat had a different strain gage configuration depending on the locus of maximum tension, such that as many gages as possible were placed near the anticipated locus of maximum tension. Gage redundancy was also used in such sections, such that if a gage became nonfunctional, data would still be available from another gage at a similar position. Plan views for each of the instrumented mats showing each of the strain gage positions are shown in the Bay et al. (2003a, Report No. UT-03.11) and in Goodsell (2000). For both the primary only and the primary and intermediate reinforced sections of the wall, the primary bar mats have the same strain gage configuration at each level. Fig. 3.5 shows a photograph showing one of the instrumented bar mats during construction of the wall.

For the intermediate mats three of the six layers were instrumented with strain gages. For each intermediate instrumented layer, six to seven strain gage points were chosen. Fig. 3.6 gives a plan view description of the gage configuration of the intermediate bar mat located 1.25 ft (0.38 m) from the base of the wall. The strain gage positions for the two additional instrumented intermediate mats are shown in Bay et al. (2003a, Report No. UT-03.11) and in Goodsell (2000).

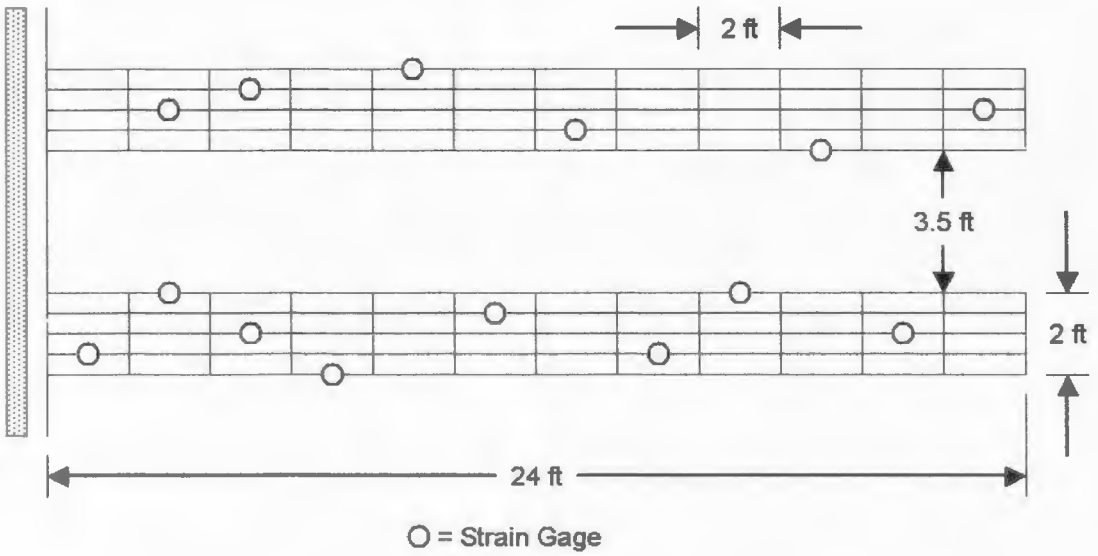

Fig. 3.4 Plan view of instrumented primary bar mats at base of wall

Fig. 3.5 Photograph showing an instrumented bar mat during construction

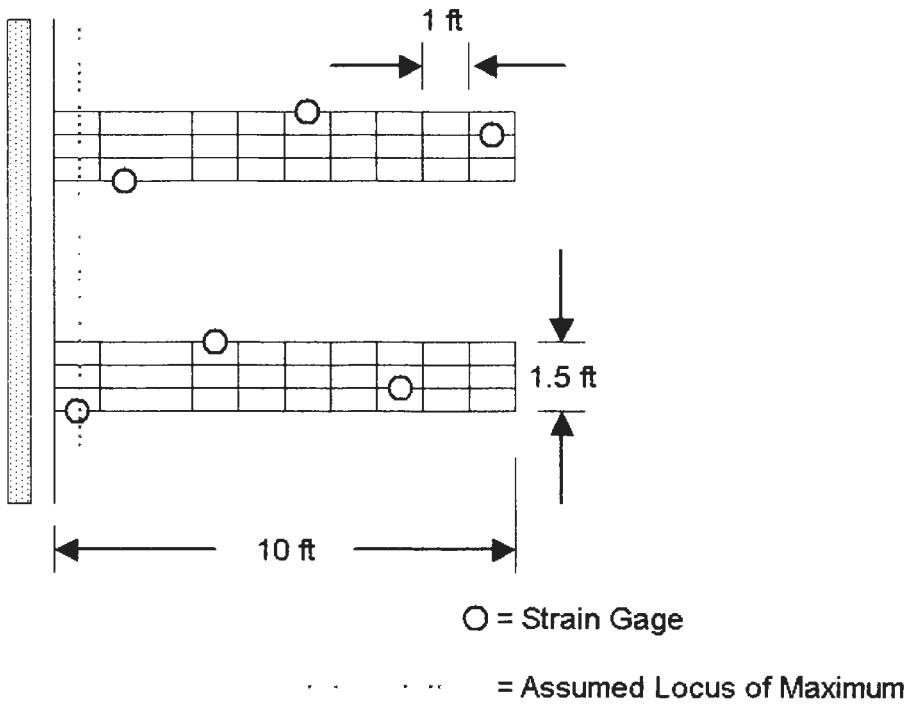

Fig. 3.6 Plan view of instrumented intermediate bar mats 1.5 ft from base of wall

For the primary and intermediate bar mats, each instrumentation point consists of two strain gages that are glued opposite each other on the top and bottom of the longitudinal bars. The gages for each instrumentation point were wired individually. However, the top and bottom gages were read in a full bridge format that causes bending stresses in the bar mats to cancel, thereby measuring the axial tension. In the event that either the top or bottom gage became damaged the good gage was read in a half-bridge configuration. The bridge was completed in the multiplexer. A total of three different readings were required for each instrumentation point: a full bridge reading, a half bridge reading using the top strain gage, and a half bridge reading using the bottom strain gage.

The gages used are manufactured by Micro-Measurements, Inc. and are of the type EA-06-125M-120. The gages are arranged such that a single matrix has two foil elements oriented perpendicular to one another. One of these elements measures the axial strain, while the other is used to monitor Poisson's effects. Such a dual gage provides for two specific benefits. First, having two gages in essentially the same position allows for temperature compensation to be made. Second, such gages have a higher sensitivity than those containing only a single element.

One major disadvantage of the dual gage system is that the gages are less robust than other types of gages. During the course of construction, a substantial percentage of the strain gages became nonfunctional. Of the 215 gages initially placed on the longitudinal reinforcement, for example, only 96 gages were providing reasonable data at the end of construction, and additional gages have lost function since that time. It is possible that a more robust gage would have been more successful in surviving the rigors of the construction process. For future projects of a similar nature, it is recommended that a more robust strain gage be used to monitor tension in the reinforcement.

3.2.1.2 Pressure Plates. To measure the overburden pressure within the wall, five 9 inch (228.6 mm) diameter SINCO vibrating wire total pressure cells were installed at a fill height of about 6 ft (1.83 m). The position of these pressure plates is shown in Fig. 3.2. Fig. 3.7 shows the pressure cell located 30 ft (9.14 m) from the face prior to burial.

Fig. 3.7 Photograph showing an installed total pressure cell before burial

3.2.2 Instrumentation to Measure Deformations

3.2.2.1 Vertical Inclinometers. To measure horizontal movement within the walls soft foundation soils, three vertical slope inclinometers were installed to a depth of 90 ft (27.4 m) in order to penetrate the soft clay deposits. The vertical inclinometers were installed in a linear array shown in Fig. 3.8. Fig. 3.1 gives an elevation view of the vertical inclinometers as they are positioned within the wall and subsurface soils. The inclinometers are identified as I1 (located 3 ft (0.91 m) within the wall footprint), I2 (located 8 ft (2.4 m) outside the wall footprint), and I3 (located 31 ft (9.4 m) outside the wall footprint).

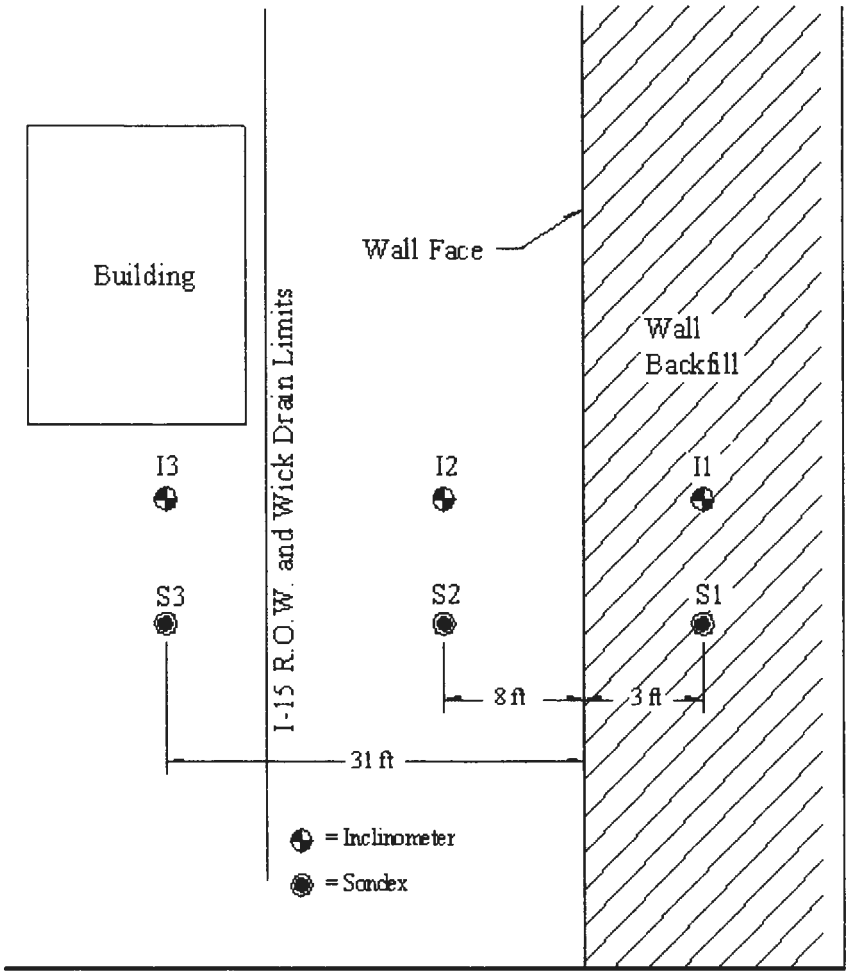

Fig. 3.8 Plan view of vertical inclinometers, I1, I2, and I3

Inclinometer No. 1 (I1) was installed inside the wall footprint and is inside the wick drain boundary zone. Inclinometer No. 2 (I2) was installed 8 ft (2.44 m) away from the bar mat fascia face of the wall and it is also located within the wick drain boundary zone. Inclinometer No. 3 (I3) was installed 31 ft (9.45 m) away from the face of the wall and it is located about 9 ft (2.74 m) outside the wick boundary zone. Since I1 was installed within the footprint of the wall, inclinometer casing was added as the wall fill height increased.

3.2.2.2 Horizontal Inclinometers. Two 3.75 inch (95.25 mm) diameter horizontal inclinometers were installed in the foundation of the wall and within the wall fill. Horizontal inclinometer H1 is located near the base of the wall and requires a manhole for access. It extends 52 ft (15.8 m) through the foundation fill material. Fig. 3.9 shows a reading being taken on H1 from inside the manhole. Horizontal inclinometer H2 is located within the wall fill, originates at the wall face as shown by Fig. 3.1 and Fig. 3.10, and extends 42 ft (12.8 m) into the wall fill. Installation of these horizontal inclinometers was done with the assistance of Terracon, a geotechnical engineering consulting firm.

Fig. 3.9 Photograph showing the inside of the manhole where horizontal inclinometer No.1 (H1) is located

Fig. 3.10 Photograph of horizontal inclinometer No. 2 (H2)

3.2.2.3 Horizontal Extensometers. Measurement of horizontal movement at various locations within the wall fill was done with 60 horizontal extensometers. These extensometers vary in length and identify any movement that may exist at their respective distances back into the wall as shown in Fig. 3.11. The lengths of the extensometers are 1 ft, 2 ft, 4 ft, 8 ft, and 16 ft (305 mm, 610 mm, 1.22 m, 2.44 m, and 4.88 m., respectively). These extensometers were built in the lab at Utah State University and consist of 0.5 inch (12.7 mm) schedule 40 PVC pipe and a 0.187 inch (4.75 mm) steel rod illustrated in Fig. 3.12. A hook was bent in the steel bar at one end so a plumb bob could be hung to measure any horizontal movement. At the opposite end of the steel bar a small piece of steel bar was welded perpendicular to the main isolated steel bar. Before welding, the main piece of steel bar was threaded through the PVC pipe and capped with

0.5 inch (12.7 mm) PVC end caps to prevent soil from entering the pipe. Fig. 3.13 is a photograph showing the horizontal extensometers protruding out of the face of the wall.

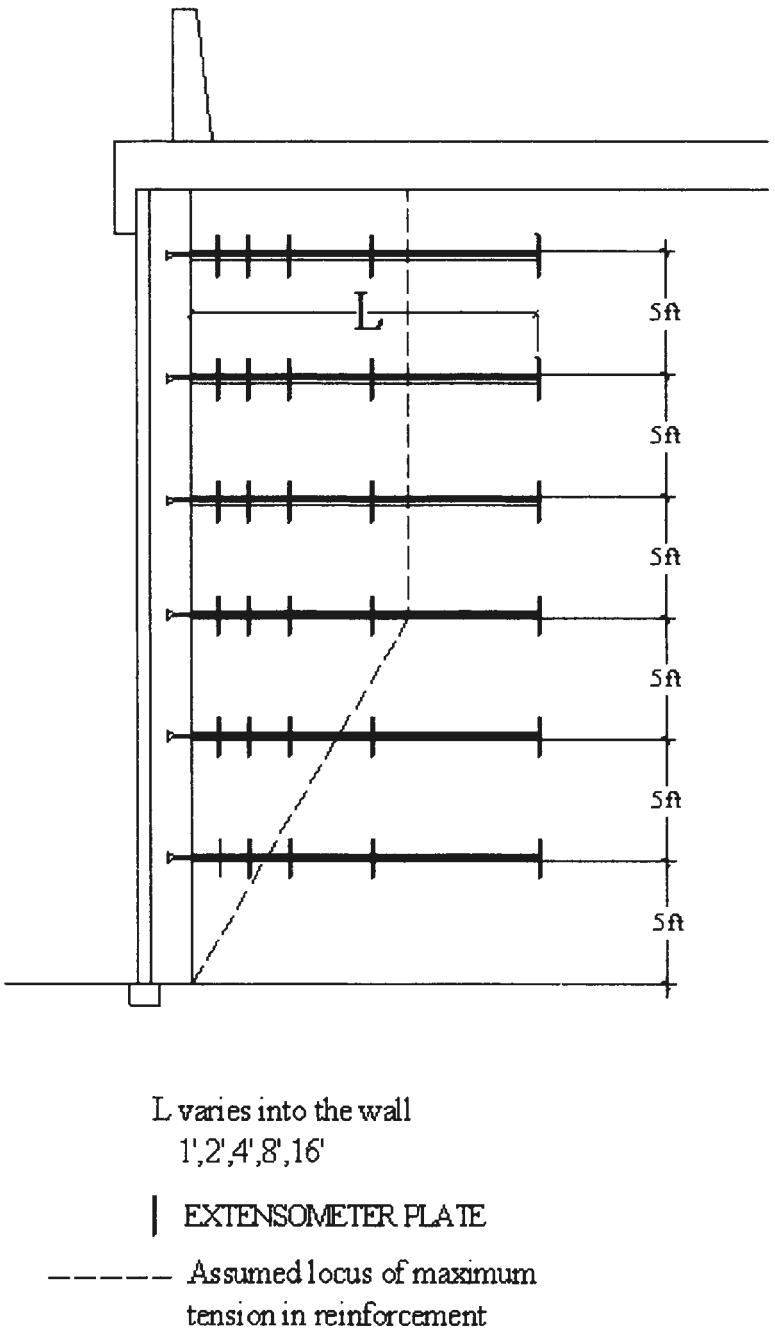

Fig. 3.11 Elevation view of the instrumented section with horizontal extensometers

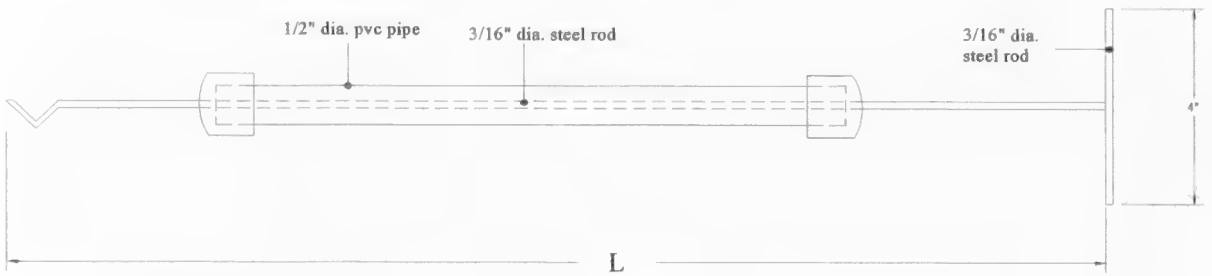

L varies 1',2',4',8',16'

Fig. 3.12 Plan view showing the design of a horizontal extensometer

Fig. 3.13 Photograph showing horizontal extensometers protruding from wall face

3.2.2.4 Sondex Settlement System Vertical Extensometers. The Sondex Settlement System was used to monitor total settlement and the depths at which incremental settlement occurs. Sondex instruments were installed adjacent to the vertical inclinometers previously shown in Fig. 4.20. The Sondex instruments are identified as S1 (located 3 ft (0.91 m) within the wall footprint), S2 (located 8 ft (2.4 m) outside the wall footprint), and S3 (located 31 ft (9.4 m) outside the wall footprint).

Sondex instruments S1 and S2 are located adjacent I1 and I2, respectively, and they are both located within the wick drain zone, which extends to the I-15 right-of-way. Sondex instrument S3 is adjacent to I3 and it is located about 9 ft (2.74 m) outside the wick drain zone.

Three Sondex settlement tubes were installed to a depth of 90 ft (27.4 m) by a truck-mounted drill as illustrated by Fig. 3.14. The Sondex settlement system involves several components: a reel with stainless steel sensing rings, corrugated pipe, and 2.75 inch (69.85 mm) SINCO casing. As shown in Fig. 3.15, the Sondex probe is lowered inside the 2.75 inch (69.85 mm) casing, which is encased by the corrugated pipe, which in turn has a number of stainless steel sensing rings that have been vertically positioned prior to installation every 3 ft (0.914 m) along the casing. In the soft foundation soils the sensing rings are fixed to the continuous length of compressible corrugated pipe, which slips along the 2.75 inch (69.85 mm) casing and allows the rings to move with the surrounding ground. These Sondex rings are allowed to move independently of one another. Installation of the Sondex Settlement System was done in accordance with suggestions given by the Slope Indicator Company (SINCO).

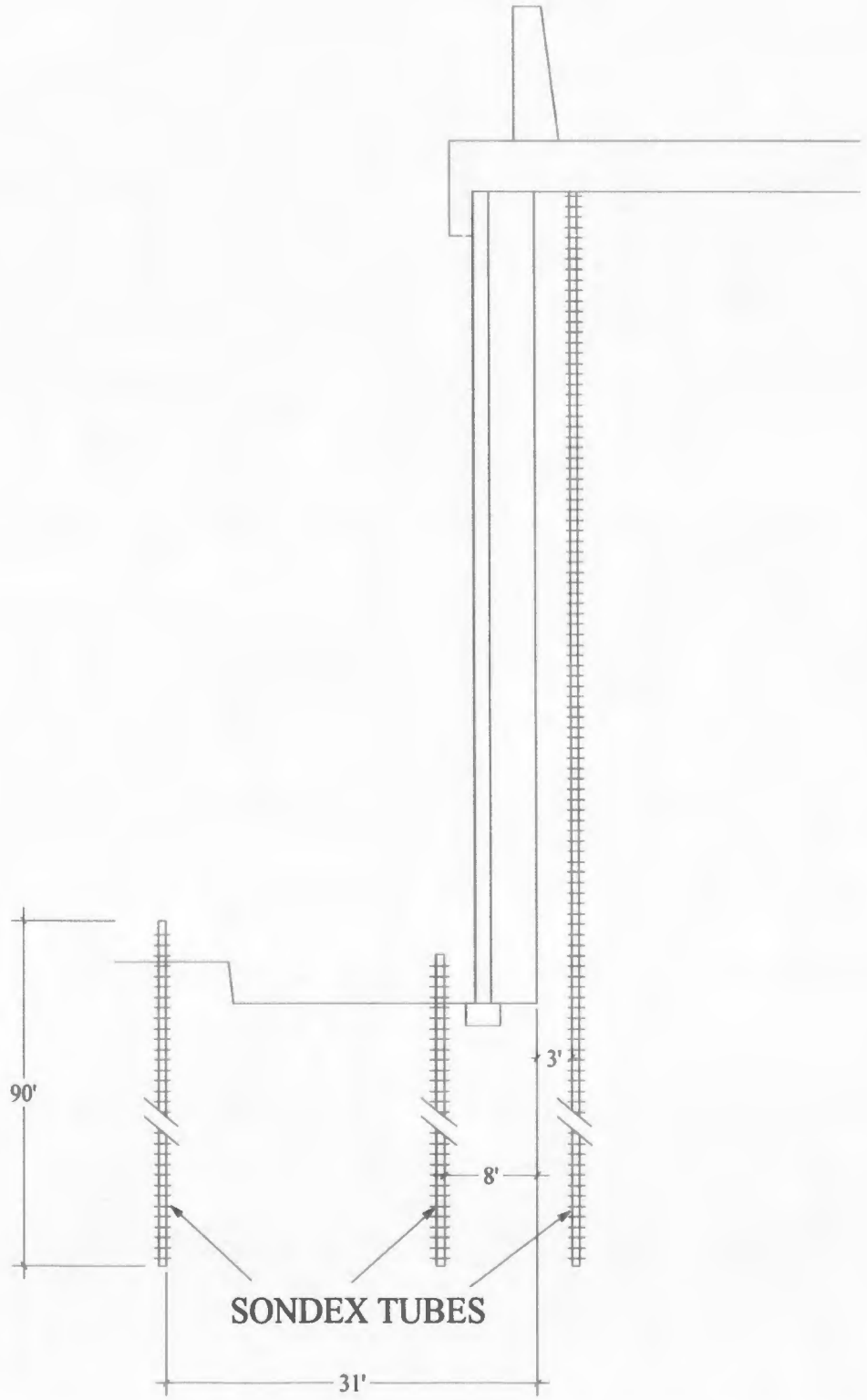

Fig. 3.14 Elevation view of the instrumented section with the Sondex tubes S1, S2, and S3

Fig. 3.15 Photographs showing Sondex sensor and readings being taken in the field

3.3 MEASURED FORCES AND PRESSURES

3.3.1 Tensile Forces in the Reinforcing Mats

Both the section of the wall containing primary reinforcement only and the section containing primary and intermediate reinforcement were determined to be internally stable, based on strain gage measurements. The strain gages placed on the bar mats measured strain throughout the construction process. These strain measurements were converted to stresses in the reinforcement, which were compared to the allowable stresses in the steel.

Fig. 3.16 presents an example of the tension distribution in the longitudinal bars for one of the bar mats located approximately 20.0 ft (6.1 m) from the base of the wall. The tension is plotted with respect to the distance from the face of the wall for a number of measurements taken throughout the construction process. As seen, the locus of maximum tension can be determined for any given bar mat, establishing the maximum tension in the reinforcement. In this case, the maximum tension in the longitudinal bars occurs approximately 13 ft (4.0 m) from the wall face for each of the measurements taken.

The maximum tension measured in the individual longitudinal bars was much less than the allowable tension to which the bars could be subjected. The minimum ratio of the allowable yield stress to the tensile stress existing in the longitudinal bars of the reinforcement is 2.5 for one strain gage position, with only four gage positions having ratios less than 5.0 (out of more than 90 functional positions). Thus, the vast majority of the bar mats are subjected to tensile forces less than 20 percent of the yield strength of the

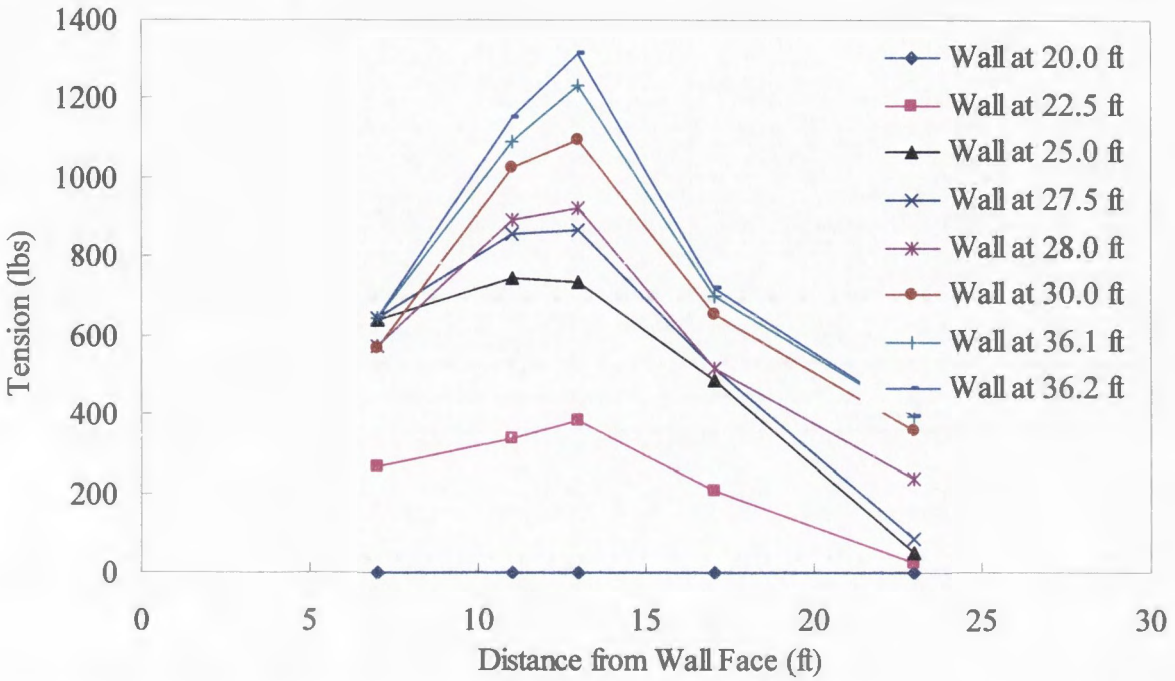

Fig. 3.16 Example of measured tension distribution in the longitudinal wires for a bar mat positioned 20.0 ft from the base of the wall in the primary and intermediate reinforced section

material. The allowable stresses used in calculating these ratios considered the entire cross section of the longitudinal bar, not taking into account corrosion of the steel over time, which decreases the cross-sectional area.

AASHTO requires MSE wall design to account for corrosion of reinforcement steel throughout the design life of the wall (AASHTO, 1998). For a 75-year design life, and allowing 16 years for loss of the galvanization, the minimum ratio of the allowable yield stress to the tensile stress existing in the longitudinal bars of the reinforcement is 2.0 for one strain gage position (out of more than 90 functional positions). Only four gages have ratios less than 4.2 after the same 75-year design life. The vast majority of the bar mats are subjected to tensile forces less than 25 percent of the yield strength of the material at the end of the design life of the wall.

A number of steps were required in order to take post-construction measurements of the forces in the reinforcing bar mats used in the construction of Wall R-346-1C. The first problem was met upon placement of the secondary stage concrete fascia panels. The cables connected to the strain gages on the bar mats were initially between the primary stage bar mat fascia panels and the concrete fascia panels, such that the cables were inaccessible. Thus, a 6-inch (152.4 mm) hole was cored in the concrete panels at each section of the wall that was instrumented to allow access to the cables. These holes are similar to the cored hole shown in Fig. 3.17, which is actually the access hole for the upper horizontal inclinometer H2.

Once the holes were cored in the concrete fascia panels and the cables pulled through, it was noted that many of the connectors had been splattered with concrete during the construction of the concrete fascia panels. After discussing the matter with a number of sources (including the Utah Department of Transportation and Intermountain Concrete Specialties), it was determined that the best method for cleaning the connectors was to soak the connectors in diesel fuel to soften the concrete, then use a brass brush to remove the concrete. This would provide minimal damage to the connector pins while allowing removal of the concrete. Several hours of work were required to clean these connectors, but the outcome was positive, with what appears to be very minimal damage to the connectors.

Once the connectors were cleaned, they were sprayed with contact cleaner to remove any remaining diesel fuel from the connectors. The fuel would have eventually volatilized, but contact cleaner was used to make sure that no trace of fuel remained.

Fig. 3.17 Hole cored in secondary stage concrete fascia panel to allow access (Inclinometer H2)

The connectors were initially labeled using a permanent marker. However, after being subject to sunlight, inclement weather, and concrete splattering during and after the construction process, the marker was beginning to fade. The connector labels were still legible, but it was decided that a more permanent label was necessary to maintain legibility for the number of years that readings would be taken. Small aluminum tags were created which were stamped with the appropriate labels and clamped to the connectors. The tags are quite permanent and inexpensive, and much more durable than the marker labels previously relied on. An example of such a tag is shown in Fig. 3.18.

Once the connectors were cleaned and labeled, they were placed in weatherproof electrical boxes that were bolted to the concrete fascia panels. Several pictures of these boxes are given in Fig. 3.19 and Fig. 3.20. Silicone was used to seal the small gap between the concrete fascia panels and the electrical boxes, such that the connectors and cables are protected from the weather. With the connectors and cables in good condition and protected from vandalism and the elements, gage readings were taken to measure forces in the bar mats.

Strain gage readings were taken in the same manner as used during construction. Data were collected and stored using the same datalogger and PC as used previously. The data were processed and analyzed using the same Excel Spreadsheet used to process the data collected during construction.

A number of the strain gages that were functioning near the end of construction are no longer functional. Also, for many of the gages that yielded readings the results were not credible, deviating from expected values by factors of anywhere from 2 to 20. Further investigation is required to determine whether there is a problem in the procedure followed in reading the gages, or whether there is an electrical or mechanical problem that is causing the inaccurate readings. The bar mat specimens used to calibrate the strain gages can be tested again to repeat the calibration process and determine whether or not the procedure is causing problems. If no problem is determined from that trial, the resistance for each of the strain gages will be checked to make sure the gages have maintained the proper resistance over time. Beyond that, there is not much that can be done to validate any readings taken in the future.

Fig. 3.18 Aluminum tags used to label the strain gage connectors

3.3.2 Lateral Earth Pressure Coefficient, K

Lateral earth pressure coefficient K-values (back-calculated from tension measurements in the bar mats) indicate that K-values currently required by AASHTO (1998) are conservative. Fig. 3.21a shows the K-values back-calculated in the wall, for the section containing primary reinforcement only throughout construction, and Fig. 3.21b shows the K-values back-calculated for the section containing primary and intermediate reinforcement throughout construction.

Fig. 3.19 Views from the north and south, respectively, showing the two electrical boxes containing strain gage cables and connectors for the two instrumented sections of wall

Fig. 3.20 Close up views of the north box containing strain gage cables and connectors

A number of the back calculated K-values shown in Fig. 3.21a appear to exceed the current AASHTO design envelope, but closer inspection shows that these values occurred in the mats near the bottom of the wall early in the construction process when horizontal stresses in the fill would have been high due to compaction stresses. The horizontal stresses in this portion of the wall are higher than the AASHTO envelope predicts. However, because the stresses are low in a short wall, these stresses do not represent overstressing of the reinforcement. The same mats show values well within the design envelope after construction progressed. It is concluded that these higher values of K can be attributed to residual compaction stresses (Mitchell and Villet, 1987), and are not of concern.

The section containing both primary and intermediate reinforcement was subjected to higher tensile stresses than the section with only primary reinforcement. This can be seen by comparing Fig. 3.21a to Fig. 3.21b, where higher K-values were calculated in the section of the wall containing the intermediate reinforcement. One possible explanation is that the section with additional reinforcement is more rigid, resulting in less internal deformation. This causes the soil conditions to be closer to the at-rest condition. The increased stresses in the soil are transferred to the reinforcement, causing the increased stresses to be observed in the section with additional reinforcement. However, even with increased stresses in this section, the reinforcement was not overstressed during any stage of construction.

Since the calculation of the lateral earth pressure coefficient K is based on tension measurements in the bar mats, and since the data collected from the strain gages on the bar mats appears to be suspect (see Section 3.3.1), no additional data has been collected

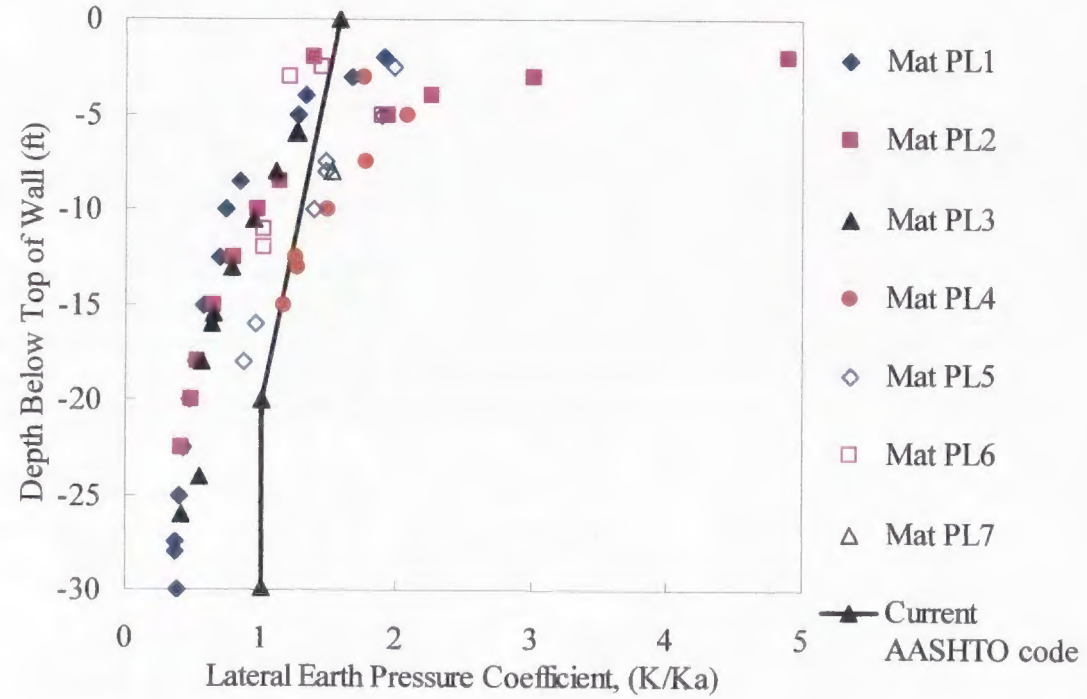

(a) Primary reinforced only section

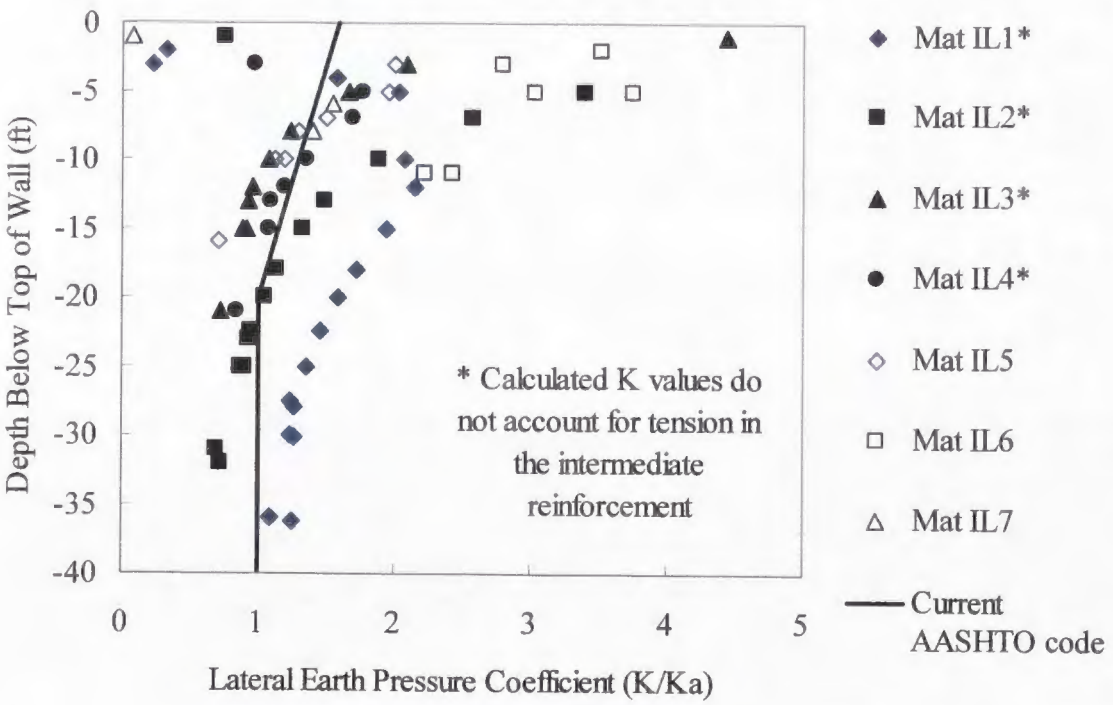

(b) Primary and intermediate reinforced section

Fig. 3.21 Normalized values of lateral earth pressure coefficient K for two sections of MSE wall

with respect to lateral earth pressure coefficient K. Until the problem in strain gage measurements can be determined and hopefully corrected, no additional data relating to K will be available.

3.3.3 Vertical Earth Pressures

Fig. 3.22 shows the maximum vertical stresses measured at the pressure plates in the wall at the time of surcharge. The vertical stress distribution followed a pattern similar to that measured in other instrumented MSE walls (Sampaco et al., 1994; Anderson et al., 1987; Sampaco, 1996), with low vertical stresses near the face of the wall, stresses increasing to a maximum value several feet (in this case, approximately 6 ft (1.83 m)) from the wall face, then decreasing to the stress expected from overburden ($\sigma_v = \gamma h$) at some distance from the wall face.

Also shown in Fig. 3.22 is the vertical stress calculated due to overburden (γh) at the time the surcharge was applied, as well as the stress calculated using the Meyerhof equation (AASHTO (1998)). This equation assumes higher toe stresses due to eccentric loading. Due to the significant wall height (36 ft (11 m) with maximum surcharge), the eccentricity is large, producing large calculated vertical stresses near the toe of the wall when using the AASHTO equation. No such large toe stresses were measured in the wall. Thus, the vertical stress distribution measured in this wall is not reflective of the design stresses required by AASHTO.

The cables connected to the pressure cells were pulled through the same hole in the concrete fascia panels as the strain gage cables in order for readings to be taken (Section 3.3.1). The vibrating wire reader provided by UDOT was again used to take the

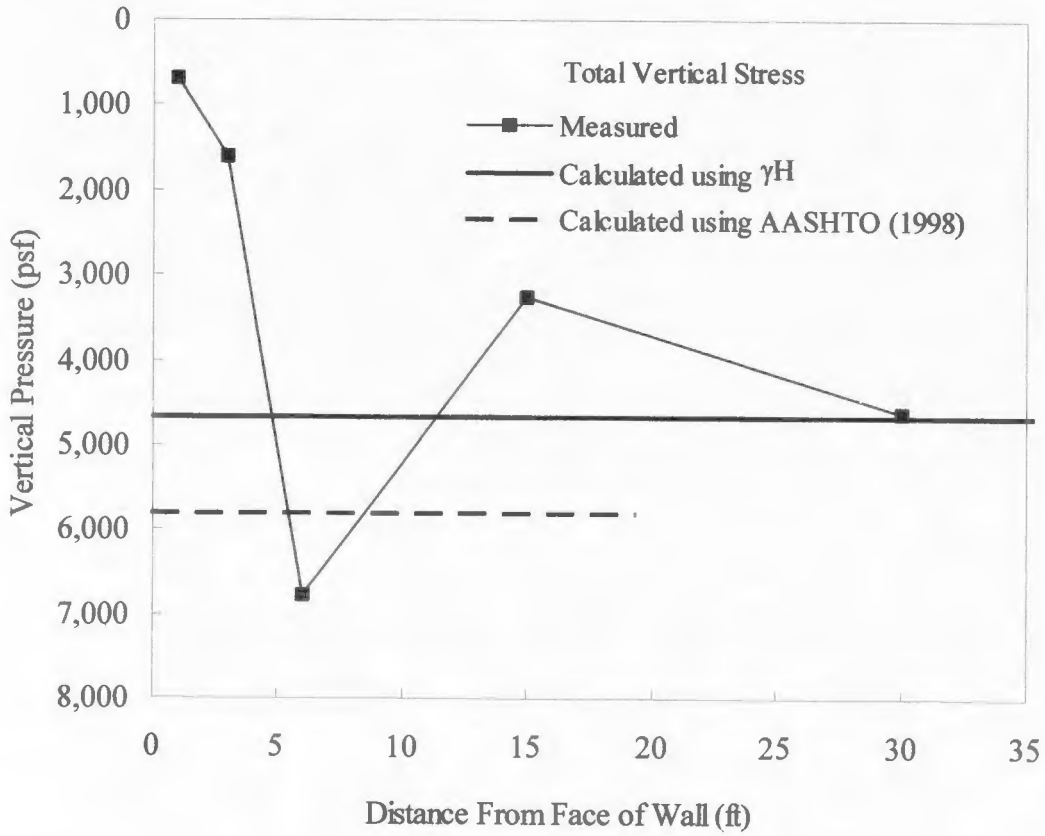

Fig. 3.22 Plot of vertical pressure versus distance from wall face during application of surcharge

post-construction readings. A vibrating wire reader acquired by Utah State University was also used to take post-construction readings, and the two sets of readings are compared in this section.

The vibrating wire reader purchased by USU does not use the same thermistor as the pressure cells contain, so independent temperature readings are not possible. However, the temperature readings taken using the vibrating wire reader provided by UDOT were used to correct the pressure readings given.

Fig. 3.23 and Fig. 3.24 show the additional readings taken from the pressure cells using the UDOT vibrating wire reader. A tabular comparison of the most recent set of pressure cell readings for the two vibrating wire readers is shown in Table 4.1.

As noted in comparing the two sets of data, the results from each vibrating wire reader were quite precise for each of the pressure plates that appear to be still functional. As also seen in the data, it appears that Pressure Plate TPC5 (located 30 ft (9.1 m) from the wall face) is no longer yielding reasonable results.

Another point to bring out is the decrease in pressure upon removal of the surcharge. As seen in the figures, a pressure decrease was present for each of the functional pressure plates from the second surcharge reading (36 ft fill height (11.0 m) above pressure plates) to the final grade readings (wall at 30 ft (9.1 m)) taken after construction.

Table 3.1 Tabular Comparison of Pressure Plate Results Using the UDOT Vibrating Wire Reader and the USU Vibrating Wire Reader

Date	02-Nov-02		02-Nov-02	
	Final Grade - UDOT		Final Grade - USU	
Pressure Plate	Pressure (psi)	Temp (deg C)	Pressure (psi)	Temp (deg C)
22 - 1 ft from wall face	2.115	10.578	2.341	10.578
23 - 3 ft from wall face	6.846	13.025	6.948	13.025
24 - 6 ft from wall face	41.621	16.791	41.904	16.791
25 - 15 ft from wall face	20.738	18.154	20.764	18.154
26 - 30 ft from wall face	8.119	252.000	4.014	18.154

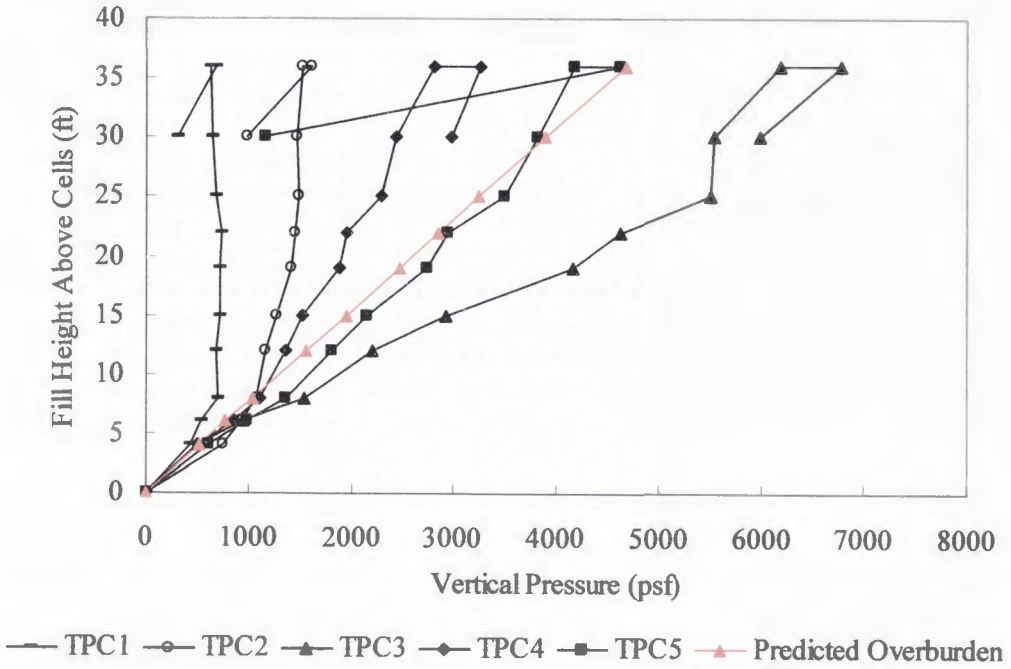

Fig. 3.23 Measured vertical wall pressures for different heights of fill above the total pressure cells beginning at 6 ft within the wall backfill (UDOT vibrating wire reader results)

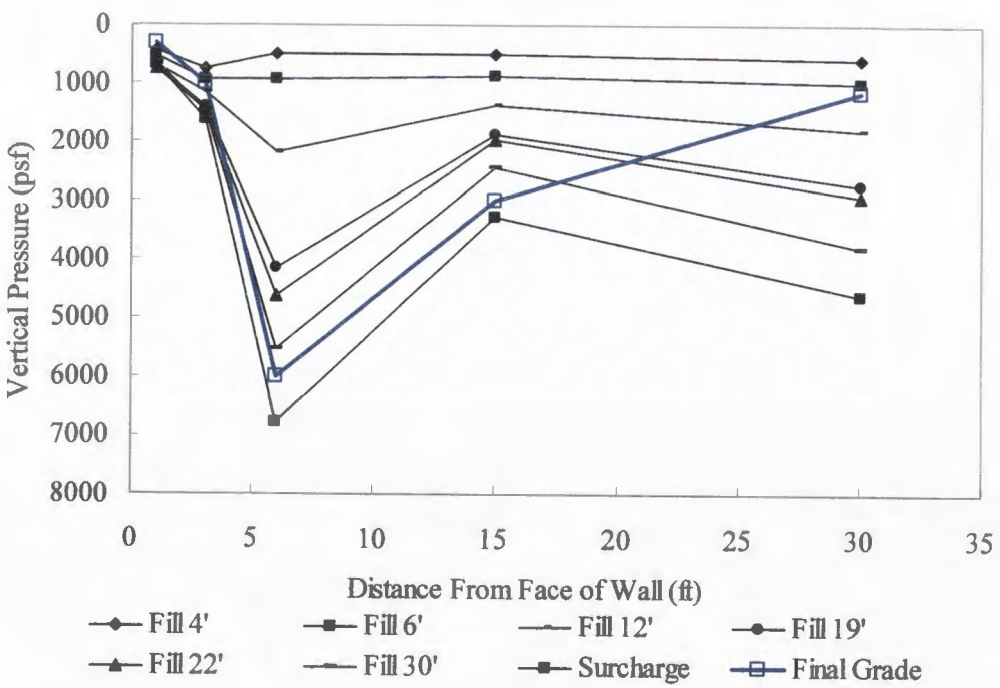

Fig. 3.24 Measured vertical wall pressures versus pressure plate position within the wall (UDOT vibrating wire reader results)

3.4 VERTICAL AND HORIZONTAL DEFORMATIONS

3.4.1 Vertical Inclinometers

Horizontal deformations of the wall and foundation material were measured using vertical inclinometers. The positions of these inclinometers are shown in Fig. 3.1. The overall results of each of the three vertical inclinometers used on this project are shown in Fig. 3.25, Fig. 3.26, and Fig. 3.27.

Fig. 3.25 shows the measurements made at a vertical inclinometer located 3 ft (0.9 m) from the wall face within the wall footprint. This inclinometer shows about 3.5 in. (89 mm) of horizontal movement at the base of the wall, with nearly all horizontal movement confined to soil down to 20 ft (6.1 m) beneath the base of the wall. This inclinometer casing was gradually extended as the wall was built.

Fig. 3.26 shows the measurements made at a vertical inclinometer located 8 ft from the wall face outside the wall footprint. This inclinometer casing experienced the most lateral movement of the three vertical inclinometers, with maximum deflections of more than 6 in. (152 mm) occurring at the top of the soft clay layer beneath the rubble backfill. This is indicative of localized shear and mass movement of the soft clay layers.

Fig. 3.27 shows the measurements made at a vertical inclinometer located 31 ft (9.4 m) from the wall face outside the wall footprint and also outside the zone containing PVDs. Less than 0.75 in. (19 mm) of horizontal movement has occurred in this location outside of the right of way.

Additional measurements have been taken at each of the three vertical inclinometer casings and both of the horizontal casings since completion of the

construction process. However, as with the strain gage and pressure plate readings, some additional work was required to allow readings to be taken.

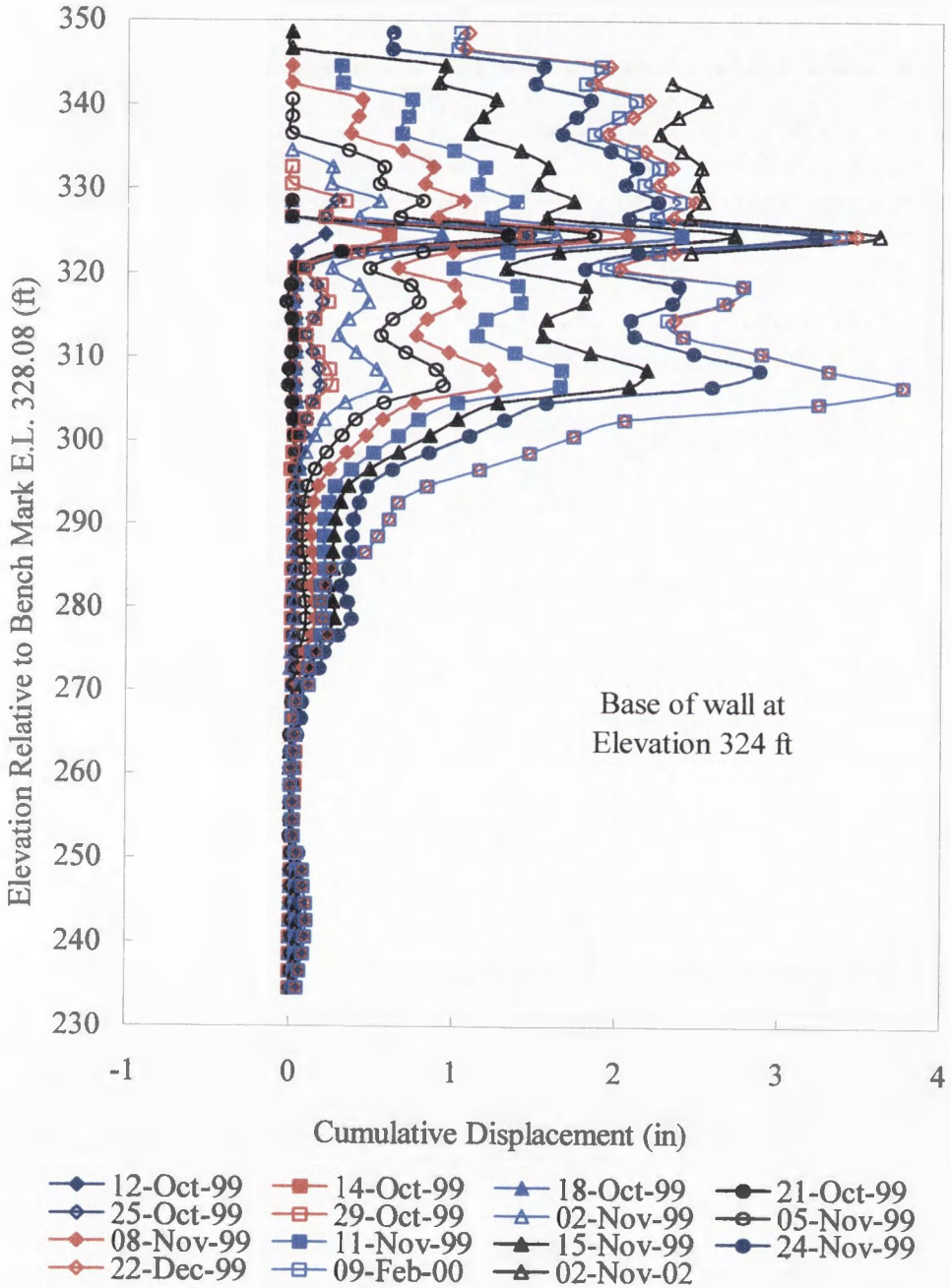

Fig. 3.25 Plot of vertical inclinometer measurements for inclinometers located 3 ft from wall face, within wall footprint

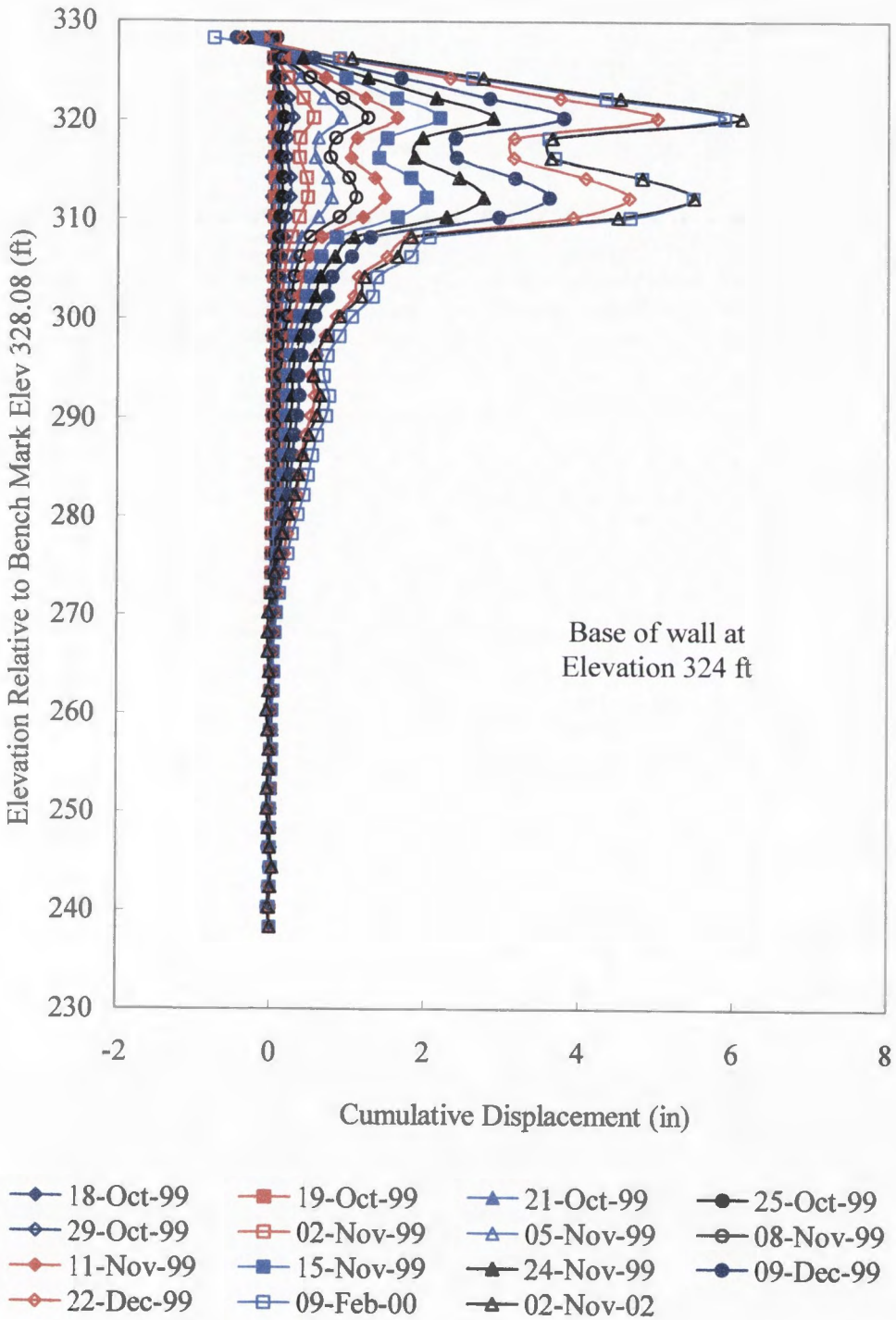

Fig. 3.26 Plot of vertical inclinometer measurements for inclinometers located 8 ft from wall face, outside wall footprint

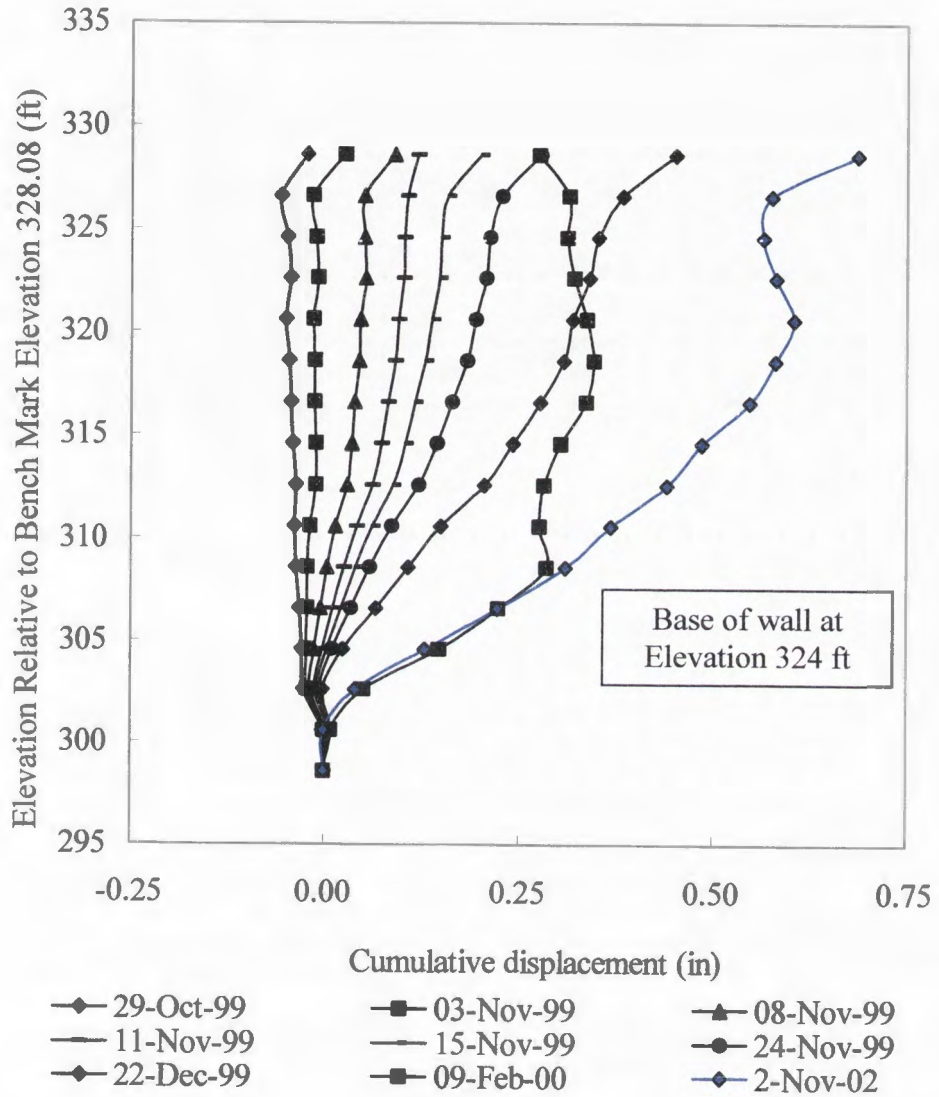

Fig. 3.27 Plot of vertical inclinometer measurements for inclinometers located 31 ft from wall face, outside wall footprint and outside wick drain zone

There were several obstacles to overcome in taking readings from Inclinometer casing I1, which was the inclinometer within the wall footprint extending to the top of the wall. First, UDOT required fall protection in order for anyone to gain access to the upper casing. This is due to the fact that only a 6 ft (1.8 m) shoulder exists between the Jersey barrier and the edge of the wall.

A number of alternatives were considered, including tying off to a vehicle on the traffic side of the Jersey barrier, installing tie-off loops on the Jersey barrier itself, creating some type of cable system to tie-off fall protection to, and several other ideas. A non-permanent system was desired that would have minimal effect on traffic yet have the safety of the persons taking the measurements as highest priority.

Eventually, a steel bracket was designed that could be set on top of the barrier like a saddle, and fall protection harnesses could be attached to this bracket, allowing a person to be constantly protected from a possible fall. This prevented the need for a bumper vehicle on the traffic side of the barrier (which would have been required to protect whatever vehicle would have been used to tie-off to), and met the criterion of not being a permanent fixture. A photograph of the fall protection system that was devised is given in Fig. 3.28.

Another problem associated with Inclinometer I1 was the fact that the Jersey barrier was positioned such that the access hole cap was partially covered by the barrier. The concrete was chiseled at the base of the barrier just enough to allow the cap to be removed, thus allowing the inclinometer to be dropped into the hole and readings be made. Photographs showing the chisel work on the Jersey barrier are shown in Fig. 3.29.

Problems were also encountered with Inclinometer I2. Once the secondary concrete fascia panels were constructed, additional fill was placed along the edge of the right of way and a drainage ditch constructed. To facilitate this drainage ditch, inclinometer casing I2 was cut off and subsequently buried under several feet of fill. Luckily, the caps used to cover the casings were replaced, such that minimal fill material

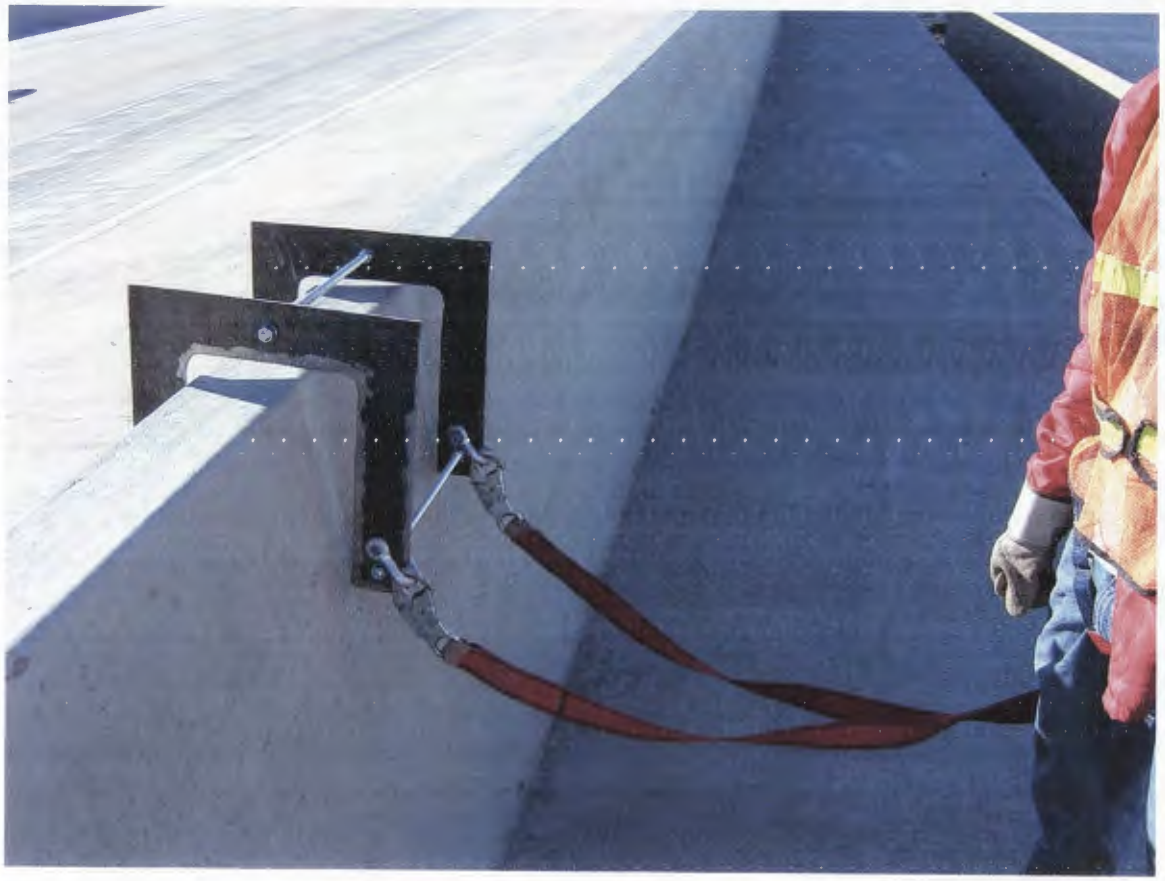

Fig. 3.28 Photograph of the fall protection system devised for access to the upper inclinometer casing

fell into the casing. However, substantial time using a pick-axe and a shovel were devoted to digging up the casing. Photos showing the recovered casing are given in Fig. 3.30 and Fig. 3.31. Once the casing was discovered, readings were again taken.

The casing for Inclinometer I3, positioned outside the right of way for I-15 and outside of the wick drain zone, was not affected by construction. Readings were easily obtained.

Fig. 3.32 and Fig. 3.33 show the updated horizontal deformations of the wall and foundation soils with the results from Inclinometer I1. Fig. 3.32 shows only the most

current reading and the previous reading in order to show post-construction movement. Fig. 3.33 focuses on the section for which new data was obtained, as will be explained.

Problems were encountered in analyzing the data, due to the fact that the inclinometer would not pass through the casing beyond a point 26 ft (7.9 m) below the top of the casing. Since movement was calculated with respect to an assumed stationary point at the deepest point possible, and a cumulative deflection with respect to that point calculated, another point of reference was required. It was decided that the most accurate alternative was to assume this point of reference to be at Elevation 322.6 ft, which was 2 ft (0.6 m) below the deepest reading taken from Inclinometer I1. It was assumed that the increase in horizontal deflection from the previous reading at this elevation for I1 would be the same as the increase in horizontal deflection from the previous reading at the same elevation for Inclinometer I2. This was considered to be slightly conservative, since Inclinometer I1 had shown less movement than I2 at that elevation during the construction process.

Another factor that required some adjustment was the fact that the casing was cut off upon removal of the surcharge and prior to placement of the concrete pavement at final grade. The raw data were shifted such that the best agreement between peak readings was achieved, then the raw data were interpolated in order to calculate displacements with respect to the baseline. These displacements are given in the figures here.

As noted, from the limited data obtained due to the obstruction in the casing, it appears that some movement (on the order of 0.5 inches (12.7 mm) at the uppermost elevation with valid readings) has taken place since the completion of the wall.

Fig. 3.29 Photographs showing the chisel work required for inclinometer casing I1

Fig. 3.30 Photographs showing the recovered inclinometer I2 casing (on the left in upper photo)

Fig. 3.31 Additional photographs showing the recovered inclinometer I2 casing

Presumably this movement is only within the wall itself and not in the foundation soils beneath the wall, as will be seen in the results from Inclinometer I2. Continuing measurements over coming years will monitor the drift occurring within the wall and in the soils beneath the wall, to determine how much additional movement may occur.

The readings for Inclinometer I2 also required some manipulation, due to the fact that the casing had been cut off upon construction of the drainage ditch, as mentioned above. The raw data were plotted to compare the newest set of readings to the most recent previous readings, with the intent of matching peaks to determine how the data needed to be adjusted to match the baseline data. Fortunately, it appears that exactly 4 ft (1.2 m) of the casing was cut off, which allowed a simple shift of data to solve the problem with no interpolation necessary. The updated data for Inclinometer I2 are given in Fig. 3.34.

As seen in these figures, negligible movement has occurred in Inclinometer I2 from the end of construction to the time the most recent readings were taken (02 November 2002). Continued monitoring will occur, but one would not expect substantial post-construction movements to transpire.

Inclinometer I3 required the least data manipulation before results could be obtained. However, one problem was noted upon inspection of the data. Readings throughout the course of the construction process were only taken in the top 30 ft (9.14 m) beneath the ground surface. Thus, there is only baseline data for this uppermost soil that dates to the beginning of construction. The most recent data obtained (02 November 2002) recorded data from the ground surface to the bottom of the inclinometer casing (90 ft or 27.4 m). From the results from Inclinometer I2, it appears that some movement

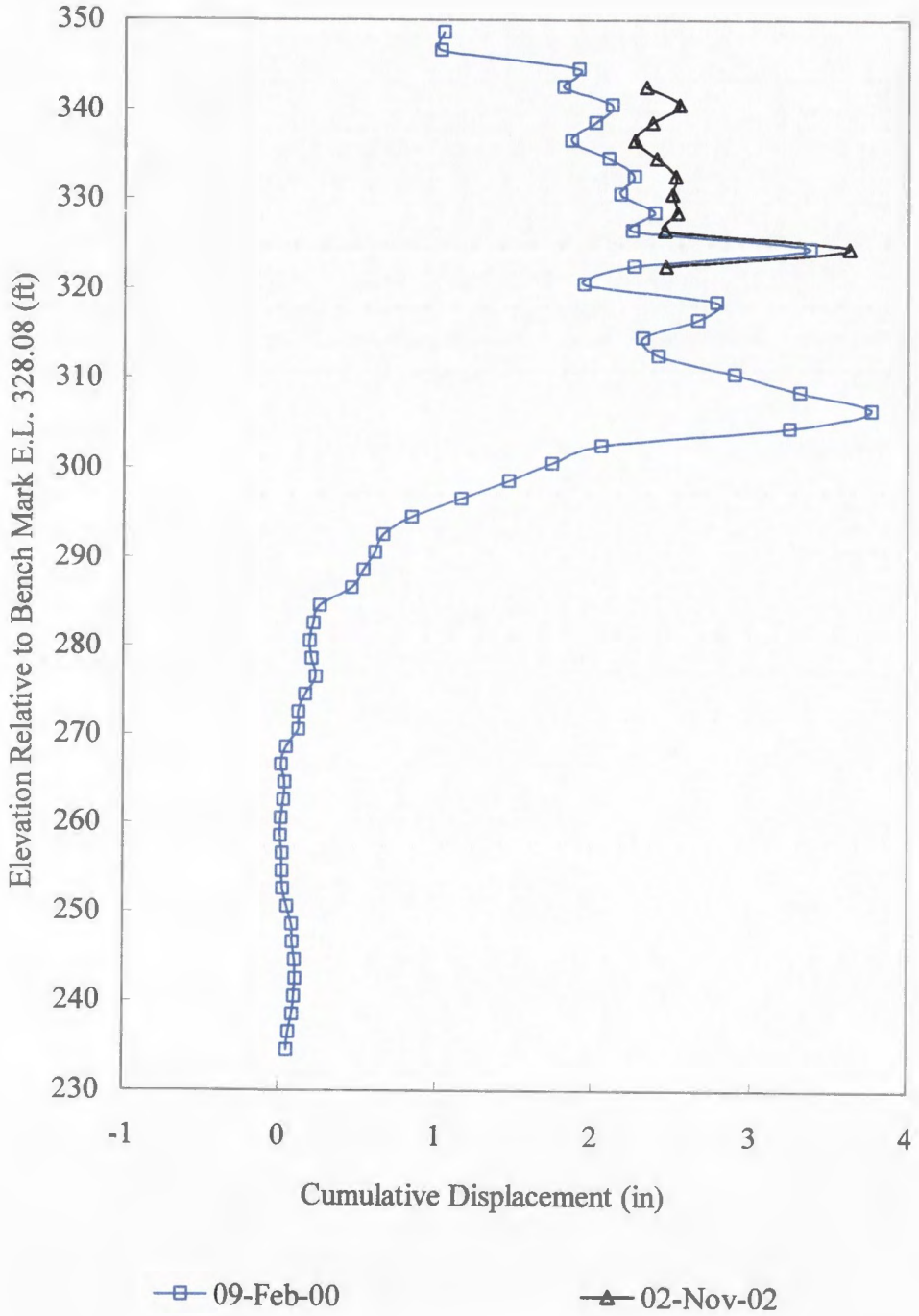

Fig. 3.32 Updated horizontal deformations of wall as collected from inclinometer I1 (two most recent sets of data showing post-construction deformations)

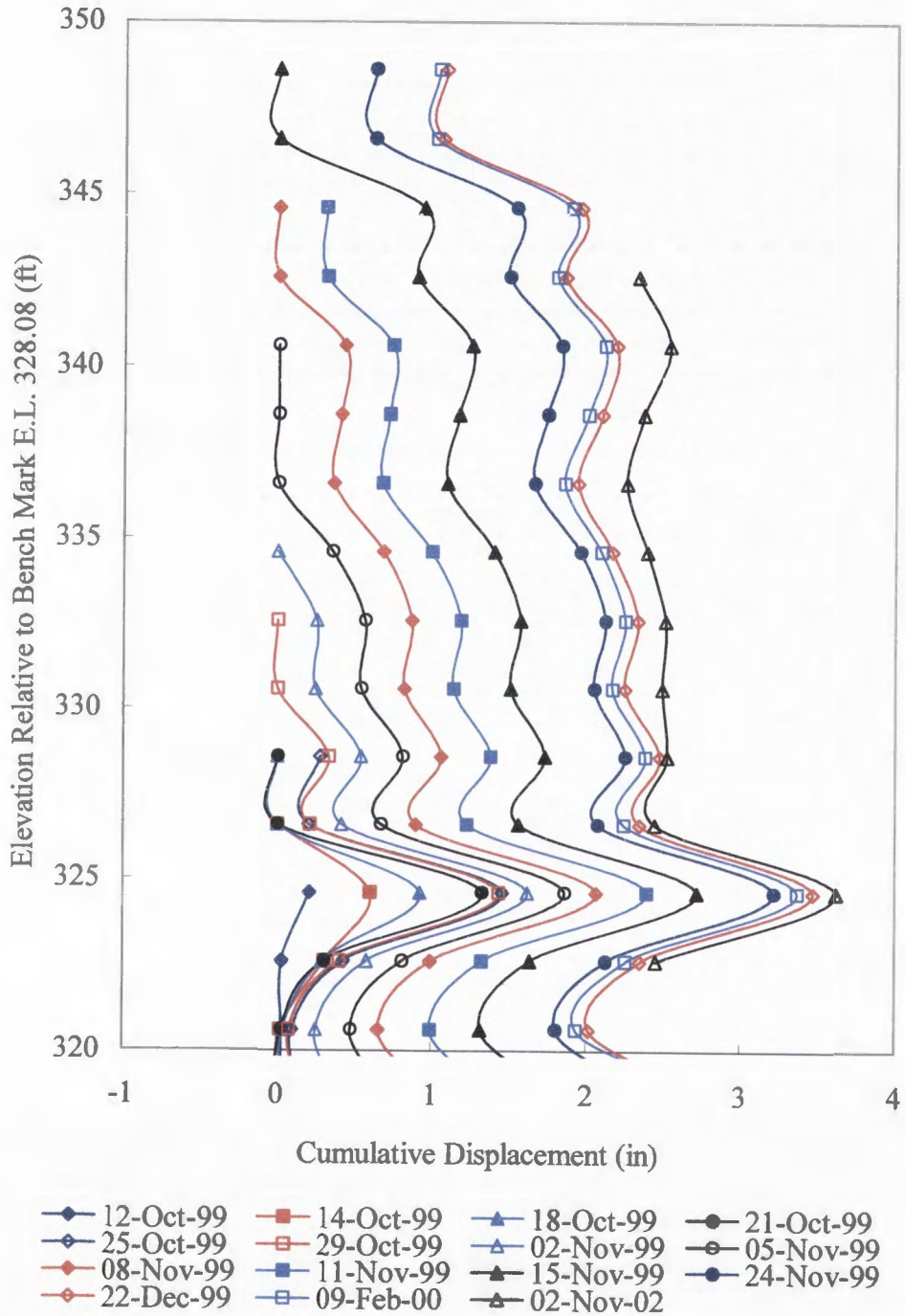

Fig. 3.33 Updated horizontal deformations of wall as collected from inclinometer I1 (zoomed to clarify most recent data collected)

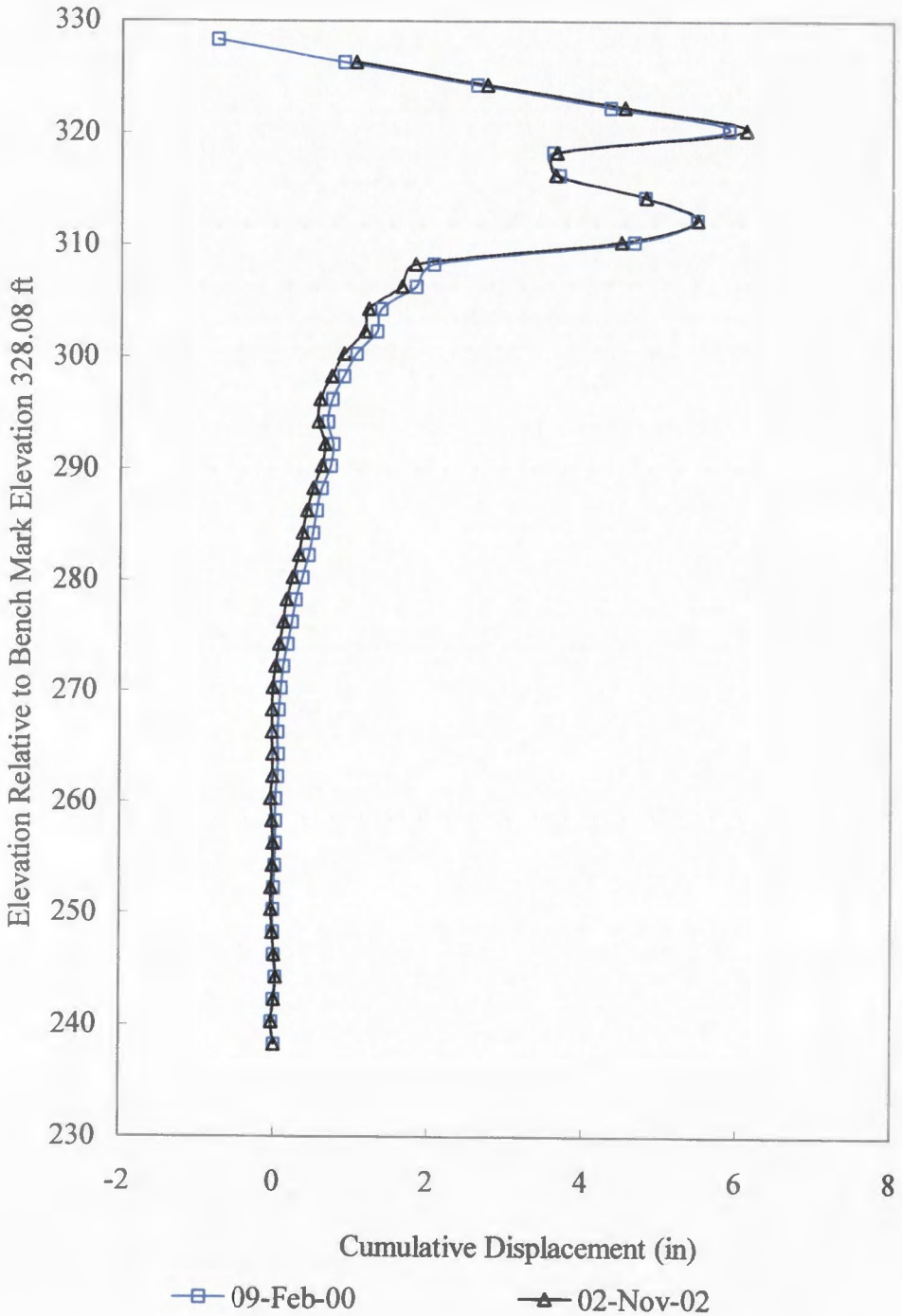

Fig. 3.34 Updated horizontal deformations of wall as collected from inclinometer I2 (two most recent sets of data showing post-construction deformations)

likely occurred in I3 at the 30 ft (9.14 m) depth during construction of the wall, but due to the data only being collected for that uppermost 30 ft (9.14 m), the displacement at that depth was required to be zero. An adjusted baseline was created, using a combination of the initial baseline and the new data obtained. Future readings will be able to use the this adjusted baseline, which will assume that no displacement occurs at a 90 ft (27.4 m) depth, which is a more valid assumption. The updated results of Inclinometer I3 are given in Fig. 3.35.

To facilitate long-term monitoring of horizontal movement, plots of the horizontal drift (displacement with respect to the zero readings) versus the log of time have been constructed. These will allow primary and secondary movements to be monitored over extended periods of time. Comparison of movements at a given elevation for the three inclinometers can be made over time, as well as comparison of displacements at various depths for a given inclinometer over time. These plots, as mentioned, will be of great benefit in the prediction of long-term horizontal movement within the wall and in the foundation soils beneath the wall. An example of such a plot is given in Fig. 3.36.

As seen in Fig. 3.36, minimal horizontal displacement has occurred near the base of the wall over the log cycle from the end of construction (124 days) to the most recent readings (1121 days). As an example, Inclinometer I1 has moved 0.25 inches at the given elevation (324.6 ft) during this period of time. Assuming the movement follows a pattern similar to secondary soil consolidation, the increase in deflections over the next log cycle (i.e. 1000 days to 10,000 days) will be the same as the increase shown over the previous log cycle. Thus, over the next approximately 27 years the increase in deflections will only be about the same (0.25 inches) as the minimal increase over the

past 2.7 years, such that hardly noticeable displacements will be taking place in coming years. It will be of great interest to note whether or not the horizontal displacements follow these expected trends.

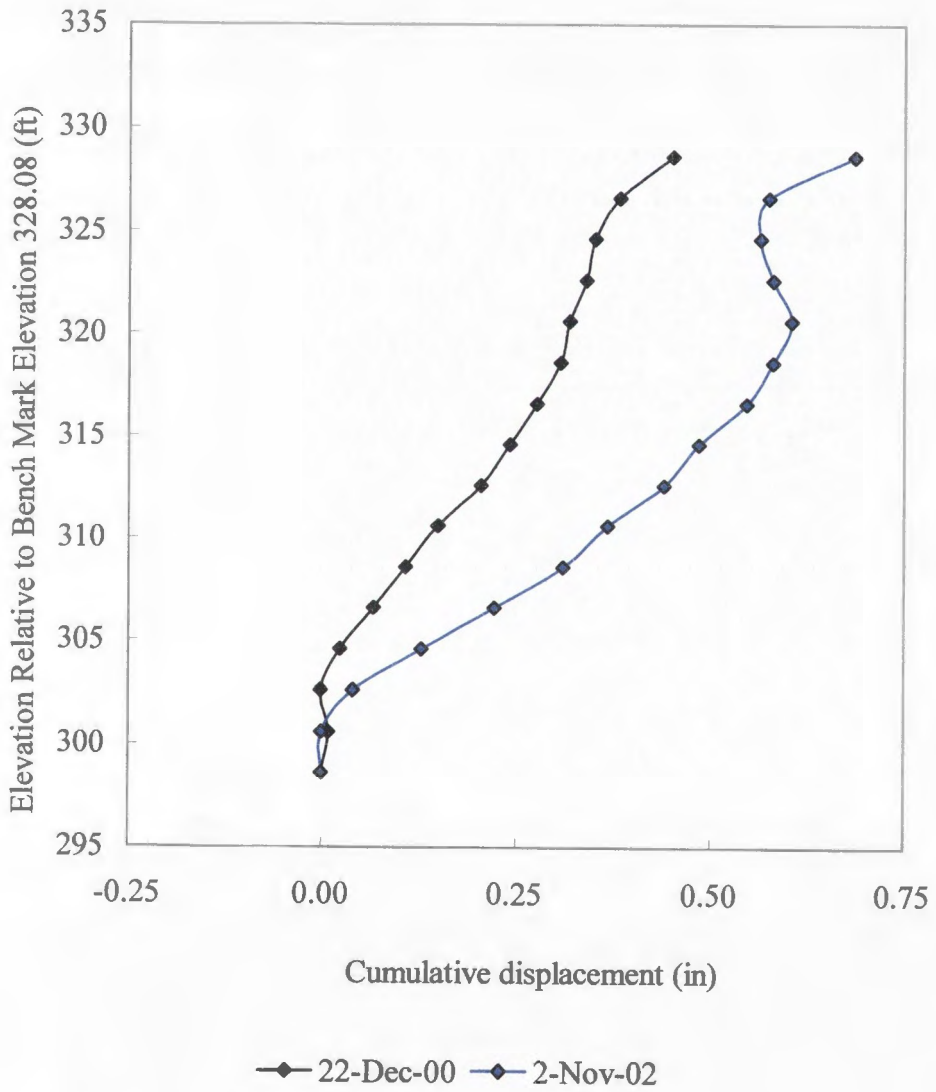

Fig. 3.35 Updated horizontal deformations of wall as collected from inclinometer I3 (two most recent sets of data showing post-construction deformations)

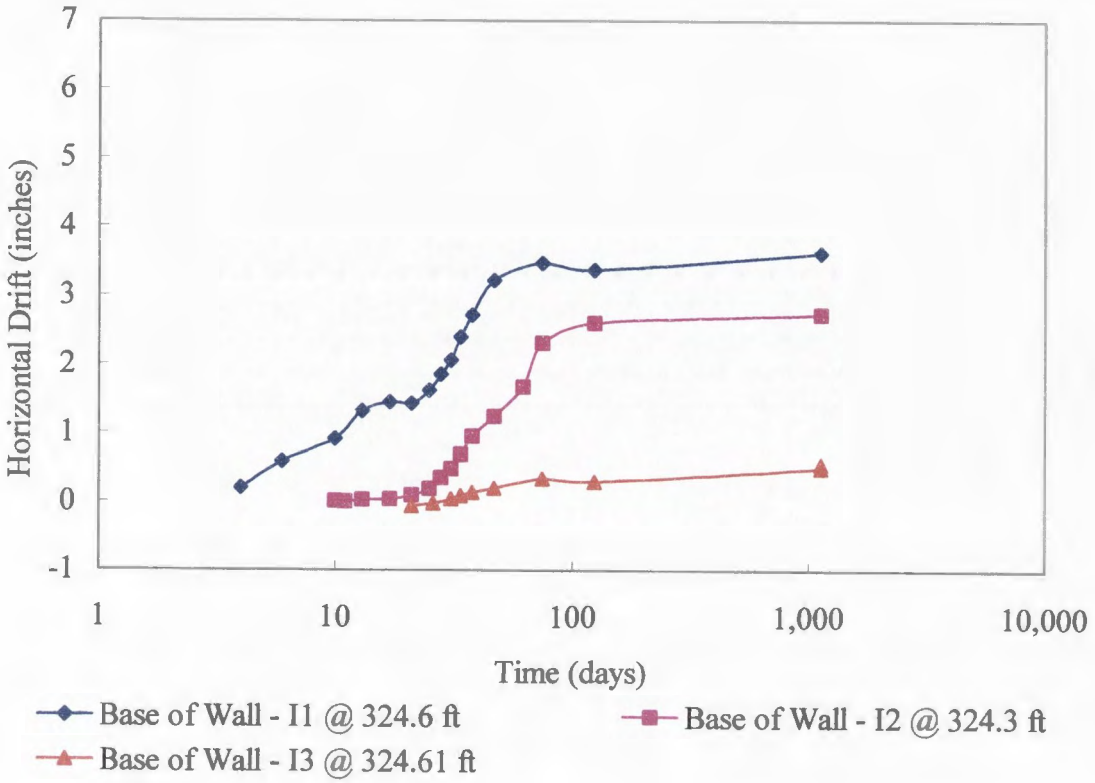

Fig. 3.36 Example of long-term plot to monitor horizontal movement over time

3.4.2 Horizontal Inclinometers

Horizontal inclinometer results are plotted in Fig. 3.37 and Fig. 3.38 for the two horizontal inclinometers used on this project. As seen in Fig. 3.1, the inclinometer placed at the base of the wall backfill material extended to a manhole located 14 ft (4.3 m) from the bar mat wall face. Fig. 3.37 shows settlements measured at the inclinometer at the base of the wall. Negligible settlement of the manhole occurred, while settlement of the soil outside the wall footprint increased to the face of the wall.

Fig. 3.38 shows settlements measured at the second horizontal inclinometer, placed in the wall when the wall height was approximately 8 ft (2.4 m). The overall settlement of the second inclinometer was surveyed when each inclinometer

measurement was performed. Both inclinometers show maximum settlement near the toe of the wall, with slightly less settlement further into the wall. This could be due to localized shearing at the wall toe and preconsolidation of the foundation beneath the wall due to preexisting fill.

Some work was required in order to take readings on the two horizontal inclinometers. Horizontal Inclinometer H1 (located in the manhole, extending beneath the wall) was intact, such that all that was required to take the readings was to obtain a small fan to provide ventilation in the manhole for several minutes before entrance to ensure that any toxic fumes that may have entered the manhole were dispersed. Again, this was a safety concern, not an equipment concern. The cable used to pull the inclinometer into the casing was intact, and the readings were obtained fairly easily.

The upper Horizontal Inclinometer (H2), however, required more work before readings could be obtained. As with the strain gage and pressure plate cables, a hole had to be cored in the concrete fascia panels in order to have access to the inclinometer casing. The cored hole for this inclinometer was shown in Fig. 3.17.

During the time between the coring of the hole through the fascia panels and the initial attempts to take additional readings, the cable strung through the casing that was used to pull the inclinometer into the hole was stolen. Numerous attempts were made using a variety of tools to make an effort to restring the cable, such as attempting to push a steel fishtape into the casing, around the pulley, and back out. However, these attempts were fruitless.

After discussing the matter with a representative of SINCO, Inc., it was decided to create an extensible rod that could be used to push the inclinometer into the casing

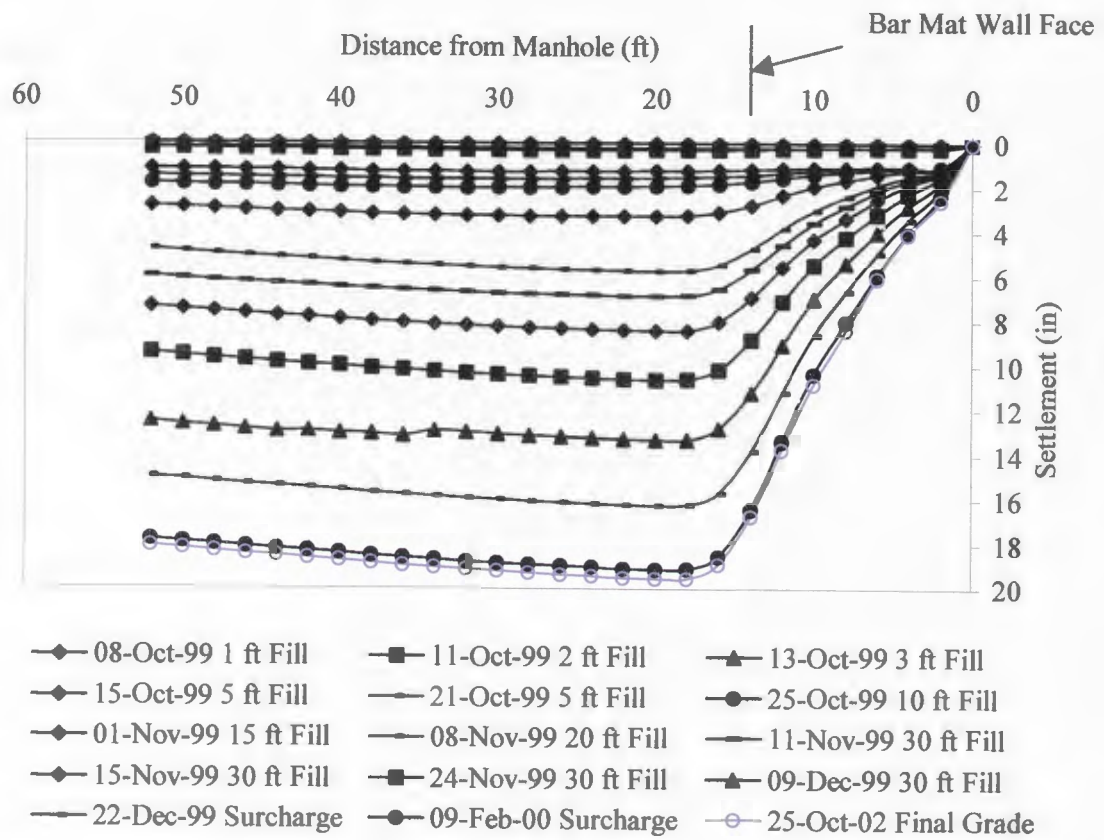

Fig. 3.37 Updated movement of horizontal inclinometer H1 originating from a manhole and going beneath the wall face at about 14 ft

instead of attempting to rethread a cable to pull the inclinometer into the casing. As a result, ten 5 ft pieces of 0.75 inch PVC pipe were purchased with connection sleeves glued to one end of each. A rope was threaded through the pipes and sleeves, such that the pipes would not become disconnected in the hole and become irretrievable. As the inclinometer was pushed into the hole in 5 ft lengths, additional sections of pipe were added that allowed the inclinometer to be pushed the entire distance into the hole. This allowed the problem with the missing cable to be overcome. A photograph of these interconnectable PVC pipes is given in Fig. 3.39.

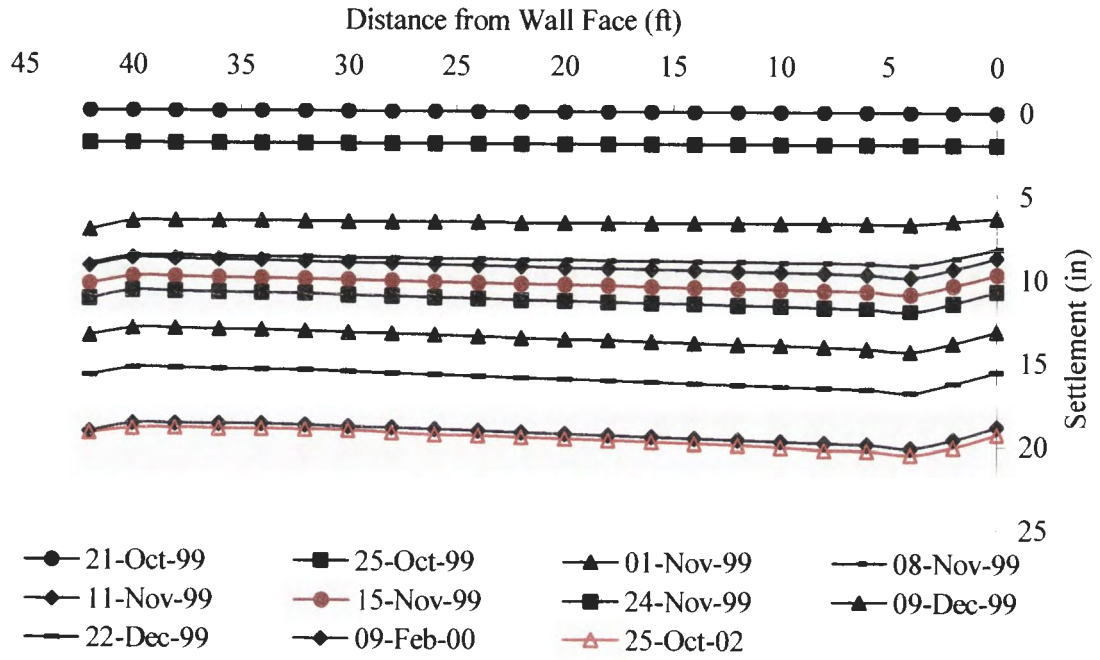

Fig. 3.38 Updated horizontal inclinometer H2 beginning at an initial height of 8 ft in the wall fill and originating at the wall face

One final obstacle to overcome was also present. Near the back of the casing, an obstruction was encountered. The obstruction did allow the inclinometer past with some effort. However, upon removal of the inclinometer some rotten remains and an awful stench were attached to the inclinometer and a portion of the cable. It appears that some sort of animal (a rat, perhaps) climbed into the inclinometer casing, proceeded a long distance into the casing, and was unable to turn around to escape and died. The cap that had been in place to cover the casing was apparently removed and/or stolen when the cable was stolen, allowing access to the casing hole. Before the next set of readings are taken, attempts will be made to flush out the animal remains to make taking measurements a much less offensive matter, and a cap will be replaced over the end of the casing to prevent such an occurrence from happening again.

Fig. 3.39 Photograph showing the interconnectable PVC pipes used to push the horizontal inclinometer into the H2 casing

Settlement calculations using the data collected from the horizontal inclinometers were much more straightforward than the calculations for the vertical inclinometers, since neither casing had been altered in any way from the previous readings. Since the manhole had not settled at all during the construction process, it was assumed that it has not settled at all in the months following construction. The manhole position will be monitored over time to make sure no settlement does occur, but negligible change is anticipated.

The updated results from Inclinometer H1 are given in Fig. 3.37. As noted in observing this figure, some additional movement has taken place in the years following

construction. Continued observation over several years will show such continued secondary consolidation taking place, as will be further shown later.

One problem was present in processing the results of Horizontal Inclinometer H2. The presence of the concrete fascia panel made it much more difficult to accurately survey the elevation of the casing. It was certain that the wall had settled during the time since the previous readings, but since accurate surveying through the cored hole was very difficult, the extent of settlement was not directly available. Throughout construction the incremental settlement of Inclinometer H2 at the face of the wall closely matched the settlement of H1 about 4 ft (1.2 m) within the wall footprint. Inclinometer H2 readings were adjusted accordingly, assuming the same increment of settlement as occurred at H1 at that position. The updated results from Inclinometer H2 are given in Fig. 3.38.

As seen in this figure, some movement is still occurring, and this movement will continue to be monitored over time. As noted in the discussion of the vertical inclinometer results, much of the movement is expected to follow the behavior of secondary consolidation. It is thus appropriate to monitor settlement results with respect to the log of time. Such figures are included here, as given in Fig. 3.40 through Fig. 3.42. These figures show the settlement at the toe of the wall (18 ft readings for H1 and 4 ft readings for H2) as well as the back of the wall (52 ft readings for H1 and 38 ft readings for H2). The data presented in Fig. 3.40 is repeated in Fig. 3.41 and Fig. 3.42 for clarity in observing the results of the H1 readings at the toe and back and the H2 readings at the toe and back, respectively.

As seen in these figures, and as noted in the discussion of the vertical inclinometers, minimal vertical movement (0.3 inches (7.6 mm)) has occurred over the

past log cycle of time at the base of the wall. Assuming secondary consolidation theory applies, again one would expect the same amount of movement to occur over the next log cycle (1000 to 10,000 days) as has occurred during the past log cycle (100 to 1000 days). From this data one would expect minimal additional movement over the next 27 years.

One of the design criteria for the I-15 reconstruction related to long-term deformations due to secondary consolidation. UDOT required that no more than 3.0 inches (76.2 mm) of post-construction movement be measured in the first 10 years after construction. It appears at this point, that this criterion will be easily met, at least for this MSE wall. It will be of great interest to monitor this vertical movement over time and see if this is indeed the case.

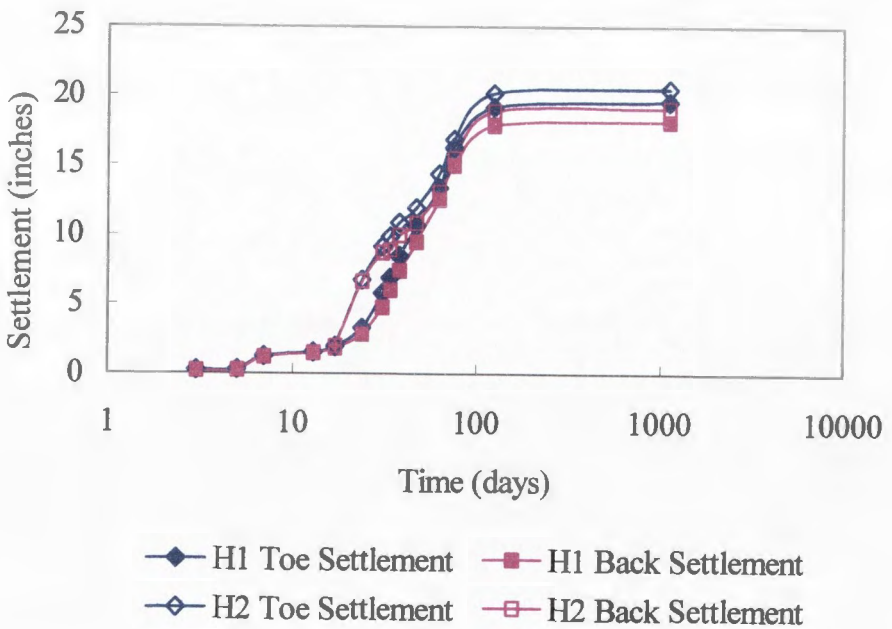

Fig. 3.40 Wall settlement at toe and back of wall as measured by horizontal inclinometers H1 and H2

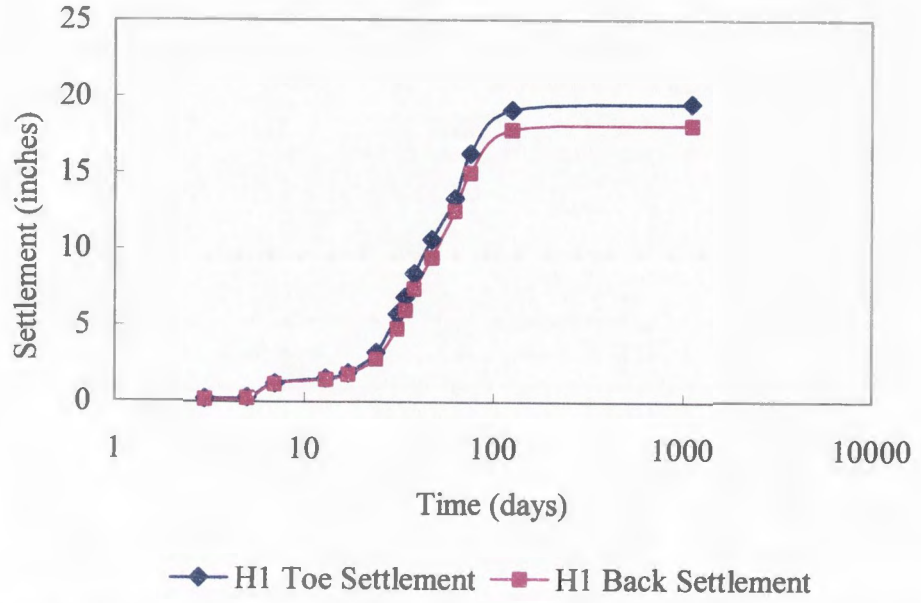

Fig. 3.41 Wall settlement at toe and back of wall as measured by horizontal inclinometer H1

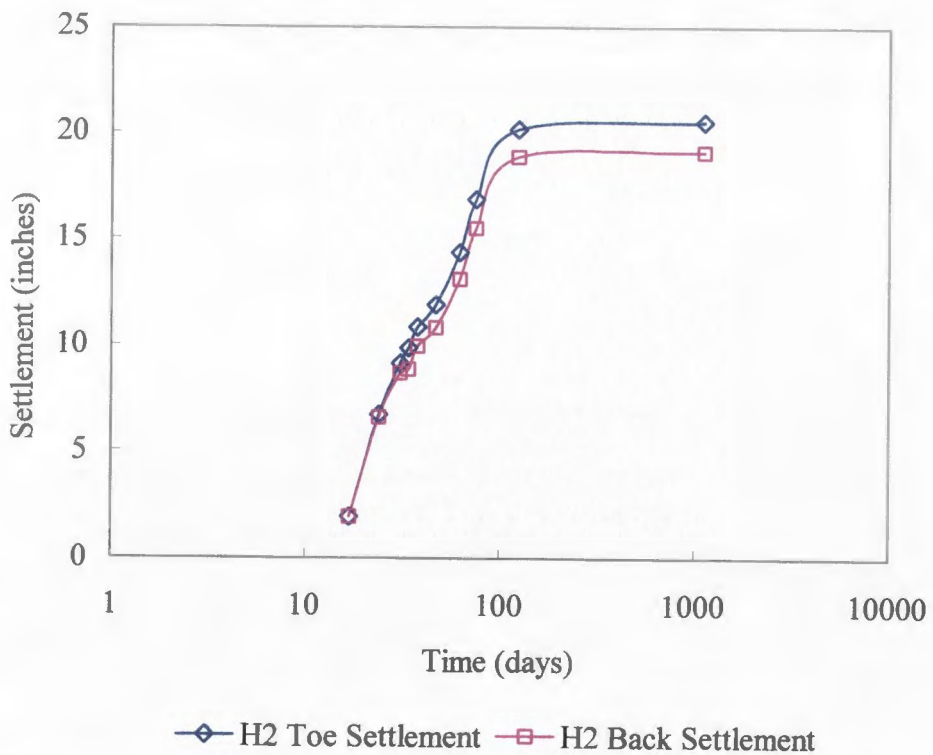

Fig. 3.42 Wall settlement at toe and back of wall as measured by horizontal inclinometer H2

One additional tool in monitoring movement over coming years will be to measure the rotation of the wall according to the horizontal inclinometers. The angle of rotation for each of the inclinometers was calculated using the points given for the toe and the back of the wall given above (Fig. 3.40). The difference in elevation from the toe to the back was easily determined, and the horizontal distance between the two points was known. Simple trigonometry allowed the angle of rotation to be calculated. The results of these calculations are plotted with respect to the log of time in Fig. 3.43.

As seen in the figure, rotation of the wall is minimal, being less than a quarter of a degree. As also seen, the increase in rotation again appears to follow secondary consolidation theory, such that increased rotation over the next log cycle would be expected to approximate the increase in rotation over the past log cycle. Again, monitoring this rotation over a number of years will be of great interest.

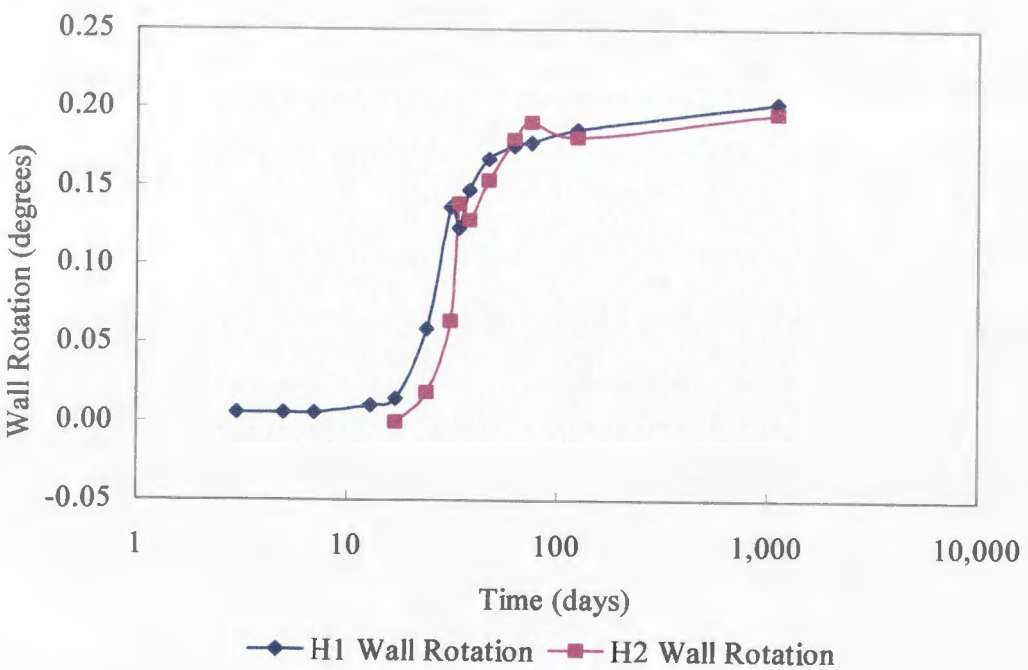

Fig. 3.43 Wall angle of rotation as determined from measurements by horizontal inclinometers H1 and H2

3.4.3 Horizontal Extensometers

Horizontal extensometers were used to measure the horizontal movements within the wall backfill. These horizontal extensometers consisted of a longitudinally placed steel rod placed in a PVC pipe, with a hook on one end to which a plumb bob was attached. At the other end, a steel bar was welded perpendicular to the longitudinal rod at the point of interest. Using the plumb bob, the horizontal displacement of the opposite end of the rod with respect to a known reference line was monitored.

The horizontal extensometers measured significant deformations in the wall within 4 ft (1.2 m) from the face of the wall, but minimal deformations were measured in the wall beyond 4 ft (1.2 m) from the wall face. The final horizontal extensometer measurements taken for each section of the wall before the second-stage concrete panels were installed are shown in Fig. 3.44. Fig. 3.44a shows the maximum horizontal extensometer measurements made before second-stage face was constructed for the primary reinforced only section of the wall, while Fig. 3.44b shows the maximum horizontal extensometer measurements for the primary and intermediate reinforced section of the wall.

The deformation in the soil mass near the wall face was probably due to the fact that less compaction was achieved close to the wall face. Since the VSL system provides little support of the wall face during compaction, less compaction can be obtained near the face of the wall than further into the fill. The movement of the extensometers further from the wall face was on the same order as the movement of the entire wall measured by the vertical inclinometer measurements, confirming the rigid movement of the wall as a whole. On average, the vertical inclinometers measured a horizontal displacement of 3.5

in. (89 mm) at the base of the wall. Horizontal extensometers in the same general area also near the base of the wall showed 3.1 in. (79 mm) of movement 16 ft (4.9 m) from the wall face, with increasing movement toward the face of the wall. Extensometer measurements showed a decrease in lateral movement moving from the base of the wall to the top of the wall, with incremental movements decreasing near the base of the wall throughout the construction process. In comparing Fig. 3.44a and Fig. 3.44b, the primary and intermediate reinforced section of the wall had significantly greater deformation than the section of wall containing only primary reinforcement. This situation has yet to be explained.

Obviously, once the concrete fascia panels were in place, the horizontal extensometers were no longer accessible. Even if attempts to core holes at each extensometer position had been made, there would have been no way to replace the stringline or make the appropriate measurements, making any additional measurements impossible. Thus, no additional data will be obtained from the horizontal extensometers.

3.4.4 Sondex Settlements

Sondex readings were taken throughout the construction process to measure the vertical deformation of the foundation material as construction progressed. The measured deformations throughout construction and the post-construction measurement are shown in Fig. 3.45, Fig. 3.47, and Fig. 3.49 for the Sondex casings located 3 ft (0.9 m) within the wall footprint, 8 ft (2.4 m) outside the wall footprint, and 31 ft (9.4 m) outside the wall footprint, respectively.

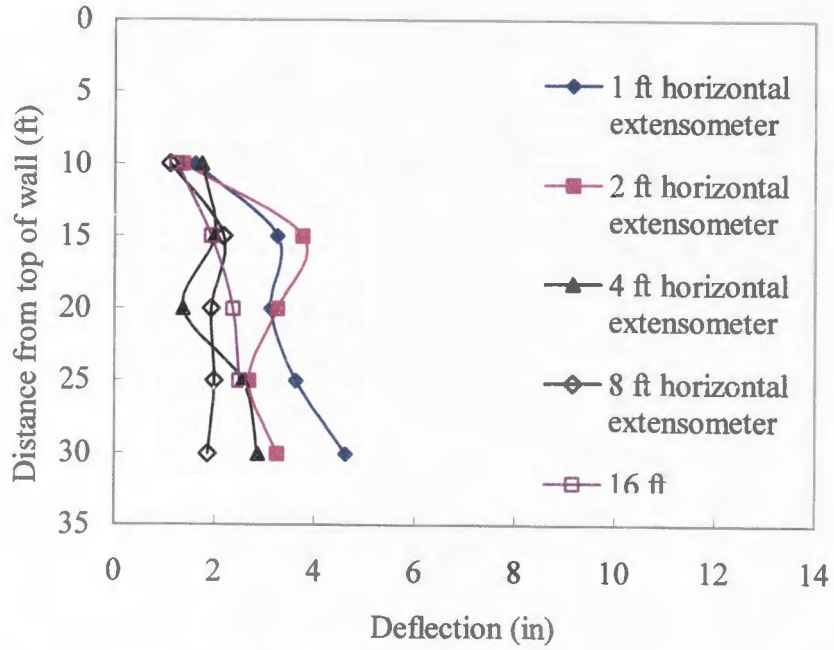

(a) Primary reinforced only section

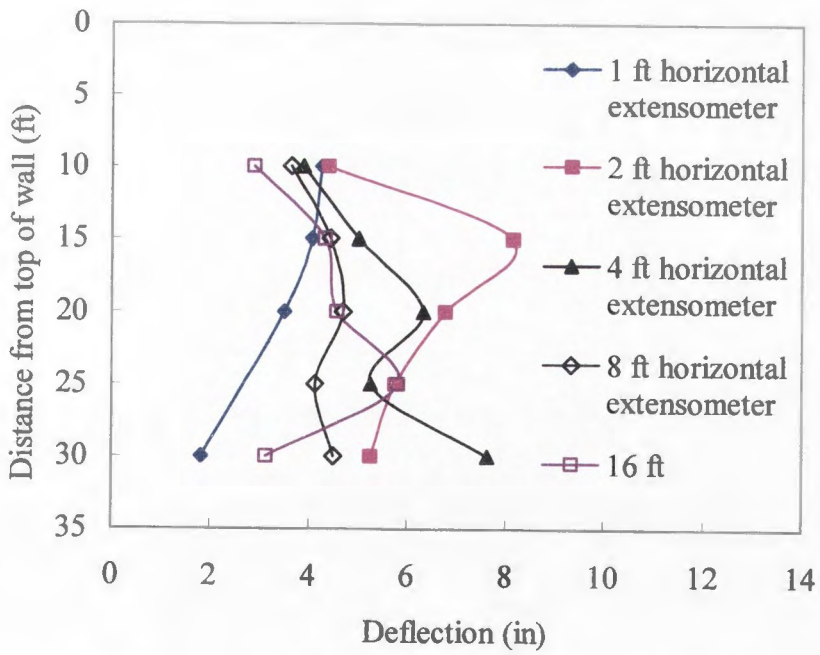

(b) Primary and intermediate reinforced section

Fig. 3.44 Final horizontal extensometer measurements

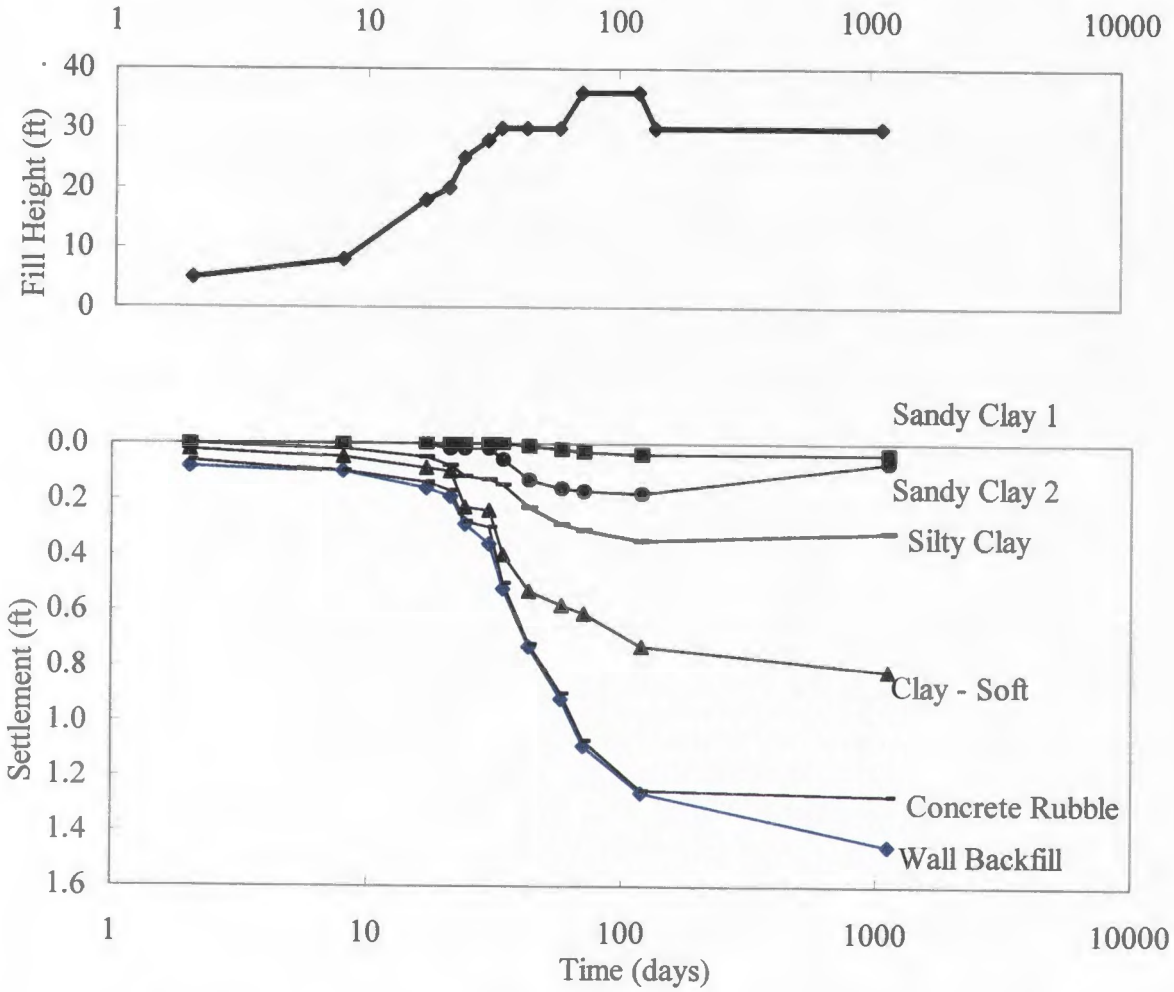

Fig. 3.45 Updated results from Sondex tube S1 settlement measurements

The same problems were present at the end of construction with respect to the Sondex casings as were present for each of the vertical inclinometer casings, as mentioned in Section 3.4.1. Again, fall protection was required to access the Sondex casing on the top of the wall (S1), and chiseling of the Jersey barrier was required in order to remove the cover plate over the casing and allow measurements to be taken.

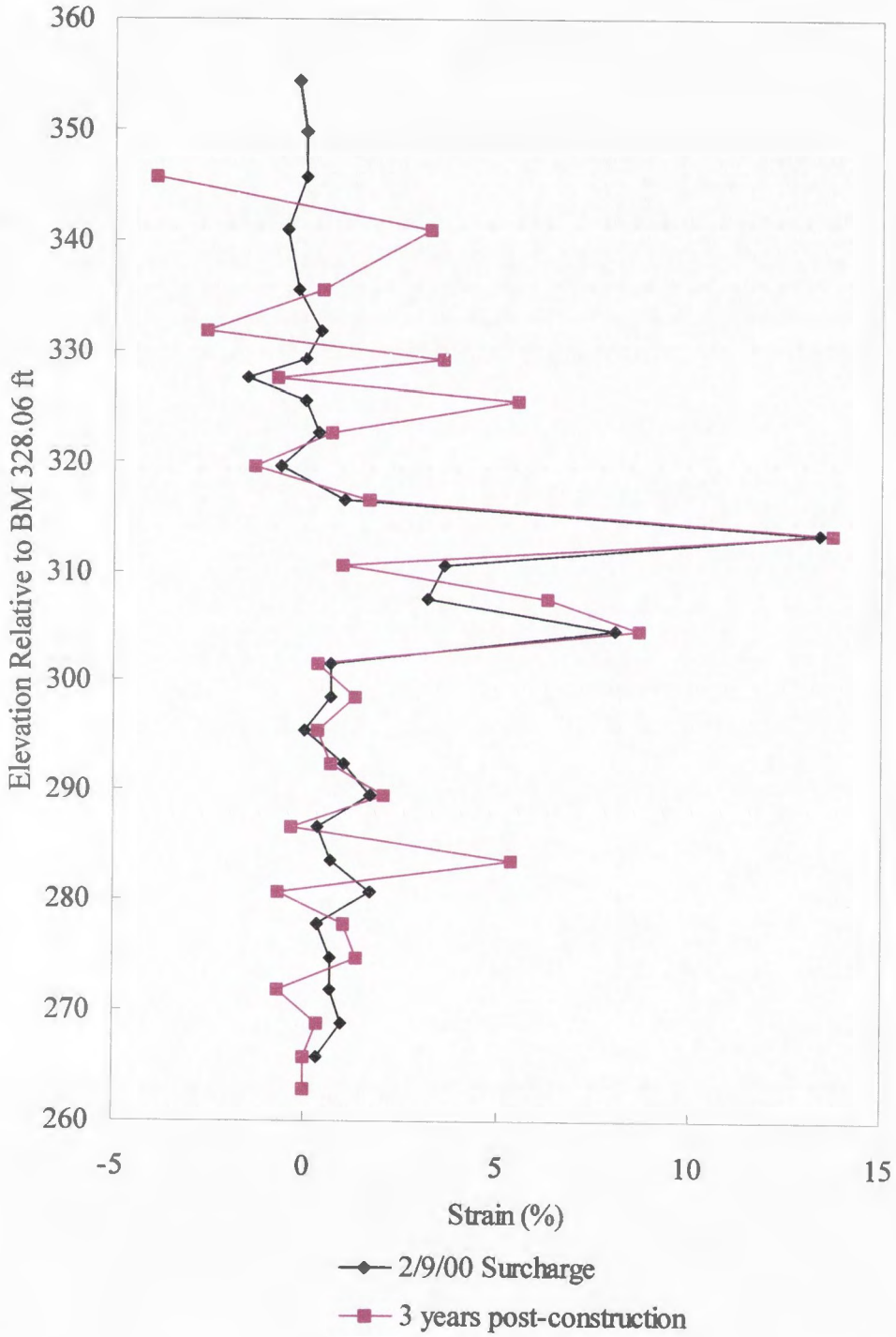

Fig. 3.46 Updated results from Sondex tube S1 strain measurements

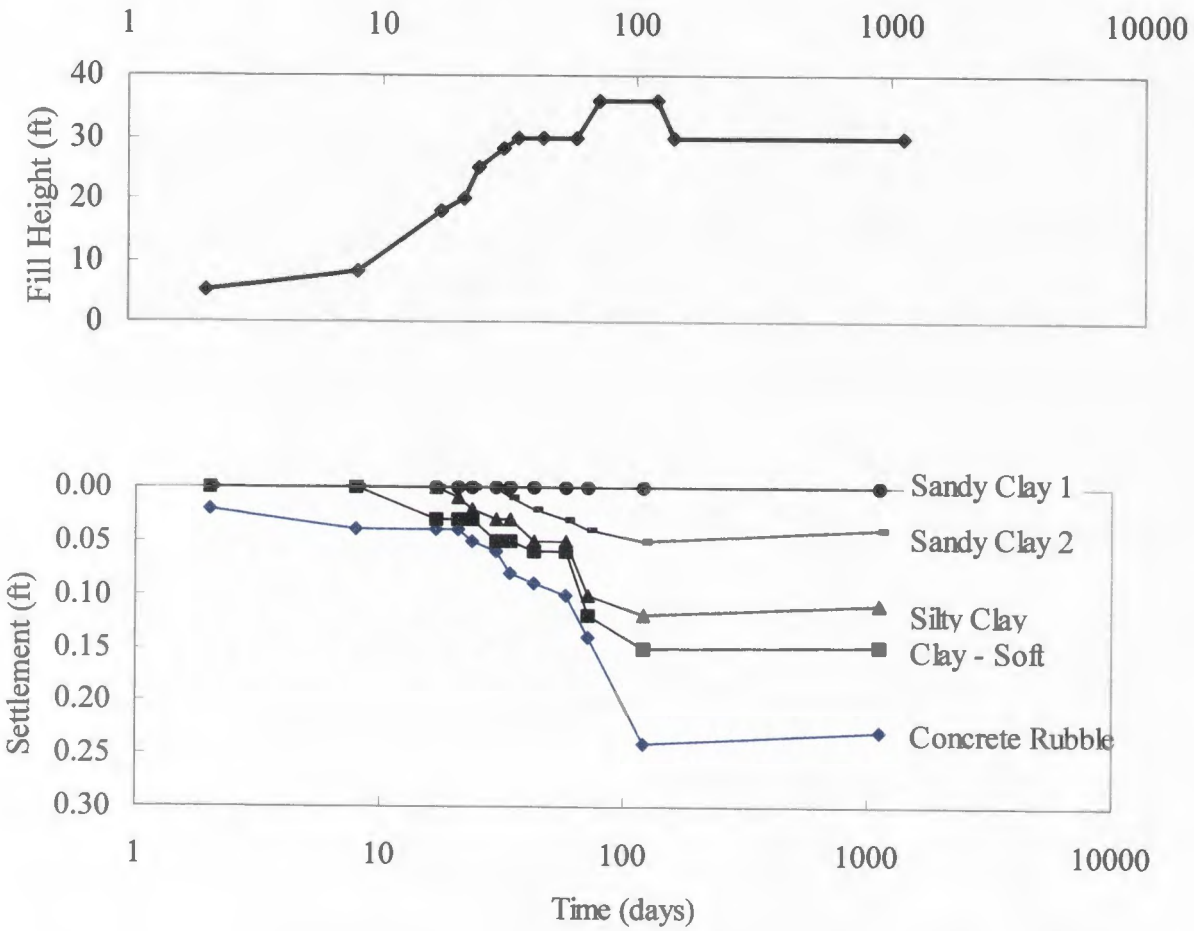

Fig. 3.47 Updated results from Sondex tube S2 settlement measurements

Sondex casing S2 was found after substantial digging, again having been cut off and buried when the drainage ditch was constructed. Photographs of recovered Sondex casing S2 are shown in Fig. 3.51. Sondex casing S3 was undisturbed, and measurements were obtained without additional work. The same spreadsheets used to compute strains and settlements for measurements taken during construction were again used for calculations for the most recent data collected. Adjustments were again necessary for the two casings (Sondex casings S1 and S2) that had been cut off since

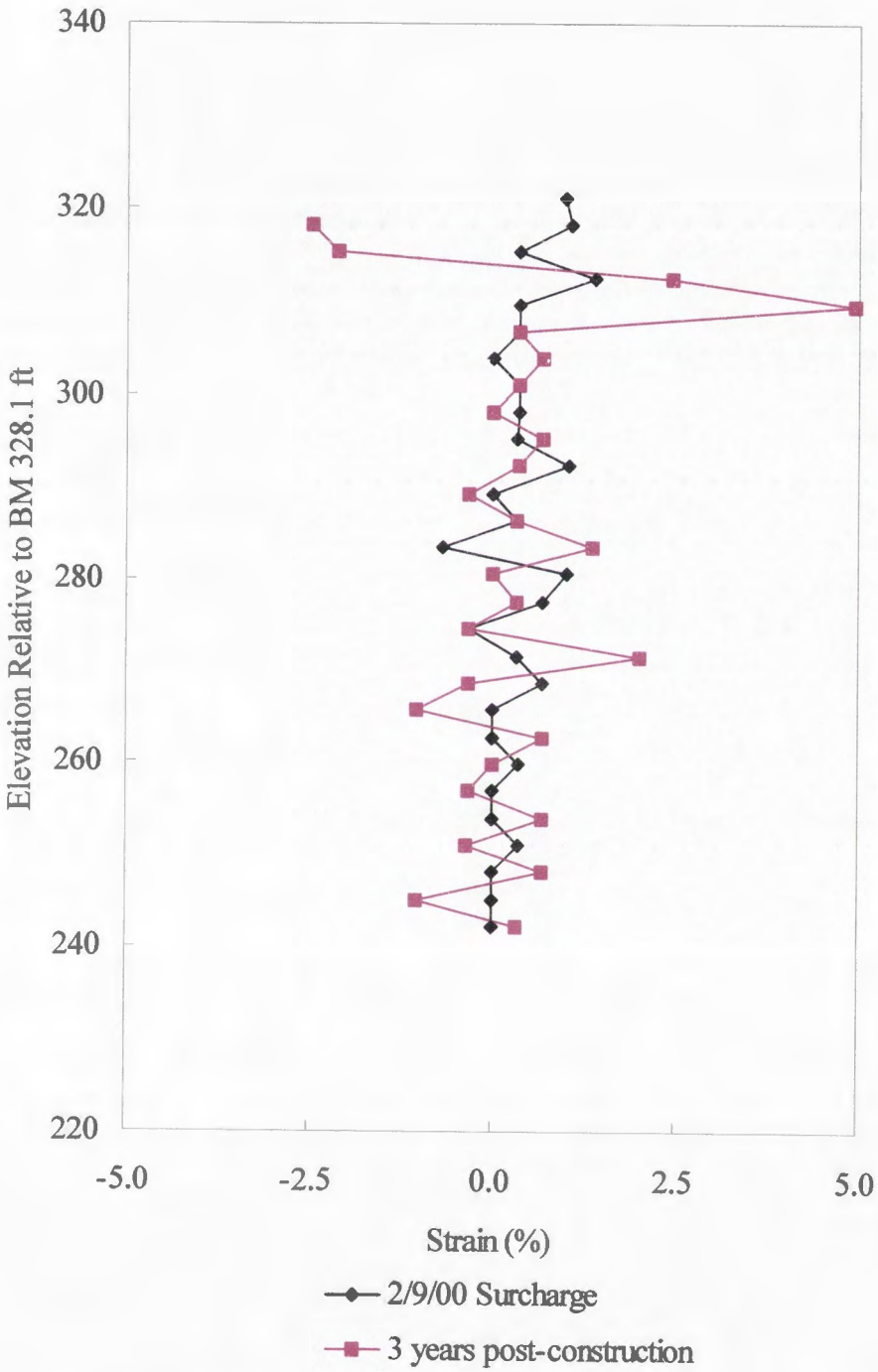

Fig. 3.48 Updated results from Sondex tube S2 strain measurements

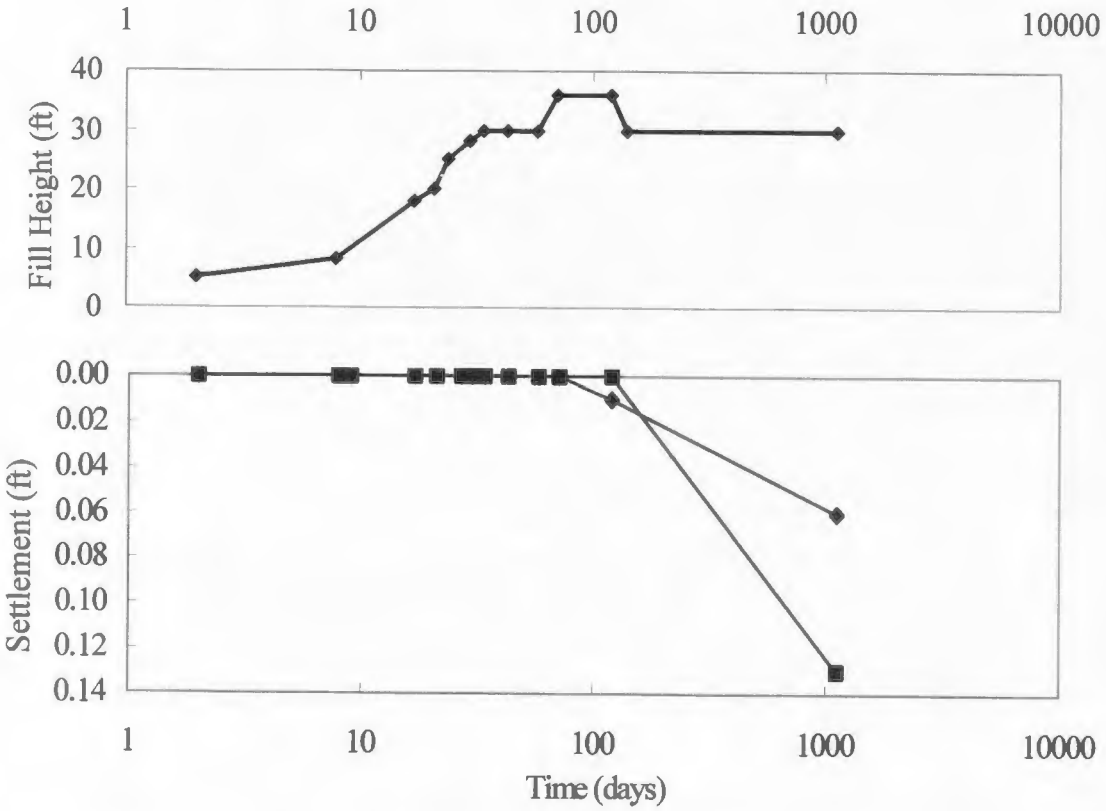

Fig. 3.49 Updated results from Sondex tube S3 settlement measurements

the previous measurements were made. These adjustments were made in a manner similar to the adjustments required for Vertical Inclinometer casings I1 and I2.

As noted in the figures given, minimal change has occurred with respect to the Sondex measurements since the end of wall construction. In some cases, slight rebound appears to have occurred according to the data. This may be due to slight rebound due to the removal of surcharge. However, this apparent rebound may simply be due to slight inconsistencies in the taking of the measurements. The technique involved in reading the Sondex positions is not precise beyond perhaps 0.03 ft, such that minor discrepancies

may appear to create such unexpected behavior as the rebound mentioned or the negative strains that have been presented throughout construction.

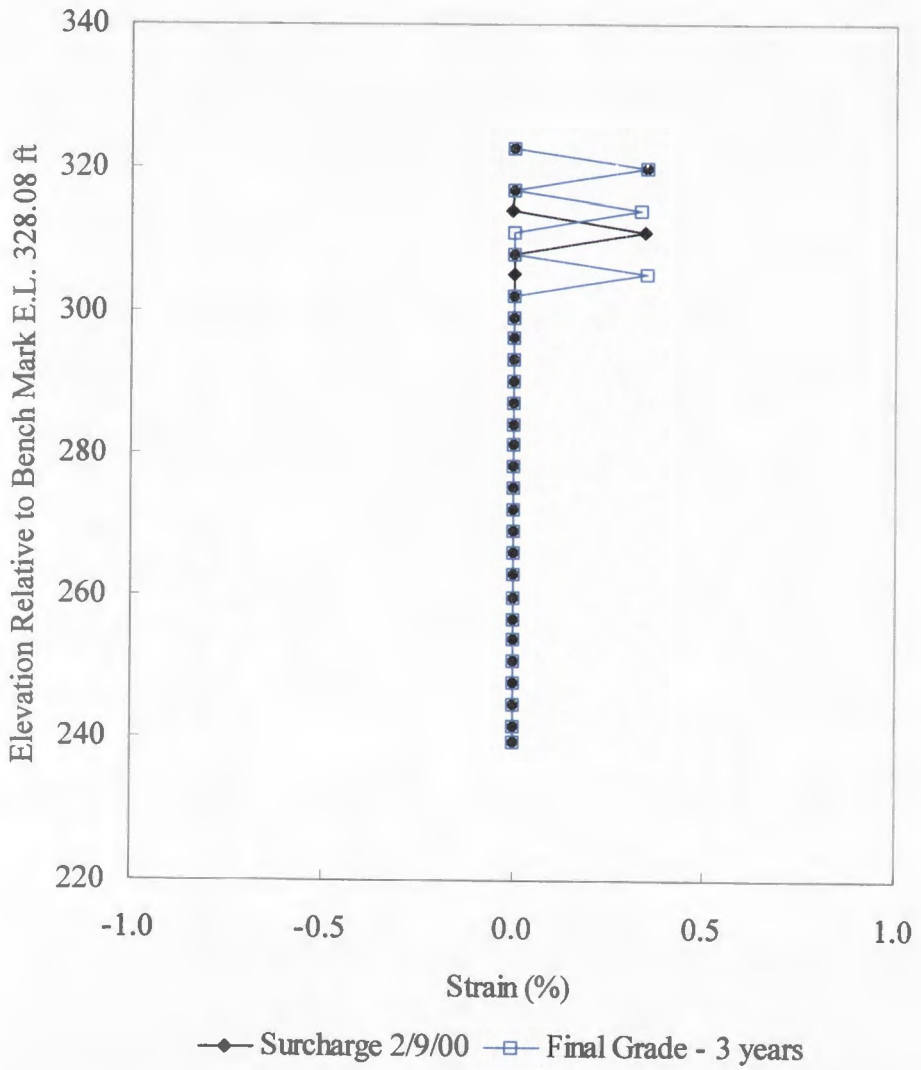

Fig. 3.50 Updated results from Sondex tube S3 strain measurements

Fig. 3.51 Photographs of recovered Sondex casing S2 (at right in upper photograph)

3.4.5 Deformation of Wall Face

In the section of wall containing only primary reinforcement, a bulge on the order of 4 inches (102 mm) developed during wall construction and extended over a fairly large distance (approximately 17 ft (5.2 m)). The maximum bulge found in the section of wall containing both primary and intermediate reinforcement was only 2.7 inches (69 mm) and was only prominent for a distance of approximately 4 ft (1.2 m). Plots showing the measured bulge displacements versus wall height are shown in Fig. 3.52.

It appears that the addition of intermediate reinforcement did reduce the bulging near the toe of the wall significantly. It should be noted, however, that neither of the bulges monitored at the two sections of wall was found to be indicative of a stability problem. Other solutions besides the use of intermediate reinforcement could have been used to eliminate the excessive toe bulging. Additional solutions include using a uniform gravel as fill near the wall face or providing temporary support of the wall face during compaction.

As with the Horizontal Extensometers, once the secondary stage concrete fascia panels were in place, measurements of the deformation of the wall face were no longer possible. Thus, no additional data will be available with respect to the deformation of the wall face.

3.4.6 Overall Deformation

Both the vertical and horizontal movements of the wall were monitored throughout the construction process. Based on survey monuments and the horizontal inclinometer at the base of the wall, during construction and primary consolidation the

wall settled approximately 18 in. (0.46 m). This was less consolidation than several other walls on the same project had experienced, but the magnitude of settlement is still significant. Results of the vertical extensometers show that the majority of this consolidation occurred in the two soft clay layers (shown in Fig. 3.1) located in the upper 22 ft (6.7 m) of the soil profile beneath the rubble backfill on which the wall was constructed.

Survey monuments showed that no measurable settlement occurred outside the wick drain zone, while monuments within the wick drain zone verified the settlements measured using the horizontal inclinometers and vertical extensometers.

Exaggerated wall deformations are shown in Fig. 3.53, to show the directions of movement. Wall settlement was approximately 20 inches (0.51 m) at the time the most recent measurements were taken. Horizontal movement at the base of the wall was 3.5 inches (89 mm). Rotation of the wall was on the order of 0.0035 horizontal feet per vertical foot. Each of these deformations will continue to be monitored over time to observe secondary consolidation effects.

3.5 CONCLUSIONS REGARDING INSTRUMENTATION AND WALL MONITORING

Overall, throughout construction and in the years following construction the wall is performing well. Results of this study show that there is adequate reinforcement within the wall, with stresses in the reinforcement being well below the allowable. The wall is internally stable, in spite of large deformations near the face of the wall. The wall is externally stable. The expected large primary settlement of the wall did occur, but little secondary settlement has taken place. There is no evidence of deep-seated wall

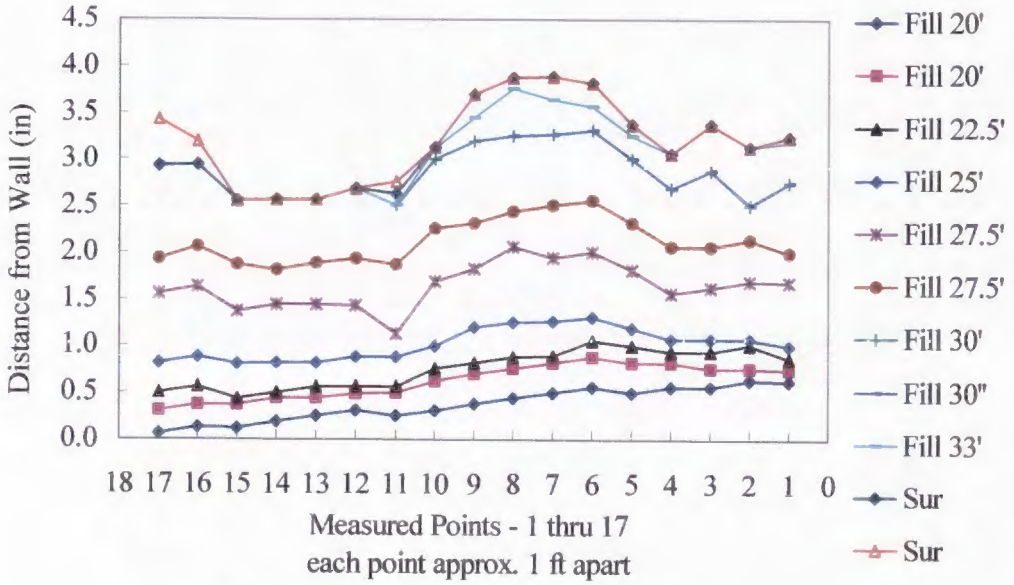

(a) Primary reinforced only section

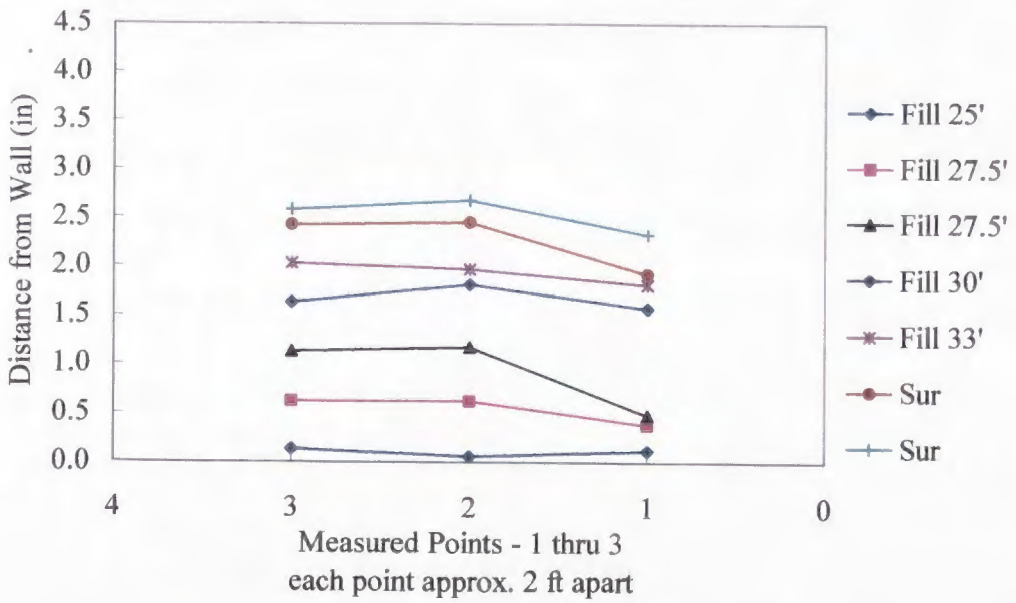

(b) Primary and intermediate reinforced section

Fig. 3.52 Plots of measured toe bulge deformations two sections of MSE wall

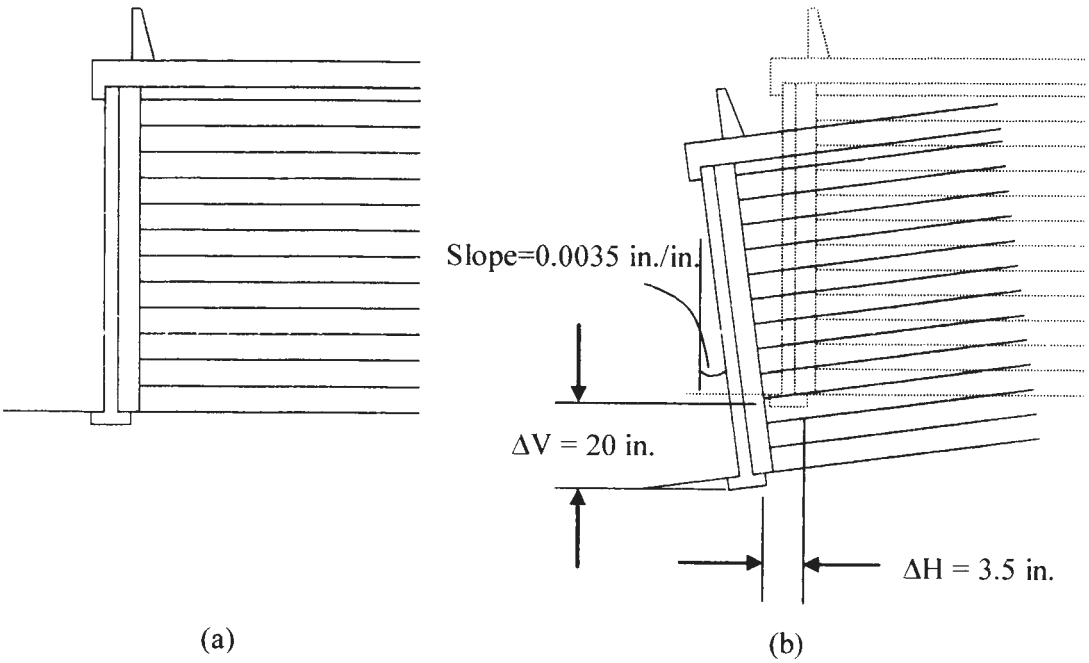

Fig. 3.53 Comparison of the undeformed wall (a) to an exaggeration of the deformed wall (b)

movement. Finally, a comparison of the section of wall containing only primary reinforcement to that containing primary and intermediate reinforcement led to the following conclusions:

- Intermediate reinforcement was not necessary for stability of the wall, since the section of wall not containing additional reinforcement was found to be both internally and externally stable,
- Intermediate reinforcement did decrease the deformations of the wall face in the lower portion of the wall, resolving the constructibility issues that had been a problem with previous walls not containing the intermediate reinforcement, and

- Intermediate reinforcement could be omitted without consequence if another method to control deformations of the wall face is utilized.

A number of steps were required to allow additional measurements to be taken and to protect the instrumentation for long-term monitoring. A number of challenges that were overcome were explained. Each of the instruments for which data was collected during construction was discussed to illustrate the post-construction changes in the wall and any changes in the ability to take such measurements. As noted, the instrumentation is now protected to allow future readings to take place, and the measurement changes in the years following construction were shown to be quite minimal.

CHAPTER 4

SOIL SAMPLING AND LABORATORY TESTING BACKGROUND

4.1 INTRODUCTION

The purpose of this portion of this research project was to evaluate the effects of sampling method on sample disturbance in the soft Bonneville clays that are common throughout northern Utah. In addition to assessing the effects of sample disturbance, which required extensive laboratory testing, laboratory tests were performed to determine the stress-strain and consolidation behavior of the foundation clays. These clays are lacustrine in nature, having been deposited during the time in which Lake Bonneville covered much of northwestern Utah and portions of southern Idaho and western Nevada.

Two drilling methods, rotary wash and hollow stem auger, were used to obtain samples for this work. Samples were obtained using a shelby tube sampler and two different piston samplers. Sample disturbance was evaluated using radiograph images of the specimens, and laboratory consolidation and triaxial tests.

Many soil samples were collected prior to this research as a part of the I-15 reconstruction project through Salt Lake City, Utah. Extensive testing of these samples was performed in order to characterize the foundation soils and predict the foundation response during the reconstruction project. However, most of these samples and the results of testing these samples were later rejected on the grounds of excessive disturbance of the samples (Bay et al., 2003b, Report No. UT-03.14). Funding was provided to Utah State University from the Utah Department of Transportation to

investigate the factors that affect sample disturbance in order to avoid such setbacks in future projects.

This chapter presents the procedures followed and the conclusions made with respect to sample disturbance of soft clay soils. The majority of the work contained in this chapter was performed by Jon C. Hagen and Todd M. Colocino. A complete version of their work is given in two reports submitted to UDOT (Bay et al., 2003b, Report No. UT-03.14 and Bay et al., 2003c, Report No. UT-03.13) and a master's thesis prepared by Hagen (2001). Todd Colocino has not yet submitted a final version of the thesis relating to his work.

The sampling equipment and the procedures followed in transporting samples to the laboratory are outlined. The procedure of using radiographs (x-rays) of the soil samples to choose the most appropriate specimens for testing is also explained. The consolidation and triaxial tests performed as a part of this investigation are summarized. A comparison of the extent of disturbance of samples obtained in shelby tubes and samples obtained in piston samplers is made. A comparison is also made between samples obtained using rotary wash and hollow stem auger drilling methods. A number of conclusions are made to provide guidelines for obtaining high-quality samples for use in laboratory testing.

4.2 SAMPLING EQUIPMENT USED AND PROCEDURES FOLLOWED

Three types of samplers were used on this research project. One sampler was a fixed-piston sampler designed at Utah State University and built specifically for this

project. The second sampler was a typical shelby tube (AW type) sampler. The third sampler was a free-piston sampler.

A cross section of the fixed-piston sampler design is shown in Fig. 4.1. The cone-shaped piston minimizes the amount of disturbed material that is allowed into the sample tube. The brass rod extends through the AW Head Assembly and up through the drill rods where it can be fixed in place using vice grips. Two photographs of the fixed-piston sampler are shown in Fig. 4.2.

When placing the tube in the borehole, the piston is at the end of the tube with the cone extended past the end of the tube. The rod and piston are locked into that position with vice grips that clamp the brass rod to the drill rod. When the piston is at the elevation where a sample is to be recovered, the vice grips are taken off. The piston rod and piston are then locked in place with a taut line from the drill rig that is connected to the eyebolt. The drill rod is then pushed while the piston remains in a fixed position relative to the ground. After the sample tube is pushed to the bottom of the sample interval, the piston rod and piston are fixed to the drill rod with vice grips to prevent the weight of the rods and piston from pushing the sample out of the tube. The sample is allowed to sit for a few minutes, after which the sample is recovered from the borehole.

A cross section of the shelby tube sampler is shown in Fig. 4.3. The ball check valve was carefully examined to make sure it was clean and functioning properly. Conventional shelby tube sampling procedures were followed in obtaining samples for testing (ASTM D 1587, 2000).

The free-piston sampler used for this project has a cone clamp that allows the piston to move upward but prevents downward movement. The piston is placed flush

with the end of the tube, after which the drill rods are attached. The sampler is then lowered to the bottom of the borehole. The piston is free to move up with respect to

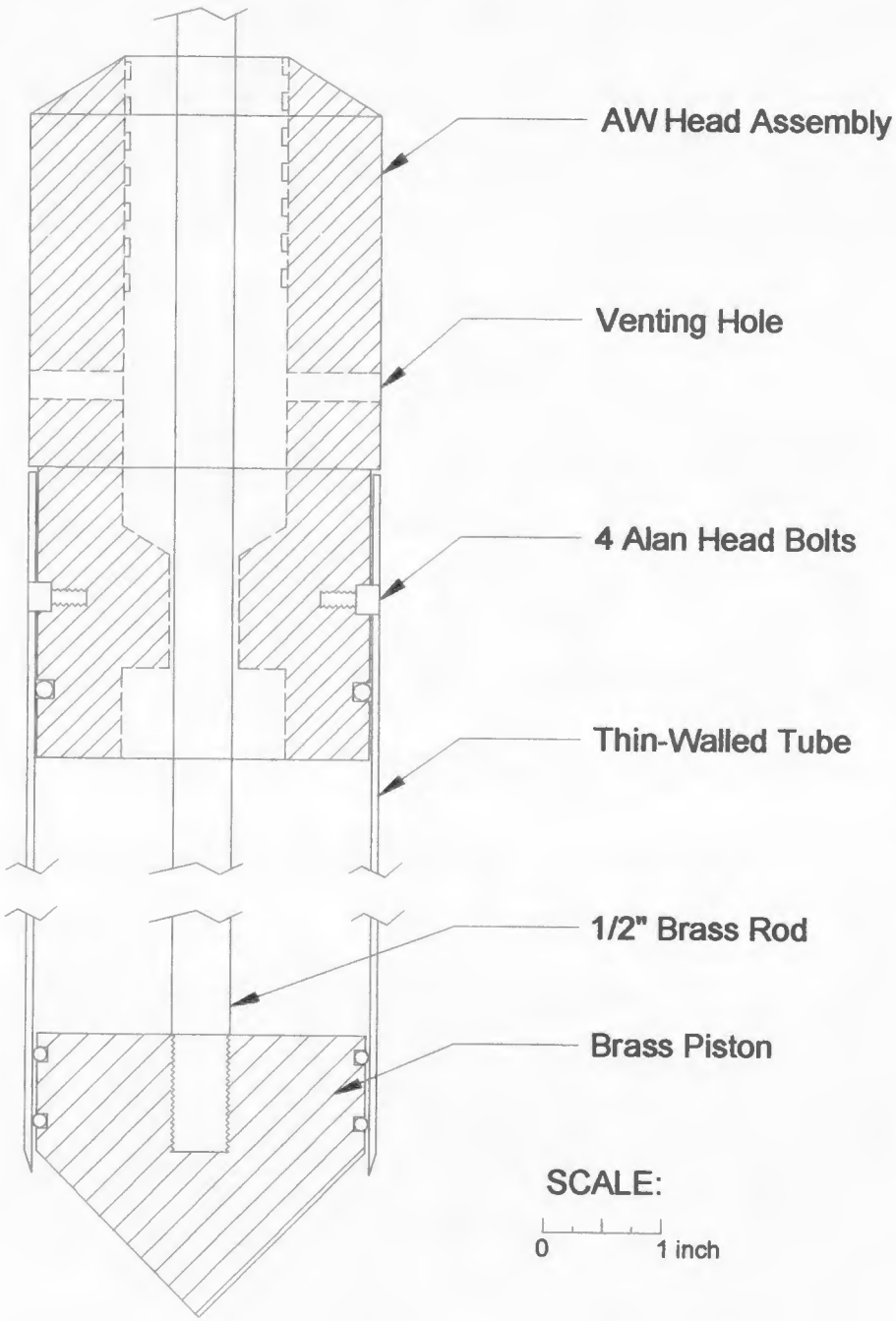

Fig. 4.1 Cross section of fixed piston sampler

Fig. 4.2 Photographs of fixed piston sampler

the tube if pressure from cuttings or slough in the bottom of the borehole provides enough force against the piston to overcome friction between the piston and the tube. The piston has a leather seal around the edges to provide a tight fit in the tube. When the

sample tube is pushed, the piston remains at the same elevation. When the tube is extracted, the piston is fixed with the cone clamp so that it does not move down with respect to the tube. This aids in sample recovery.

The drilling exploration for this study consisted of four boreholes. Two of the boreholes were drilled using rotary wash techniques and the other two were drilled with a continuous-flight hollow-stem auger. The sample tubes were pushed hydraulically at a constant rate of 0.1 ft/sec (30.5 mm/sec). The 30 in. (0.76 m) tubes were only pushed 24 in. (0.61 m) to ensure that the sample was not compressed at the upper end of the sample. All samples were allowed to sit for a minimum of 5 minutes in the hole before extraction to aid in recovery.

After each tube was extracted from the hole, the outside of the tube and the exposed inside surfaces of the tube were cleaned with a rag. A wax mixture of 50 percent bee's wax and 50 percent paraffin wax was melted in a pot over a gas flame at the site. At least 0.5 in. (12.7 mm) of hot wax was poured into the top of the tube as shown in Fig. 4.4. When it had cooled and hardened, the tube was turned over. A glazing tool was used to clean out 0.5 in. (12.7 mm) of soil from the bottom of the sample, and hot wax was poured in its place.

Problems occurred with the wax shrinking in the tube when it cooled. Different ratios of bee's wax to paraffin wax were tried, but the shrinking still occurred. It was determined that the cold weather was aggravating the shrinking problem. To get a better seal, the wax was worked into the spaces with a finger until a suitable bond with the tube was achieved.

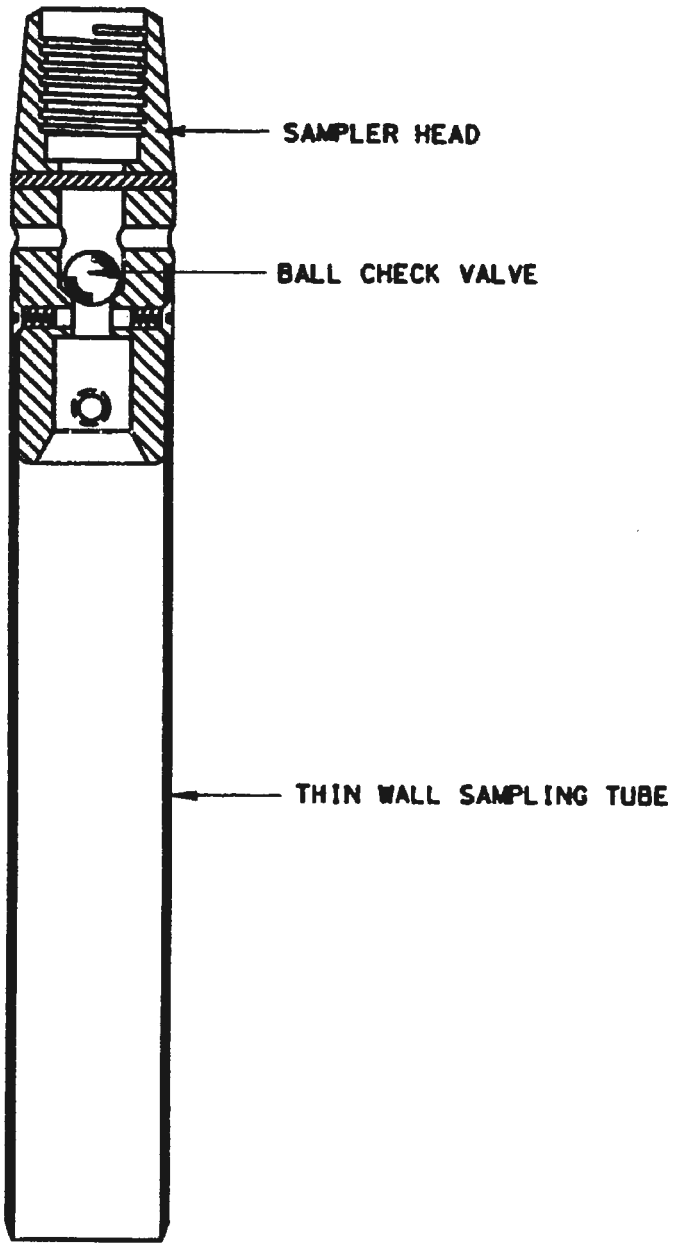

Fig. 4.3 Cross section of shelby tube sampler

When the wax was hard, caps were placed on the ends of the tube. The caps were taped with electrical tape, which provides a more airtight seal than duct tape. The caps were marked with a permanent marker "bottom" or "top" and included the boring label and sample depth.

Fig. 4.4 Photograph of wax preparation for a sample

After the sample tubes were sealed, they were placed upright in special padded boxes shown in Fig. 4.5 for transportation back to Utah State University. The boxes were tied to the bed of a pickup truck. Driving the 80-mile (129 km) trip was done cautiously and slowly in order to avoid unnecessary shocks and jolts. Sample tubes were stored upright in the laboratory at the university. Tubes stored in the lab were placed in a secure corner where they would not be bumped or knocked over until sample tubes were ready for further testing.

4.3 RADIOGRAPHY TECHINIQUES

Radiographs were extremely valuable in identifying fractures caused by sampling disturbance, which allowed the most appropriate specimens to be obtained for laboratory testing. Each sample tube collected from the exploration site was x-rayed using the machine in the Industrial Technology and Education building. The tubes were x-rayed in three 10-inch (0.25 m) segments in order to cover the entire tube. The intent of the radiographs (x-rays) was to characterize the soil and locate visible disturbance in the samples. A piece of steel with slits cut in it was laid alongside the sample tube as it was x-rayed in order to precisely locate various features found within the tube once the radiograph was developed. Additional details as to the radiograph process can be found in Hagen (2001).

The developing process for the radiographs is similar to the process used to develop photographs. The exposed film is taken into a darkroom illuminated with only red light, placed in tanks containing the developing chemical for the required amount of time, rinsed with water, and soaked in a fixer chemical to prolong the life of the x-ray. Some additional steps are taken, but eventually the radiograph is hung to dry, after which it can be evaluated by placing the image on a light table.

Close inspection of the images allowed sand, gravel, and clay to be distinguished. The more closely packed the specimen, the lighter it appears in the negative. Sand shows up darker than clay, while clay is darker than gravel. The top of the tube, which contains no sample, will be completely black, while the wax seal at the top and bottom of the sample is slightly lighter.

Fig. 6 shows a number of the radiographs from this project. As seen in Fig. 6a, the slough at the top of the sample tube is apparent, with obvious disturbance. Fig. 6b shows a number of the cracks from sample disturbance that become apparent from the radiograph image. Fig. 6c shows a sample that is essentially undisturbed, for comparison.

Fig. 4.5 Photograph of sample transport boxes

Other features that were recognized in other radiographs not included here were roots running vertically down the sample, sand and clay layers at significant angles from horizontal, etc. Such features are important to avoid when obtaining test specimens, especially for such tests as consolidation tests and triaxial shear tests.

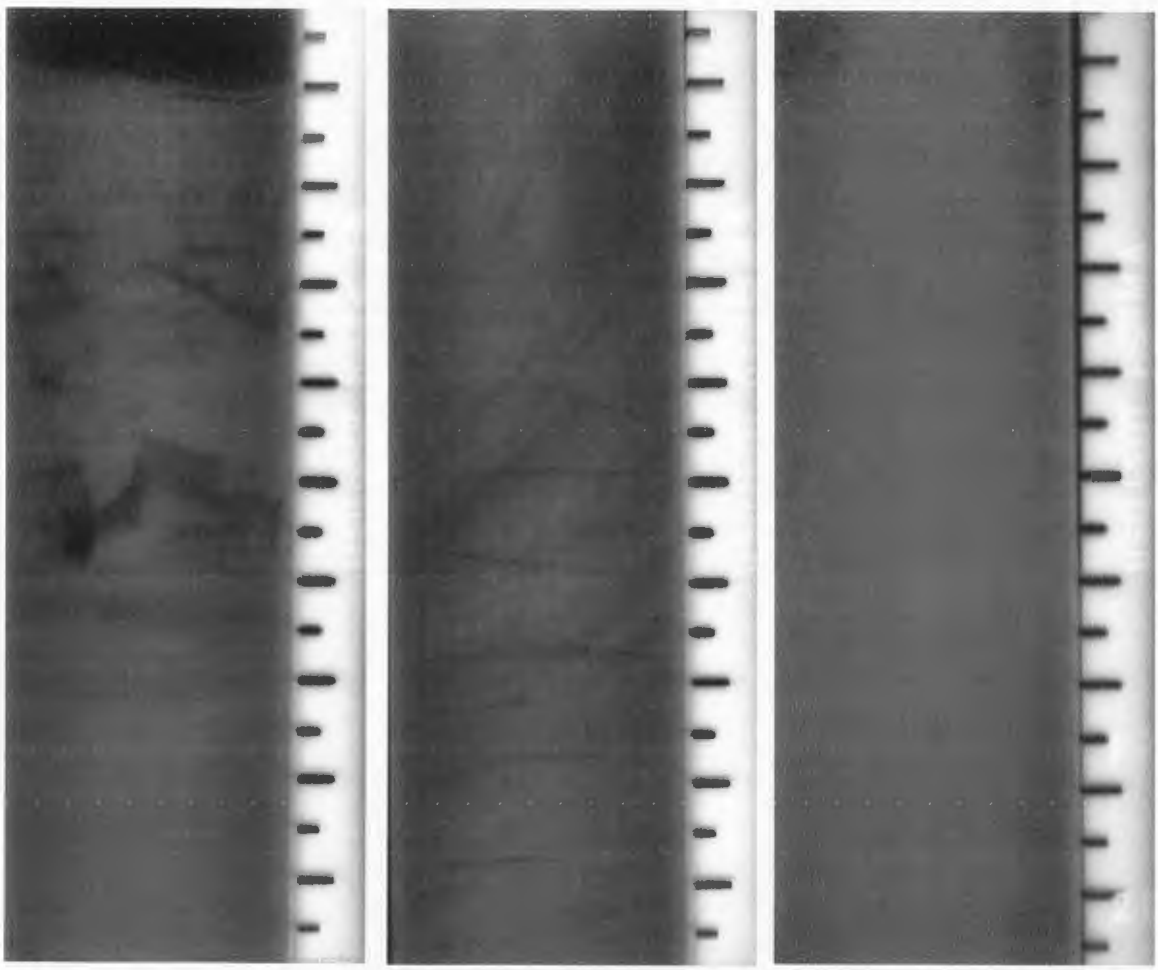

a) Slough b) Disturbance Cracking c) Minimal Disturbance

Fig. 4.6 Example radiograph images from this project

4.4 CRS CONSOLIDATION TESTING

After the sample tube radiographs were carefully examined and the most representative soil specimens selected, the sample tubes were cut at the desired locations using a pipe cutter. Once the tube was cut, a wire saw was used to cut through the sample. The tube was then cut lengthwise using a band saw. A wire saw was then slipped along the interface between the tube and the soil, allowing the sample to easily slip out of the tube.

Once the specimen was removed from the sample tube, it was carefully trimmed into a stainless steel consolidation ring with a wire-trimming tool. The consolidation ring has a sharp edge on one end that is advanced into the soil specimen a small amount by applying slight pressure to it. The excess soil was trimmed after each advance. A small amount of grease was applied to the inside of the ring to reduce friction between the ring and the soil. Once the soil was trimmed into the ring a sufficient distance, both ends were trimmed using a wire saw.

The ring and soil were placed in a loading ring between porous stones. Filter paper was placed between the stones and the soil to prevent migration of fines into the stones. The loading ring was placed in an acrylic cell with a frictionless piston on the top. The piston comes in contact with a 2.5 in. (63.5 mm) diameter acrylic cylinder placed over the porous stone, and a seating load placed on the sample until 0.2 percent strain was attained.

The cell was then filled with de-aired water and backpressure saturation was performed to ensure sample saturation. The strain was held constant throughout the backpressure saturation process. Once sample saturation was achieved, sample testing

began using a Constant Rate of Strain (CRS) consolidation test. Loading was performed at a rate of 4.5 percent per hour. This rate prevented the pore pressure ratio (pore pressure divided by total vertical stress) from exceeding 30 percent, the upper bound recommended by ASTM (D 4186, 1998).

A load cell, several pressure transducers, and a linear voltage displacement transducer (LVDT) allowed measurements of load, pressure, and displacement to be made, respectively. These measurements were recorded every minute throughout the test. The data were opened in a spreadsheet for further analysis, and the results used to compare the extent of sample disturbance as given in the following sections.

4.5 COMPARISON OF SAMPLER TYPE

Three tools were used to make a comparison of the extent of sample disturbance between the samples acquired using shelby tubes and those acquired using piston samplers. The first tool was a comparison of the average distance between fractures in the samples as determined from the radiograph images. The more fractures occurring in a given sample, the shorter the average distance between fractures, and the more disturbed the sample was determined to be. The steel scale set alongside the sample tubes during the x-ray process was used to determine the distances between fractures for each of the sample tubes. These distances were tabulated, and the average distance between fractures calculated.

The piston sampler tubes had a much greater average distance between fractures (19.3 in. (490 mm)) than the shelby tubes (2.5 in. (63.5 mm)), and the piston sampler tubes also had a much higher percentage of tubes with no visible fractures (62%) than

Table 4.1 Summary of Average Distance Between Fractures for Sample Disturbance Evaluation Comparing Shelby Tube and Piston Samplers

Sampler	Avg. distance between fractures (in.)	% of tubes with no fractures
Shelby tube	2.5	32
Piston	19.3	62

the shelby tube results (32%). No significant difference was found between the two types of piston samplers. These results are summarized in Table 4.1. From these results, it appears that the piston samplers provided significantly less disturbed samples than the shelby tube samples.

The second tool in evaluating disturbance was to compare the minimum radius of the consolidation curve, which is used in estimating the maximum past pressure of the soil sample. The smaller the radius, the less disturbed the sample is considered to be. Fig. 4.7 shows several consolidation curves for different specimens tested and the significant differences in radii for the various samples. The curves with the most distinct break in the curve and the smallest radii are the least disturbed, while the more rounded curves with larger radii are significantly disturbed.

A spiral was constructed for use in measuring the radii of the curve for each of the samples tested, and these radii were tabulated for each of the CRS tests performed. Fig. 4.8 shows a histogram comparing the results of the piston samples to the shelby tube samples. Approximately 90 percent of the piston samples tested had radii less than 2 in. (51 mm), while only 60 percent of the shelby tube samples had radii less than 2 in. (51

mm). From these results, it appears that the shelby tube samples are more disturbed than those obtained from piston samplers.

Finally, a plot of the unconfined compression test results shows that the samples obtained using piston samplers had higher initial moduli (E_{50}) values than the shelby tube samples. The plot of these tests is shown in Fig. 4.9. Having higher initial moduli is also indicative of less sample disturbance. Thus, the piston samples are again determined to be less disturbed than the shelby tube samples.

In summary, each of the three tools used to compare the degree of sample disturbance between shelby tube samples and piston samples showed that piston samplers yield less-disturbed samples than the shelby tube samples. In comparing the two, the average distance between fractures was much higher, the average radii near the point of maximum past pressure on the consolidation curves was much smaller, and the initial modulus (E_{50}) was higher for the piston samples, each suggesting that the piston samples were less disturbed than samples obtained using a shelby tube.

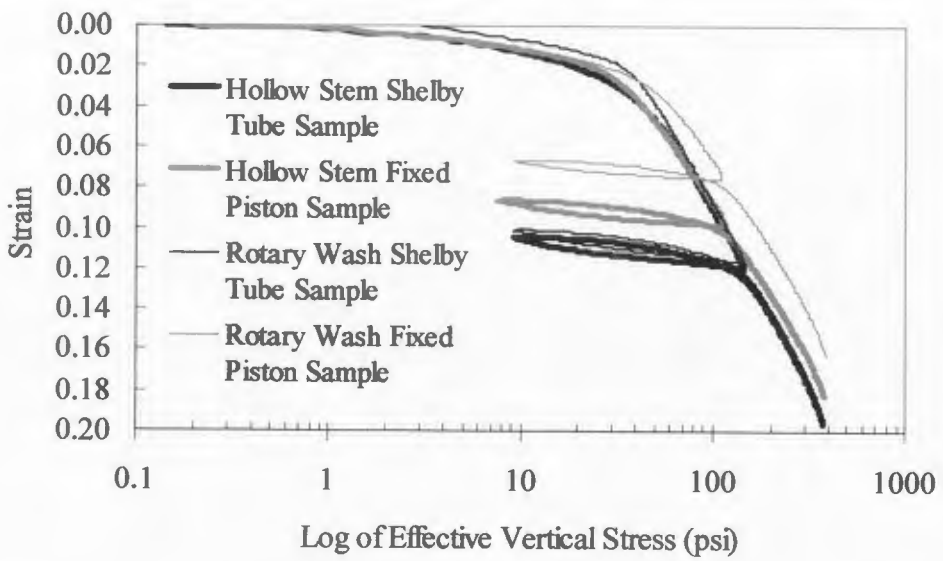

Fig. 4.7 Typical consolidation curves for samples tested

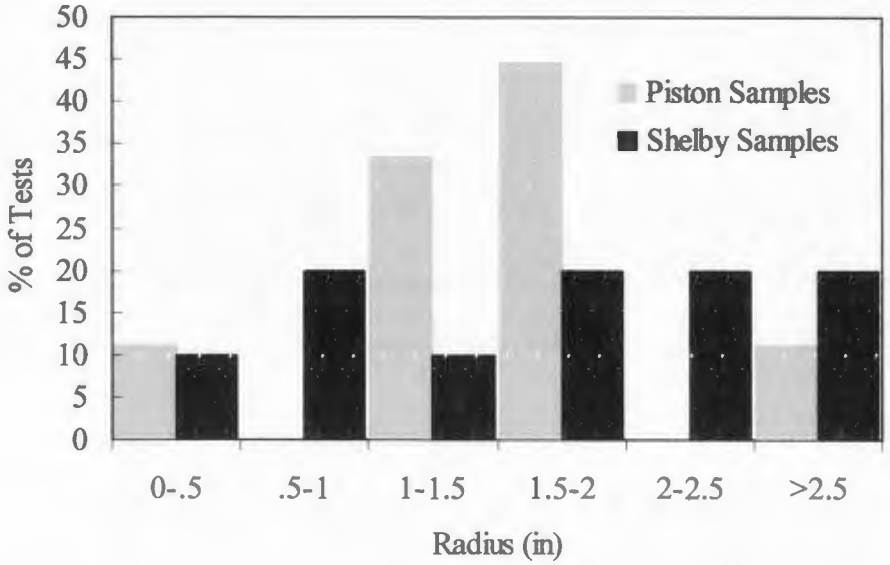

Fig. 4.8 Comparison of piston sample and shelby tube sample consolidation results

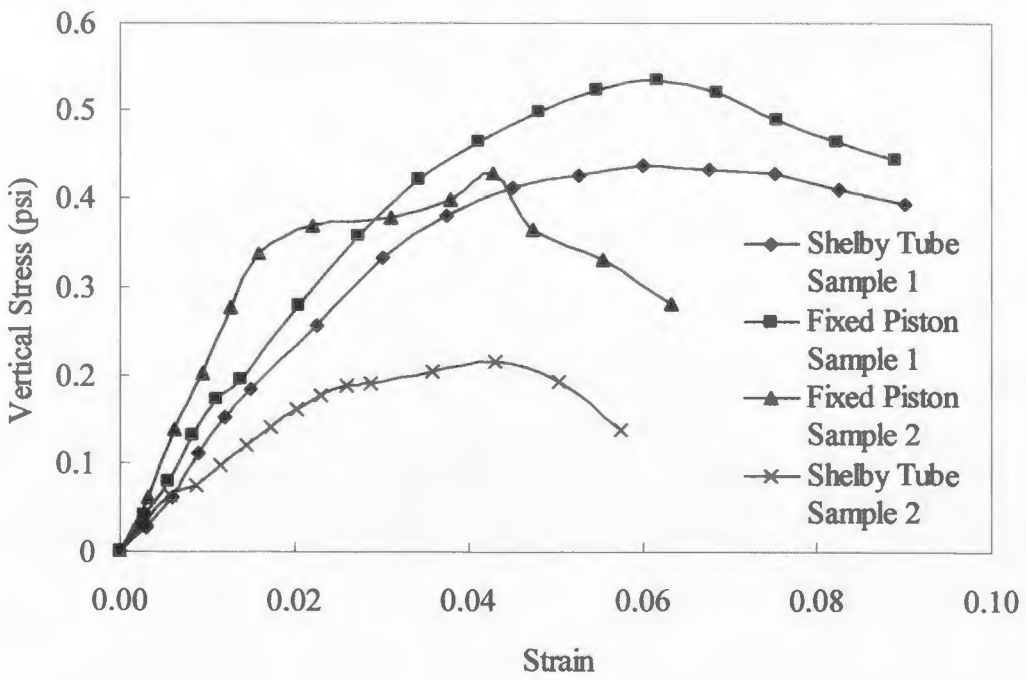

Fig. 4.9 Comparison of piston sample and shelby tube sample unconfined compression test results

4.6 COMPARISON OF DRILLING METHODS

The same three criteria were examined in order to compare the rotary wash drilling method to the hollow stem augering method. Again, the average distance between fractures was compared, the radii of the consolidation curves were evaluated, and the initial moduli (E_{50}) from unconfined compression tests were compared.

One important note must be addressed before the results are discussed. The driller helping with this research was very highly recommended due to the extreme care used in obtaining samples. When performing the hollow stem augering, slow rotation of the auger was maintained throughout the drilling process. A slow advance was also sustained, and care was taken to preserve the water level at a desired point during the augering process. Such care is not always taken when using a hollow stem auger, though such practice should be required.

From the results of the x-ray evaluation of the average distance between fractures, no significant conclusion can be made as to which drilling method yields less disturbed samples. As shown in Table 4.2, the average distance between fractures for the hollow stem auger was 7.3 in. (185 mm), compared to 3.0 in. (76 mm) for the rotary wash samples. From this aspect the hollow stem auger appears to yield less disturbed samples than the rotary wash method. However, it is also noted that 52 percent of the rotary wash samples had no visible fractures, while only 41 percent of the hollow stem auger samples had no visible fractures. This would suggest that the rotary wash method may yield less-disturbed samples. Thus, the results of the radiograph evaluation in comparing the two drilling methods are inconclusive.

Table 4.2 Summary of Average Distance Between Fractures for Sample Disturbance Evaluation Comparing Rotary Wash and Hollow Stem Auger Drilling Methods

Drilling method	Avg. distance between fractures (in.)	% of tubes with no fractures
Rotary wash	3.0	52
Hollow stem auger	7.3	41

A more definite conclusion was made with respect to a comparison of the radii of the consolidation curve for the two drilling methods. Fig. 4.10 shows a histogram containing the results of this comparison. Approximately 88 percent of the tests performed on rotary wash samples had radii less than 2 in. (51 mm), while 65 percent of the tests performed on hollow stem auger samples had radii less than 2 in. (51 mm). This would suggest that the rotary wash samples are slightly less disturbed than the hollow stem auger samples. However, this deduction is still fairly inconclusive.

A final comparison of the two drilling methods is again made in comparing the unconfined compression test results. The plot of these tests is shown in Fig. 4.11. The samples obtained using the hollow stem auger had an average initial modulus (E_{50}) value almost identical to the average initial modulus obtained from the rotary wash samples.

From these results, no conclusion can be made as to whether one drilling method provides less sample disturbance than the other.

In summary, there appears to be very little difference in the extent of sample disturbance when comparing the hollow stem auger drilling method to the rotary wash method, especially when extreme care is used in performing the hollow stem augering. No definite conclusion can be made in comparing the average distance between fractures

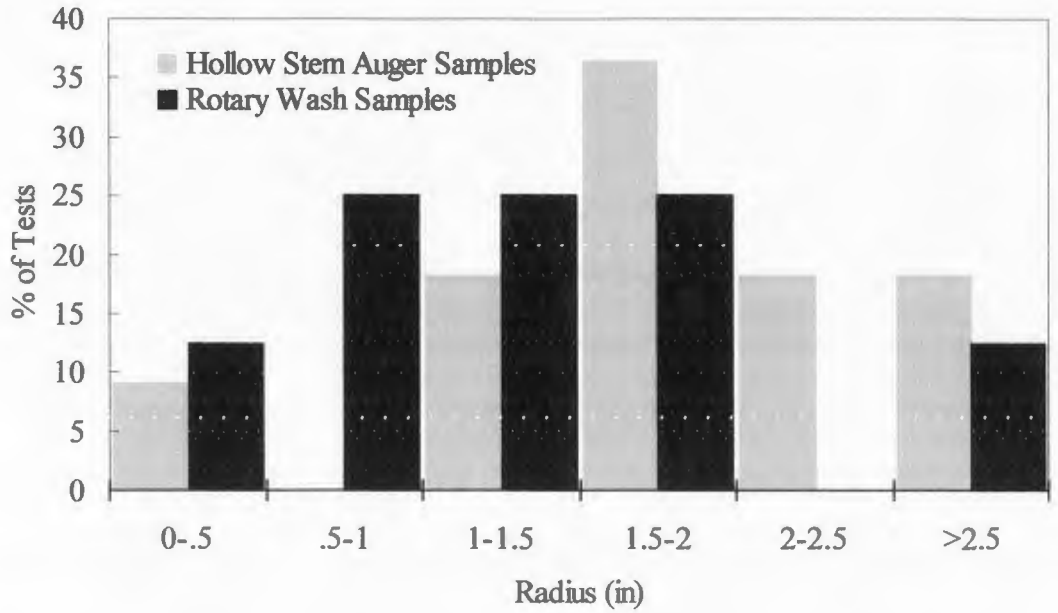

Fig. 4.10 Comparison of hollow stem auger and rotary wash sample consolidation results

or in comparing the initial moduli obtained from the unconfined compression tests. Comparing the radii of the consolidation tests showed that the rotary wash samples are slightly less disturbed than the hollow stem auger samples.

4.7 CONCLUSIONS REGARDING SOIL SAMPLING AND TESTING METHODS

Comparisons of piston and shelby tube samples indicate that piston samples are less disturbed than shelby tube samples. X-rays show significantly fewer fractures in piston samples than shelby tube samples. The average radius of the consolidation curves at the points of maximum past pressure was less (indicating a sharper break between reconsolidation and virgin consolidation) for the piston samples than the shelby tube samples, resulting in less uncertainty in maximum past pressure predictions.

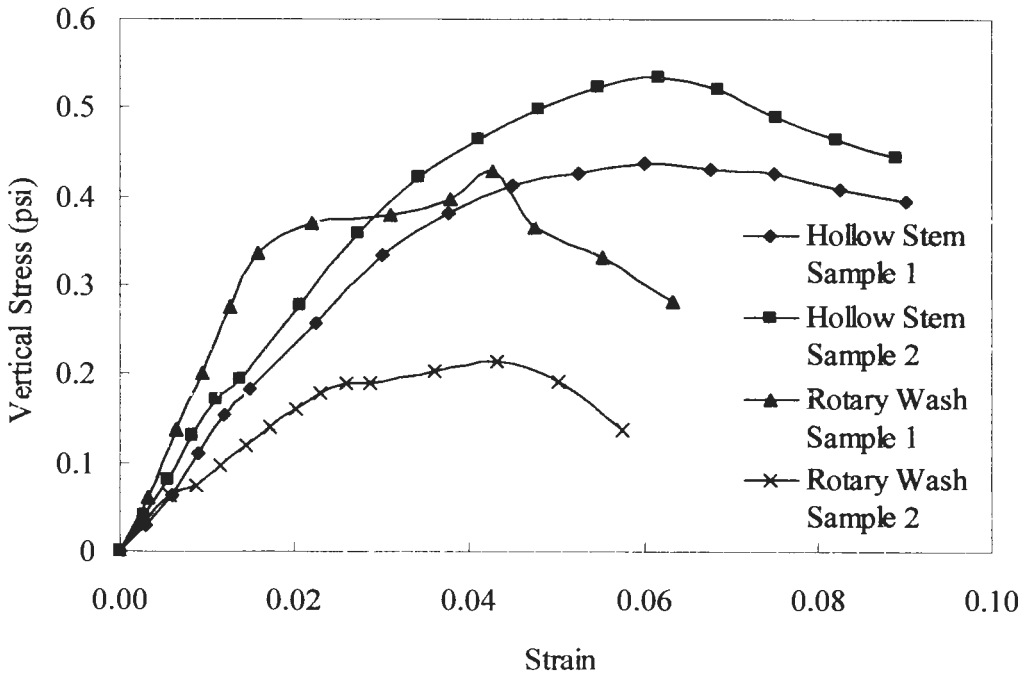

Fig. 4.11 Comparison of hollow stem auger versus rotary wash drilling method from unconfined compression test results

Interestingly, there was no significant difference in maximum past pressure or $C_{c\varepsilon}$ between the piston and the shelby tube samples. This may be because the radiograph images were used to select portions of the sample to use in consolidation tests. Thus, themost disturbed portions of the samples were not tested. The piston samples also exhibited higher initial moduli (E_{50}) values than the shelby tube samples in the unconfined compression test. This is also indicative of less sample disturbance. The shape of the consolidation curves for piston samples are generally better than those of shelby tube samples with the same drilling method.

The differences in sample disturbance were not as recognizable or significant between the two drilling methods. The quantities of fractures and cracks identified in

radiograph images were similar for the two drilling methods. The CRS tests show slightly less disturbance in the rotary wash samples than the hollow stem auger samples. The average radius of the consolidation curves at the points of maximum past pressure was somewhat lower for the rotary wash samples than the hollow stem auger samples, resulting in less uncertainty in maximum past pressure for the rotary wash samples. Again, there was no significant difference in the average maximum past pressure or $C_{c\varepsilon}$ between rotary wash and hollow stem auger samples.

Based upon this research, several recommendations can be made as to methods that should be employed in drilling and sampling to minimize the effects of sample disturbance in Bonneville clays or similar soft clays. These are:

- Piston samplers along with thin-walled sampling tubes should be used rather than shelby tube samplers for obtaining specimens for consolidation, triaxial, and other critical geotechnical tests.
- It was observed that fixed piston and free piston samplers obtain samples of similar high quality.
- Radiograph (x-ray) images of the soil specimens provide a powerful tool for assessing sample disturbance, selecting the least disturbed portions of the sample for critical tests, and identifying locations of sand lenses in soft clay samples.
- Very careful rotary wash drilling methods may result in slightly less sample disturbance than hollow stem auger drilling, but the results were inconclusive.

- When hollow stem auger drilling is used, the auger should be advanced slowly using slow rotation (as was done in this work) to minimize disturbance to the surrounding soil.

- Sample recovery can be increased by waiting a period of several minutes after pushing a sample tube before attempting to extract the sample from the ground.

CHAPTER 5

MECHANICALLY STABLIZED EARTH WALL FINITE ELEMENT MODEL

5.1 INTRODUCTION

This chapter is the culmination of extensive research into the behavior of an MSE wall at I-15 and 3600 South in Salt Lake City, Utah. The wall is about 30 ft (9.1 m) tall and is constructed on a compressible, soft clay foundation. This project has included extensive instrumentation and monitoring of stresses and deformations in the wall and its foundation, a study of the effects of drilling and sampling method on disturbance of samples, and extensive laboratory testing to determine strength and deformation properties of soils at the site. All of this work has been used to develop and calibrate an analytical model of the MSE wall. This chapter describes this analytical model.

The analytical model of this wall is a valuable and powerful tool to understand the behavior of tall MSE walls on compressible foundations. Using such a model, the effects of pore pressure dissipation during construction can be evaluated. This allows for accurate evaluation of the stability of the embankment during construction and long-term for any construction sequence. The model can be used to evaluate soil reinforcement interaction and to evaluate different reinforcement configurations.

This chapter contains discussions of the soil model that was developed for Bonneville clay, a comparison between measured and calculated deformations in the wall foundation, the time-settlement behavior of the wall, soil-reinforcement interactions, and

stability evaluations, as well as a comparison of traditional slope stability analysis results to the finite element results obtained from this model.

5.2 SOIL MODEL FOR BONNEVILLE CLAY

One of the critical components of a model for the MSE wall is an appropriate constitutive model for the soil. A constitutive soil model must properly represent the soil's shear strength, dilative behavior, compressibility, and time dependent behavior. Most of the deformations that occurred at the MSE wall at I-15 and 3600 South occurred in the soft Bonneville clays underlying the site. Therefore, the critical soil model for this site is the Bonneville clay model. Values of parameters used to model the soft Bonneville clay were obtained from a combination of laboratory tests on undisturbed soil specimens and matching analytical model outputs to field measurements.

5.2.1 The Hardening Soil Model

The soil model used in this study is the Plaxis hardening soil model (Plaxis, 2001). This effective stress model accounts for the effects of confinement and stress history on the soil moduli. It uses a hyperbolic stress-strain relationship for shear deformations. Ultimate shear strengths are characterized using a Mohr-Coulomb failure envelope. It utilizes the associated flow rule to predict plastic deformations, and a dilation angle to predict the volume change associated with plastic deformations.

The hardening soil model is probably the most comprehensive soil model available today in commercial modeling software. However, it has some deficiencies. The shear strength of soil is partially dependent on the soil's stress history. This cannot be modeled using a Mohr-Coulomb strength envelope. This is especially a problem for

soils that are initially over-consolidated, but loaded beyond their maximum past pressure. This weakness can be partially overcome by using an appropriate failure envelope for the range of stresses the soil will experience.

Real soils exhibit dilative (or contractive) behavior at intermediate strain levels. The hardening soil model does not induce dilative behavior until there are plastic strains in the soil. This means that pore pressures are not induced in soils during undrained loading until the soil is at failure. This leads to small errors in predicting undrained strength in dilative soils, but can lead to large over-predictions of undrained shear strength in contractive soils. One adjustment to compensate for this problem is to use lower strength parameters when modeling the undrained strength of contractive soils.

Time dependent consolidation in soil is often divided into primary and secondary consolidation. The time rate of settlement due to primary consolidation is inversely proportional to the soil modulus and permeability, and proportional to the square of the length of the drainage path. The rate of secondary consolidation is controlled by the viscous properties of the soil. The hardening soil model does an excellent job of modeling primary consolidation, but does not account for any secondary consolidation.

Table 5.1 shows the parameters used in the Plaxis hardening soil model. The equation given is used to determine the modulus values as a function of confining pressure, σ'.

5.2.2 Laboratory Consolidation Measurements

Initial estimates of consolidation parameters for the foundation soils at the site were obtained from constant rate of strain (CRS) consolidation tests performed on

Table 5.1 Plaxis Hardening Soil Parameters

Hardening Soil Parameter	Units	Description
γ	lb/ft^3	Total unit weight
k_x	ft/day	Horizontal permeability
k_y	ft/day	Vertical permeability
ϕ'	degrees	Effective friction angle
c'	lb/ft^2	Effective cohesion
ψ	degrees	Dilation angle
E_{50}^{ref}	lb/ft^2	Reference Young's modulus
E_{oed}^{ref}	lb/ft^2	Reference constrained modulus
E_{ur}^{ref}	lb/ft^2	Reference unload/reload modulus
ν_{ur}		Unload/reload Poisson's ratio
p_{ref}	lb/ft^2	Reference stress
m		Stress exponent

$$E = E^{ref}\left(\frac{\sigma'}{p_{ref}}\right)^m \qquad (1)$$

Where E is E_{50}, E_{oed}, or E_{ur},

and E^{ref} is E_{50}^{ref}, E_{oed}^{ref}, or, E_{ur}^{ref},

σ' is effective vertical stress, and

$m \approx 1.0$ for clays, and $m \approx 0.5$ for granular soils.

undisturbed soil samples obtained from the site. Results from all of these consolidation tests are presented in Report No. UT-03.14, "Factors Affecting Sample Disturbance in Bonneville Clays," (Bay et al., 2003b) and in the thesis prepared by Jon Hagen (Hagen,

2001). Fig. 5.1a. is a consolidation curve from a typical CRS test on one of the more compressible clays.

The hardening soil model uses a stress dependent modulus rather than a consolidation coefficient to model the consolidation behavior, therefore, the modulus versus effective stress is plotted in Fig. 5.1b. In Fig. 5.1b the virgin loading is represented by the low, linearly increasing modulus values. The higher modulus values represent the reload and unload behavior. Fig. 5.2 shows the consolidation and modulus plots from a typical soil exhibiting lower compressibility.

Tables 5.2, 5.3, 5.4, and 5.5 contain summaries of all of the consolidation results from samples obtained from the four boreholes at the site. The average E_{oed}^{ref} for the top 16 ft (4.9 m) at the site is 26,900 psf (1,288 kPa), and for 16-36 ft (4.9-11.0 m) is 30,800 psf (1,475 kPa). These results are summarized from work done by Hagen (2001).

5.2.3 Maximum Past Effective Vertical Stress

Another important parameter in predicting consolidation behavior is the maximum past effective vertical stress. These values were also determined from CRS testing, and are tabulated in Table 5.2 through Table 5.5. The in situ effective vertical stress and the measured maximum past effective vertical stress are plotted in Fig. 5.3. As is usually the case, there is considerable scatter in the maximum past effective vertical stress values. The site has a desiccated surface layer with high maximum past pressure, and below the desiccated layer the maximum past pressure roughly parallels the in situ effective vertical stress. The maximum past effective vertical stress used in the Plaxis model is also plotted in Fig. 5.3.

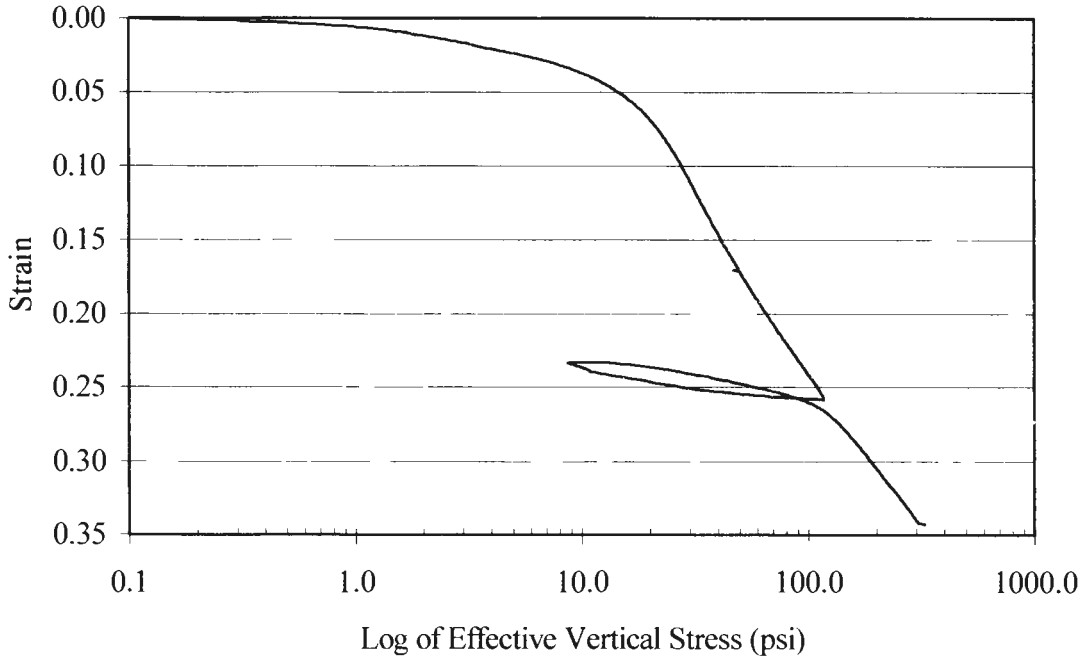

a) Consolidation Curve

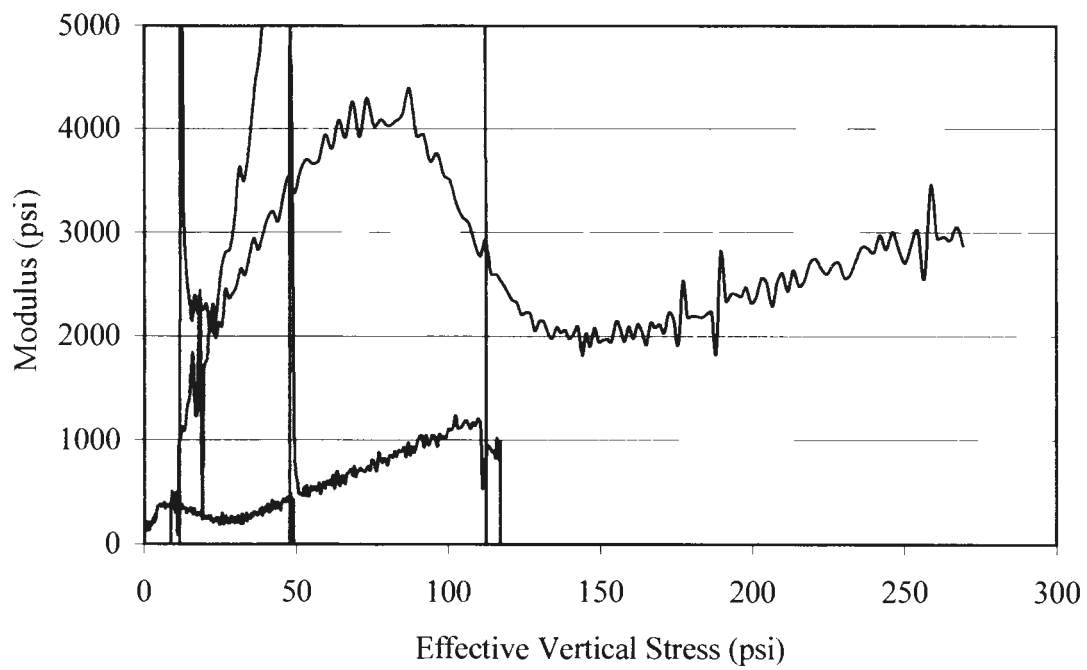

b) Modulus Curve

Fig. 5.1 Consolidation and modulus curve from boring HF-2 at 17-19 ft

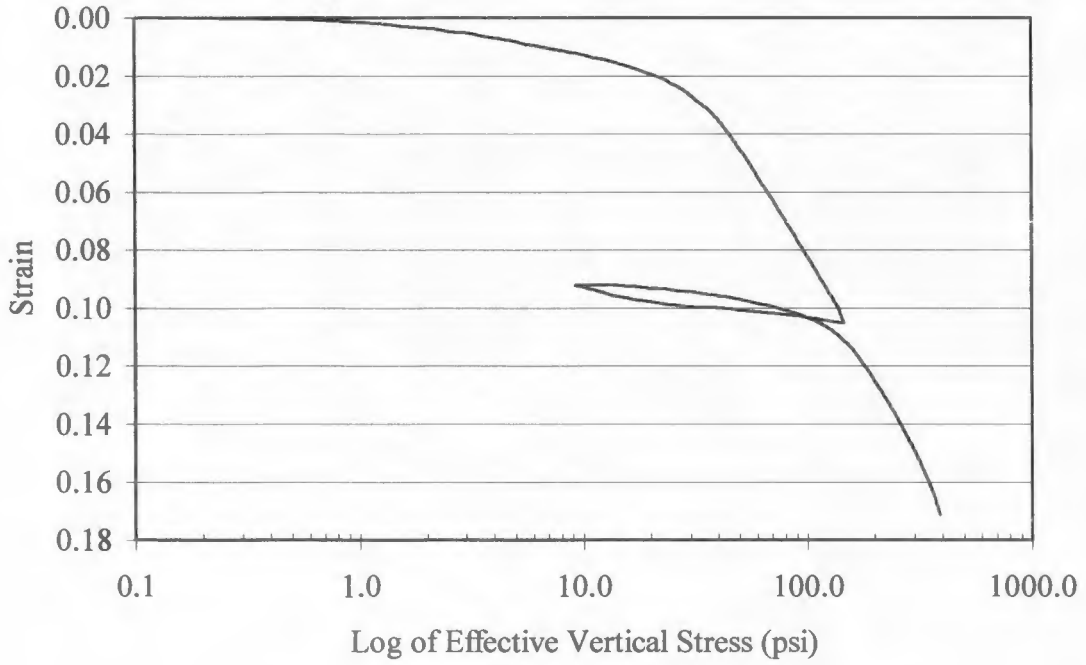

a) Consolidation Curve

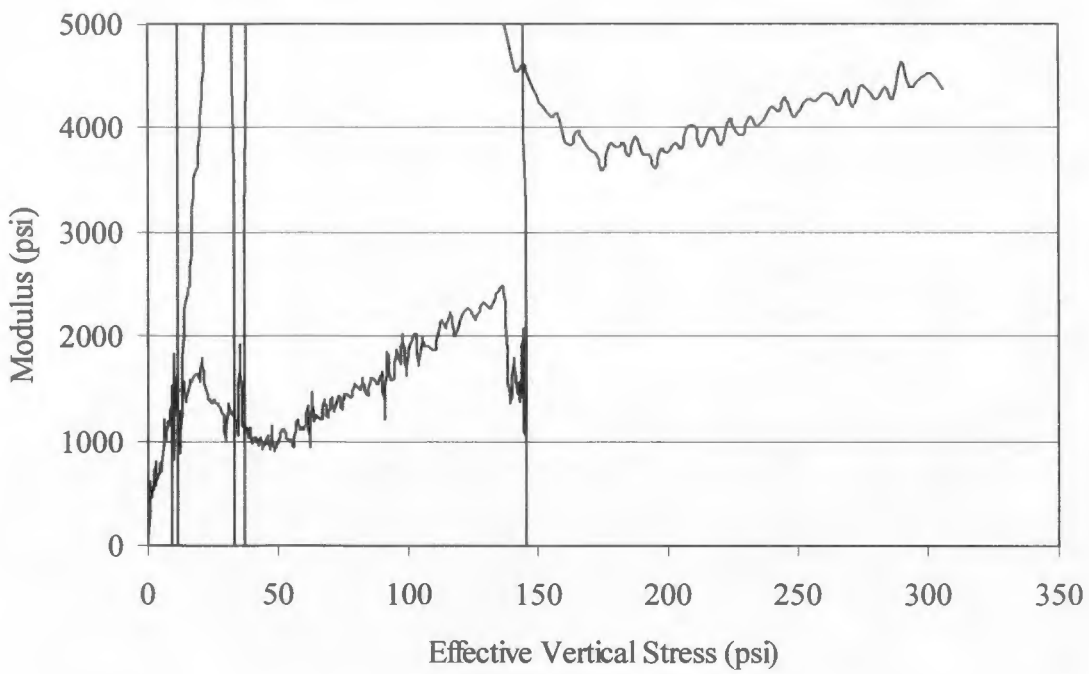

b) Modulus Curve

Fig. 5.2 Consolidation and modulus curves from boring RF-4 at 24.5-26.5 ft

Table 5.2 Results of CRS Consolidation Test on Soil Samples from Borehole HS-1

Depth (ft)	σ'_{vo} (psf)	σ'_{p} (psf)	E^{ref}_{oed} (psf)	$C_{c,\varepsilon}$	W_n %	PL %	LL %	% Fines	Grain size %<2μm
9.5-11.5	1080			0.135		19	32		31
12-14	1440	3312	25474	0.134		18	27		38
14.5-16.5	1555	5616	28606	0.162	31.0	23	34	99	35
17-19	1699	3456	19001	0.500	58.0	26	36	97	35
19.5-21.5	1786								
22-24	1958	4320	30485	0.139	36.4	23	32		33
24.5-26.5	2074	4464	36122	0.129	26.4	18	22	82	20
27-29	2261	4752	40925	0.112				86	19
29.5-31.5									
32-34									
34.5-36.5	2750							74	23

Table 5.3 Results of CRS Consolidation Test on Soil Samples from Borehole HF-2

Depth (ft)	σ'_{vo} (psf)	σ'_{p} (psf)	E^{ref}_{oed} (psf)	$C_{c,\varepsilon}$	W_n %	PL %	LL %	% Fines	Grain size %<2μm
9.5-11.5	1080	7632	24012	0.156	30.3	22	32	99	40
12-14	1440	4320	27979	0.159	33.2	22	30	98	20
14.5-16.5	1555	5040	30067	0.132	27.8	19	31	99	30
17-19	1699	2880	25056	0.269	48.7	24	37	98	38
19.5-21.5									
22-24									
24.5-26.5									
27-29									
29.5-31.5									
32-34									
34.5-36.5									

Table 5.4 Results of CRS Consolidation Test on Soil Samples from Borehole RS-3

Depth (ft)	σ'_{vo} (psf)	σ'_p (psf)	E^{ref}_{oed} (psf)	$C_{c,\varepsilon}$	W_n %	PL %	LL %	% Fines	Grain size %<2μm
9.5-11.5	1080								
12-14	1440	5328	28606	0.138	33.4	23	32	99	38
14.5-16.5	1555	6192	28606	0.170	32.6	23	33	99	30
17-19	1699	3168	25056	0.419	67.0			94	34
19.5-21.5	1786								
22-24	1958								
24.5-26.5	2074								
27-29	2261								
29.5-31.5									
32-34									
34.5-36.5	2750				21.3	19	23	89	32

Table 5.5 Results of CRS Consolidation Test on Soil Samples from Borehole RF-4

Depth (ft)	σ'_{vo} (psf)	σ'_p (psf)	E^{ref}_{oed} (psf)	$C_{c,\varepsilon}$	W_n %	PL %	LL %	% Fines	Grain size %<2μm
9.5-11.5	1080								
12-14	1440	6480	26309	0.136					
14.5-16.5	1555	7920	22133	0.129	28.3	24	32	98	40
17-19	1699	4032	27144	0.490	58.4	23	47	99	37
19.5-21.5	1786								
22-24	1958	3024	40507	0.093	32.3	18	25	77	30
24.5-26.5	2074	5040	32573	0.126	27.1	17	26	94	39
27-29	2261								
29.5-31.5									
32-34									
34.5-36.5	2750								

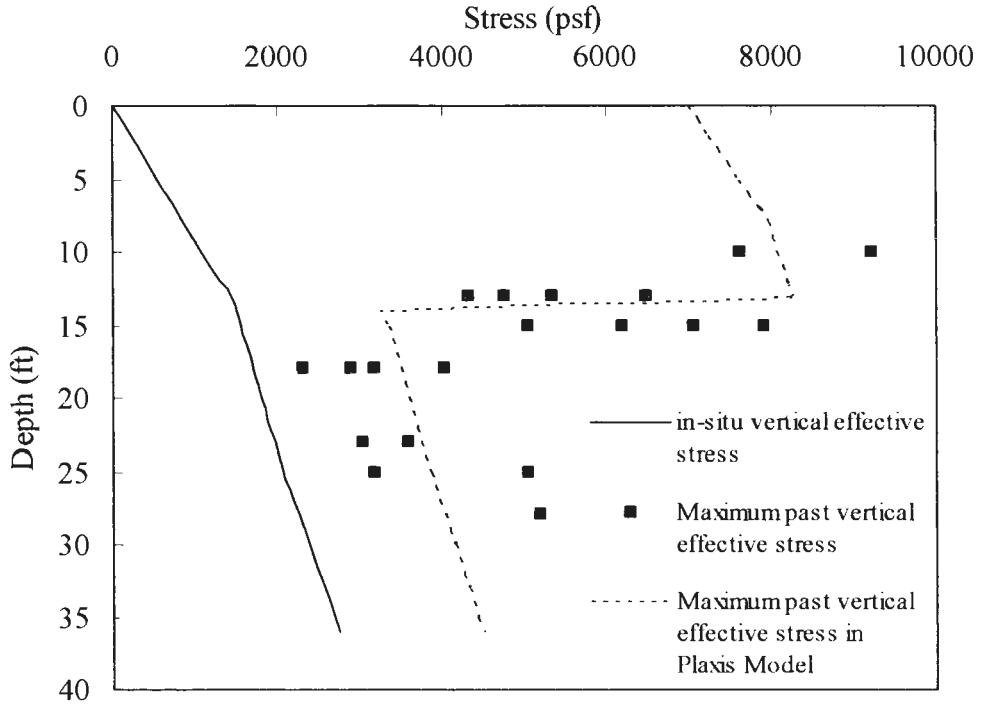

Fig. 5.3 In situ and maximum past effective vertical stress at MSE wall site

5.2.4 Shear Strength Parameters

Effective shear strength parameters for the hardening soil model were obtained from $\overline{CK_0U}$ triaxial compression tests. A typical stress-strain plot from one of these tests is presented in Fig. 5.4. Tabulated strength parameters from these tests are presented in Table 5.6.

One of the strengths of the hardening soil model is that it uses effective strength parameters and a pore pressure model to determine the undrained behavior of a soil model. These clays, like most clays, have an effective cohesion of zero when the clay is normally consolidated. At over consolidation ratios greater than 1 the clays will have some effective cohesion and a lower effective friction angle. Because the hardening soil

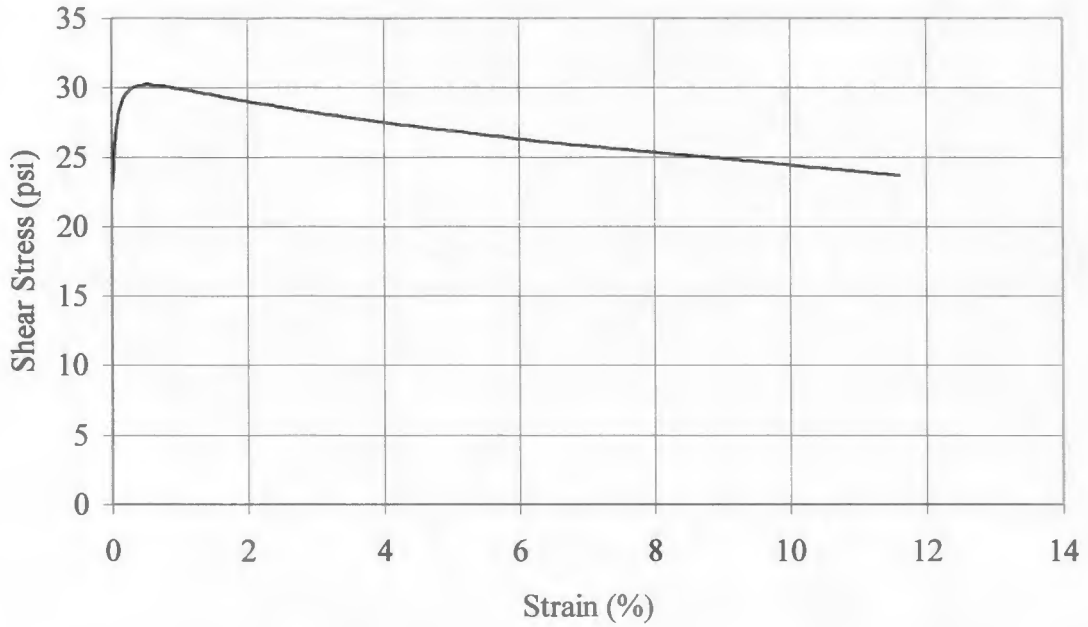

Fig. 5.4 Shear stress versus strain for the 4.0 x σ'_{v0} normally consolidated specimen from boring HF-2, depth of 18.6 ft

Table 5.6 Results of $\overline{CK_0U}$ Triaxial Compression Testing of Samples from 17-19 ft Depth

Boring	σ'_{v0} (psi)	σ'_{vm} (psi)	OCR	A_f	S_u/σ'_{vm}	ϕ' (deg)*
HS-1	36	36	1.0	1.55	0.317	26.99
RS-3	60	60	1.0	1.58	0.326	27.08
HF-2	96	96	1.0	1.45	0.315	26.36
RF-4	30	60	2.0	0.36	0.595	-
RF-4	15	60	4.0	0.13	0.989	-
RF-4	10	60	6.0	0.04	1.398	-

* assuming c'=0.

model cannot account for the effect of stress history on shear strength, it was decided to use the normally consolidated strength parameters in the model. This assumption is justified because most of the foundation soils are normally consolidated after being

consolidated by the embankment, and the assumption is somewhat conservative for soils that are not normally consolidated.

Modeling the undrained behavior of the embankment requires an accurate pore pressure model for the foundation. Pore pressures are generated from consolidation behavior of the embankment and from dilation (or contraction) of the soils during shear. The hardening soil model does a very good job of model consolidation and pore pressures during consolidation. Unfortunately, the hardening soil model does not accurately reflect the behavior of real contractive soils. From A_f values shown in Table 5.6 it can be seen that, in its normally consolidated state, Bonneville clay is highly contractive. The errors due to problems modeling the dilative (or contractive) behavior of the soil are probably quite low because almost all of the generated pore pressures are from consolidation and because the soils drain quite rapidly (as will be shown later), making the undrained behavior less critical.

5.2.5 Soil Permeability

The time-settlement behavior and pore pressure dissipation are functions of the soil modulus, permeability and the length of the drainage paths. Prefabricated vertical drains (PVD's) were used to decrease the lengths of drainage paths and accelerate the foundation consolidation. Flow into a PVD is a three-dimensional problem, but Plaxis is limited to two-dimensional problems. To work around this limitation trench drains were used in the Plaxis model to simulate the PVD's. Closely spaced drains were not practical for efficient calculations, so widely spaced trench drains were utilized.

The equivalent two-dimensional spacing of a trench drain for PVD's installed on a five-foot (1.5 m) square grid was determined to be approximately 7 ft (2.1 m). For the model, the trench drains were placed at approximately 14 ft (4.3 m) spacings, effectively doubling the length of the equivalent horizontal drainage path. In order compensate for the large spacings between drains, higher soil permeabilities were used. An iterative procedure was used to adjust the permeability until the time-settlement behavior in the model accurately matched the measured time settlement. Therefore, permeabilities used in the model do not accurately represent the actual permeability of soil at the site, but rather the combination of permeability and drain spacing simulates the site with PVD's.

5.2.6 Hardening Soil Parameters Used in Plaxis Model

Initial estimates of parameters were arrived at from laboratory tests. Then these values were adjusted based upon comparisons between analytical model outputs and measured deflections at the site presented in Report No. UT-03.11 "Instrumentation and Installation Scheme of a MSE Wall on I-15 with Results of Wall and Foundation Behavior" (Bay et al., 2003a). These results were summarized in Chapter 3. After numerous iterations a calibrated wall model was obtained. Table 5.7 contains the values of parameters in this calibrated model.

5.3 GEOMETRIC MODEL OF MSE WALL

5.3.1 Development of Wall Geometry

Fig. 5.5 shows the basic geometry of the final Plaxis MSE wall model. The complexity of the model increased throughout the modeling process. Initially, a very

simple foundation was used, containing only one soil type to represent the clay material and a second soil type to represent the granular backfill. Both the original embankment and the new wall were represented by an elastic material with the same unit weight values as anticipated for the final model. Using an elastic material allowed the foundation to be modeled without having to worry about the reinforcement in the new wall, and the additional unknown parameters associated with the reinforcement. A drained analysis was performed such that the time settlement effects were not taken into account.

Having only one type of soil did not allow the model to adequately replicate the deformations measured in the foundation material. Even though the hardening soil model DID provide for variation in the soil modulus as a function of depth, and even though uniform loads could be applied to overconsolidate the near-surface soil, no combination of modulus values was found that was able to match the deformations measured in the foundation soil profile.

The next step was to use two soils to represent the foundation material. One soil was used to model the deeper, stiffer material, and a second soil was used to model the softer soil and the desiccated material near the surface. Again, uniform loads could be applied to provide overconsolidation for the near-surface layer. A drained analysis was again performed. The deformations in the foundation provided a better estimate of the measured deflections, but the results were still not adequate.

Additional soil layers were added that correlated to the layers obtained from boring logs, until eventually the five clay and silt soils and the granular fill provided a close match to the measured results. Soils underlying the site are identified as medium

Table 5.7 Hardening Soil Parameters for Calibrated Wall Model (Foundation Material)

Hardening Soil Parameters	Units	Medium Stiff Surface Clay	Soft Clay	Stiff Sandy Silt	Very Stiff Sandy Clay
γ	lb/ft^3	119.2	113	120	120
k_x	ft/day	3.5 E -03	3.5 E -03	3.5 E -03	3.5 E -03
k_y	ft/day	3.5 E -03	3.5 E -03	3.5 E -03	3.5 E -03
ϕ'	degrees	27	27	30	27
c'	lb/ft^2	750	10	750	100
ψ	degrees	0	0	0	0
E_{50}^{ref}	lb/ft^2	1.8 E 04	1.65 E 04	2.2 E 05	2.85 E 04
E_{oed}^{ref}	lb/ft^2	1.8 E 04	1.65 E 04	2.2 E 05	2.85 E 04
E_{ur}^{ref}	lb/ft^2	9.0 E 04	1.65 E 05	2.2 E 06	2.85 E 05
ν_{ur}		0.2	0.2	0.2	0.2
p_{ref}	lb/ft^2	2088	2088	2088	2088
m		1.0	1.0	0.5	1.0

Table 5.8 Hardening Soil Parameters for Calibrated Wall Model (Fill Material)

Hardening Soil Parameters	Units	Original Embankment	Granular Fill (Wall Footprint)	New Fill Material / Surcharge	Near-Face Material
γ	lb/ft^3	125	119.2	126	125
k_x	ft/day	50	50	50	50
k_y	ft/day	50	50	50	50
ϕ'	degrees	36	34	40	38
c'	lb/ft^2	10	100	10	10
ψ	degrees	0	0	0	0
E_{50}^{ref}	lb/ft^2	2.5 E 05	2.5 E 05	2.5 E 05	2.0 E 05
E_{oed}^{ref}	lb/ft^2	2.5 E 05	2.5 E 05	2.5 E 05	2.0 E 05
E_{ur}^{ref}	lb/ft^2	2.5 E 06	2.5 E 06	2.5 E 06	2.0 E 06
ν_{ur}		0.2	0.2	0.2	0.2
p_{ref}	lb/ft^2	2088	2088	2088	2088
m		0.5	0.5	0.5	0.5

stiff surface clay, soft clay, stiff sandy silt, very stiff sandy clay, and semi-rigid material. As mentioned, there is also a region of granular fill beneath the toe of the wall. It should be again noted that modulus of each layer is not homogeneous, but rather it varies continuously with depth. This makes it possible to accurately model a complex site with relatively few soil layers.

At this point, an undrained analysis was performed in an attempt to match the time-settlement behavior of the foundation material. The equivalent drain system used identical strength and stiffness parameters as the surrounding soil, the only difference being a higher permeability. Three drains, simulating the PVD's, extend from the granular layer to the bottom of the soft clay layer. One value of permeability was used for all of the materials (except the equivalent drains) below the water table, and one value of permeability was used for all soils above the water table. This oversimplifies the consolidation behavior of the foundation, since there are likely many more permeabilities associated with many more soil layers than used in the model. However, it was desired to begin with as few parameters as possible, and add complexity as necessary from that point.

Soils above the water table (and the equivalent drains) were treated as drained soils, since the strength parameters used in Plaxis depend on whether the soil is drained or undrained. Treating the layers above the water table as undrained with a high permeability was causing some strange strength behavior to occur. Treating the layers as drained with the same permeability allowed the anticipated behavior to take place.

Several iterations with adjusted permeabilities provided a model that replicated both the ultimate deformation of the foundation material and also the time settlement

behavior of the foundation material. At this point, a more appropriate model of the MSE wall system was developed.

Again, to minimize the complexity in developing the model, the first step in establishing the MSE wall model was to place the wall on a compressible, yet much less complicated foundation material. The original embankment was again modeled as an elastic material, but the new wall and backfill material were modeled using an appropriate hardening soil model. Reinforcement was added by using the geotextile model provided in Plaxis. This reinforcement model is somewhat limited, especially when comparing the model to the actual field reinforcement. The Plaxis model gives essentially sheet reinforcement, due to the two-dimensionality of the software. This sheet reinforcement is defined by the tensile strength of the material, given as an EA term per unit length of the wall.

In order to best approximate the equivalent EA term of the actual wall, an equivalent cross sectional area of the longitudinal bars for each given layer of bar mats was calculated. Since the number of longitudinal bars varied over the height of the wall, the model reinforcement also varied. The equivalent cross sectional area for the center-to-center spacing of the bar mats was determined. This value was multiplied by the modulus of elasticity for the steel reinforcement, and these values were used to model the reinforcement in the wall.

Again, the Plaxis model is forced to oversimplify the actual mechanisms associated with the lightly reinforced MSE wall. In actual fact, the existing reinforcement in the wall is not continuous, since there are gaps between reinforcement in some layers as much as 3 ft (0.9 m) wide between consecutive mats. No attempt was

made to try to model the transverse bars in the bar mats. However, the best approximation of the reinforcement was obtained that Plaxis would allow.

Once an appropriate model of the new wall backfill and reinforcement was obtained, it was applied to the full model of the MSE wall. The entire foundation model was used, an appropriate hardening soil model was used for the original embankment, and the reinforcement/backfill model was used to model the new wall. The final wall model consists of three parts; the original I-15 embankment, the new MSE wall fill (including surcharge), and a near-face material with slightly reduced unit weight and increased compressibility due to less possible compaction effort near the face of the wall. Initially, a drained analysis was run. Strength and stiffness parameters were adjusted slightly to match ultimate deformations beneath the wall.

Once the appropriate long-term deformations were obtained, the permeabilities were again adjusted slightly to obtain a match of the time settlement behavior. Once the long- and short-term behavior of the wall was matched appropriately, the model was considered to be adequate.

5.3.2 Loading Sequence

A complicated loading sequence was utilized to simulate the stress history and construction sequence at the site. This sequence is explained below.

First, the foundation material at the site was loaded to simulate the stress history. With all embankment parts deactivated, a downward uniform load of 7000 psf (335 kPa) was applied at the ground surface and an upward uniform load of 5000 psf (239 kPa) was

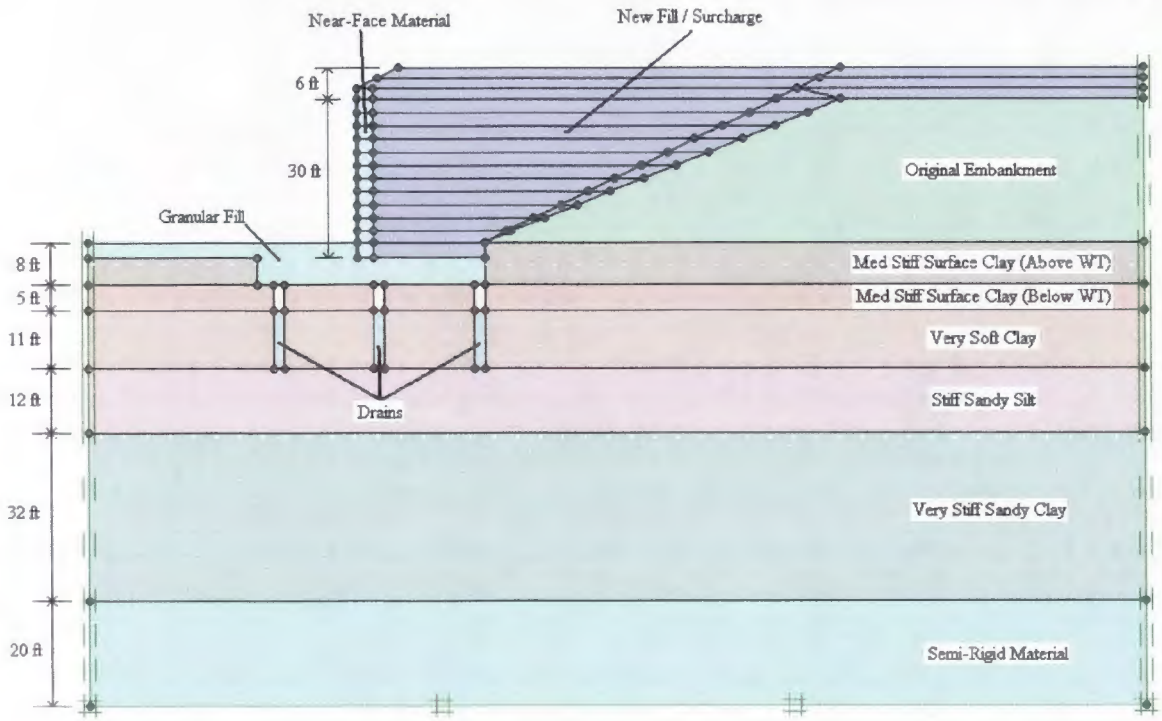

Fig. 5.5 Simplified geometry of Plaxis MSE wall model

applied at a depth of 13 ft (4.0 m). After consolidating under these loads, the maximum past effective vertical stress profile shown in Fig. 5.3 was imposed at the site.

Next, the original embankment plus a 6 ft (1.8 m) surcharge at the top of the embankment and a wedge-shaped surcharge along the slope of the embankment were activated. The site consolidated under these loads.

Next, the surcharge applied to the original embankment was deactivated, and site was allowed to swell. This replicates aging effects that will cause soils beneath the original embankment to be slightly over consolidated.

Next, the MSE wall was constructed in 5 ft (1.5 m) increments. Each 5 ft (1.5 m) increment was applied instantly. After applying each increment, the wall was allowed to

consolidate for a period of time equal to the time it took to construct that increment of wall. This procedure continued until the wall and surcharge were constructed.

Next, consolidation continued (with the surcharge applied) for an additional 90 days. Then, the surcharge was removed (deactivated).

Last, consolidation continued for another 1200 days.

5.4 LONG-TERM BEHAVIOR

One of the important goals of the model was to be able to represent the long-term behavior of the MSE wall. The model should be able to replicate the settlement of the wall, vertical and horizontal movement in the foundation soil, and pressure within the wall at the conclusion of primary consolidation.

5.4.1 Total Deformations

The total deformations of the wall model compared well to the deformations measured at the end of wall construction. Settlement of the wall was measured to be about 1.26 ft (0.38 m) and 1.6 ft (0.49 m) using the Sondex settlement data and the Horizontal Inclinometer data, respectively. These measurements were positioned at the base of the wall, within the wall footprint, and three feet from the wire mesh face. The apparent discrepancy between the inclinometer reading and the Sondex reading (measured at essentially the same point) is assumed to a function of the slurry that was used to backfill the casing annulus. It appears that the slurry near the top of the hole was too stiff, such that minimal deformation between adjacent sensor rings was measured. Thus, the settlement measured by the inclinometer at that point was considered to be more appropriate than the Sondex value.

From the Plaxis model, settlement was estimated to be approximately 1.56 ft (0.48 m) at the base of the wall, matching the inclinometer reading at that point. Horizontal movement of the wall face was measured to be from 0.25 ft (76 mm) to 0.30 ft (91 mm) as given by vertical inclinometer data and horizontal extensometer data, respectively. The Plaxis model gives a horizontal deflection of approximately 0.22 ft (67 mm) at the toe of the wall. Fig. 5.6 shows the deformed mesh at the end of primary consolidation. Fig. 5.6a shows the deformed mesh at the true scale, and Fig. 5.6b shows exaggerated deformations.

5.4.2 Vertical Deformations

Much of the calibration of the Plaxis model focused on the vertical deformation of the wall. A comparison of the Plaxis model results and the measured results for two of the Sondex tubes and one of the horizontal inclinometers is made below.

5.4.2.1 Comparison with Sondex Measurements. Only two of the three Sondex tubes showed measurable deformations during the construction of the wall. Sondex tube S1 was located 3 ft (0.91 m) within the wall footprint, while Sondex tube S2 was located 8 ft (2.4 m) from the wall face, outside the wall footprint. Fig. 5.7 shows a comparison of the Sondex tube S1 measurements taken at the end of primary consolidation compared to Plaxis model deformations at the end of consolidation.

As mentioned, it appears that the grout used to backfill the Sondex casing was too stiff, and did not give the appropriate measurements near the original ground surface. The S1 measurements were adjusted to match the horizontal inclinometer vertical deflection at Elevation 325 ft (99.1 m). It was assumed that the measured deflections at

Elevation 315 ft (96.0 m) were correct. It was further assumed that approximately 80 percent of the deformation between Elevation 315 ft (96.0 m) and Elevation 325 ft (99.1 m) would be in the 5 ft (1.5 m) of medium stiff surface clay, while the remaining 20 percent of deformation would occur in the 5 ft (1.5 m) region of granular material. Fig. 5.8 shows the actual Sondex data compared to the adjusted Sondex data for the readings taken at the end of primary consolidation.

Fig. 5.9 shows a comparison of the Sondex tube S2 measurements taken at the end of primary consolidation compared to Plaxis model deformations at the end of consolidation. The Plaxis model estimates the amount of vertical deformation of the wall with depth reasonably well for both Sondex tube locations.

5.4.2.2 Comparison with the Horizontal Inclinometer. A comparison of the vertical deformation was also made between the Plaxis model and Horizontal Inclinometer H1 that is located at the base of the wall backfill at elevation EL 325 ft (99.1 m) . This inclinometer extends from a manhole located approximately 14 ft (4.3 m) from the wire face of the MSE wall, and extends approximately 38 ft (11.6 m) into the wall. The Plaxis results are compared to the measured inclinometer results in Fig. 5.10.

The Plaxis model does a very good job of replicating the deformations beneath the MSE wall (14 ft (4.3 ft) to 52 ft (15.8 ft) from the manhole). However, in the soil between the manhole and the toe of the wall (0 ft (0 m) to 14 ft (4.3 m) from the manhole), the model underestimates the vertical deformations that were measured. This likely means that the model does not precisely replicate the shear behavior that is occurring between the manhole and the toe of the wall. Even with this variation, the

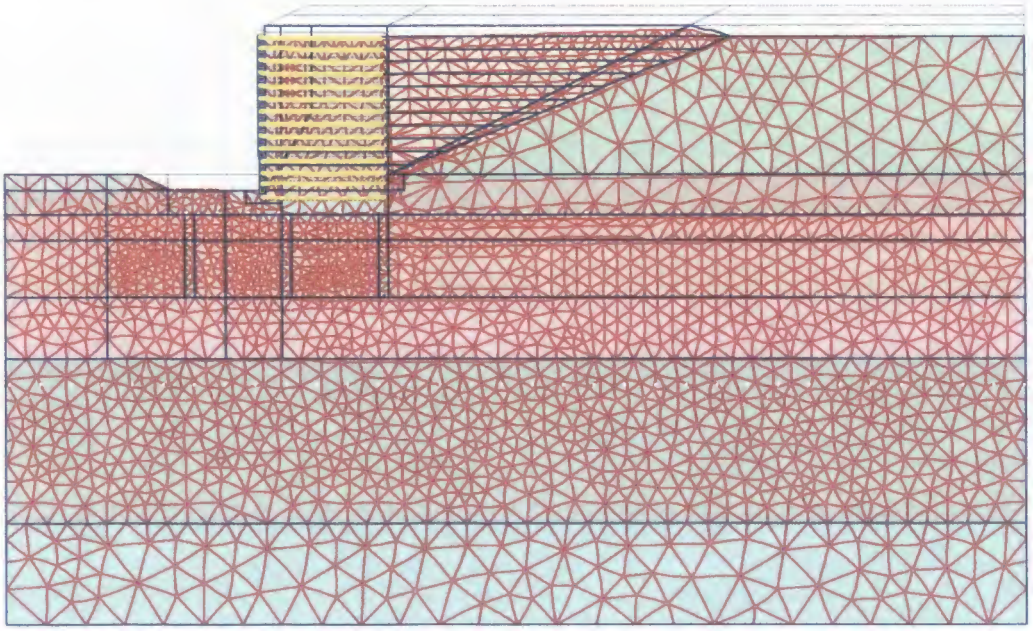

a) True Scale

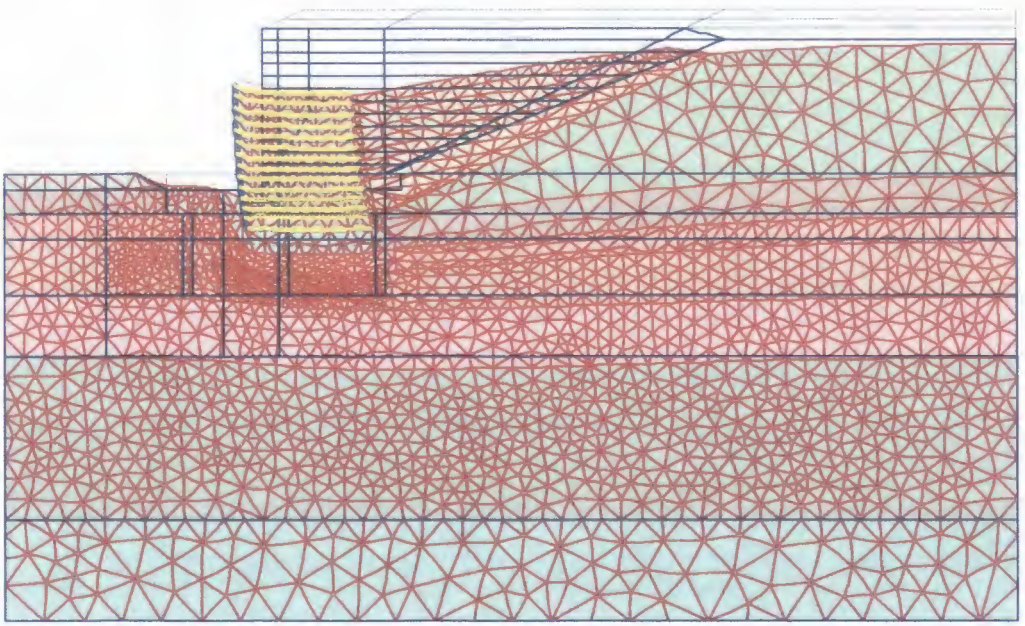

b) Exaggerated 5 times

Fig. 5.6 Deformed Plaxis mesh at the end of primary consolidation

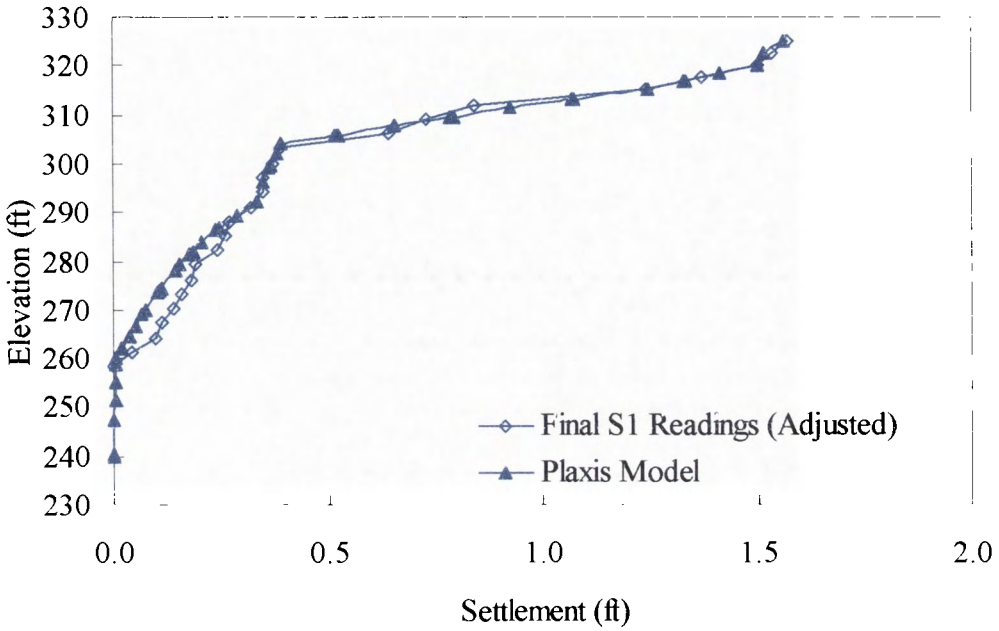

Fig. 5.7 Comparison of Plaxis model and adjusted Sondex tube S1 measurements of vertical deflection

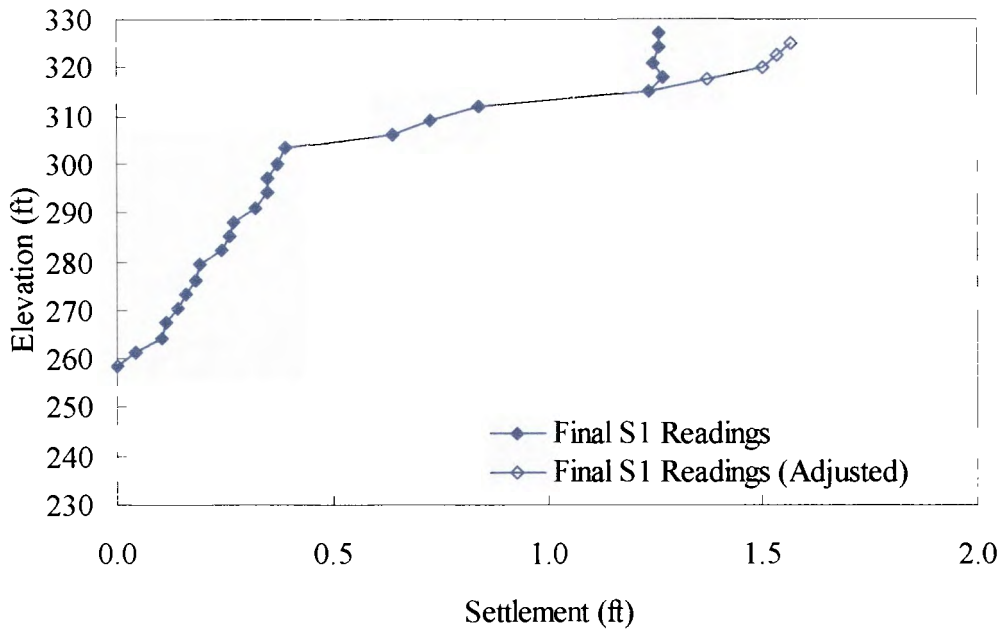

Fig. 5.8 Comparison of actual Sondex tube S1 measurements of vertical deflection to the adjusted Sondex tube S1 measurements used for model calibration

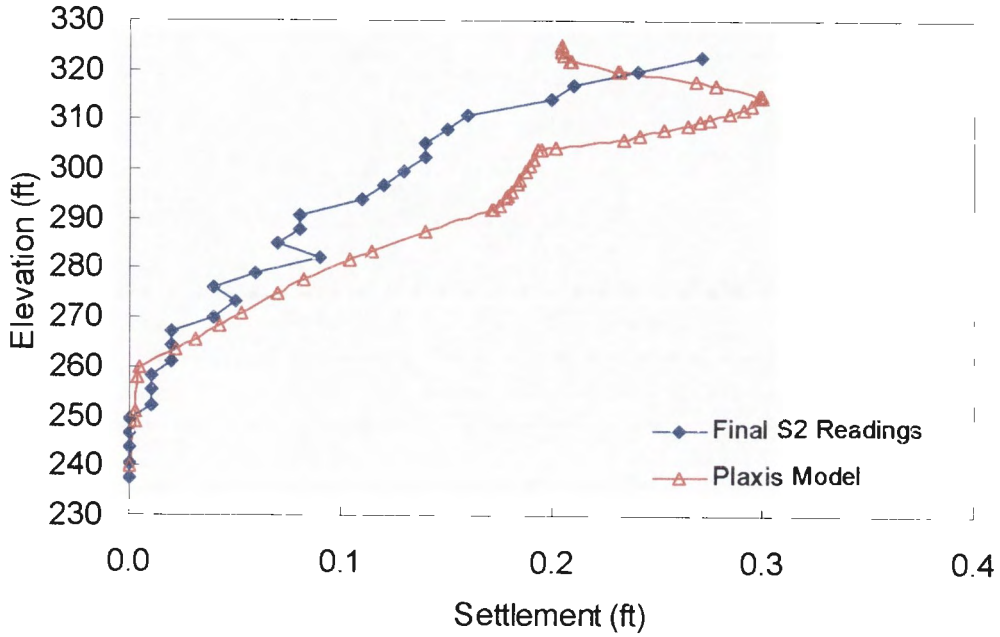

Fig. 5.9 Comparison of Plaxis model and Sondex tube S2 measurements of vertical deflection

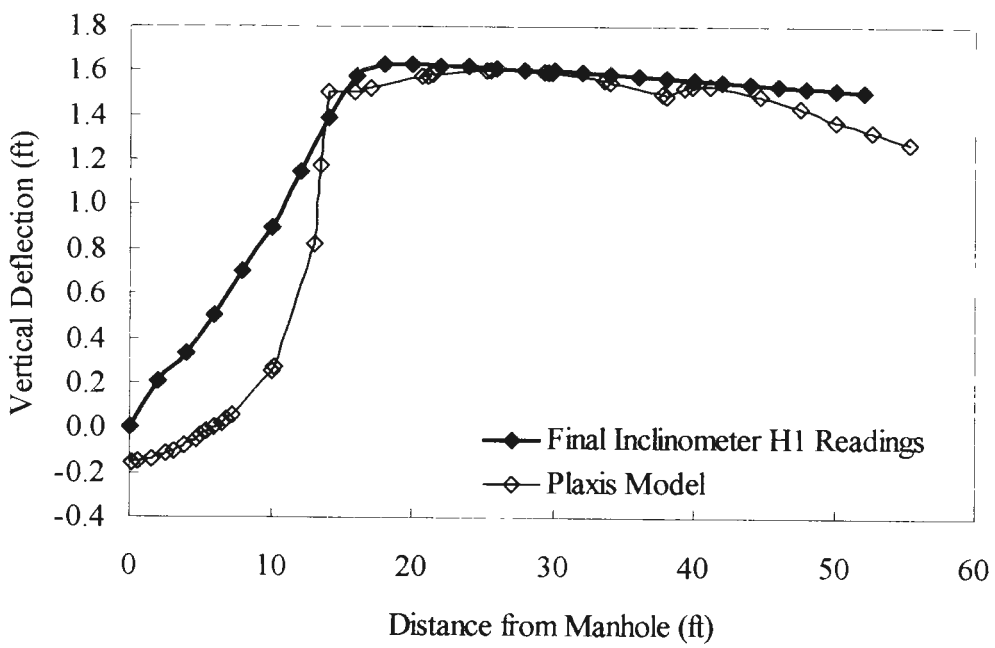

Fig. 5.10 Comparison of Plaxis model and horizontal inclinometer H1 measurements of vertical deflection

model seems to do very well in predicting deformations due to compression (rather than shear deformations) of the soil, which includes the vast majority of the deformations measured in the foundation material.

5.4.3 Horizontal Deformations

Two of the three Vertical Inclinometers at the wall showed significant horizontal deformations during wall construction. Vertical Inclinometer I1 is located 3 ft from the face of the wall, within the wall footprint, and Vertical Inclinometer I2 is located 8 ft from the wall, outside the wall footprint. The third vertical inclinometer (I3), located 31 ft from the wall face, outside the wall footprint and outside the zone of PVDs, showed less than 0.06 ft of horizontal movement at the most recent measurement.

A comparison of the Plaxis model results and the measured results for inclinometer I1 and inclinometer I2 are given in Fig. 5.11 and Fig. 5.12, respectively. The deformations predicted by the model compare very well to those measured by the vertical inclinometer located outside the footprint of the wall (Figure 11). The reverse spike noticed between elevation 305 and elevation 292 is somehow due to the layer of silt in the model. Why the spike occurs has not yet been determined. Apart from the apparent spike, the model does a very good job at matching the measured results.

The model and the measured results do no match very well for the inclinometer located within the wall footprint. The horizontal movement in the model is very similar to the movement occurring in the measured and modeled results for the inclinometer outside the wall footprint, but does not match the measured results inside the wall footprint. The measurements taken throughout construction appear to be valid, so the

difference between the model and the measured results has yet to be explained. As is quite apparent, assuming the measured results are indeed valid, the model does of poor job of replicating the horizontal deformations within the wall footprint.

Again, since the horizontal movement in the foundation was considered to be much more important than the horizontal movement within the wall, Figure 10 only compares the horizontal movement between the measured and model results for the foundation material, not comparing the movement measured within the wall to the movement modeled by Plaxis.

5.4.4 Vertical Stresses

Pressure plates were placed in the wall approximately 6 ft (1.8 m) vertically from the base of the wall, located from 1 ft (0.3 m) inside the wall footprint to 30 ft (9.1 m)

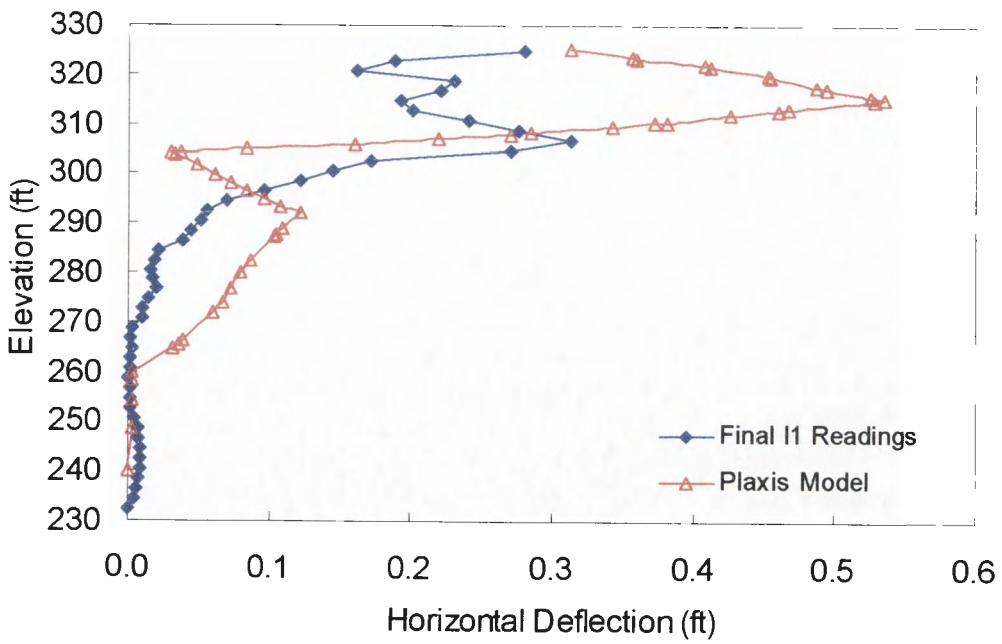

Fig. 5.11 Comparison of Plaxis model and vertical inclinometer I1 measurements of horizontal deflection

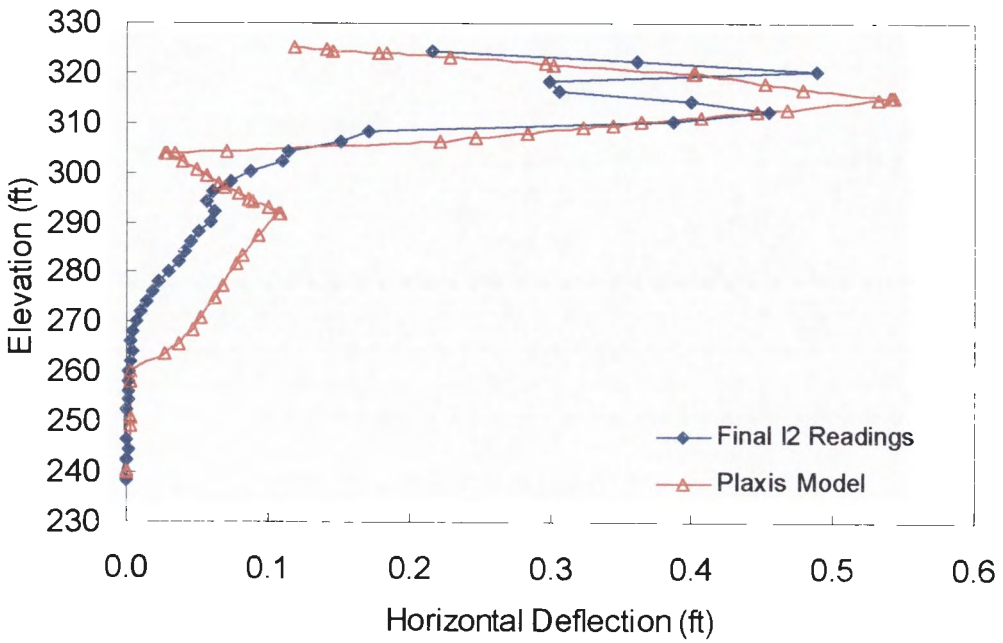

Fig. 5.12 Comparison of Plaxis model and vertical inclinometer I2 measurements of horizontal deflection

inside the wall footprint. The measured values (with surcharge applied) at the end of primary consolidation are compared to the Plaxis model values in Fig. 5.13.

The Plaxis model does a fair job of replicating the vertical stresses within the wall. The decreased stress occurring near the wall face is reproduced quite well, though the model still overpredicts the stress near the face. The position of the peak stress occurring 6 to 8 ft from the wall face is modeled very well, but the magnitude of this peak stress is underpredicted significantly. The stresses further into the wall are approximated quite well by the Plaxis model.

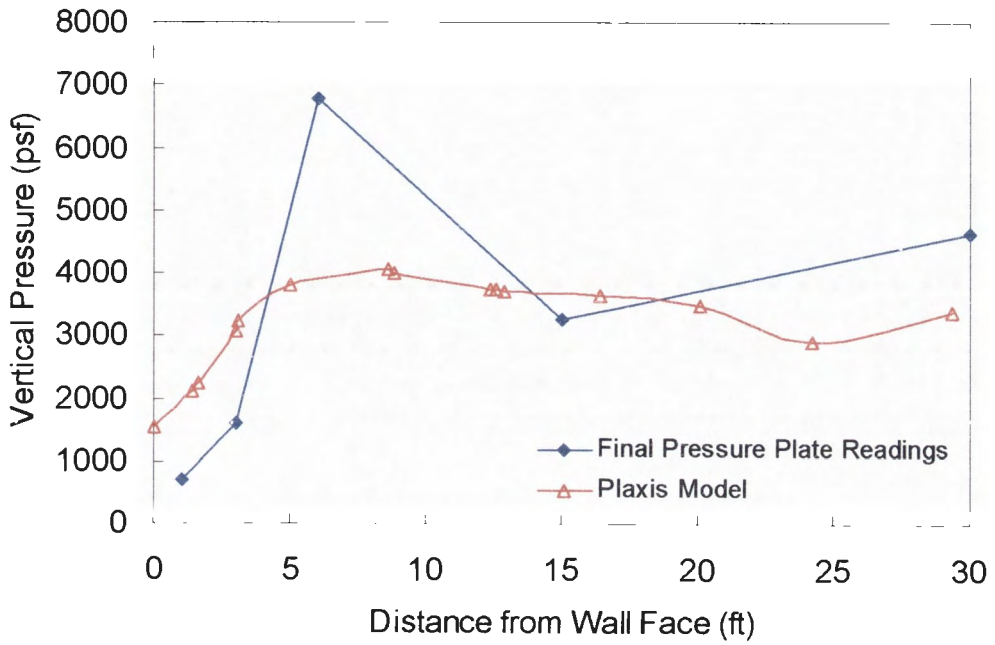

Fig. 5.13 Comparison of Plaxis model and pressure plate measurements of vertical pressure

5.5 TIME SETTLEMENT BEHAVIOR

5.5.1 Time Settlement Curves

The Plaxis model time settlement behavior was calibrated to the actual wall by matching the time settlement curves for a point at the base of the wall, 3 ft (0.9 m) within the wall footprint. Construction records were used to determine the staging sequence of the analytical model. Fig. 5.14 shows the measured construction sequence compared to the staged construction sequence followed by the Plaxis model. A comparison between the measured and calculated settlement curves is shown in Fig. 5.15. Fig. 5.15a shows the time settlement up to 200 days and Fig. 5.15b shows the long-term time settlement. The match between the model and measurements is extremely close up until 200 days. This time corresponds with the end of primary consolidation. After this time there is no

additional settlement in the analytical model while the measurements continue to show some settlement. This is expected because the analytical model does not include secondary consolidation or creep.

The close agreement between analytical and measured time settlement curves gives a high degree of confidence in the models pore pressure dissipation and settlement evaluations.

5.5.2 Pore Pressure Dissipation

A series of figures showing the excess pore pressures in the foundation are plotted in Fig. 5.16 through Fig. 5.23. These plots show the excess pore pressures during construction and continue through the end of primary consolidation. The highest excess pore pressure that occurred during staged construction was 1710 psf (81.9 kPa). The contour interval for each figure is the same for easy comparison.

Undrained strength parameters are often used to evaluate the stability of embankments. This assumes that no drainage is allowed. This condition can also be evaluated in Plaxis by applying the entire embankment instantly. The excess pore pressures from this loading condition are shown in Fig. 5.24. Note that the contour interval was adjusted from the plots showing the staged construction, since the pore pressure magnitude was much higher. The highest pore pressure that occurred during instantaneous construction was 3760 psf (180 kPa), or more than two times the maximum excess pore pressure that occurred during staged construction. This indicates that the use of undrained strength parameters without accounting for pore pressure dissipation is quite conservative for loading conditions like those encountered at this site.

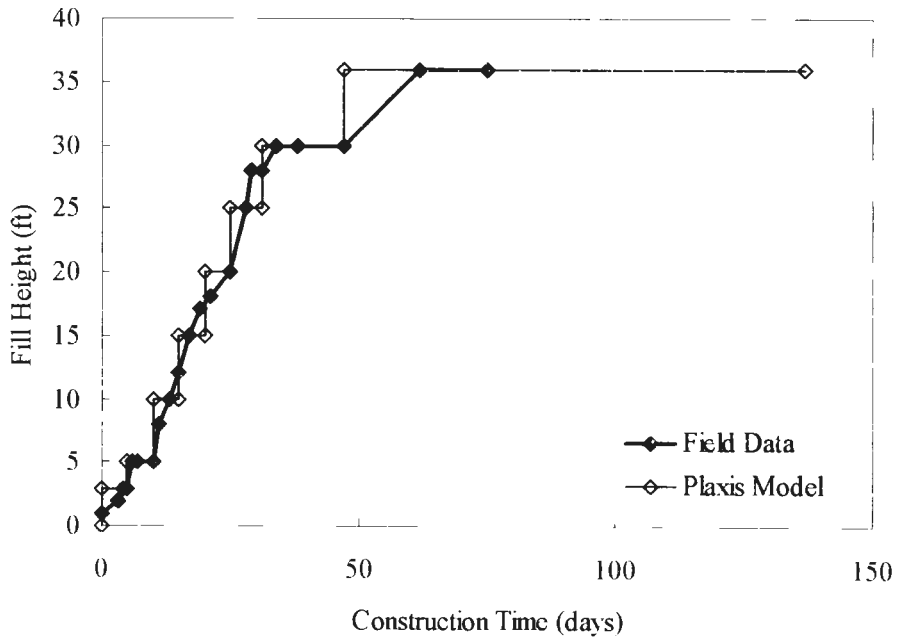

Fig. 5.14 Field construction sequence versus Plaxis model construction sequence

Fig. 5.25 shows plots of maximum excess pore pressure versus time for staged and instantaneous construction. For instantaneous construction the highest excess pore pressure occurs at time = 0. For the staged construction the excess pore pressures reach a peak at 48 days, which is the time at which the surcharge load was applied.

It should be noted that the stepwise function for the staged construction is entirely a function of the loading sequence for the model. Lifts were chosen that corresponded well with the position of the reinforcement within the soil (i.e. five foot (1.5 m) lifts allowed for exactly two reinforcement layers to be added, complete with backfill.) These lifts were applied instantaneously, as mentioned earlier, then consolidation was allowed for the time during which construction of that list actually occurred. Thus, the model does not exactly follow the sequence of construction, but is a close approximation of the construction process.

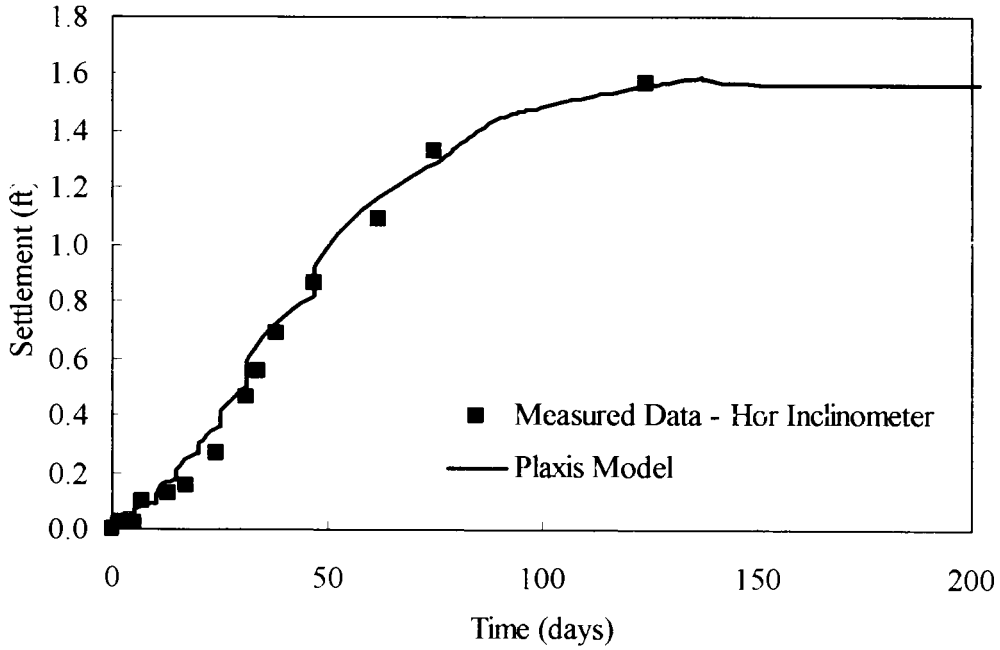

a) First 200 days after beginning of construction

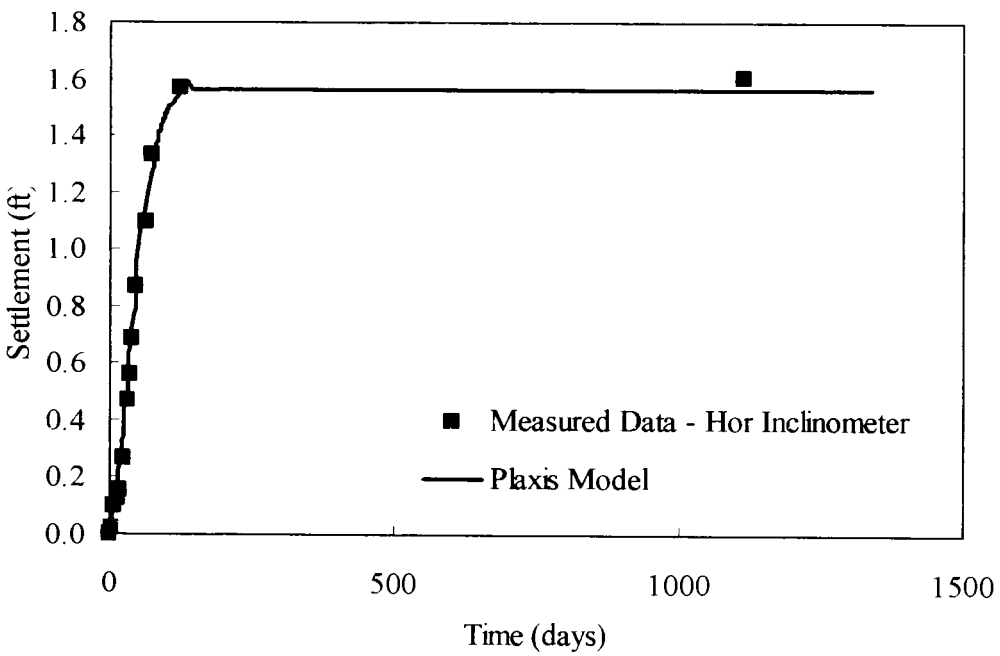

b) First three years after beginning of construction

Fig. 5.15 Time settlement plot comparing Plaxis model with measured results of settlement at the base of the MSE wall

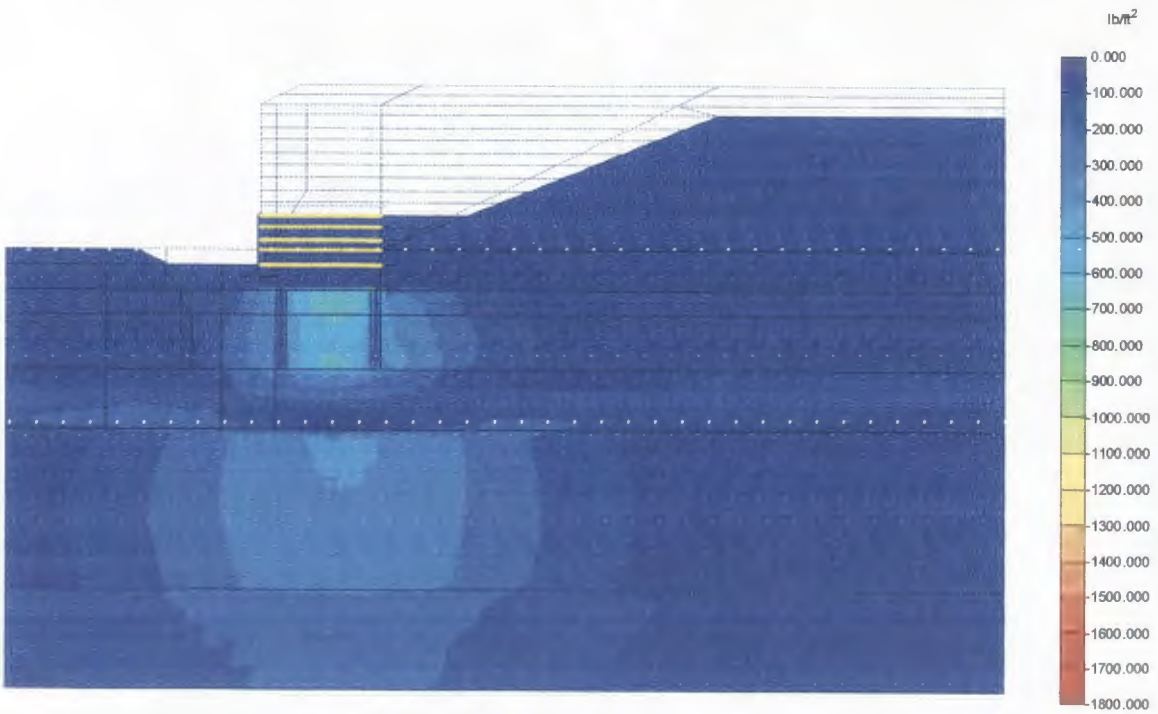

Fig. 5.16 Excess pore pressures at lift of 10 ft

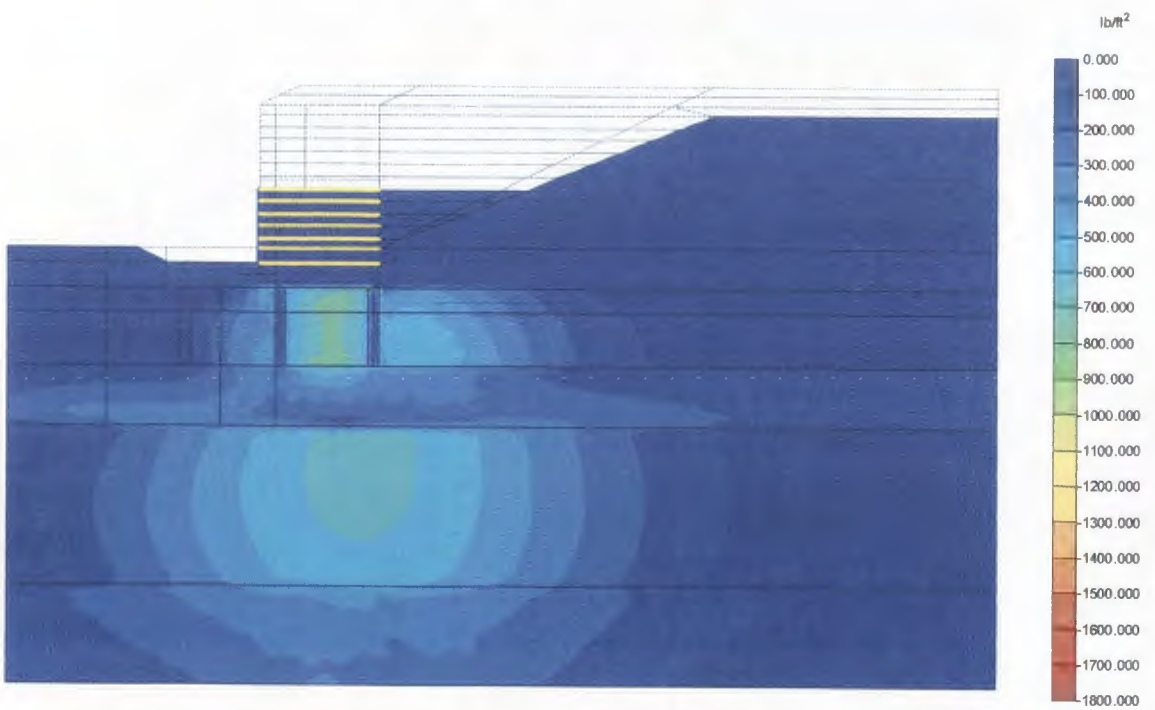

Fig. 5.17 Excess pore pressures at lift of 15 ft

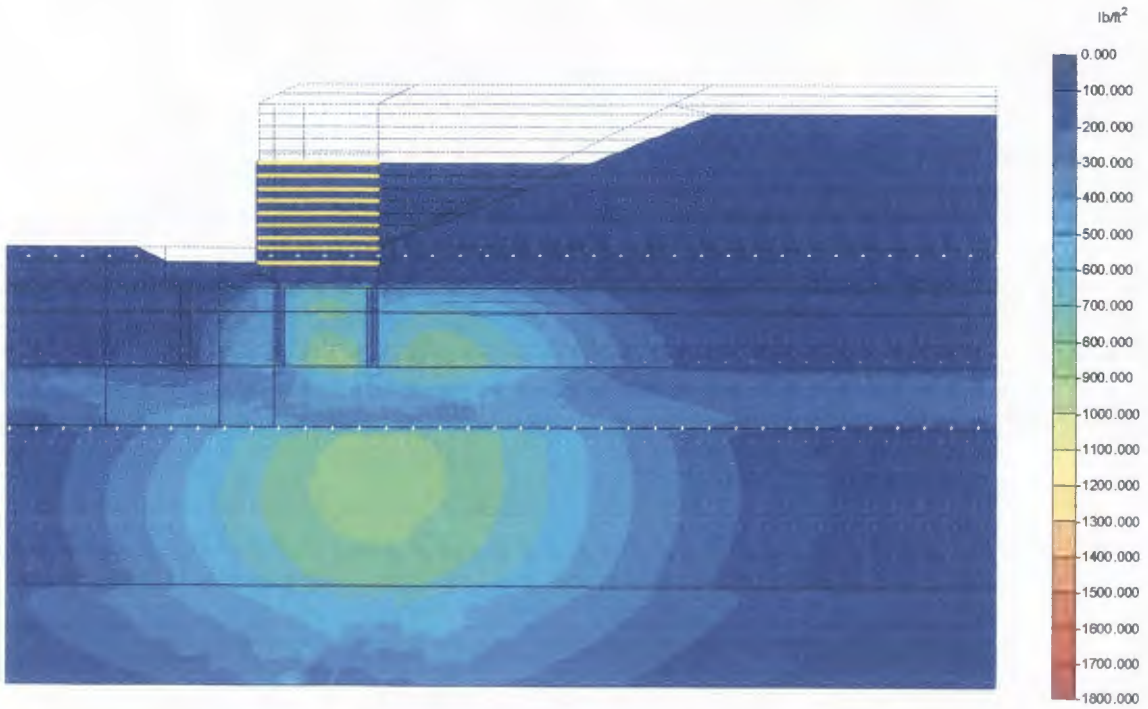

Fig. 5.18 Excess pore pressures at lift of 20 ft

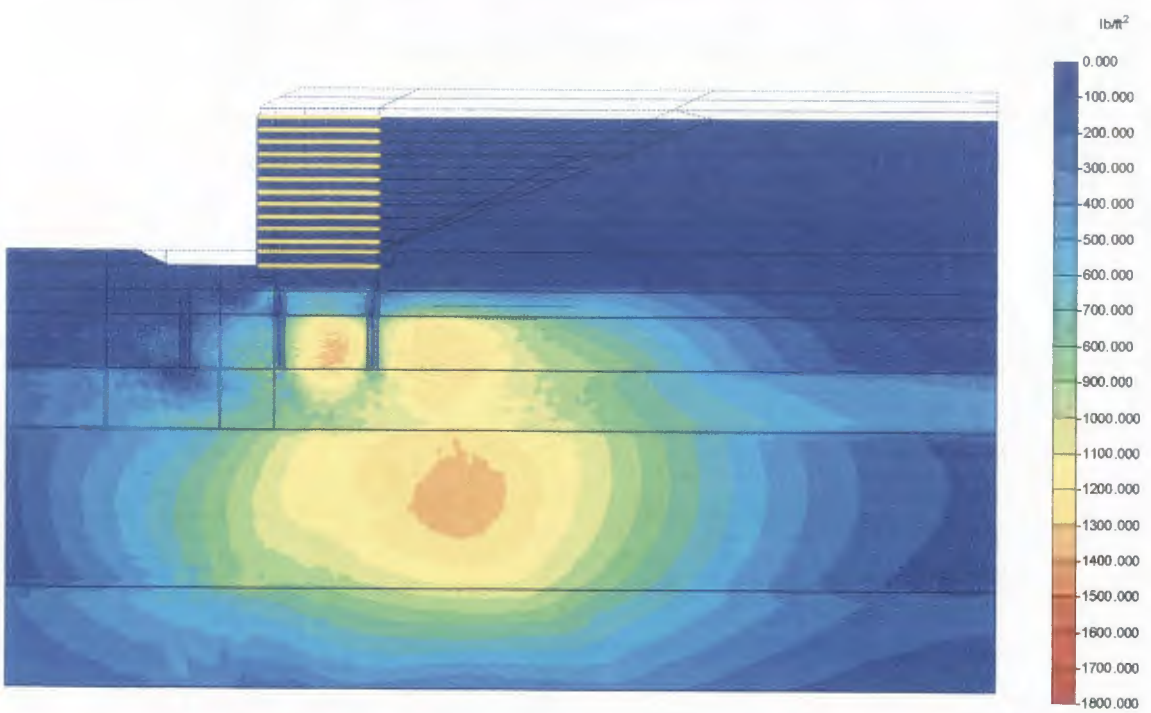

Fig. 5.19 Excess pore pressures at lift of 30 ft

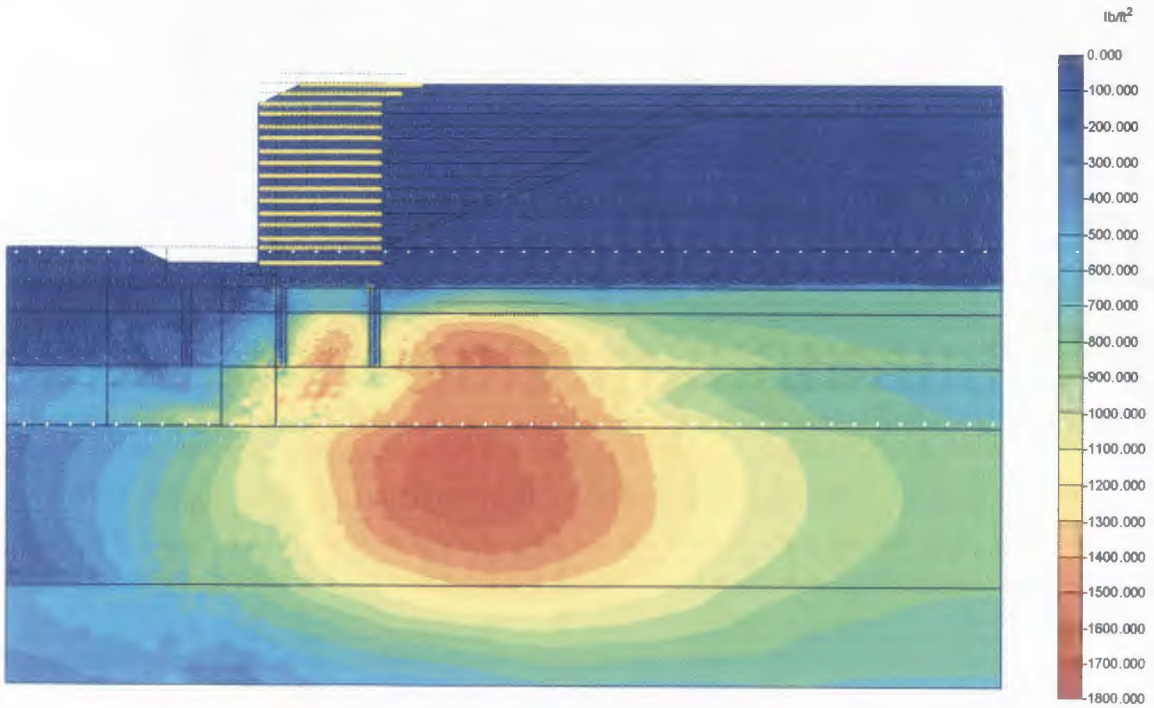

Fig. 5.20 Excess pore pressures at lift of 36 ft

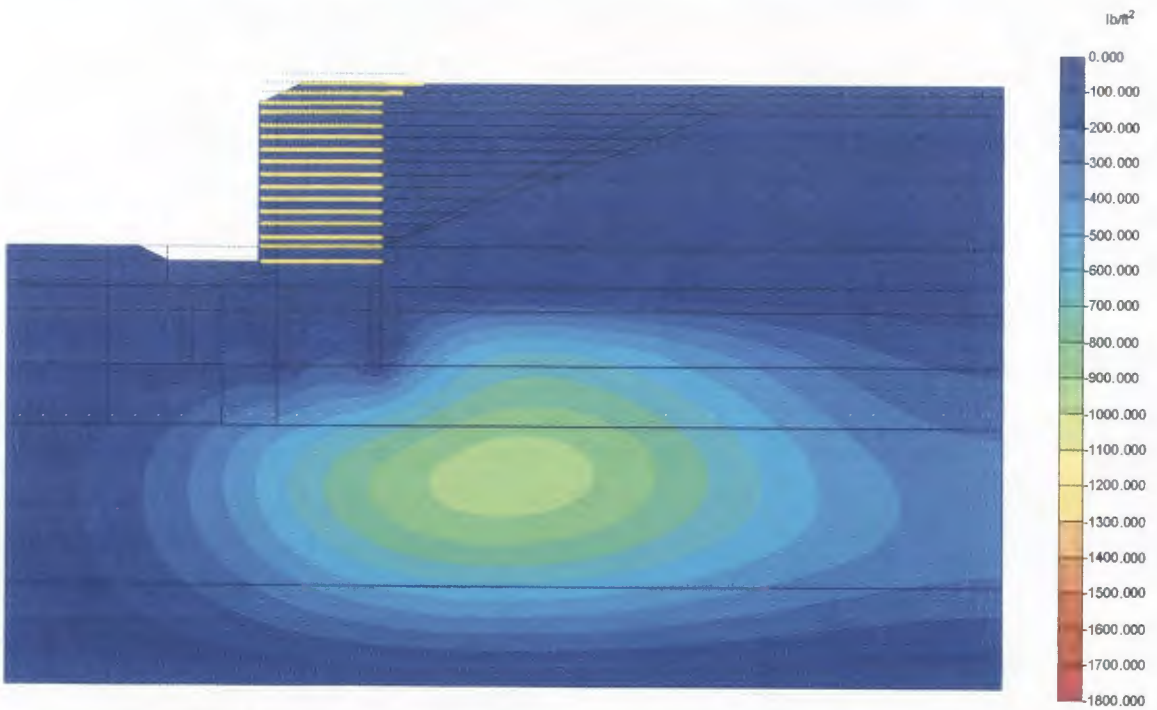

Fig. 5.21 Excess pore pressures 45 days after placement of surcharge

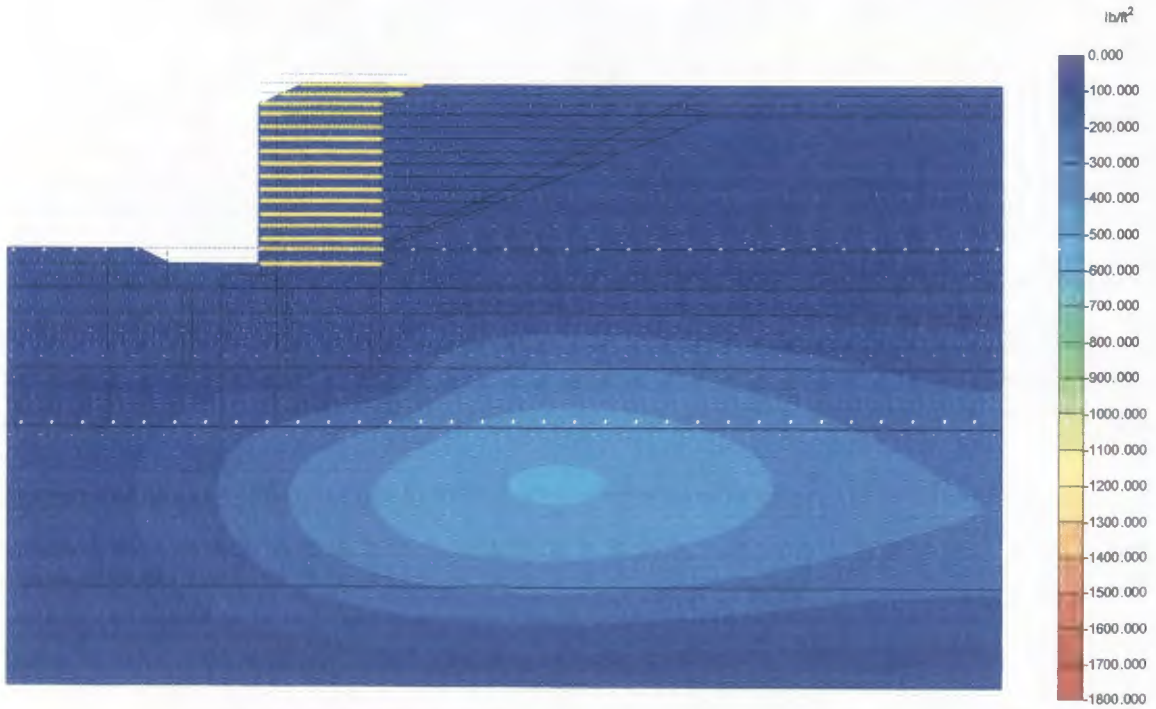

Fig. 5.22 Excess pore pressures 90 days after placement of surcharge

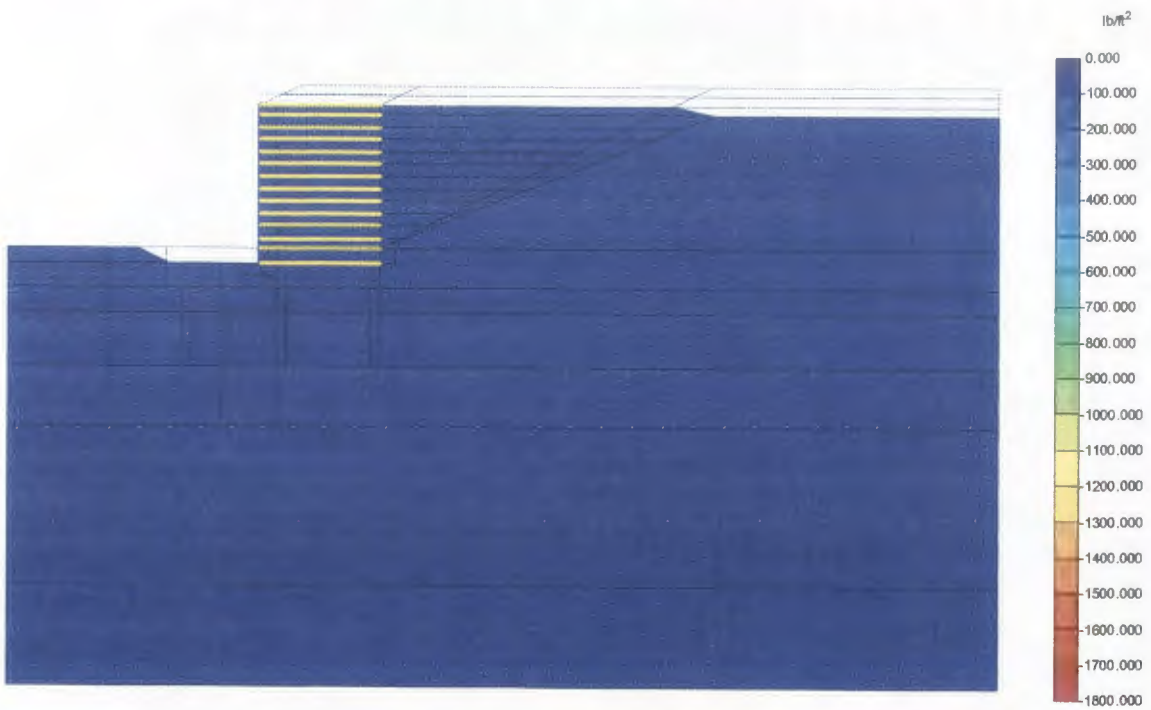

Fig. 5.23 Excess pore pressures 100 days after removal of surcharge

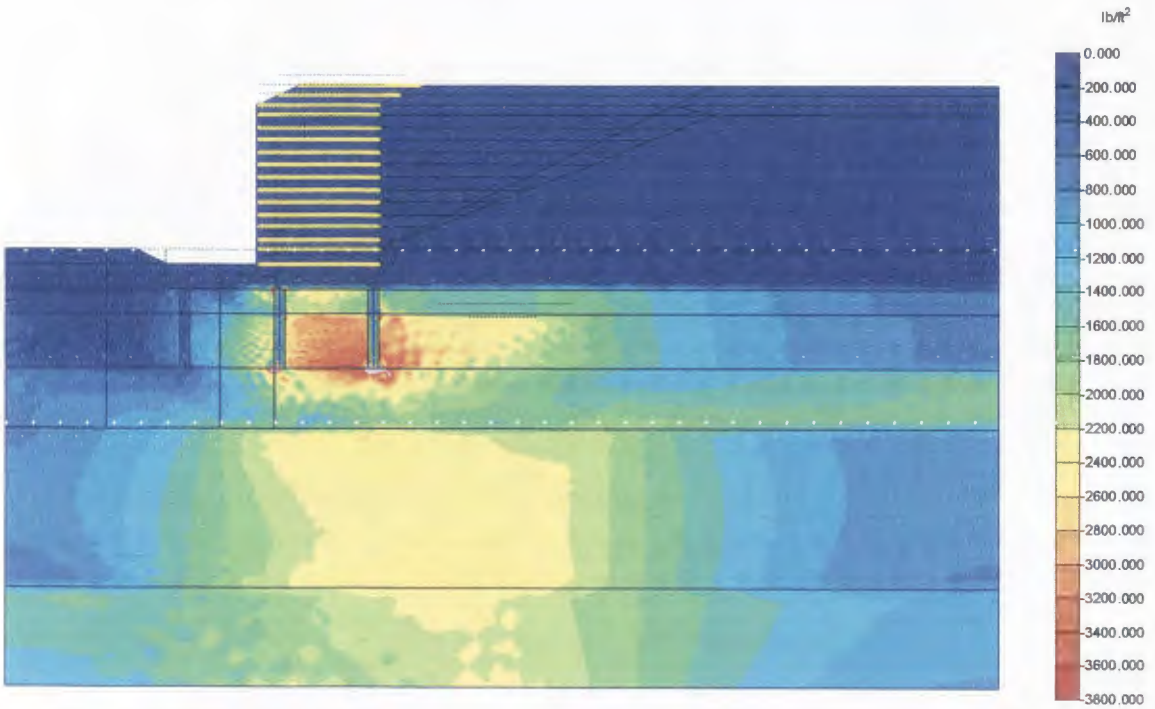

Fig. 5.24 Excess pore pressures after instantaneous wall construction

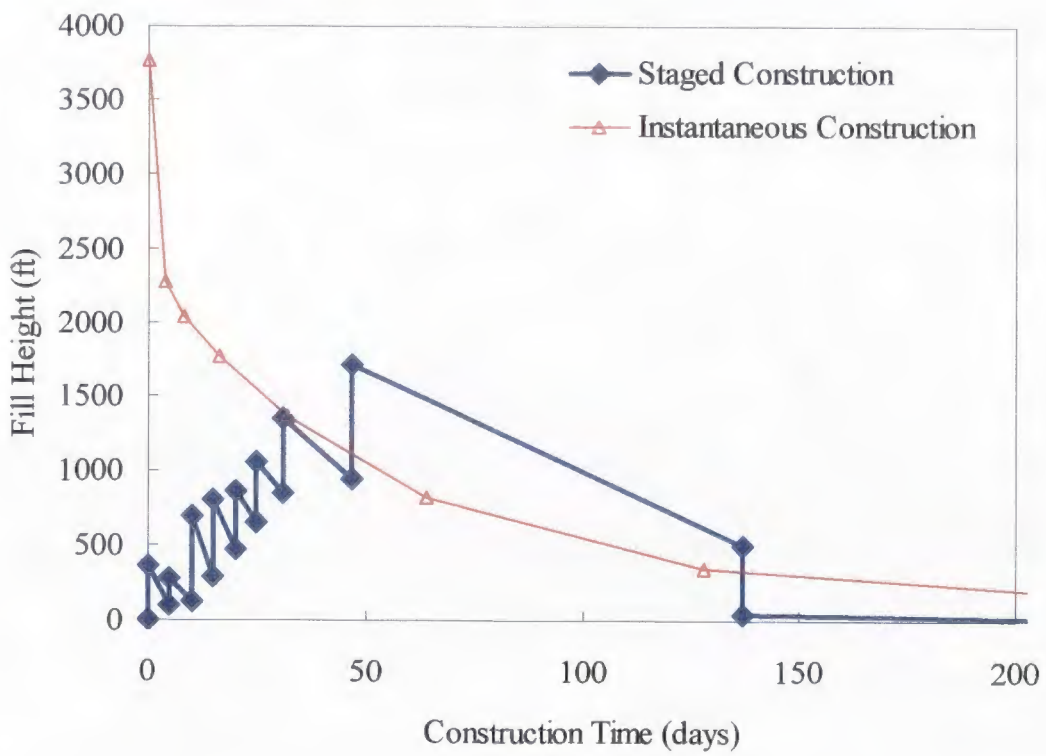

Fig. 5.25 Excess pore pressures versus time for instantaneous and staged construction

5.6 SOIL-REINFORCEMENT INTERACTION

The interaction between the backfill material and the bar mat reinforcement in the MSE wall is a complex three-dimensional phenomenon. Friction along the longitudinal bars, combined with passive resistance from the transverse bars, provide the soil-reinforcement interaction for the system. Plaxis does not have the capacity to fully model such complicated three-dimensional phenomena. Therefore, a highly simplified model was employed. This simplified model is adequate for modeling the external stability of the wall, where the soil reinforcement plays only a minor role. However, the model is inadequate for detailed analysis of the internal stability of the wall.

Modeling this interaction was rather difficult, for several reasons. First, the amount of reinforcement within the wall was not constant throughout the wall height. Although the center-to-center spacing of the bar mats was constant (5.5 ft (1.7 m)), the width of the bar mats varied depending on the position of the reinforcement within the wall. The mats varied from being 1.5 ft (0.5 m) wide (four longitudinal bars spaced at 0.5 ft (152 mm)) to 2.5 ft (762 mm) wide (six longitudinal bars spaced at 0.5 ft (152 mm)). This also implies that the horizontal distance between successive bar mats (ie. "unreinforced soil") varies from 3.0 ft (0.9 m) to 4.0 ft (1.2 m), depending on the width of the bar mats at a particular position.

Another difficulty was the fact that the reinforcement model (geotextile model) in Plaxis only allows the property EA (Young's modulus times the cross sectional area) for the sheet reinforcement. It was determined that the best approach was to use an equivalent EA term for a given layer of reinforcement, using an appropriate modulus of

elasticity for steel and the appropriate equivalent cross sectional area for the longitudinal bars for a given layer of reinforcement.

The final input value that influenced the behavior of the soil-reinforcement interaction was the R_{inter} value. This value is the strength reduction factor for the interfaces, and is a property of the soil that is in contact with the reinforcement. This value allows the strength of the interface to be a function of the soil strength (Plaxis, 1998).

The Plaxis user's manual (1998) notes that R_{inter} may be assumed to be on the order of 0.67 for sand-steel contact, in the absence of more detailed information. Numerous iterations were made to determine the effects of the R_{inter} values on the behavior of the reinforcement as the wall was constructed. It was determined that the strength reduction factor does play a significant role, especially when examining the position and magnitude of the maximum tension within the reinforcement.

5.6.1 Reinforcement Parameters

In comparing the measured tension during construction to the tension in the reinforcement in the model, it was found that the predicted tension distribution and the maximum tension observed in a given mat did not compare very well to the measured values. The maximum tension significantly overestimated the measured values in the lower portion of the wall, while underestimating the tension in the upper section of the wall, as shown in Fig. 5.26. Table 5.9 summarizes the values used to model the soil-reinforcement interaction.

A 3 ft (0.9 m) length of reinforcement near the face of the wall was given a lower EA value than the remaining reinforcement to make it more compliant. Initial model runs produced higher-than-reasonable tensions near the wall face. Making the reinforcement more compliant near the face allowed more reasonable values.

Fig. 5.27 shows a comparison of the measured tension in bar mat PL5 (as given in the Instrumentation report, Bay et al., 2003a, UT-03.11), which is located approximately 20 ft (6.1 m) from the base of the wall. The model is fairly good at predicting the magnitude of maximum tension in this bar mat, and it shows the tension decreasing near the face of the wall, as is expected. However, the overall tension distribution is not very good, and the position of the locus of maximum tension does not correspond to the expected point of maximum tension.

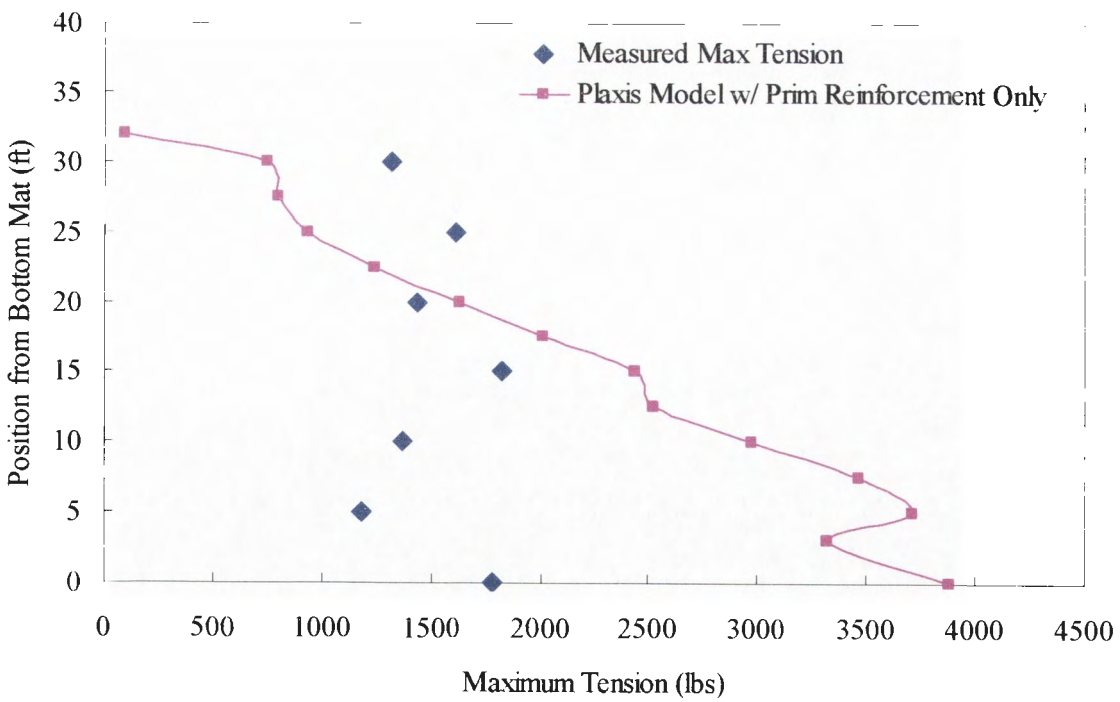

Fig. 5.26 Plaxis model maximum tension versus measured maximum tension plotted with respect to reinforcement position within wall

Table 5.9 Reinforcement Parameters

Description of Bar Mat	EA Value for Geotextile
Four-Bar Longitudinal Bar Mat Near Wall Face	2.07 E 05
General Four-Bar Longitudinal Bar Mat	2.07 E 06
Five-Bar Longitudinal Bar Mat Near Wall Face	2.59 E 05
General Five-Bar Longitudinal Bar Mat	2.59 E 06
Six-Bar Longitudinal Bar Mat Near Wall Face	3.105 E 05
General Six-Bar Longitudinal Bar Mat	3.105 E 06

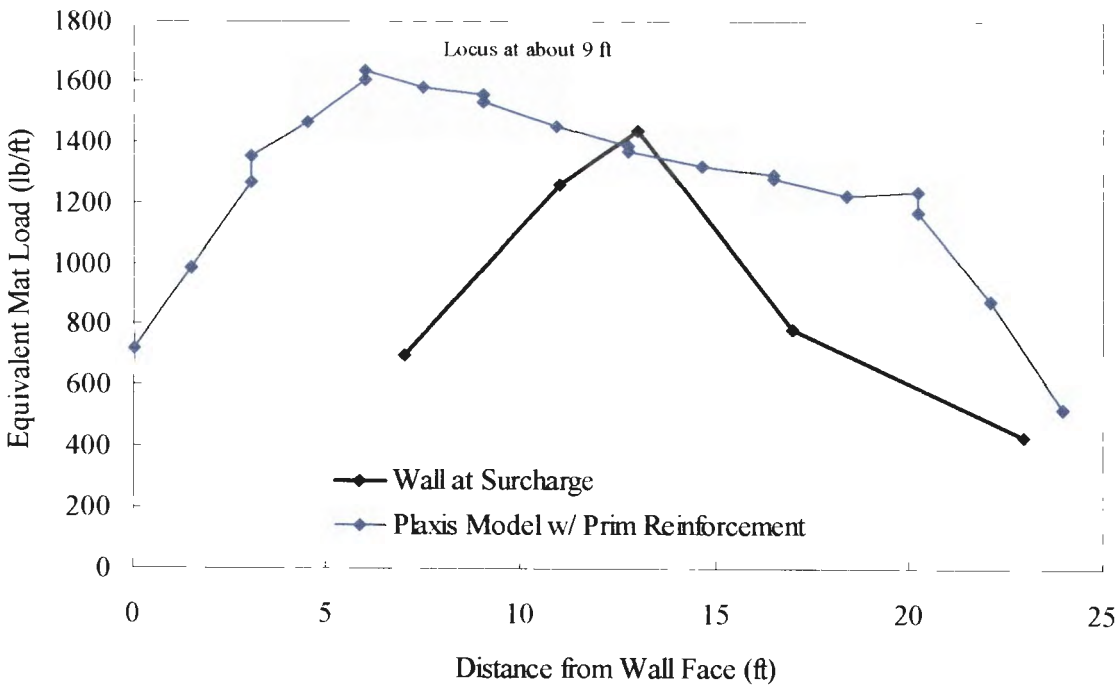

Fig. 5.27 Plaxis model tension versus measured tension in bar mat PL5

5.6.2 *Effects of Intermediate Reinforcement on Wall Behavior*

One of the important purposes of this study was to compare the original reinforcement design (containing only primary reinforcement) to the revised reinforcement design (containing the additional intermediate reinforcement). The observed differences in wall behavior were given in Chapter 3, along with conclusions regarding the effects of the intermediate reinforcement.

It has been mentioned that the simple reinforcement model used in Plaxis does not do a very good job of replicating the measured reinforcement behavior in the field. Again, in attempting to model a three-dimensional problem with complex soil-reinforcement interactions using a two-dimensional geotextile with limited properties and limited soil-interaction capabilities, the shortcomings of the Plaxis model with respect to reinforcement are obvious.

With these limitations in mind, an additional model was created that included the intermediate layers of reinforcement in the lower half of the wall. This intermediate reinforcement would not be expected to affect the overall behavior of the wall to any measurable extent, especially with respect to wall deformation. However, the additional reinforcement would be expected to affect the predicted tension in the primary reinforcement layers. Some comparison was made concerning the measured tension values in the two sections of wall in Chapter 3.

Fig. 5.28 shows a graph similar to that given in Fig. 5.26, but showing both the tension values for the model containing primary reinforcement only and the values for the model containing both primary and intermediate reinforcement. Fig. 5.29 shows a

comparison of the measured tension in bar mat PL2 (located 5 ft (1.5 m) from the base of the wall), the Plaxis model results for PL2 with primary reinforcement only, and the Plaxis model results for PL2 when both primary and intermediate reinforcement were present. As seen, the additional reinforcement had a significant effect on the tension in the lower layers of reinforcement within the wall.

5.7 STABILITY VERSUS TIME

5.7.1 Global Stability Analysis

Once a model was constructed that adequately replicated the measured behavior of the wall and foundation material, a stability analysis was performed to evaluate the stability of the wall. The global stability was investigated using the phi-c reduction

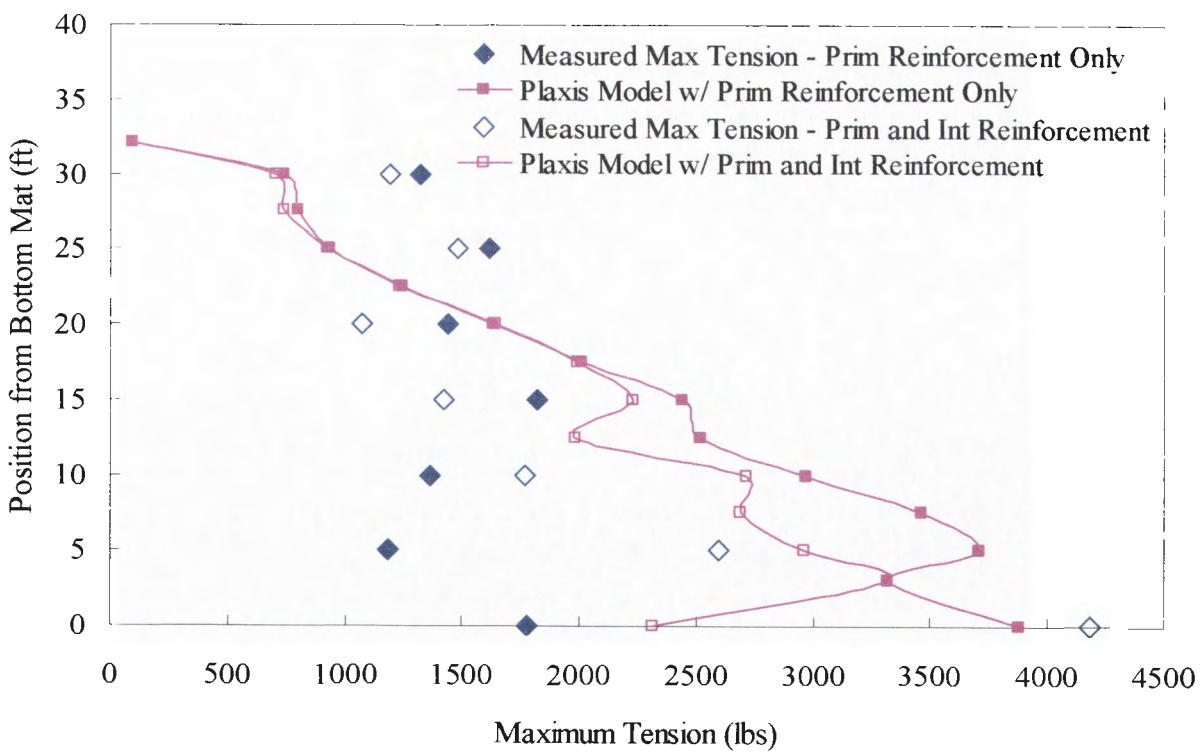

Fig. 5.28 Plaxis model maximum tension versus measured maximum tension plotted with respect to reinforcement position within wall

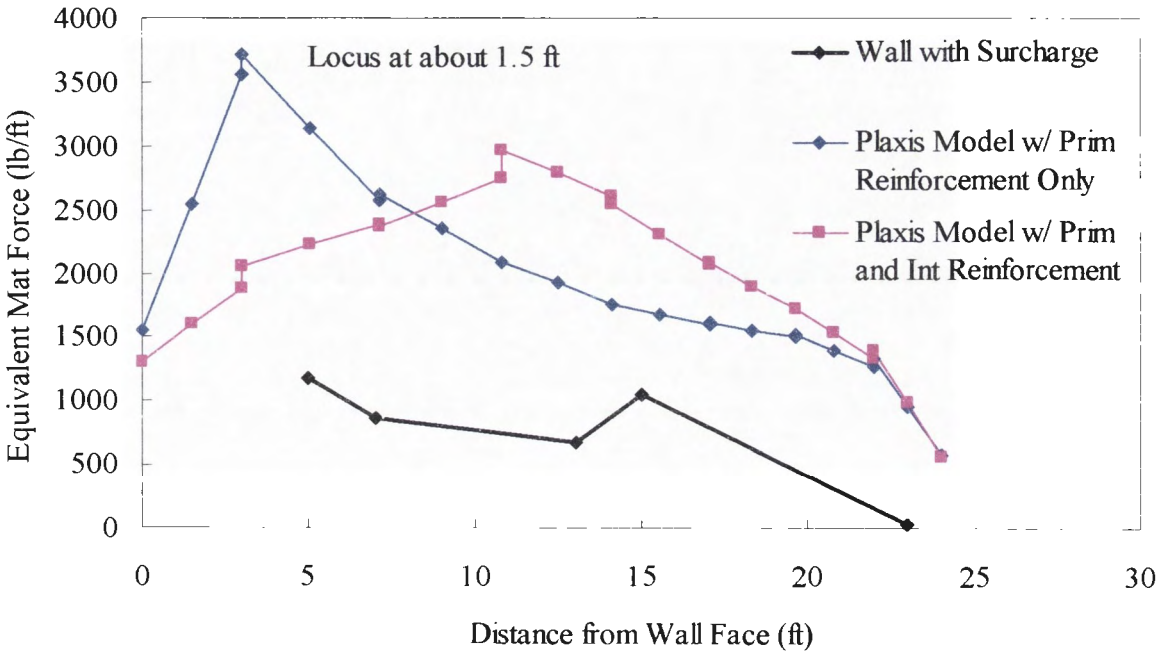

Fig. 5.29 Plaxis model tension versus measured tension in bar mat PL2

method in the Plaxis software. Using this procedure, a factor of safety is calculated by monitoring deformations at points within the model while reducing the soil's strength parameters (tanϕ and c) by a factor of ΣMsf. When the wall stability becomes critical, deformations will become large, and the value of ΣMsf represents the factor of safety.

Fig. 5.30 compares the global stability (as a factor of safety) versus time for the construction sequence of the wall, as estimated from field notes during the project. Also shown in Fig. 5.30 is the factor of safety versus time as calculated for the instantaneous construction mentioned previously. As expected, the instantaneous construction had a much lower initial factor of safety due to much higher excess pore pressures in the foundation material. However, as consolidation occurs, the instantaneous factor of safety

converges to a value nearly identical to the long-term factor of safety for the staged construction.

It should be noted that the factor of safety calculated by Plaxis for the original I-15 embankment was 1.96, with a failure surface that will be shown later. The reason for the increase in the factor of safety during the construction of the wall is that initially the wall behaves as a berm for the embankment, forcing the failure surface further up the embankment, and increasing the factor of safety. However, when the wall becomes high enough, the failure surface is forced into the foundation soil, which again decreases the factor of safety. The long-term factor of safety for the wall is 1.81 for the staged construction at the final embankment height.

Fig. 5.31 compares the global stability (as a factor of safety) as a function of the wall height for the construction sequence of the wall. The significance of the initial 20 ft (6.1 m) of wall acting as a berm for the original embankment is evident in this figure. Slight increases in the factor of safety as the soil consolidates at a given wall height are due to increases in the soil strength with consolidation.

Fig. 5.32 through Fig. 5.39 show the progression of the failure surfaces through the staged construction process. These figures show the deformation vectors calculated during the phi-c reduction procedure. These vectors show the extent of the sliding soil mass and the location of the failure surface. As noted, initially the failure surface was a surficial failure in the original embankment. The factor of safety for the original embankment was 1.96. The initial several lifts of the wall provided a berm for the embankment failure, which increased the factor of safety from about 2.0 to a maximum of about 2.4 when the wall height was 20 ft (6.1 m). However, as construction

progressed, and as the effect of the berm was overcome, the failure surface was forced into the foundation soil, as seen in the later figures. The factor of safety dropped to a minimum value of 1.57 when the surcharge was applied, then increased to a final value of 1.81 for the final wall configuration as consolidation occurred.

Of particular note is the shape of the failure surface for the final wall configuration. As seen in Fig. 5.39, for example, the failure surface has a V-shape, with total movement being downward and away from the original embankment in the backfill material and the foundation material beneath the wall backfill, and with total movement being upward and away from the wall in the foundation material outside the wall footprint. It is noteworthy that such a failure surface would NOT be predicted using a traditional slope stability analyses, where a circular or spiral failure surface would be used to compute a factor of safety. Thus, for this case, it appears that a traditional slope stability approach would not be conservative.

Fig. 5.40 shows the failure surface for the instantaneous construction of the wall. It should be noted that the minimum factor of safety for the instantaneous construction (immediately after applying the load) is a value of 1.25 for applying the entire surcharge, while a value of 1.38 is obtained when applying the final wall height (ie. no surcharge) instantaneously. These values are both significantly less than the factors of safety calculated during the staged construction process.

5.7.2 Additional External Stability Failure Modes

Once the analysis of the global stability of the wall was completed, an analysis of some additional external failure modes was performed. This analysis was completed

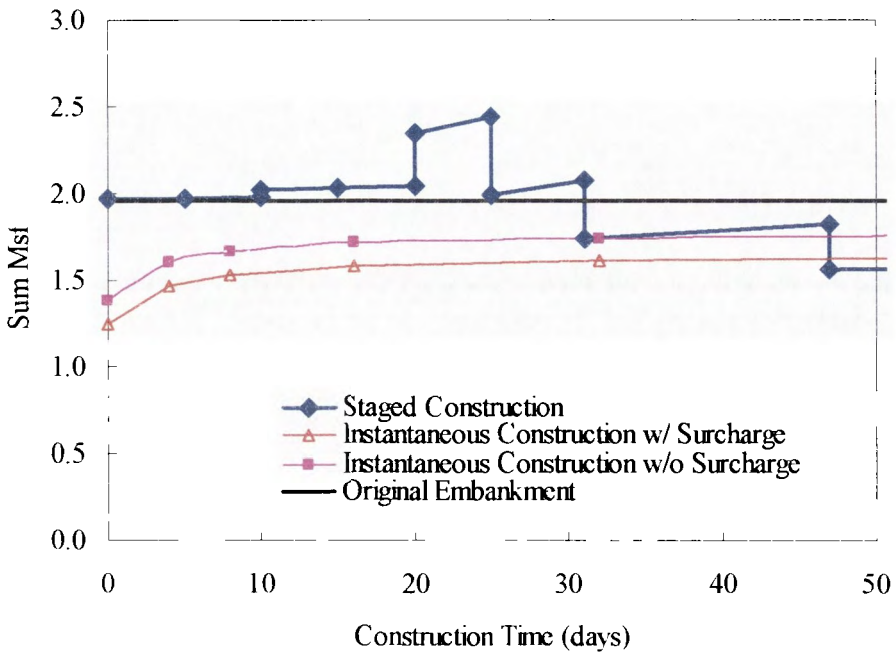

a) First 50 days

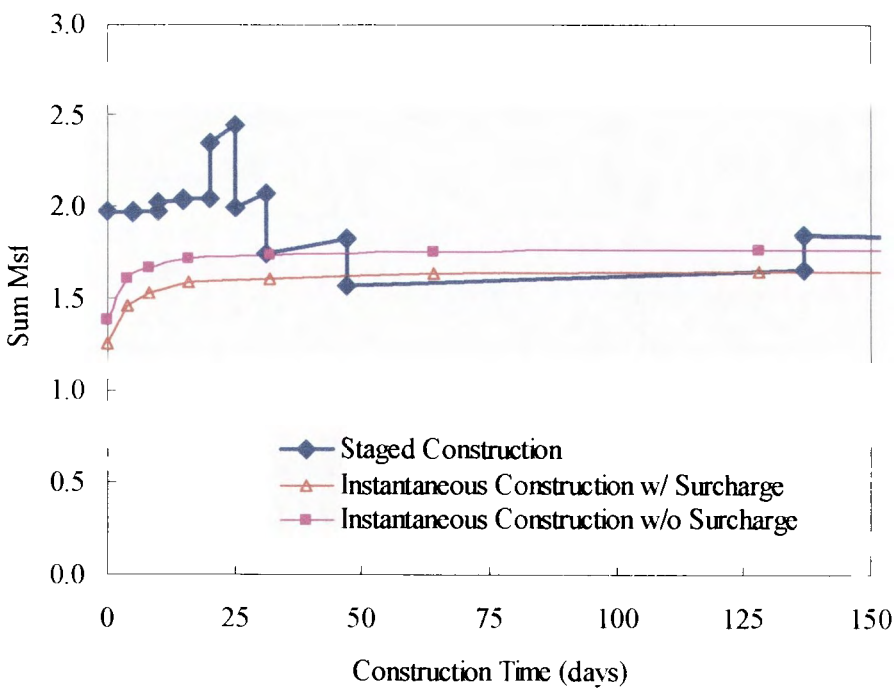

b) First 150 days

Fig. 5.30 Global stability of MSE wall versus time

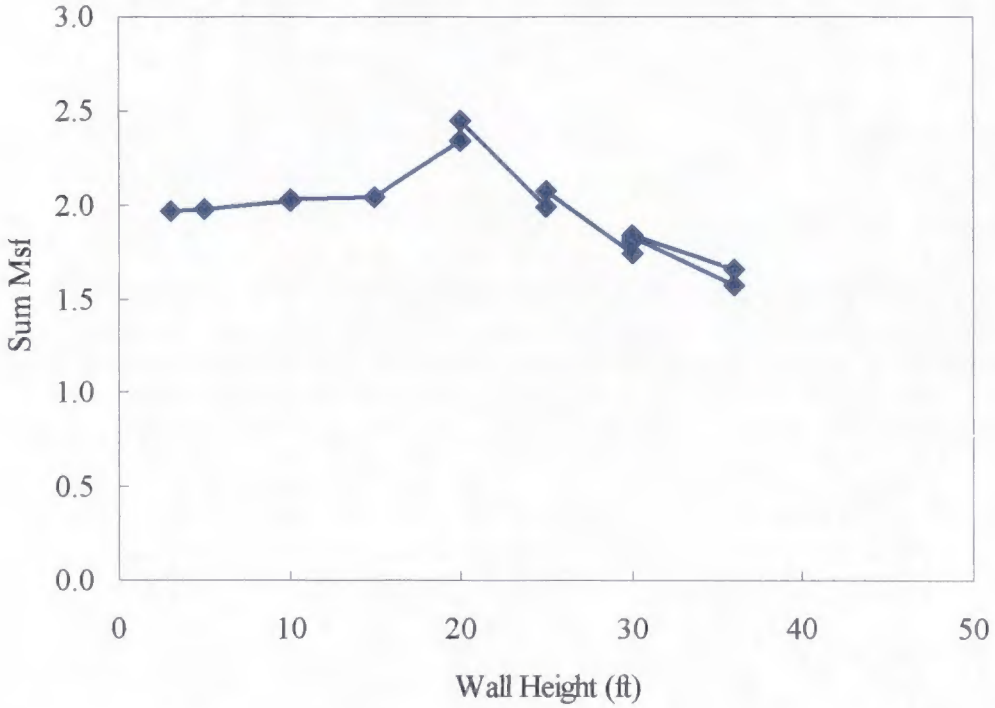

Fig. 5.31 Global stability of MSE wall as a function of wall height

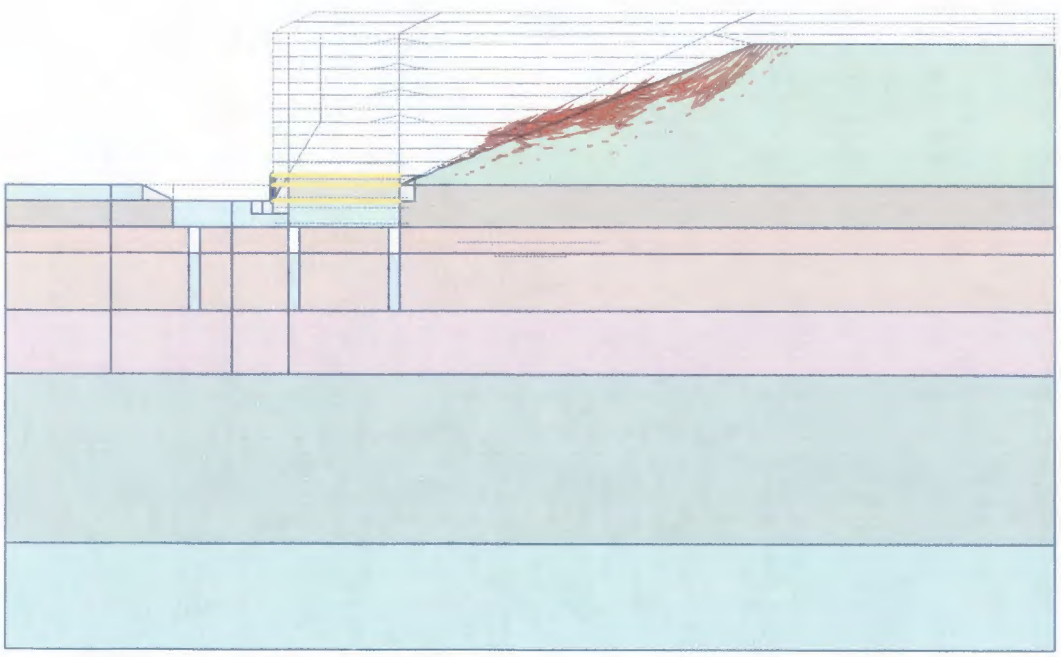

Fig. 5.32 Deformation vectors after Phi-C reduction for 5 ft wall

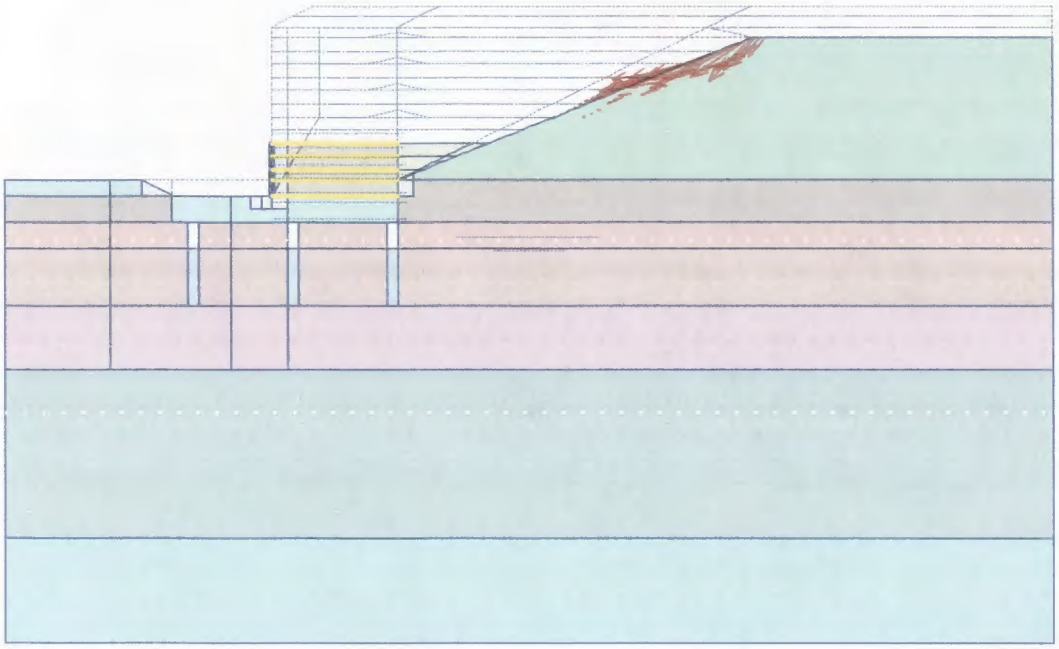

Fig. 5.33 Deformation vectors after Phi-C reduction for 10 ft wall

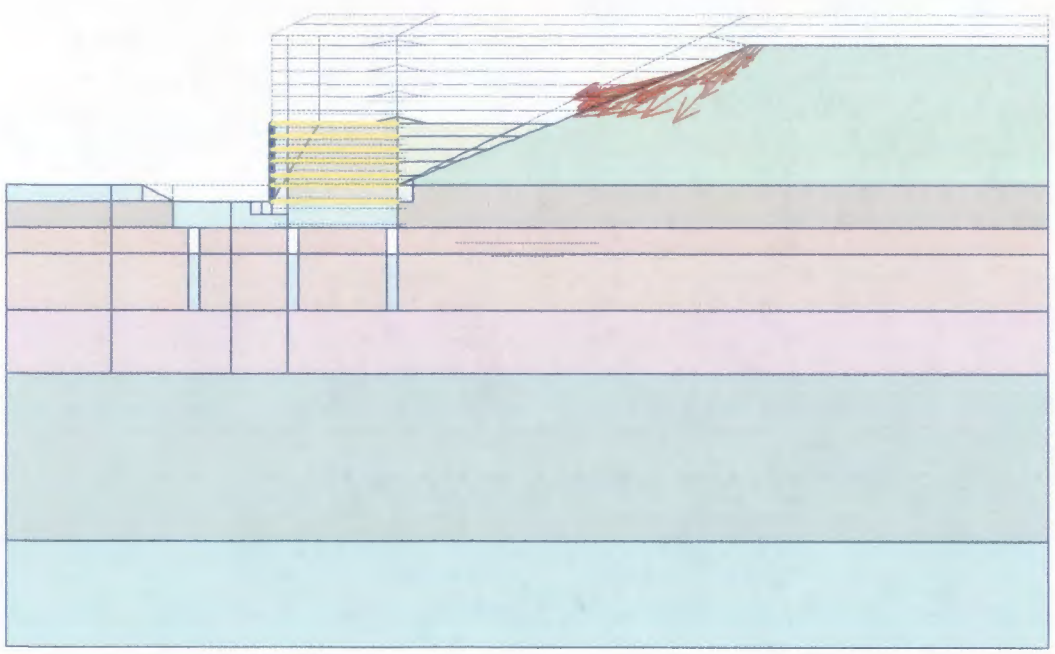

Fig. 5.34 Deformation vectors after Phi-C reduction for 15 ft wall

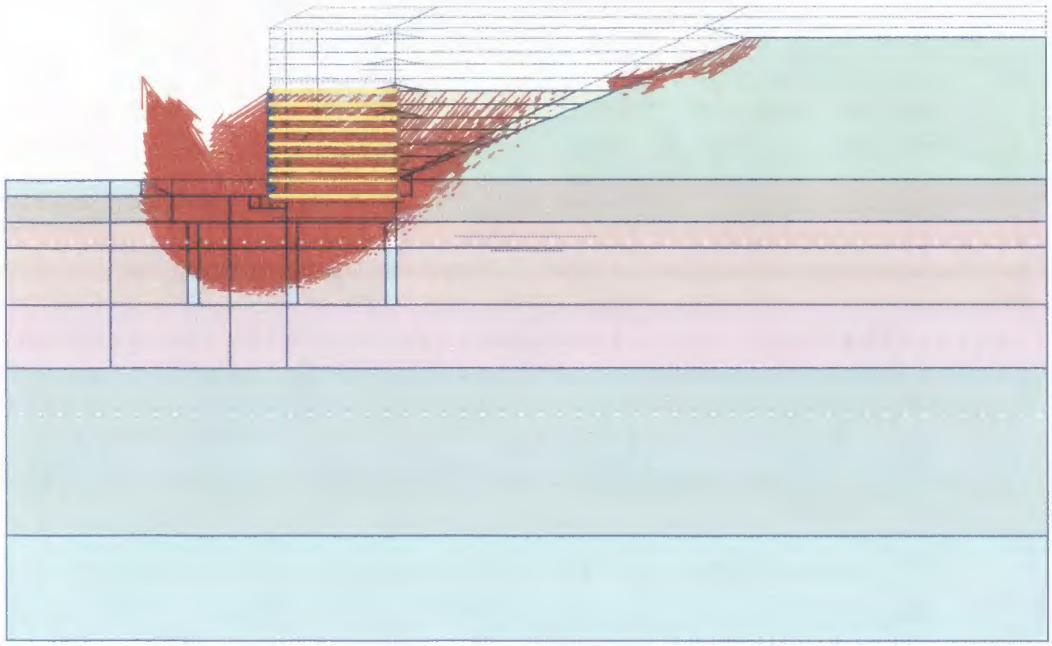

Fig. 5.35 Deformation vectors after Phi-C reduction for 20 ft wall

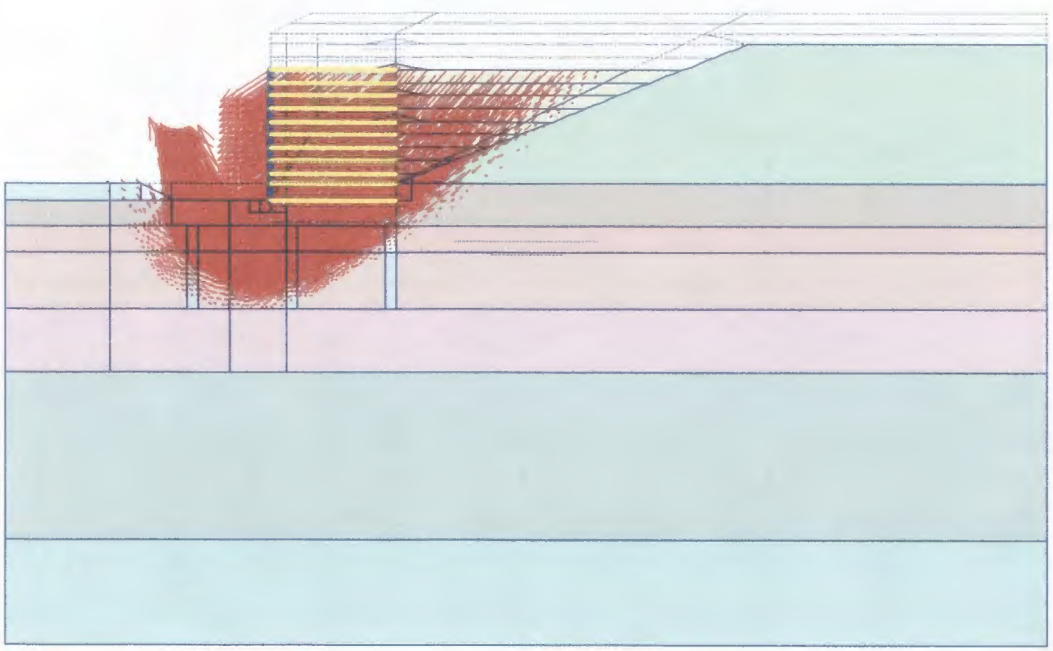

Fig. 5.36 Deformation vectors after Phi-C reduction for 25 ft wall

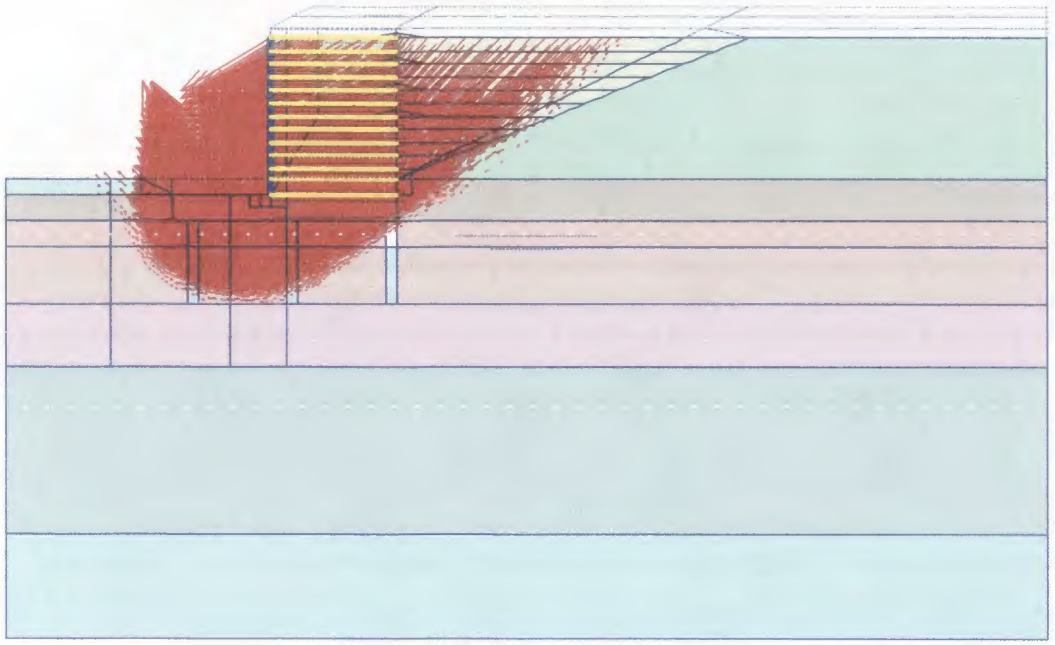

Fig. 5.37 Deformation vectors after Phi-C reduction for 30 ft wall

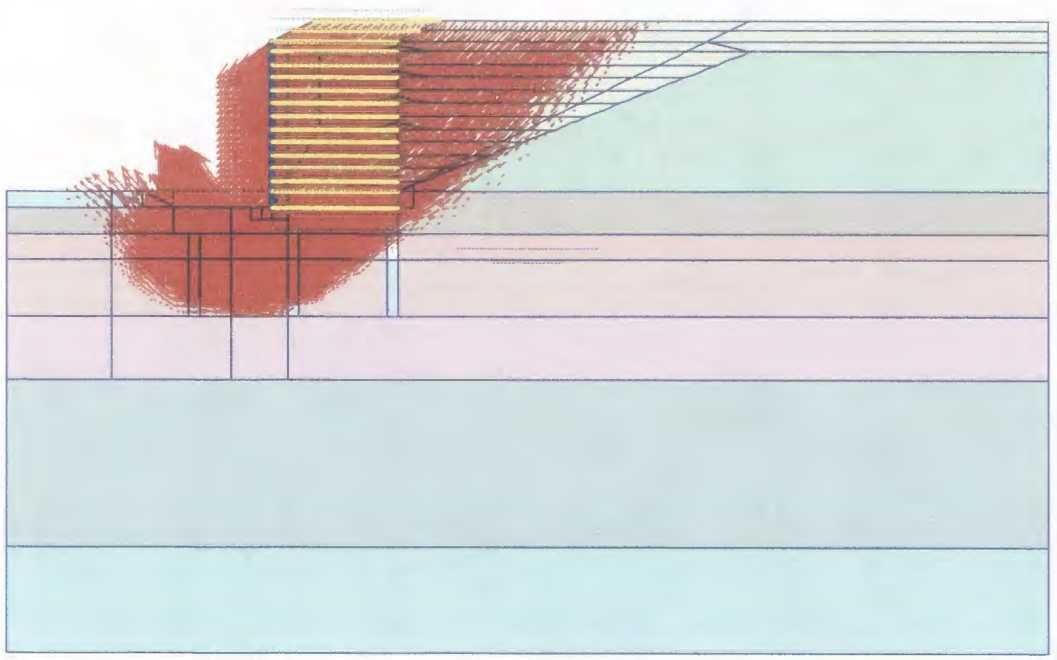

Fig. 5.38 Deformation vectors after Phi-C reduction for wall with surcharge

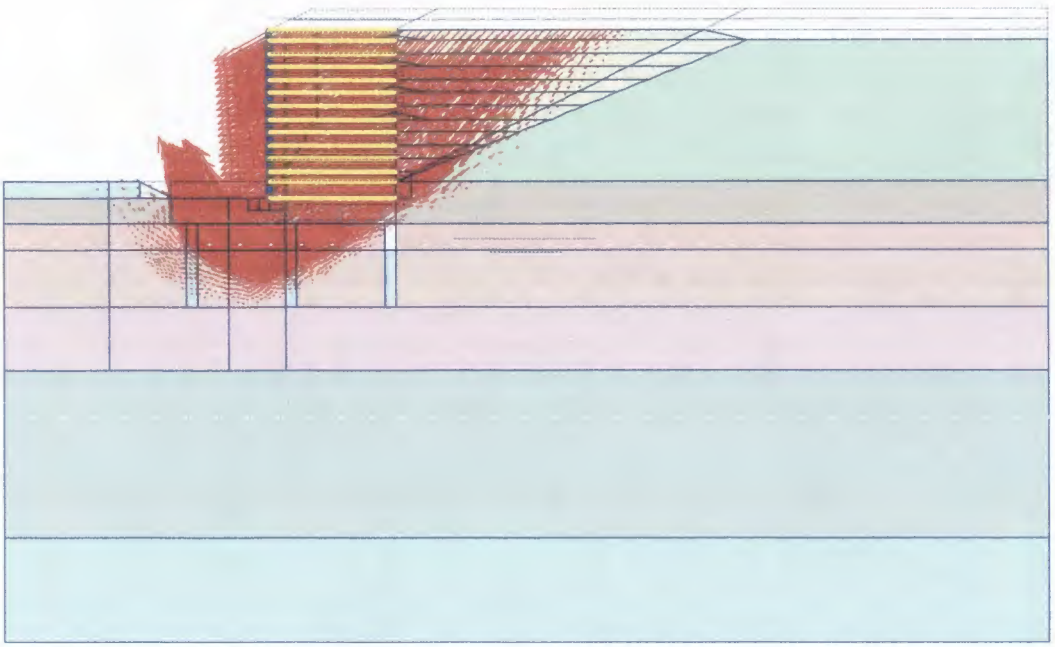

Fig. 5.39 Long-term deformation vectors after Phi-C reduction for final wall

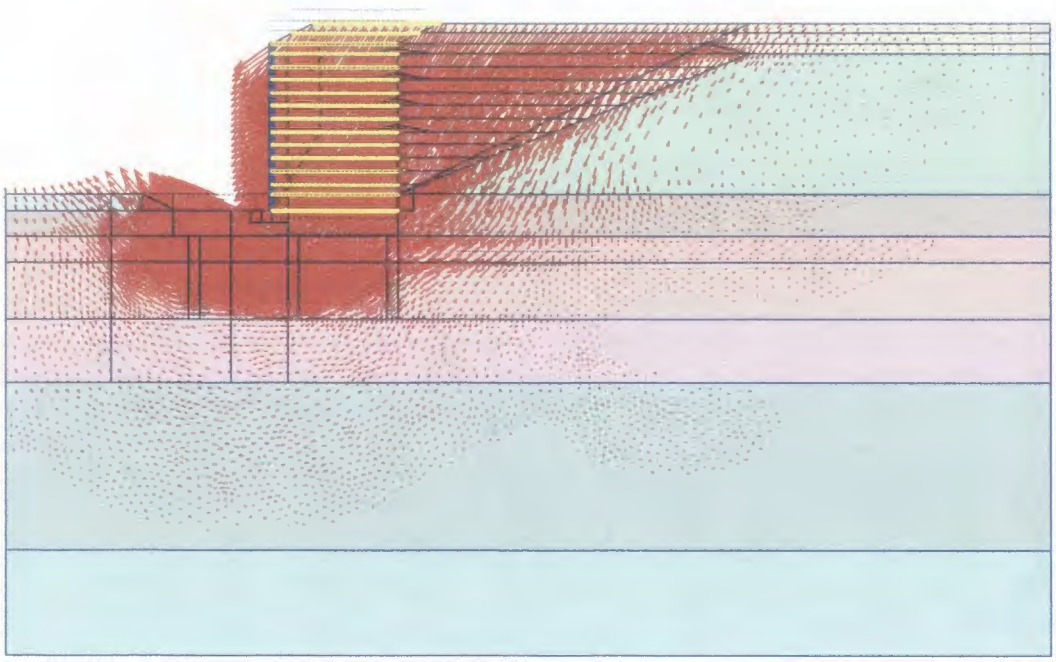

Fig. 5.40 Deformation vectors after Phi-C reduction for instantaneous wall construction

using two additional wall models, which were simplified from the full model to decrease computation time and to achieve the desired failure mode.

5.7.2.1 Overturning Failure. The first model used to investigate a specific failure mode utilized an elastic material for the foundation soil beneath the MSE wall. This would prevent failure of the foundation material and force failure to occur within the wall itself. The modulus values needed to be adjusted from the soil hardening modulus values used for each soil type in the original model (E_{ref}, E_{oed}, E_{ur}) to a single E_{50} value for each soil type. Recall that the elastic soil model will NOT take into consideration the stress history of the soil, adjusting the modulus to account for confinement and stress history. The E_{50} values were adjusted so that roughly the same settlement of the wall occurred as had been achieved during the actual construction of the wall.

Once the foundation materials were adjusted accordingly, the wall was constructed instantaneously, ignoring undrained behavior. The ultimate settlement of the wall was checked to ensure that roughly the same settlement was present. At this point, a Phi-C reduction was used to determine the factor of safety (given in Plaxis as ΣM_{sf}) for the wall and the failure mode.

Fig. 5.41 shows a plot of the factor of safety versus deflection for a point within the wall backfill. The deflections are extreme, as is expected from a Phi-C reduction using the Plaxis software. Both the case investigating the wall at full height with surcharge and the case of the wall at final height are given in the figure. As seen, there is no significant difference between the two cases, with a factor of safety against overturning being about 2.1 for both cases.

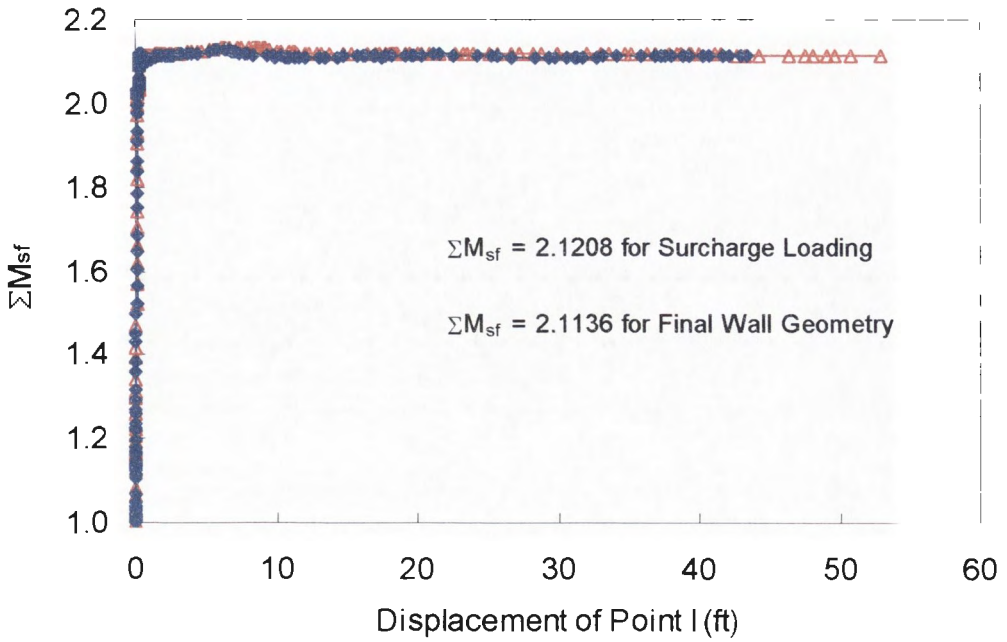

Fig. 5.41 Factor of safety versus deflection of point within wall backfill for overturning failure

Fig. 5.42 shows a plot of the deformed mesh following the Phi-C reduction. With the entire foundation being an elastic material, the failure mode is forced to be an overturning failure, as seen in the figure.

5.7.2.2 Sliding Failure. Next, the failure mode of sliding was investigated. To allow sliding to occur, the granular fill beneath the wall and the clay soil above the water table were again given the hardening soil properties assigned for the full model. The remaining foundation materials were left with the elastic properties as given in the overturning investigation. A loading sequence identical to the full model investigation was performed, such that the granular fill and the upper clay would have identical modulus values as the full wall model. At this point, the entire wall was constructed instantaneously, again ignoring undrained behavior, and a Phi-C reduction was performed

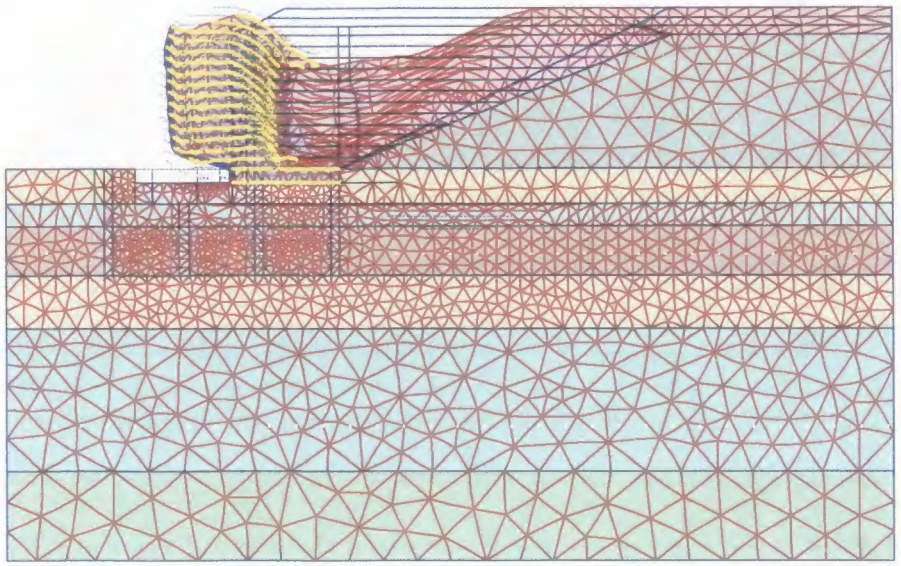

Fig. 5.42 Deformed mesh following Phi-C reduction for overturning failure

to determine the factor of safety. As before, factors of safety were calculated for both the wall with surcharge applied and the wall at final height. A plot of the factor of safety versus deflection for a point within the wall backfill is given in Fig. 5.43, with a plot of the deformed mesh following the Phi-C reduction given in Fig. 5.44. Again, the factor of safety is essentially identical in comparing the wall with surcharge to the final wall geometry.

As seen in comparing Fig. 5.40 to Fig. 5.42, it appears that the factor of safety is lower for the sliding mode of failure (1.93) than for the overturning mode of failure (2.12). However, both failure mechanisms have a higher factor of safety than that found for the wall when investigating the global stability (1.81), such that the global stability appears to be the controlling method of failure.

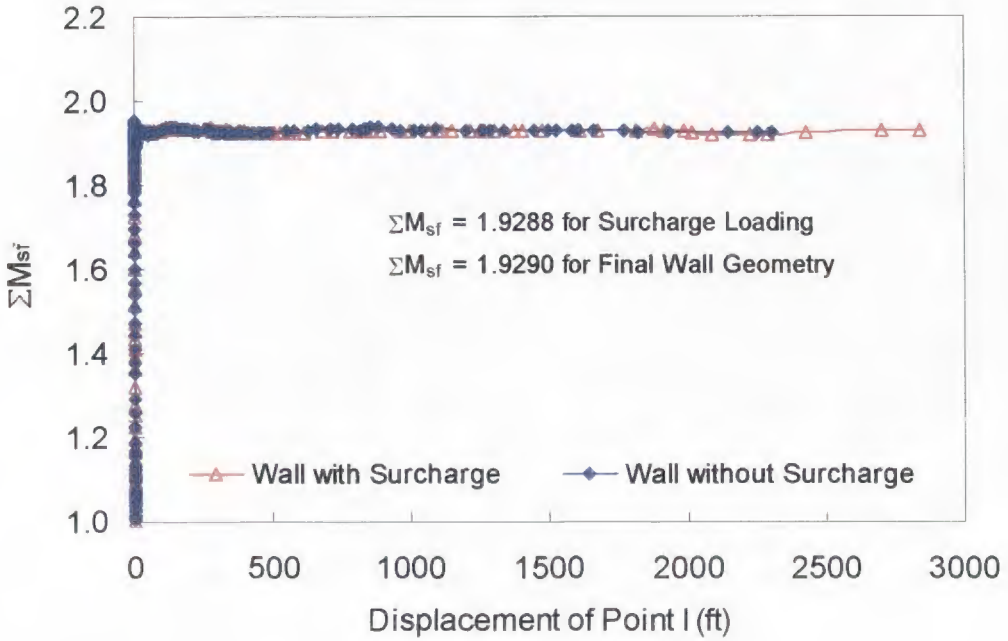

Fig. 5.43 Factor of safety versus deflection of point within wall backfill for sliding failure

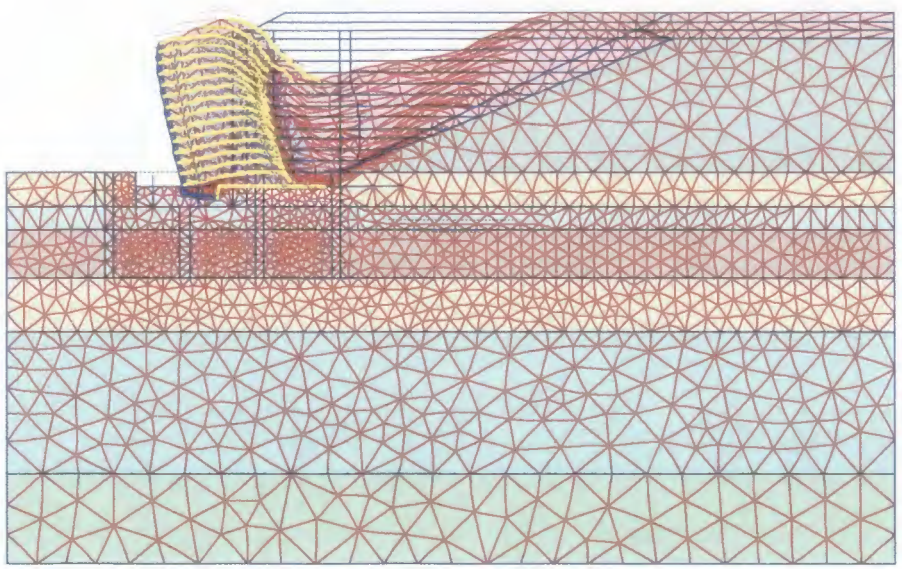

Fig. 5.44 Deformed mesh following Phi-C reduction for sliding failure

5.7.3 Internal Stability Analysis

As discussed in section 5.1, the Plaxis model is unable to adequately model the complex, three-dimensional behavior of steel bar mats. Therefore, an internal stability analysis would be flawed and incomplete. Issues such as pull-out resistance and tensile failure are not considered. Mention of the internal stability is included in this report to show the capacities and limitations of Plaxis, but should not be used to infer the internal stability of the wall.

5.8 CONCLUSIONS REGARDING THE FINITE ELEMENT MODEL

This report presents the results of a finite element model of the mechanically stabilized earth (MSE) wall located on I-15 at 3600 South in Salt Lake City, Utah. The model was created and calibrated using data collected at the construction site during and after construction of the wall, as well as using the results of extensive laboratory testing on samples collected at the site. Such a model is a powerful tool in understanding the behavior of a tall MSE wall on a compressible foundation.

This analytical model includes a number of soil models to represent the range of soils in the foundation of the wall, as well as additional soil models to represent the fill material used for the original I-15 embankment and the new material used to construct the MSE wall. Trench drains, with adjusted soil permeabilities, were used to represent the prefabricated vertical drains (PVDs) used at the site. The bar mat reinforcement used to construct the wall was also modeled, with special consideration as to the effects of soil-reinforcement interaction.

The analytical model was calibrated to match the measured long-term horizontal and vertical deflections at the wall site. Once this was accomplished, the effective permeability of the foundation soil was adjusted and the construction sequence approximated in order to match the time settlement behavior of the wall. When the model was considered to accurately represent the MSE wall for both the long- and short-term behavior, a stability analysis was performed at various stages of construction to observe the external stability of the wall throughout the construction process and in the years following construction.

For the model following the staged construction of the wall, the factor or safety for the original embankment was 1.96. This value increased slightly as the wall was built, since initially the wall acted as a berm, forcing the failure surface up the embankment. However, once the wall was approximately halfway constructed, the failure surface was forced into the foundation material, and the factor of safety decreased to a minimum value of 1.57 at the application of the surcharge load, then increased with consolidation to a value of 1.81 for the long-term factor of safety for the MSE wall at final grade. A minimum factor of safety of 1.25 was calculated for instantaneous construction of the wall, which increased with consolidation to a value nearly identical to the long-term value obtained from the staged construction.

As determined during the external stability analysis, the failure surface has a V-shape, with total movement being downward and away from the original embankment in the backfill material and the foundation material beneath the wall backfill, and with total movement being upward and away from the wall in the foundation material outside the wall footprint. It is noteworthy that such a failure surface might not be predicted using

traditional slope stability analyses, where a circular or spiral failure surface would typically be used to compute a factor of safety. Thus, for this case, it appears that a traditional slope stability approach would not be conservative. This is a key reason for using a finite element program to perform slope stability (or other stability) evaluations instead of the more traditional software packages that are limited to circular or spiral failure surfaces.

The effects of pore pressure dissipation during construction can be evaluated, and were taken into account during the stability analyses and in calibrating the time-settlement behavior. The effects of excess pore pressure were significant. Substantial excess pore pressures developed during the construction process, and dissipated with time. However, the pore pressures that developed were much less than those that would occur if an immediate, undrained construction had occurred. Thus, an undrained strength approach would be quite conservative, while a drained strength approach would be unconservative. Using a soil model that accounts for the generation and dissipation of pore pressures and accounts for those excess pore pressures in performing stability analyses is of the utmost importance.

The ability to model the interaction between the soil and the reinforcement is somewhat limited, due to the limitations in the Plaxis software. However, a model was developed that overestimates the tension in the reinforcement in the lower portion of the wall while underestimating the tension in the upper portion of the wall. With this limited and simplified model of the soil-reinforcement interaction, an analysis of some additional external failure modes was performed. The modes of overturning and sliding were investigated, while internal modes relating to pull-out failure and tensile failure of the

reinforcement were not considered. These additional analyses resulted in a factor of safety for sliding of approximately 1.9 and a factor of safety for overturning of approximately 2.1.

CHAPTER 6

SUMMARY AND CONCLUSIONS

6.1 WALL PERFORMANCE

Overall, throughout construction and in the years following construction the wall is performing well. Results of this study show that there is adequate reinforcement within the wall, with stresses in the reinforcement being well below the allowable. The wall is internally stable, in spite of large deformations near the face of the wall. The wall is externally stable. The expected large primary settlement of the wall did occur, but little secondary settlement has taken place. There is no evidence of deep-seated wall movement. Finally, a comparison of the section of wall containing only primary reinforcement to that containing primary and intermediate reinforcement led to the following conclusions:

- Intermediate reinforcement was not necessary for stability of the wall, since the section of wall not containing additional reinforcement was found to be both internally and externally stable,
- Intermediate reinforcement did decrease the deformations of the wall face in the lower portion of the wall, resolving the constructibility issues that had been a problem with previous walls not containing the intermediate reinforcement, and
- Intermediate reinforcement could be omitted without consequence if another method to control deformations of the wall face is utilized.

A number of steps were required to allow additional measurements to be taken and to protect the instrumentation for long-term monitoring. A number of challenges that were overcome were explained. Each of the instruments for which data was collected during construction was discussed to illustrate the post-construction changes in the wall and any changes in the ability to take such measurements. As noted, the instrumentation is now protected to allow future readings to take place, and the measurement changes in the years following construction were shown to be quite minimal.

6.2 SOIL SAMPLING AND LABORATORY TESTING

Comparisons of piston and shelby tube samples indicate that piston samples are less disturbed than shelby tube samples. X-rays show significantly fewer fractures in piston samples than shelby tube samples. The average radius of the consolidation curves at the points of maximum past pressure was less (indicating a sharper break between reconsolidation and virgin consolidation) for the piston samples than the shelby tube samples, resulting in less uncertainty in maximum past pressure predictions. Interestingly, there was no significant difference in maximum past pressure or $C_{c\varepsilon}$ between the piston and the shelby tube samples. This may be because the radiograph images were used to select portions of the sample to use in consolidation tests. Thus, the most disturbed portions of the samples were not tested. The piston samples also exhibited higher initial moduli (E_{50}) values than the shelby tube samples in the unconfined compression test. This is also indicative of less sample disturbance. The shape of the consolidation curves for piston samples are generally better than those of shelby tube samples with the same drilling method.

The differences in sample disturbance were not as recognizable or significant between the two drilling methods. The quantities of fractures and cracks identified in radiograph images were similar for the two drilling methods. The CRS tests show slightly less disturbance in the rotary wash samples than the hollow stem auger samples. The average radius of the consolidation curves at the points of maximum past pressure was somewhat lower for the rotary wash samples than the hollow stem auger samples, resulting in less uncertainty in maximum past pressure for the rotary wash samples. Again, there was no significant difference in the average maximum past pressure or $C_{\alpha\varepsilon}$ between rotary wash and hollow stem auger samples.

Based upon this research, several recommendations can be made as to methods that should be employed in drilling and sampling to minimize the effects of sample disturbance in Bonneville clays or similar soft clays. These are:

- Piston samplers along with thin-walled sampling tubes should be used rather than shelby tube samplers for obtaining specimens for consolidation, triaxial, and other critical geotechnical tests.
- It was observed that fixed piston and free piston samplers obtain samples of similar high quality.
- Radiograph (x-ray) images of the soil specimens provide a powerful tool for assessing sample disturbance, selecting the least disturbed portions of the sample for critical tests, and identifying locations of sand lenses in soft clay samples.
- Very careful rotary wash drilling methods may result in slightly less sample disturbance than hollow stem auger drilling, but the results were inconclusive.

- When hollow stem auger drilling is used, the auger should be advanced slowly using slow rotation (as was done in this work) to minimize disturbance to the surrounding soil.
- Sample recovery can be increased by waiting a period of several minutes after pushing a sample tube before attempting to extract the sample from the ground.

6.3 MECHANICALLY STABILIZED EARTH WALL FINITE ELEMENT MODEL

This research presents the results of a finite element model of the mechanically stabilized earth (MSE) wall located on I-15 at 3600 South in Salt Lake City, Utah. The model was created and calibrated using data collected at the construction site during and after construction of the wall, as well as using the results of extensive laboratory testing on samples collected at the site. Such a model is a powerful tool in understanding the behavior of a tall MSE wall on a compressible foundation.

This analytical model includes a number of soil models to represent the range of soils in the foundation of the wall, as well as additional soil models to represent the fill material used for the original I-15 embankment and the new material used to construct the MSE wall. Trench drains, with adjusted soil permeabilities, were used to represent the prefabricated vertical drains (PVDs) used at the site. The bar mat reinforcement used to construct the wall was also modeled, with special consideration as to the effects of soil-reinforcement interaction.

The analytical model was calibrated to match the measured long term horizontal and vertical deflections at the wall site. Once this was accomplished, the effective permeability of the foundation soil was adjusted and the construction sequence

approximated in order to match the time settlement behavior of the wall. When the model was considered to accurately represent the MSE wall for both the long- and short-term behavior, a stability analysis was performed at various stages of construction to observe the external stability of the wall throughout the construction process and in the years following construction. For the model following the staged construction of the wall, the factor or safety for the original embankment was 1.96. This value increased slightly as the wall was built, since initially the wall acted as a berm, forcing the failure surface up the embankment. However, once the wall was approximately halfway constructed, the failure surface was forced into the foundation material, and the factor of safety decreased to a minimum value of 1.57 at the application of the surcharge load, then increased with consolidation to a value of 1.81 for the long term factor of safety for the MSE wall at final grade. A minimum factor of safety of 1.25 was calculated for instantaneous construction of the wall, which increased with consolidation to a value nearly identical to the long term value obtained from the staged construction.

As determined during the external stability analysis, the failure surface has a V-shape, with total movement being downward and away from the original embankment in the backfill material and the foundation material beneath the wall backfill, and with total movement being upward and away from the wall in the foundation material outside the wall footprint. It is noteworthy that such a failure surface would NOT be predicted using traditional slope stability analyses, where a circular or spiral failure surface would be used to compute a factor of safety. Thus, for this case, it appears that a traditional slope stability approach would not be conservative. This is a key reason for using a finite element program to perform slope stability (or other stability) evaluations instead of the

more traditional software packages that may be limited to circular or spiral failure surfaces.

The effects of pore pressure dissipation during construction can be evaluated, and were taken into account during the stability analyses and in calibrating the time-settlement behavior. The effects of excess pore pressure were significant. Substantial excess pore pressures developed during the construction process, and dissipated with time. However, the pore pressures that developed were much less than those that would occur if an immediate, undrained construction had occurred. Thus, an undrained strength approach would be quite conservative, while a drained strength approach would be unconservative. Using a soil model that accounts for the generation and dissipation of pore pressures and accounts for those excess pore pressures in performing stability analyses is of the utmost importance.

The ability to model the interaction between the soil and the reinforcement is somewhat limited, due to the limitations in the Plaxis software. However, a model was developed that overestimates the tension in the reinforcement in the lower portion of the wall while underestimating the tension in the upper portion of the wall. With this limited and simplified model of the soil-reinforcement interaction, an analysis of some additional external failure modes was performed. The modes of overturning and sliding were investigated, while internal modes relating to pull-out failure and tensile failure of the reinforcement were not considered. These additional analyses resulted in a factor of safety for sliding of approximately 1.9 and a factor of safety for overturning of approximately 2.1.

LITERATURE CITED

"AASHTO LRFD Bridge Design Specifications." (1998). AASHTO, Washington, D.C.

Abdi, R., de Buhan, P., and Pastor, J. (1994). "Calculation of the critical height of a homogenized reinforced soil wall: A numerical approach." *Int. J. for Numer. and Anal. Methods in Geomechanics,* 18(7), 485-505.

Adib, M., Mitchell, J.K., and Christopher, B. (1990). "Finite element modelling of reinforced soil walls and embankments." *Geotechnical Special Publication No. 25 - 1990 Specialty Conference on Design and Performance of Earth Retaining Structures.* ASCE, New York, N.Y., 409-423.

Anderson, L.R., Sharp, K.D., and Harding, O.T. (1987.) "Performance of a 50-foot high welded wire wall." *Geotechnical Special Publication No. 12 - 1987 Specialty Conference on Soil Improvement - A Ten Year Update.* ASCE, New York, N.Y., 280-308.

ASTM Standard D 1587-00. (2000). "Practice for thin-walled tube geotechnical sampling of soils." *ASTM Standards in Building Codes: Specifications, Test Methods, Practices, Classifications, Terminology.* ASTM International, West Conshohocken, Penn, 905-908.

ASTM Standard D 4186-89. (1998). "Test method for one-dimensional consolidation properties of soils using controlled-strain loading." *ASTM Standards in Building Codes: Specifications, Test Methods, Practices, Classifications, Terminology.* ASTM International, West Conshohocken, Penn, 780-785.

Bay, J.A., Anderson, L.R., Budge, A.S., and Goodsell, M.W. (2003a). "Instrumentation and installation scheme of a mechanically stabilized earth wall on I-15 with results of wall and foundation behavior." Report No. UT-03.11, Utah Department of Transportation, Salt Lake City, Utah.

Bay, J.A., Anderson, L.R., Hagen, J.C., and Budge, A.S. (2003b). "Factors affecting sample disturbance in Bonneville clays." Report No. UT-03.14, Utah Department of Transportation, Salt Lake City, Utah.

Bay, J.A., Anderson, L.R., Colocino, T.M., and Budge, A.S. (2003c). "Evaluation of SHANSEP parameters for soft Bonneville clays." Report No. UT-03.13, Utah Department of Transportation, Salt Lake City, Utah.

Bergado, D.T., Anderson, L.R., Muira, N., and Balasubramaniam, A.S. (1996). *Soft Ground Improvement in Lowland and Other Environments.* ASCE Press, New York.

Bergado, D.T., Chai, J.C., Alfaro, M.C., and Balasubramaniam, A.S. (1992). "Improvement techniques of soft ground in subsiding and lowland environment." Division of Geotechnical and Transportation Engineering, Asian Institute of Technology, Bangkok, Thailand.

Cadden, A.W., and Harris, R.S., Jr. (1998). "Foundation evaluation for 8.5 m MSE wall." *Geotechnical Special Publication No. 77 - Proc., 1998 GeoCongress.* ASCE, Reston, Va., 69-78.

Chang, J.C., Hannon, J.B., and Forsyth, R.A. (1977). "Pull resistance and interaction of earthwork reinforcement and soil." Transportation Research Board Record 640, Transportation Research Board, National Research Council, Washington, D.C., 1-7.

Federal Highway Administration. (2001). *Mechanically Stabilized Earth Walls and Reinforced Soil Slopes.* Publication No. FHWA NHI-00-043. U.S. Department of Transportation, Washington, D.C., 418 p.

Goodsell, M.W. (2000). "Instrumentation and installation scheme on a mechanically stabilized earth wall on I-15." Unpublished MS thesis. Utah State University, Logan, Utah. 133 p.

Hagen, J.C. (2001). "Factors affecting sample disturbance in Bonneville clays." Unpublished MS thesis. Utah State University, Logan, Utah. 233 p.

Hermann, L.R. (1978). "User's Manual for REA (General Two Dimensional Soils and Reinforced Earth Analysis Program)." University of California at Davis, Davis, Calif.

Hird, C.C., and Kwok, C.M. (1989). "FE studies of interface behavior in reinforced embankments on soft ground." *Computers and Geotechnics,* 8, 111-131.

Ishii, K., and Suzuki, M. (1987). "Stochastic finite element method for slope stability analysis." *Structural Safety*, 4(2), 111-129.

Kiousis, P.D., Voyiadjis, G.Z., and Tumay, M.T. (1986). "Large strain theory for the two dimensional problems in geomechanics." *Int. J. Numer. and Anal. Methods in Geomechanics,* 10(1), 17-39.

Koga, K., Aramaki, G., and Valliappan, S. (1988). "Finite element analysis of grid reinforcement." *International Geotechnical Symposium on Theory and Practice of Earth Reinforcement*, Fukuoka, Japan, 407-411.

Laba, J.T., and Kennedy, J.B. (1986). "Reinforced earth retaining wall analysis and design." *Can. Geotech. J.,* 23(3), 317-326.

Lechman, J.B., and Griffiths, D.V. (2000). "Analysis of the progression of failure of earth slopes by finite elements." *Geotechnical Special Publication No. 101 - GeoDenver Conference 'Slope Stability 2000'.* ASCE, Reston, Va., 250-265.

Leshchinsky, D., and Vulova, C. (2001). "Numerical investigation of the effects of geosynthetic spacing on failure mechanisms in MSE block walls." *Geosynth. Int.,* 8(4), 343-365.

Long, P.V., Bergado, D.T., Balasubramaniam, A.S., and Delmas, P. (1997). "Interaction between soil and geotextile reinforcement." *Geotechnical Special Publication No. 69 - Ground Improvement, Ground Reinforcement, Ground Treatment: Developments 1987-1997.* ASCE, New York, 560-578.

Mitchell, J.K., and Villet, W.C.B. (1987). "Reinforcement of earth slopes and embankments." National Cooperative Highway Research Program Report No. 290, 323 p.

Mylleville, B.L.J, and Rowe, R.K. (1988). "Steel reinforced embankments on soft clay foundations." *International Geotechnical Symposium on Theory and Practice of Earth Reinforcement*, Fukuoka, Japan, 437-442.

Plaxis: Finite Element Code for Soil and Rock Analyses, Version 7. (1998). Edited by R.B.J. Brinkgreve and P.A. Vermeer. A.A. Balkema Publishers, Rotterdam, Netherlands.

Sampaco, C.L. (1996). "Behavior of welded wire mesh reinforced soil walls from field evaluation and finite element simulation." Unpublished PhD dissertation. Utah State University, Logan, Utah. 507 p.

Sampaco, C.L., Anderson, L.R., and Robertson, D.G. (1994). "Field evaluation of earth pressure on RSE walls." *Proc., Thirteenth International Conference on Soil Mechanics and Foundation Engineering.* Oxford & IBH Publishing Co. Pvt. Ltd., New Delhi, India.

Schaefer, U.R., and Duncan, J.M. (1988). "Finite element analysis of the St. Alban test embankments." *Geotechnical Special Publication No. 18.* ASCE, New York, 158-177.

Siddharthan, R.V., Ganeshwara, V., Kutter, B.L., El-Desouky, M., and Whitman, R.V. (2004a). "Seismic deformation of bar mat mechanically stabilized earth walls. I: Centrifuge tests." *J. Geotech. and Geoenviron. Eng.*, 130(1), 14-25.

Siddharthan, R.V., Ganeshwara, V., Kutter, B.L., El-Desouky, M., and Whitman, R.V. (2004b). "Seismic deformation of bar mat mechanically stabilized earth walls. II: A multiblock model." *J. Geotech. and Geoenviron. Eng.*, 130(1), 26-35.

Vidal, H. (1969). The Principal of Reinforced Earth. Highway Research Record 282, Highway Research Board, National Research Council, Washington, D.C., 16 p.

Yamanouchi, T., Muira, N., and Ochiai, H. Editors. (1988). *Theory and Practice of Earth Reinforcement: Proceedings of the International Geotechnical Symposium on Theory and Practice of Earth Reinforcement.* A.A. Balkema Publishers, Brookfield, Vt.

Zhang, X. (1999). "Slope stability analysis based on the rigid finite element method." *Geotechnique,* 49(5), 585-593.

VITA

Aaron S. Budge
1618 West Budge Lane
Pleasant View, UT 84414
(801) 786-0544 Home
(435) 797-2945 Office
asbudge@cc.usu.edu

EDUCATION

Doctor of Philosophy, Civil Engineering, Utah State University
(Coursework completed at Utah State University and the University of Texas at Austin)
Dissertation: Analytical and Numerical Investigation of a Mechanically Stabilized Earth Wall on I-15
Expected: December 2004

Master of Science, Civil Engineering, Utah State University
Thesis: Cyclic Lateral Loading of Model Pile Groups in Clay Soil: Phase 3C
Received: December 2000

Bachelor of Science, Civil and Environmental Engineering, Utah State University
Magna Cum Laude
Senior Design Project: Lightweight Concrete Reinforcement Design
Received: June 1998

EXPERIENCE

Instructor, Utah State University, Logan, UT, 2001-present

Provided class instruction and coordinated field laboratory exercises for undergraduate civil engineering surveying course (Fall 2001, Fall 2002, Fall 2003) and provided class instruction for undergraduate engineering statics course (Spring 2004); substituted as instructor for undergraduate courses in statics, soil mechanics, and foundation design as well as a graduate course in deep foundation design; advised undergraduate students

Graduate Research Assistant, Utah State University, Logan, UT, 1998-present

Performed extensive investigation of the response of a model pile group to cyclic lateral loads and assisted other graduate students in additional phases of the investigation; prepared Masters Thesis and several papers and presentations relating to the results of the model pile group study; Assisted in performing Spectral Analysis of Surface Waves (SASW) studies at the Yucca Mountain Nuclear Waste Depository site and numerous sites in Turkey; Performed forward modeling to determine soil profiles at Yucca Mountain site; Completed extensive Finite Element analyses of several versions of a soil

testing apparatus as part of a research proposal submitted by Dr. James A. Bay; Assisted in analysis of optimum drop weight mass and drop height for various soil profiles for SASW testing; Obtained readings and performed data manipulation for instrumentation associated with an MSE wall located on I-15 in Salt Lake City, Utah; Prepared, edited, and submitted three reports to Utah Department of Transportation related to the Mechanically Stabilized Earth (MSE) wall study; Prepared additional papers and presentations relating to the MSE wall for other audiences; Currently performing extensive Finite Element analysis (Plaxis software) of the MSE wall as PhD Dissertation research to be submitted as another report to Utah Department of Transportation; Also currently working on three additional professional papers to be submitted as a portion of the fulfillment of the requirements for a PhD

Engineering State Instructor, Utah State University, Logan, UT, 2000-2004

Provided instruction and supervision for high school students participating in the "Engineering State" program sponsored by the College of Engineering at Utah State University; taught basic retaining wall theory and design to high school students; assisted students in construction and testing of scale model mechanically stabilized earth walls

Soil Mechanics Laboratory Instructor, Utah State University, Logan, UT, 1999-2000

Provided laboratory instruction and coordinated laboratory activities for exercises associated with undergraduate soil mechanics course; maintained laboratory equipment; collected necessary soil samples for testing

Civil Engineering Intern, Utah Department of Transportation Region One Materials Laboratory, Ogden, UT, 1997-1998

Performed extensive material testing in laboratory and field, including soil particle size analyses, asphalt oil content burnoffs, concrete cylinder strength tests, soil California Bearing Ratio (CBR) tests, Dynamic Cone Penetrometer (DCP) field tests; Assisted in data collection and analysis for Ground Penetrating Radar (GPR) studies; Assisted in data collection and analysis for Falling Weight Deflectometer (FWD) studies, Assisted in obtained pavement coring samples for Portland Cement Concrete Pavements (PCCP) and Bituminous Pavements (Asphalt); Performed extensive computer modeling to determine pavement and subgrade profiles corresponding to those obtained from FWD tests; Assisted in instruction relating to the determination of the extent of spall damage in PCCP

TEACHING INTERESTS

Engineering Surveying

Engineering Statics

Mechanics of Materials

Introductory Soil Mechanics

Advanced Soil Mechanics

Undergraduate-level Foundation Design

Graduate-level Deep Foundation Design
Earth Structure Design (Embankment and Earth-fill Dam)
Geotechnical Earthquake Engineering
Buried Structures (Pipe Mechanics)
Advanced Geotechnical Modeling (Finite Element / Finite Difference)
Saturated, Partially Saturated, and Multiphase Flow through Soil
(Appropriate for an Environmental Geotechnics course)

RESEARCH GOALS AND INTERESTS

Advanced Studies of Soft Soils
- Geophysical in-situ testing (SASW and crosshole testing)
- Advanced laboratory studies (resonant column tests, cyclic triaxial tests, cyclic direct simple shear tests, consolidation testing, etc.)
- Development of Stress History and Normalized Soil Engineering Properties (SHANSEP) parameters for soft clays

MSE Wall Behavior Modeling
- Finite Element Modeling
- Finite Difference Modeling
- Instrumentation and Monitoring of New Walls

Liquefaction Susceptibility Studies

Deep and Shallow Foundation Response to Cyclic Loading

SCHOLARSHIPS

Superior Student Scholarship, Utah State University, 1992-93, 1995-98
Dean F. and Bessie Peterson Engineering Scholarship, Utah State University, 1992-93

INVITED PRESENTATIONS

Budge, A.S. Liquefaction Investigation Following the Kocaeli, Turkey Earthquake. Presentation to Graduate Student Seminar for Department of Civil Engineering at Brigham Young University, Provo, UT, 2003.

Budge, A.S. Factors Affecting Sample Disturbance in Bonneville Clays. Presentation of Report No. UT-03.14. Utah Department of Transportation, Salt Lake City, UT, 2003.

Budge, A.S. Instrumentation and Installation Scheme of a Mechanically Stabilized Earth Wall on I-15 with Results of Wall and Foundation Behavior. Presentation of Report No. UT-03.11. Utah Department of Transportation, Salt Lake City, UT, 2003.

Budge, A.S. Instrumentation and Behavior of a Mechanically Stabilized Earth Wall on I-15. The 37th Annual Symposium on Engineering Geology & Geotechnical Engineering, Boise, ID, 2002.

Budge, A.S. Lateral Loading of Model Pile Groups. The 36th Annual Symposium on Engineering Geology & Geotechnical Engineering, Las Vegas, NV, 2001.

Budge, A. S., J. E. Apedaile, and K. Jelinek. Geophysical Measurements to Estimate Degree of Consolidation for Model Lateral Load Tests. The 34th Annual Symposium on Engineering Geology & Geotechnical Engineering, Logan, UT, 1999.

REFEREED PUBLICATIONS

Budge, A. S. and J. A. Caliendo. Cyclic Lateral Loading of Model Pile Groups in Clay Soil.
Submitted to *Journal of Geotechnical and Geoenvironmental Engineering,* American Society of Civil Engineers, Reston, VA, 2003. (Submitted June 2003 - currently under revision.)

Several additional publications to be submitted for review by September 2004.

OTHER PUBLICATIONS AND REPORTS

Bay, J.A., L.R. Anderson, J.C. Hagen, and **A.S. Budge**. *Factors Affecting Sample Disturbance in Bonneville Clays.* Report No. UT-03.14. Utah Department of Transportation, Salt Lake City, UT, 2003.

Bay, J.A., L.R. Anderson, T.M. Colocino, and **A.S. Budge**. *Evaluation of SHANSEP Parameters for Soft Bonneville Clays.* Report No. UT-03.13. Utah Department of Transportation, Salt Lake City, UT, 2003.

Bay, J.A., L.R. Anderson, **A.S. Budge**, and M.W. Goodsell. *Instrumentation and Installation Scheme of a Mechanically Stabilized Earth Wall on I-15 with Results of Wall and Foundation Behavior.* Report No. UT-03.11. Utah Department of Transportation, Salt Lake City, UT, 2003.

Budge, A.S. and M.W. Goodsell. Instrumentation and Behavior of a Mechanically Stabilized Earth Wall on I-15. *Proceedings of the 37th Annual Symposium on Engineering Geology & Geotechnical Engineering*, Boise, ID, 2002.

Budge, A.S. and J.A. Caliendo. Lateral Loading of Model Pile Groups. *Proceedings of the 36th Annual Symposium on Engineering Geology & Geotechnical Engineering*, Las Vegas, NV, 2001.

Budge, A.S., J.E. Apedaile, and K. Jelinek. Abstract - Geophysical Measurements to Estimate Degree of Consolidation for Model Lateral Load Tests. *Proceedings of the 34th Annual Symposium on Engineering Geology & Geotechnical Engineering*, Logan, UT, 1999.

Vandre, B., **A.S. Budge,** and S. Nussbaum. DCP: A Useful Tool for Characterizing Soil Properties at Shallow Depths. *Proceedings of the 34th Annual Symposium on Engineering Geology & Geotechnical Engineering*, Logan, UT, 1999.

SERVICE

Block Captain / Interim Section Leader, Pleasant View City Community Emergency Response Team (CERT), 2002-present
Instructor, Engineering State Program, Utah State University, 2000-2002
Vice President, Best of America Program, Golden Key National Honor Society, Utah State University, 1997-1998
Vice President, Tau Beta Pi, Utah State University, 1997-1998
Chapter Historian, Golden Key National Honor Society, Utah State University, 1996-1997
Records Secretary, Tau Beta Pi, Utah State University, 1996-1997
Academic Council Representative, Utah State University, 1996-1997

PROFESSIONAL AFFILIATIONS

Phi Kappa Phi, 2001-present
Tau Beta Pi, 1997-present
Golden Key National Honor Society, 1996-present

REFERENCES

Dr. Loren R. Anderson, Professor and Department Head, Department of Civil and Environmental Engineering, Utah State University, 4110 Old Main Hill, Logan, UT 84322-4110, (435) 797-2938, (435) 797-1185 fax, loren@cc.usu.edu

Dr. James A. Bay, Assistant Professor, Department of Civil and Environmental Engineering, Utah State University, 4110 Old Main Hill, Logan, UT 84322-4110, (435) 797-2947, (435) 797-1185 fax, jim.bay@usu.edu

Dr. Joseph A. Caliendo, Associate Professor and Division Head, Department of Civil and Environmental Engineering, Utah State University, 4110 Old Main Hill, Logan, UT 84322-4110, (435) 797-2896, (435) 797-1185 fax, joe@cc.usu.edu

Dr. Marvin Halling, Associate Professor, Department of Civil and Environmental Engineering, Utah State University, 4110 Old Main Hill, Logan, UT 84322-4110, (435) 797-3179, (435) 797-1185 fax, halling@cc.usu.edu

Dr. Stephen G. Wright, Professor, Department of Civil Engineering, University of Texas at Austin, 1 University Station Stop C1700, Austin, TX 78712, (512) 471-4929, (512) 471-6548 fax, swright@mail.utexas.edu

Dr. Ellen M. Rathje, Assistant Professor, Department of Civil Engineering, University of Texas at Austin, 1 University Station Stop C1792, Austin, TX 78712, (512) 471-4929, (512) 471-6548 fax, e.rathje@mail.utexas.edu